

EXPERIMENTAL AND ANALYTICAL STUDIES OF BEHAVIOR OF SINGLE
PILES IN SAND UNDER LATERAL AND AXIAL LOADING

by

Frazier Parker, Jr.
Lymon C. Reese

Research Report Number 117-2

Development of Method of Analysis of Deep
Foundations Supporting Bridge Bents

Research Project 3-5-68-117

conducted for

The Texas Highway Department

in cooperation with the
U. S. Department of Transportation
Federal Highway Administration

by the

CENTER FOR HIGHWAY RESEARCH
THE UNIVERSITY OF TEXAS AT AUSTIN
AUSTIN, TEXAS

November 1970

The opinions, findings, and conclusions expressed in this publication are those of the authors and not necessarily those of the Federal Highway Administration.

PREFACE

This report is the second of three reports dealing with the findings of Research Project 3-5-68-117, "Development of Method of Analysis of Deep Foundations Supporting Bridge Bents." The first report contains documentation of a procedure which was developed for analysis of pile-supported foundations and the use of the procedure to analyze two bridge bents which were designed and built by the Texas Highway Department.

This report presents the results of an investigation of the behavior of single piles in sand. The procedure for analyzing pile-supported foundations requires a knowledge of the lateral and axial load-deformation response of the individual piles in the foundation. In this report, the pile response used in the procedure for analyzing a foundation is emphasized.

The final report will be concerned with the modification and improvement of the proposed method for analyzing a pile-supported bridge bent.

The authors would like to acknowledge the work of a number of people who contributed to this report. Technical assistance, during the field and laboratory testing, was provided by Messrs. Olen Hudson, Harold Dalrymple, and Fred Koch. The assistance and advice of Messrs. H. D. Butler and Warren Grasso of the Texas Highway Department and Mr. Bob Stanford of the Bureau of Public Roads are greatly appreciated.

The support of the Federal Highway Administration is gratefully acknowledged.

Frazier Parker, Jr.
Lymon C. Reese

November 1970

This page replaces an intentionally blank page in the original.

-- CTR Library Digitization Team

LIST OF REPORTS

Report No. 117-1, "A Method for the Analysis of Pile Supported Foundations Considering Nonlinear Soil Behavior," by Frazier Parker, Jr., and William R. Cox, presents the documentation of a procedure which was developed for the analysis of pile supported foundations and the use of the procedure to analyze two bridge bents that were designed and built by the Texas Highway Department.

Report No. 117-2, "Experimental and Analytical Studies of Behavior of Single Piles in Sand Under Lateral and Axial Loading," by Frazier Parker, Jr., and Lymon C. Reese, presents criteria for describing families of nonlinear axial and lateral pile-soil interaction curves for piles in sand, and solves example problems using the proposed criteria.

This page replaces an intentionally blank page in the original.

-- CTR Library Digitization Team

ABSTRACT

This report contains the results of a study of the behavior of piles subjected to axial and lateral forces. Pile-soil interaction can be represented by families of interaction curves, and in this study criteria for describing such families of interaction curves from soil properties are investigated. Specifically, attention is directed toward formulation of criteria for piles in sand.

To study the interaction, 2-inch-diameter piles were buried in submerged sand with controlled density. Instrumentation was provided for the measurement of axial load and bending moment distributions. From these distributions, axial and lateral interaction curves were generated and correlated with measured soil properties. Based on the correlations, criteria for describing the interaction curves were formulated.

Axial and lateral interaction curves, generated using the proposed criteria, are used to predict analytically the response of the test piles. The proposed criteria are also used to compute the response of a number of piles which have been tested and the results reported in the literature. The computed response of the piles is compared with the measured response of the piles to check the validity of the proposed criteria.

KEY WORDS: piles, axial behavior, lateral behavior, shear transfer, lateral resistance, soil properties, soil criteria.

This page replaces an intentionally blank page in the original.

-- CTR Library Digitization Team

SUMMARY

The purpose of this report is to present the results of a study of the response of piles, embedded in sand, that are subjected to axial and lateral loads. Emphasis is placed on formulating criteria for describing the pile-soil interaction from soil properties in the form of nonlinear curves.

Tests were performed with 2-inch-diameter piles, placed in sand with controlled properties. Results of the tests were studied to obtain information on the transfer of loads from the piles to the surrounding sand.

For axially loaded piles, load is transferred from the pile to the soil through shear along the shaft of a pile and through pressure on the tip of the pile. In this report, criteria are developed for describing nonlinear shear transfer-pile deflection curves from stress-strain data for the sand. Criteria are also suggested for obtaining tip load-tip deflection curves. The load transfer curves may be used with available computational procedures to predict the load-deformation response for the top of a pile.

For laterally loaded piles, load is transferred from a pile to the soil by lateral pressure on the shaft of the pile. In this report, criteria are developed for describing nonlinear lateral resistance-lateral deflection curves from properties of the sand. The load transfer curves may be used with available computational procedures to predict the response of a pile subjected to lateral loads.

This page replaces an intentionally blank page in the original.

-- CTR Library Digitization Team

IMPLEMENTATION STATEMENT

The results of this study are part of a program to provide a better way of analyzing bridge bents that are founded on piles. The specific objective of the program is the formulation of a procedure for analyzing the foundation when it is subjected to vertical, as well as horizontal, forces. In the portion of the program contained in this report, behavior of individual piles is considered, with emphasis placed on those aspects of the behavior of single piles that are used in the procedure for analyzing a foundation containing piles.

This report provides the user with procedures for obtaining axial and lateral load-deformation response for piles in sand. The proposed criteria result in approximations of the behavior of the sand around a pile when it is loaded. Nonlinear soil resistance-pile movement curves can be generated and used with available computational procedures to obtain pile response that is used in the analysis of a foundation.

The procedures presented in this report can be used to make a rational analysis of a pile-supported bridge bent and improve foundation designs over those made by empirical procedures.

This page replaces an intentionally blank page in the original.

-- CTR Library Digitization Team

TABLE OF CONTENTS

	<u>Page</u>
PREFACE.	iii
LIST OF REPORTS	v
ABSTRACT AND KEY WORDS	vii
SUMMARY	ix
IMPLEMENTATION STATEMENT	xi
NOMENCLATURE	xvii
CHAPTER I. INTRODUCTION	1
CHAPTER II. FORMULATION OF RELATIONSHIPS FOR DESCRIBING PILE BEHAVIOR	5
Mechanics of an Axially Loaded Pile	6
Mechanics of a Laterally Loaded Pile	14
CHAPTER III. TEST PROGRAM	25
General Considerations	25
Selection of Test Conditions	29
Design of the Piles	31
CHAPTER IV. PROPERTIES OF SAND	35
Basic Properties of the Sand	35
Density of the Compacted Sand	37
Measurement of Strength and Stress-Strain Characteristics of Sand	40
Determination of Angle of Internal Friction	42
Determination of Stress-Strain Curves	49

	<u>Page</u>
CHAPTER V. AXIAL LOAD TRANSFER	63
Concepts of Axial Pile-Soil Interaction	64
Ultimate Shear Transfer Along the Pile Shaft	64
Pile Movement-Shear Transfer Relationships	70
Ultimate Pile Tip Resistance	79
Tip Movement-Tip Resistance Relationships	81
Test Results	84
Measured Axial Load-Deformation Curves for the Top of the Piles	84
Experimental Curves Showing Distribution of Load Along the Piles	86
Development of Shear Transfer Curves from Measured Loads and Deflections	89
Correlation of Shear Transfer Curves with Stress-Strain Curves for the Sand	92
Development of Load-Deformation Curve for the Tip of the Pile	100
Comparisons of Computed and Measured Load-Deformation Curves	106
Comparisons for Two-Inch Diameter Test Piles	107
Comparisons for Four-Inch Diameter Test Piles	109
Comparisons for Field Tests	122
Summary of Criteria for Describing Axial Load Transfer	127
Comments and Discussion of Results	131
CHAPTER VI. LATERAL LOAD TRANSFER	133
Concepts of Lateral Pile-Soil Interaction	134
Ultimate Lateral Soil Resistance	137
Initial Lateral Load-Deformation Relationships	146
Test Results	149
Measured Load Versus Deflection and Load Versus Slope Curves for the Tops of the Piles	149
Measured Moment Distribution Curves	153
Development of p-y Curves	156
Comparison of Measured and Theoretical p-y Curves	168

	<u>Page</u>
Transition Between Initial Slope and Ultimate Resistance	172
Comparisons of Measured and Predicted Lateral Pile Response	175
Comparisons for Two-Inch Diameter Test Piles	176
Comparisons for Tests of Shinohara and Kubo	180
Comparisons for Tests of Mason and Bishop	181
Comparisons for Arkansas River Tests	185
Summary of Criteria for Describing Lateral Soil Resistance	187
Comments and Discussion of Results	188
CHAPTER VII. CONCLUSIONS AND RECOMMENDATIONS	193
Experimental Procedures	193
Behavior Under Axial Load	194
Behavior Under Lateral Load	197
REFERENCES	199
APPENDICES	205
Appendix A. Test Facilities	207
Appendix B. Instrumentation	213
Appendix C. Calibration of Piles	219
Appendix D. Test Equipment	231
Appendix E. Procedures Used in Placing Sand and Measuring Density	243
THE AUTHORS	251

This page replaces an intentionally blank page in the original.

-- CTR Library Digitization Team

NOMENCLATURE

<u>Symbol</u>	<u>Typical Units</u>	<u>Definition</u>
A	square inches	Net cross-sectional area of a pile
A_y , B_y , A_m , and, B_m		Nondimensional deflection and moment coefficients
a, b, n, k, and R_f		Coefficients for fitting a hyperbola to stress-strain curves
B		Skempton's pore pressure parameter
C	inches	Pile circumference
D	inches	Equivalent pile diameter or width
E	lb./sq.in.	Modulus of elasticity of the pile material
E_m	lb./sq.in.	Soil modulus of elasticity
E_s	lb./sq.in.	Secant modulus of soil reaction
F	lb./in.	Force per unit length transferred to the soil
F_p	pounds	Ultimate passive force on a cylinder moved laterally through a sand
F_s	pounds	Ultimate skin load
f_r		Reduction factor to relate soil friction angle to friction angle between pile and soil
H	inches	Depth of a cylinder moved laterally through a sand
h	inches	Increment length
I	in ⁴	Moment of inertia of the pile
I_B		Influence coefficient for relating pile tip movement and tip pressure

<u>Symbol</u>	<u>Typical Units</u>	<u>Definition</u>
I_y		Influence coefficient for relating lateral pile deflection to lateral pressure
J		Nondimensional coefficient relating sand modules of elasticity to the relative density of the sand
K		Constant for describing the variation of the coefficient of soil reaction with depth
K_a		Coefficient of active earth pressure
K_p		Coefficient of passive earth pressure
K_x		Coefficient of lateral earth pressure
k_s	lb./sq.in.	Coefficient of soil reaction
L	inches	Depth of a pile
M	in.-lb.	Moment in a pile
m		Constants for describing the variation of the coefficient of soil reaction with depth
N_c and N_t		Compression and tension skin friction coefficients
N_q^*		Bearing capacity factor for circular or square piles
P_T	pounds	Lateral load applied to a pile
p	lb./in.	Soil resistance per unit length of pile
p_a	lb./sq.in.	Atmospheric pressure
P_{uf}	lb./in.	Ultimate soil resistance for a flow around type failure

<u>Symbol</u>	<u>Typical Units</u>	<u>Definition</u>
P_{uw}	lb./in.	Ultimate soil resistance for a wedge type failure
Q	pounds	Axial force in a pile
Q_B	pounds	Axial force on a pile base
Q_T	pounds	Axial load applied to the top of a pile
q	lb./in.	Distributed lateral load
q_B	lb./sq.in.	Pressure on the tip of a pile
q_o	lb./sq.in.	Tip bearing capacity
R_c and R_t		Factors for correlating pile movement to axial strain
S	lb./sq.in.	Slope of a stress-strain curve at zero strain
SF	pounds	Spring force
s_x	lb./sq.in.	Shear stress transferred to the soil along the pile shaft at depth x
s_{xm}	lb./sq.in.	Maximum shear stress transferred to the soil along the pile shaft at depth x
U_c and U_t		Coefficients for relating shear transfer to deviator stress
x	inches	Coordinate measured along the pile axis
y	inches	Lateral pile deflection
Z		Nondimensional depth coefficient
z	inches	Axial pile movement
z_B	inches	Pile tip movement
α	degrees	Angle used to define a failure wedge for a cylinder moved laterally through a sand

<u>Symbol</u>	<u>Typical Units</u>	<u>Definition</u>
β	degrees	Failure angle from Mohr-Coulomb failure theory
Γ	inches	Relative stiffness of a pile
$\bar{\gamma}$	lb./cu.ft.	Effective soil unit weight
γ_D	lb./cu.ft.	Dry density of the sand
$\Delta\sigma$	lb./sq.in.	Deviator stress for a triaxial test
$\Delta\sigma_f$	lb./sq.in.	Maximum deviator stress
δ	degrees	Apparent angle of friction between the pile and soil
ϵ_1		Axial strain in a triaxial test
λ		Empirically derived coefficient for relating pile tip movement and tip pressure
μ_x		Coefficient of friction between the pile and soil
ν		Poisson's ratio for a soil
ρ	lb./sq.in.	Lateral pressure exerted on the pile by the soil
$\sigma_1 \dots \sigma_7$	lb./sq.in.	Normal stress in derivation of flow-around failure
$\bar{\sigma}_1$	lb./sq.in.	Effective axial stress in a triaxial test
$\bar{\sigma}_3$	lb./sq.in.	Effective confining stress in a triaxial test
σ_{nx}	lb./sq.in.	Normal stress on the pile shaft at a depth x
ϕ	degrees	Sand angle of internal friction

<u>Symbol</u>	<u>Typical Units</u>	<u>Definition</u>
$\phi(Z)$		Nondimensional soil modulus function
ψ		Function which relates shear transfer to axial pile movement

CHAPTER I
INTRODUCTION

Pile foundations are frequently used for structures when the soil immediately below the base will not provide adequate bearing capacity. The purpose of the piles is to transfer the load from the structure to soil strata which can sustain the applied loads.

If all loads from the structure and all piles are vertical, then the loads transmitted to the piles will all be principally axial. If some horizontal component of load is present, a lateral force will also be transmitted to the piles. If some of the piles are battered, an axial and lateral force will be transmitted to the piles regardless of the direction of the applied load. For most structures both horizontal and vertical components of load are present. In some instances, the horizontal component may be small and can be neglected. However, for many structures, such as offshore drilling platforms or tall bridge bents, wind and wave action will produce significant horizontal forces. Therefore, for a complete analysis of a pile foundation, the behavior of the piles must be analyzed for both lateral and axial loads.

When a pile is subjected to any load, deformation will occur. For small loads, the deformation may be proportional to the load; however, the load-deformation relationship becomes increasingly nonlinear as the load increases. This nonlinear load-deformation relationship is principally due to the nonlinear load-deformation characteristics of the soil, but may be affected by the nonlinear load-deformation characteristics of the pile. The behavior of a pile under loading will depend on a number

of variables such as pile material, soil type, pile shape, pile length, pile cross section, and method of installation.

For axial loading, the nonlinear characteristics of the pile material will usually have little or no influence on the nonlinear behavior of the pile. For most combinations of pile length and cross section a limiting load, which results in a failure of the soil surrounding the pile, is reached before the material in the pile is strained beyond the linear range.

For lateral loading, the concept of a limiting load, where all the soil around the pile is in a failure condition, does not apply. Nonlinear bending in the pile will begin when the soil around only the upper portion of the pile has reached a failure condition, and both the nonlinear pile material characteristics and the nonlinear soil characteristics will influence the nonlinear pile behavior. However, for most problems, the effect of nonlinear bending on the overall nonlinear pile behavior is secondary, and will be excluded from further discussion.

The remainder of this report will be concerned primarily with defining curves which will simulate the nonlinear interaction between the pile and the surrounding soil. Families of curves are necessary to represent the axial and lateral interaction between the pile and the supporting soil. Axial behavior and lateral behavior are considered separately.

The family of curves describing the behavior of the soil around an axially loaded pile will give axial soil reaction versus axial pile movement for a number of locations along the pile. For a given location,

a curve would show the force per unit area transferred to the soil for a given axial movement of the pile.

The family of curves describing the behavior of the soil around a laterally loaded pile will give lateral soil reaction versus lateral pile movement for a number of locations along the pile. For a given location, a curve would show the force per unit length transferred to the soil for a given lateral movement.

If families of interaction curves are available, existing procedures for numerical computation may be used to predict the response of the pile. The response of individual piles may be combined to predict the behavior of a foundation supported by these piles. A detailed knowledge of the behavior of the foundation and of the individual piles will allow a superior design, which will usually be more economical than is possible with a less rational procedure.

However, if the procedure mentioned above is to be useful in design, it will be desirable to obtain soil interaction curves from measurable soil properties. The primary concern of this study will be the investigation of the criteria for describing the families of soil interaction curves from soil properties. Specifically, attention will be directed toward formulating criteria for piles in sand. A review of the literature revealed little information on criteria for describing axial interaction curves for piles in sand. The literature review also indicated that the criteria for lateral interaction was limited, and that much of the available criteria had not been checked experimentally. Because of the lack of information on sand criteria, tests were run on a number of

small piles for the purpose of investigating the pile-soil interaction and expanding available sand criteria.

The test piles were two inches in diameter and were buried to a depth of 96 inches in a homogeneous sand. The water table was kept just above the ground surface during the tests. Six piles were loaded axially and six piles were loaded laterally. Instrumentation was provided on the piles, and axial and lateral interaction curves obtained. The measured interaction curves were correlated with measured soil properties, and criteria for describing the interaction curves were formulated.

In Chapter II, relationships for describing mathematically the behavior of axially loaded and laterally loaded piles will be summarized. The design of the test program will be discussed in Chapter III. In Chapter IV, considerable attention will be given to the determination of the properties of the sand used in the test. The results from the axial load tests of the piles will be presented and analyzed in Chapter V; and in Chapter VI, the results from the lateral load tests will be presented and analyzed. Also included in Chapters V and VI will be a comparison between experimental results available in the literature and computed results using the proposed criteria for describing the pile-soil interaction curves. Chapter VII will contain the conclusions drawn from the study, and recommendations for further study.

CHAPTER II
FORMULATION OF RELATIONSHIPS FOR
DESCRIBING PILE BEHAVIOR

The practice of solving soil mechanics problems by considering nonlinear soil behavior has developed along with the ability to handle the necessary computations. This ability has been brought about by digital computers, which are able to perform the large number of required calculations very rapidly. Problems can now be solved that were previously solved using an ultimate strength or linear elasticity approach. In particular, the behavior of an axially loaded pile and a laterally loaded pile can be predicted for any load.

In the following two sections of this chapter the basic concepts involved in the transfer of load from the pile to the surrounding soil will be summarized. In the theoretical development, it is assumed that, from the standpoint of soil behavior, the lateral and axial behavior of the pile may be treated independently. Thus, a solution for the applied axial loads may be obtained without considering any lateral loads that may also be applied, and vice versa.

In the following section, the relationships which describe the behavior of an axially loaded pile will be formulated. The second section will deal with the formulation of the relationships for a laterally loaded pile.

Mechanics of an Axially Loaded Pile

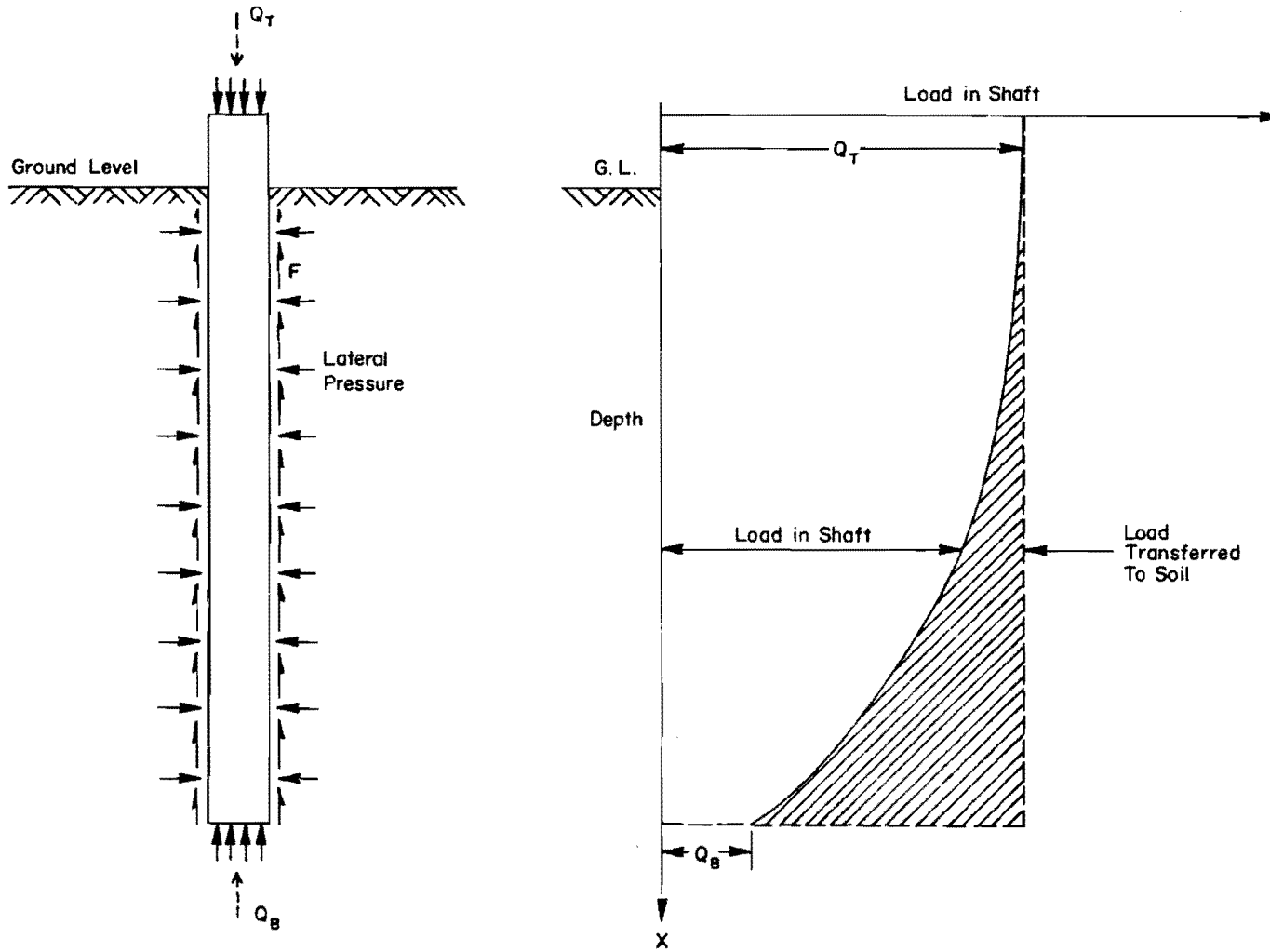
An axial load applied to the top of a pile is resisted by the shearing resistance developed along the shaft of the pile and the pressure on the base of the pile. The transfer of load from the pile to the soil is illustrated in Fig. 2.1, from Vijayvergiya, Hudson and Reese (1969), and may be stated mathematically by the equation

$$Q_T = \int_{x=0}^{x=L} F dx + Q_B \dots \dots \dots (2.1)$$

where

- Q_T = load applied to the top of a pile
- F = shear force per unit length transferred to the soil
as a function of the location along a pile
- dx = differential length over which F is transferred
- Q_B = load due to the pressure on the base of a pile.

This equation involves only statics and its solution will only assure that the forces on the pile are in equilibrium. It provides no insight into the deformation pattern that is necessary to produce the base pressure and shear transfer along the shaft for equilibrium. For the ultimate strength approach, this equation is sufficient since the deformations are not considered, and the assumption is made that the maximum base pressure and maximum shear transfer occur simultaneously. If, however, the load-deformation behavior of the pile is to be considered, the compatibility between loads and deformations must be considered. To



a. Forces acting on a pile b. Typical curve for load distribution

After Vijayvergiya, Hudson and Reese (1969)

Fig. 2.1. Illustration of Axial Load Transfer in a Pile.

represent this compatibility condition, another mathematical expression must be formulated relating load and deformation.

The derivation of an analytical expression for this purpose is suggested by Seed and Reese (1957) and expanded by Reese (1964). Considering a segment of an axially loaded pile as shown in Fig. 2.2, the expression for the strain in the pile at depth x is given by

$$\frac{dz}{dx} = \frac{Q}{EA} \dots \dots \dots (2.2)$$

where

- Q = load in pile
- E = modulus of elasticity of pile
- A = cross-sectional area of pile
- x = distance measured along axis of pile
- z = movement of pile.

This equation may be rearranged to yield

$$Q = EA \frac{dz}{dx} \dots \dots \dots (2.3)$$

Differentiation of Eq. 2.3 with respect to x , assuming EA constant, yields

$$\frac{dQ}{dx} = EA \frac{d^2 z}{dx^2} \dots \dots \dots (2.4)$$

Summing forces on the pile segment, shown in Fig. 2.2, yields the equilibrium expression

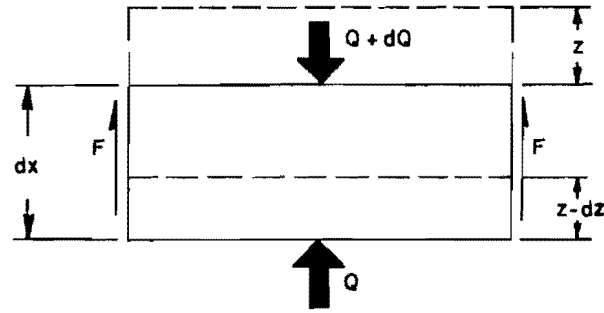


Fig. 2.2. Element from an Axially Loaded Pile.

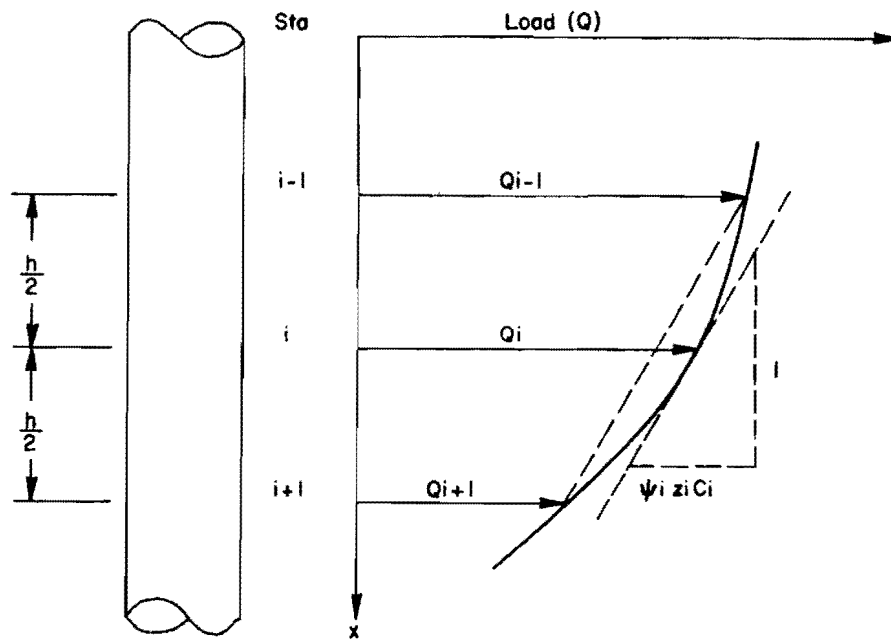


Fig. 2.3. Load Distribution Along an Axially Loaded Pile.

$$\frac{dQ}{dx} = F \dots \dots \dots (2.5)$$

The shear force per unit area is defined as

$$s_x = \frac{F}{C} \dots \dots \dots (2.6)$$

where

s_x = shear force transferred per unit area at depth x

C = pile circumference.

Equation 2.5 may now be written as

$$\frac{dQ}{dx} = s_x C \dots \dots \dots (2.7)$$

If ψ is a function which relates the shear stress to the deflection of the pile, so that

$$s_x = \psi z \dots \dots \dots (2.8)$$

then Eq. 2.7 may be written as

$$\frac{dQ}{dx} = \psi z C \dots \dots \dots (2.9)$$

Equations 2.4 and 2.9 may be equated for $\frac{dQ}{dx}$ yielding

$$EA \frac{d^2 z}{dx^2} = \psi z C \dots \dots \dots (2.10)$$

which is the desired compatibility expression. To obtain a solution for Eq. 2.10, the function ψ and two boundary conditions must be known.

For realistic problems, considering nonlinear soil behavior, the function ψ usually cannot be defined analytically, and a numerical solution is necessary.

A numerical solution to the nonlinear differential equation, Eq. 2.10, is suggested by Seed and Reese (1957), Reese (1964), and Coyle and Reese (1966). The first step in obtaining a solution is to write Eq. 2.10 in finite difference form. Referring to Fig. 2.3, the difference form of the equation for station i may be written as

$$\frac{\left(\frac{dz}{dx}\right)_{i-1} - \left(\frac{dz}{dx}\right)_{i+1}}{h} = \frac{\psi_i z_i C_i}{EA} \dots \dots \dots (2.11)$$

Substituting Eq. 2.2 into Eq. 2.11 and simplifying yields

$$Q_{i-1} - Q_{i+1} = h\psi_i z_i C_i \dots \dots \dots (2.12)$$

which is the desired form of the equation. It should be noted that, in the derivation up to this point, the assumption of a constant AE only restricts the pile size in the increment considered. In the solution process an increment is considered as having a length of h as shown in Fig. 2.3. Therefore, the distance over which AE may vary is limited to a minimum length of h .

Equation 2.12 is simply a statement that the difference between the forces in the pile at stations $i+1$ and $i-1$ is equal to the load transferred to the soil between these two points. Furthermore, the load distribution within the pile is assumed to be linear between these two points. The slope of the straight-line load distribution is approximated by the rate of load distribution at the midpoint between stations $i+1$

and $i-1$. This procedure results in a concentration of the shear force, $h\psi_i z_i C_i$, at station i . The physical significance of this assumption leads to the mechanical model of an axially loaded pile, illustrated in Fig. 2.4. This model is a combination of the overall representation of a pile as suggested by Reese (1969), but with the specific elements suggested by Matlock, Rachid, and Panak (in progress).

The mechanical model illustrated in Fig. 2.4 represents the pile by n springs, of length h , connected by rigid joints. The springs representing the pile are linear and have a spring constant as shown. The nonlinear springs, representing the load transfer to the soil, are attached to the rigid joints. The spring attached to joint 1 will represent the load transferred from the ground surface to a depth of $h/2$. The spring attached to joint $n+1$ will represent the load transferred to the soil through the pressure on the pile base. The spring attached to joint n will represent the load transferred from the pile base to a distance of $3h/2$ above the base. The interior springs represent the load transferred over a distance $h/2$ above and below the joint. With the station numbering illustrated in Fig. 2.4, Eq. 2.12 may be written as

$$Q_{j-1} - Q_j = hC_j \psi_j z_j \dots \dots \dots (2.13)$$

The concentration of the shear transfer for an arbitrary interior joint is illustrated in Fig. 2.5.

If curves are available showing the load transfer, Eq. 2.13 can be used to obtain the load deformation behavior of the pile. The solution procedure may be formulated by considering the mechanical model in

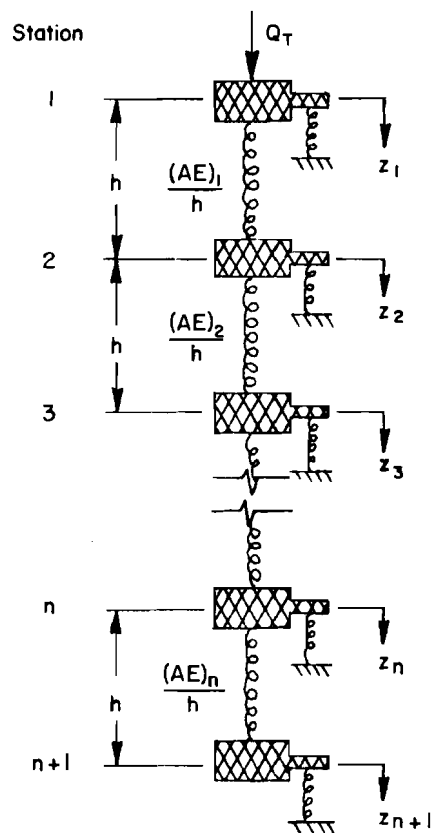


Fig. 2.4. Mechanical Model of an Axially Loaded Pile.

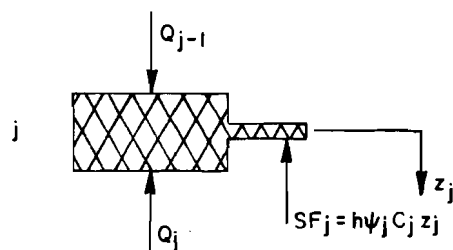


Fig. 2.5. Joint j of the Mechanical Model of an Axially Loaded Pile.

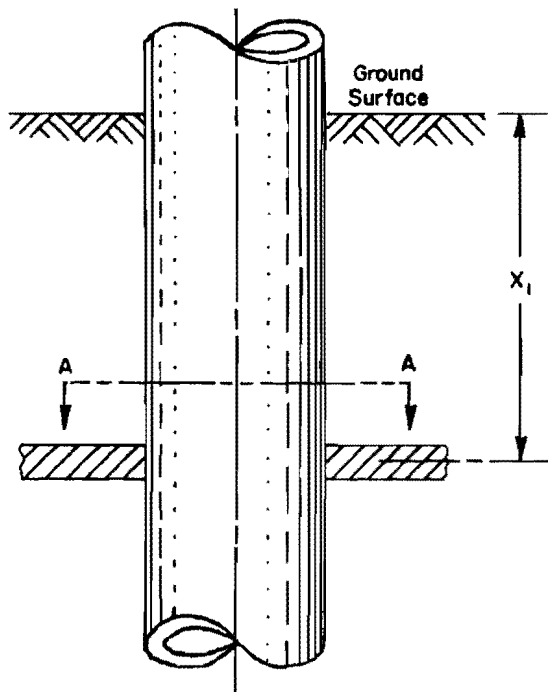
Fig. 2.4. If a load Q_T is applied to joint 1, the model will deform in such a way that conditions of equilibrium and compatibility are satisfied. The first step in the procedure is to assume a deflection of the pile base. From the nonlinear spring at joint $n+1$, the force SF_{n+1} may be found for the assumed deflection. The force Q_n may now be found by considering the equilibrium of joint $n+1$. With the force Q_n known, the deflection z_n may be obtained by considering the deformation in the linear spring between stations n and $n+1$. This is expressed mathematically as

$$z_n = z_{n+1} + \frac{Q_n h}{(AE)_n} \dots \dots \dots (2.14)$$

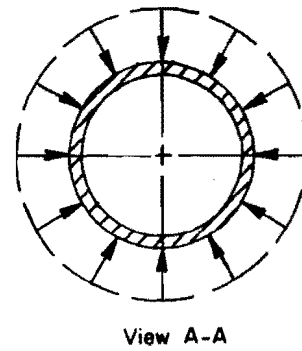
If z_n and Q_n are known, then Q_{n-1} may be found and the procedure repeated until the top of the pile is reached. This procedure will yield a top load Q_T and a top deflection z_1 . Additional values may be assumed for the base deflection and the procedure repeated until a complete load-deflection curve is obtained, for the top of the pile. A computer program for performing the necessary computations is presented by Awoshika and Reese (1971).

Mechanics of a Laterally Loaded Pile

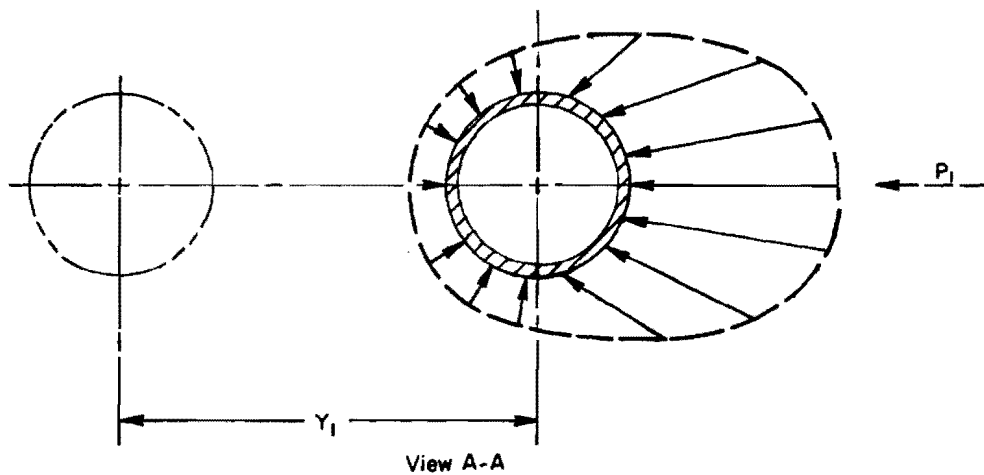
When a lateral load is applied to the top of a pile, the load is transferred to the soil surrounding the pile. This load transfer is illustrated in Fig. 2.6. A thin slice through the pile and surrounding soil is shown at a depth of x_1 below the ground surface. Before any lateral load is applied to the pile, the pressure distribution on the



a. Representation of pile segment



b. Pressure distribution before loading



c. Pressure distribution after loading

After Reese and Cox (1969)

Fig. 2.6. Illustration of Lateral Load Transfer.

pile will be similar to that shown in Fig. 2.6(b). For this condition the resultant force on the pile, obtained by integrating the pressure around the segment, will be zero. If, however, the pile is given a lateral deflection of y_1 at depth x_1 , the pressure distribution will be similar to that shown in Fig. 2.6(c). The integration of the pressure around the segment, for this condition, will yield a resultant force p_1 per unit length of pile, as shown in the figure. The same procedure may be applied for a series of deflections, resulting in a corresponding series of forces which may be combined into a p-y curve. In a similar manner, p-y curves for any depth may be defined, resulting in a set of curves as shown in Fig. 2.7.

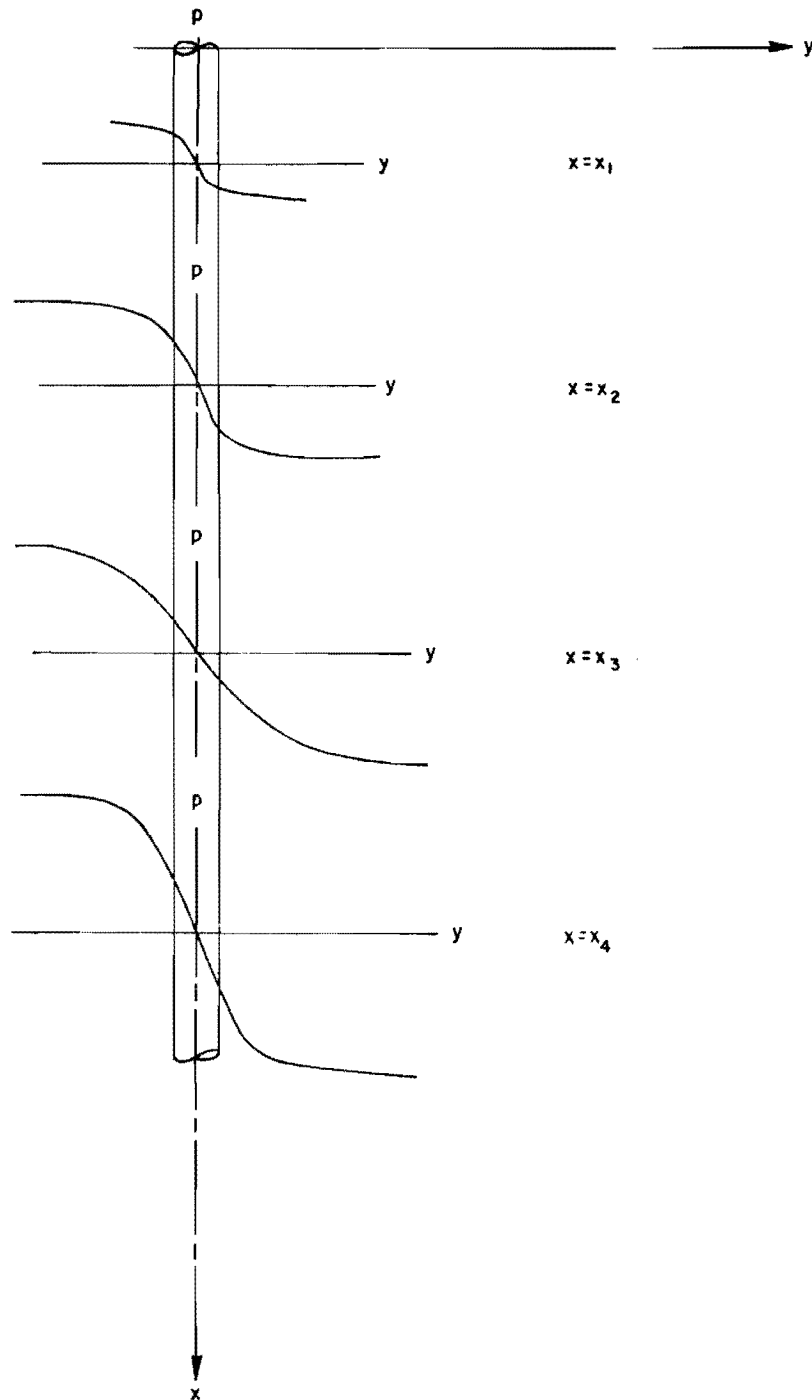
In order to use a set of p-y curves to obtain the behavior of a laterally loaded pile, a fourth-order differential equation must be solved. This is the basic equation for bending of a beam with a distributed load found in most texts on mechanics of material, and is written as

$$EI \frac{d^4 y}{dx^4} = q \dots \dots \dots (2.15)$$

where

- I = moment of inertia of the pile section
- q = distributed load applied to the pile
- y = lateral pile deflection.

The assumptions employed in the derivation of Eq. 2.15 will be considered later. For a laterally loaded pile, the distributed load q will be a



After Reese and Cox (1969)

Fig. 2.7. Family of p - y Curves.

reaction from the soil surrounding the pile. This problem was first considered by Winkler (1867). Winkler considered the soil as having linear properties, and defined a term referred to as the coefficient of soil reaction by the equation

$$k_s = -p/y \dots \dots \dots (2.16)$$

where

k_s = coefficient of soil reaction

p = soil resistance or force per unit length of pile.

Equation 2.15 may now be written as

$$EI \frac{d^4 y}{dx^4} = -k_s y \dots \dots \dots (2.17)$$

The concept of linear soil behavior has been further extended by Hetenyi (1946) and Terzaghi (1955). The extension of Eq. 2.17 to laterally loaded pile problems has been carried out by a number of investigators including Palmer and Thompson (1948), Gleser (1953), Mason and Bishop (1954), Focht and McClelland (1955), and Reese and Matlock (1960). One approach taken when the soil behavior is nonlinear is to rely on repeated applications of elastic theory where the constant coefficient of soil reaction is replaced by a secant modulus value. The secant modulus concept is illustrated in Fig. 2.8. The secant modulus of soil reaction is defined by the equation

$$E_s = -p/y \dots \dots \dots (2.18)$$

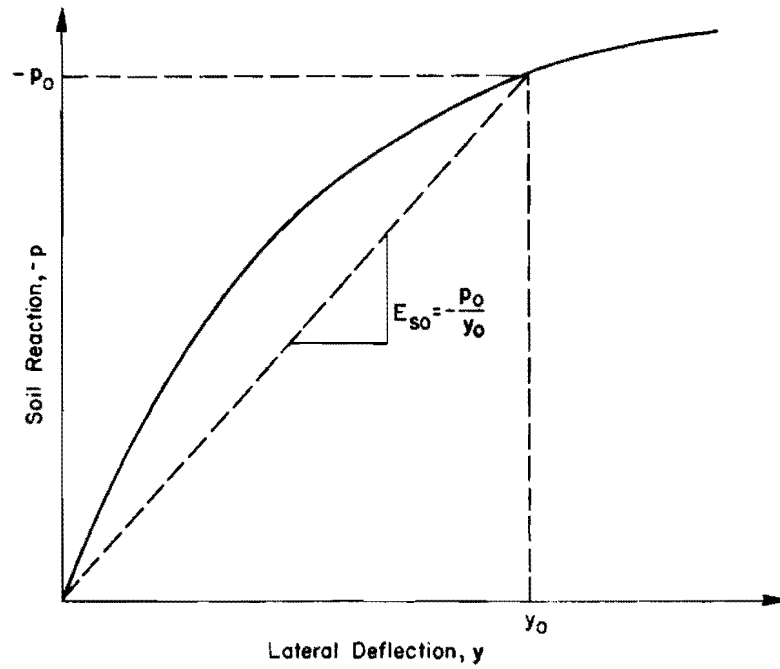


Fig. 2.8. Definition of Secant Modulus.

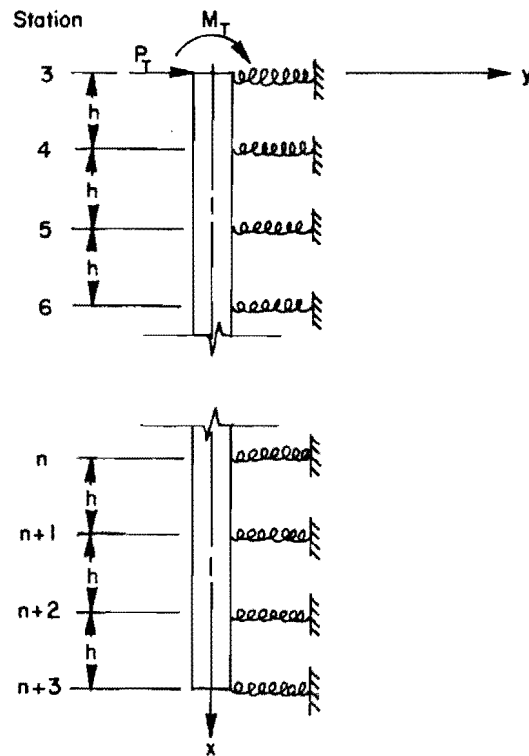


Fig. 2.9. Model of a Laterally Loaded Pile.

where

E_s = secant modulus of soil reaction.

With this definition of E_s , Eq. 2.17 may be rewritten as

$$EI \frac{d^4 y}{dx^4} = -E_s y \dots \dots \dots (2.19)$$

Equation 2.19 is the desired equation for a laterally loaded pile; but before considering a solution to this equation, the assumptions involved in the derivation up to this point will be enumerated.

The assumptions involved in the derivation of Eq. 2.15 are the assumptions made in conventional beam theory. A list of the assumptions, from Miller and Doeringsfeld (1965), is as follows:

1. The pile is straight when unloaded and has a uniform cross section.
2. The pile is in equilibrium.
3. The pile has a longitudinal plane of symmetry and the loads and reactions lie in that plane.
4. The material of the pile is homogeneous.
5. The proportional limit of the material is not exceeded.
6. The moduli of elasticity in tension and compression are equal.
7. Deformations are small.
8. A plane transverse section before bending remains plane after bending.
9. Deflections are small.

A principal assumption in the development of the family of p-y curves shown in Fig. 2.7 and in the derivation of Eq. 2.19 is that a unique curve exists at any depth. Stated in other words, the soil resistance at a point for a given lateral deflection at that point is assumed to be independent of the deflection at all other points.

The above assumption leads to the model of the pile shown in Fig. 2.9. In this model the springs act independently and, thus, satisfy the basic assumption. The load-deformation characteristics of the springs may be represented by a constant modulus of soil reaction or by a nonlinear p-y curve.

In the introduction to this chapter, it was stated that, from the standpoint of soil behavior, the lateral and axial interaction of a pile could be considered independently. However, the effect of an axial load on the lateral behavior of a pile can be considered without violating the assumption of independence of soil behavior. The modification of Eq. 2.19 to include an axial force results in the equation

$$EI \frac{d^4 y}{dx^4} + Q \frac{d^2 y}{dx^2} + E_s y = 0 \dots \dots \dots (2.20)$$

Equation 2.20 is the desired equation for a laterally loaded pile, considering the effect of an axial load. The solution procedures, discussed in the following paragraph, applies to Eqs. 2.19 and 2.20.

A solution to Eq. 2.19 or 2.20 for a laterally loaded pile, considering nonlinear soil behavior, requires an iterative procedure. The technique employed in this study is to consider the secant modulus of soil reaction as a constant and use a numerical technique for solving

the differential equation. The modulus values are then adjusted and the solution procedure repeated until the correct solution is found. The numerical procedure which is used involves the solution of a set of simultaneous equations derived from finite difference approximations.

The iterative procedure using finite difference equations has been used to obtain solutions to Eq. 2.19, by a number of investigators including Gleser (1953), Focht and McClelland (1955), and Reese and Matlock (1960). This same procedure has been applied to Eq. 2.20 by Parker and Cox (1969).

A discrete element approach to the solution of a beam, with nonlinear supports and a known distribution of axial force, has been employed by Matlock, Rachid, and Panak (in progress). Equations resulting from the discrete element technique are similar to those developed by the finite difference technique.

Both procedures yield a number of simultaneous equations. The exact form of the equations will depend on the solution technique employed and the boundary conditions applied. Because of the diversity and number of equations which result, a complete formulation of the numerical procedures will not be presented. As an example of the form of equations which result, the central-difference approximation to Eq. 2.20 for an arbitrary station i may be written as

$$\begin{aligned}
 & y_{i+2} (EI)_{i+1} + y_{i+1} \left[-2(EI)_{i+1} - 2(EI)_i + Q h^2 \right] \\
 & + y_i \left[(EI)_{i+1} + 4(EI)_i + (EI)_{i-1} - 2Q h^2 + E_{si} h^4 \right] \\
 & + y_{i-1} \left[-2(EI)_i - 2(EI)_{i-1} + Q h^2 \right] + y_{i-2} (EI)_{i-1} = 0 \dots (2.21)
 \end{aligned}$$

For this equation, the axial force in the pile is constant, the pile stiffness can vary, and the station numbering along the pile is as illustrated in Fig. 2.9. The soil resistance at each station is provided by the springs shown in Fig. 2.9. The set of simultaneous equations is formulated by writing an equation for each point along the pile in the form of Eq. 2.21, and by adding four equations for the boundary conditions. An initial estimate is made for the E_s values, and the equations solved for the deflections along the pile. The deflections are used to obtain values of soil resistance from the p-y curves. New values of E_s can now be computed. The procedure is then repeated until convergence is achieved. A computer program for performing the necessary computations is presented by Awoshika and Reese (1971).

This page replaces an intentionally blank page in the original.

-- CTR Library Digitization Team

CHAPTER III

TEST PROGRAM

In Chapter I some of the aspects of an eccentrically loaded pile foundation were considered. It was noted that certain structures, such as bridge bents, may exert significant horizontal as well as vertical forces on a foundation. These forces are transmitted to the piles, which then transfer them to the surrounding soil. It was also noted that if the load-deformation characteristics of the piles are known, the behavior of the foundation can be predicted. In Chapter II methods were presented for predicting the load-deformation behavior of the individual piles, and the nature of the soil response required for these methods was discussed.

The overall objective of the test program was the validation of a method of analysis of eccentrically loaded pile foundations, but the specific aspect considered in this study is an investigation of the load-deformation characteristics of the individual piles. The overall test program will be discussed briefly in the following section. In the remainder of the chapter, the portions of the test program considered in this study will be discussed in detail.

General Considerations

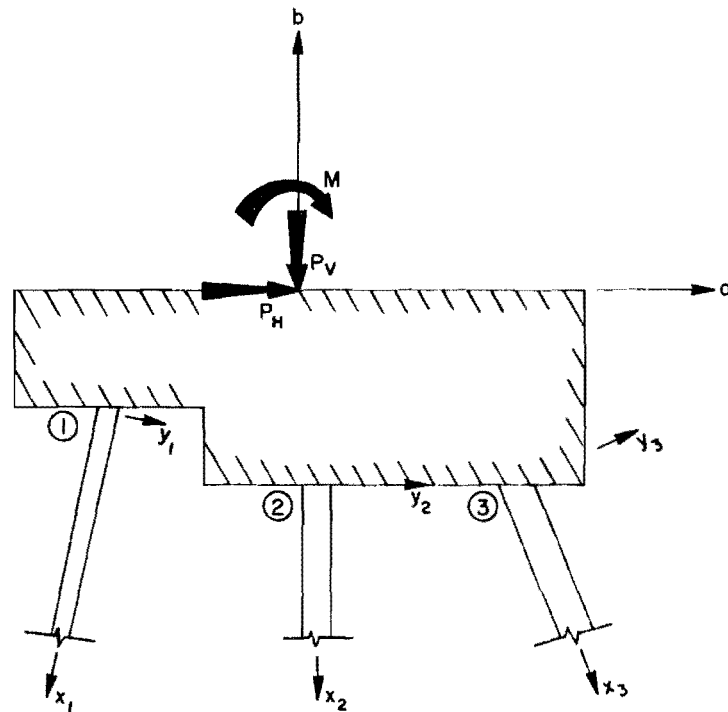
An outline of the method of analysis of eccentrically loaded foundations has been suggested by earlier investigators, Matlock and Reese (1961), and Reese and Matlock (1966). The method was proposed originally for use in analyzing off-shore structures, but it has been applied

successfully to pile foundations supporting bridge bents by Robertson (1961), Reese (1966), and Parker and Cox (1969).

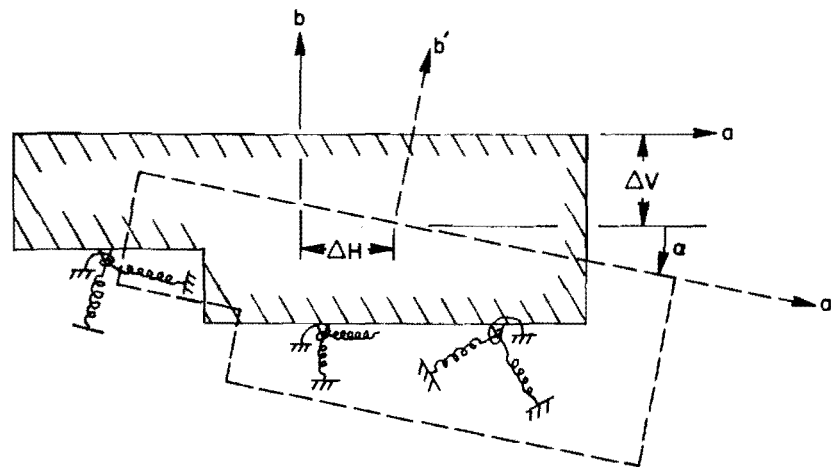
The basic scheme of the method is to represent the eccentrically loaded foundation, shown in Fig. 3.1(a), by the rigid block and spring model shown in Fig. 3.1(b). The springs in the model represent the piles and are nonlinear. The basic computational procedure requires iteration to find the deflected position of the foundation such that the applied loads and the forces exerted by the springs are in equilibrium, and that there is compatibility between the forces exerted by the springs and the movement of the springs. A number of example problems have been solved using this technique and solutions have been found which satisfy the conditions of equilibrium and compatibility. The accuracy of the solutions depend on the effect of the approximations made in the formulation of the procedure, and it was felt that a large-scale experiment would be helpful in checking the validity of the formulation.

In the test program designed, two pile foundations were tested. Each of the foundations consisted of a stiff pile cap supported by four piles. In addition, twelve individual piles were tested. The location of the piles and pile groups is illustrated in Fig. 3.2. Data from the tests of the individual piles were used in the analytical procedure to develop predictions of the behavior of the pile groups. These predictions were then compared to the experimental behavior of the pile groups.

While one aspect of the test program was the study of the pile foundations, another aspect concerned the behavior of the individual piles. As previously discussed, the analysis of a pile foundation can only be carried out if the behavior of the single piles can be predicted.

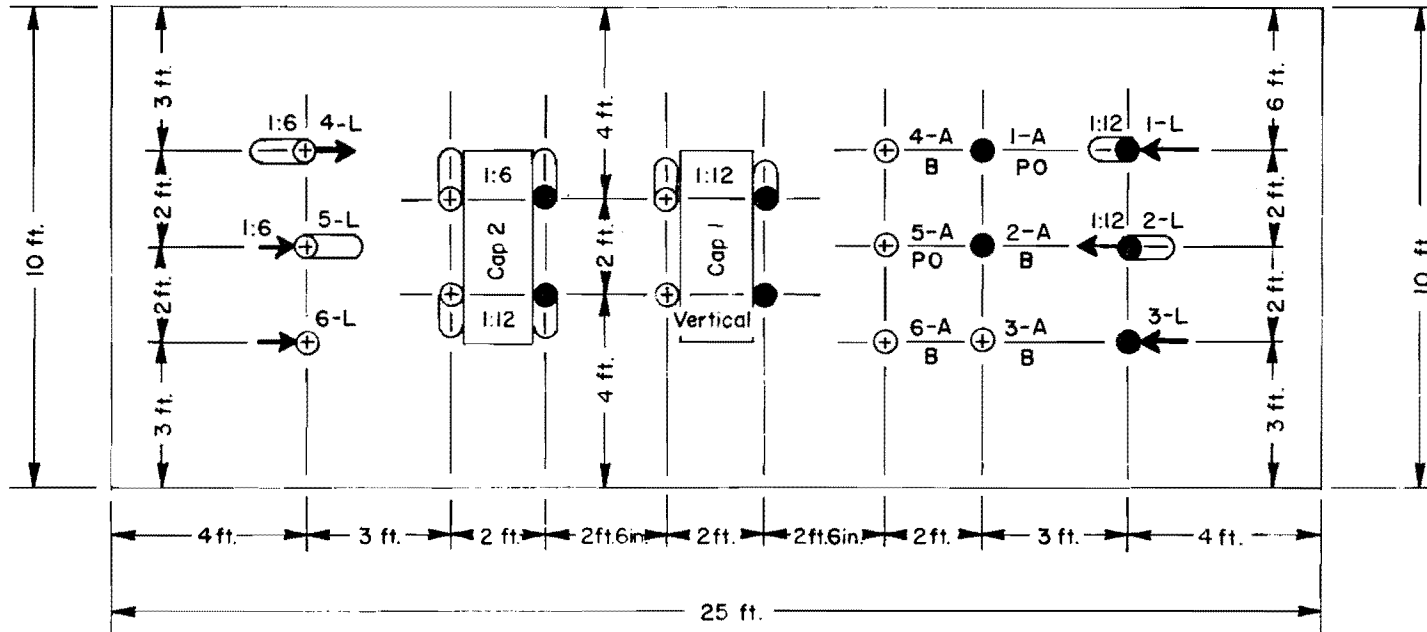


a. Loading and geometry of foundation



b. Model for foundation and movement

Fig. 3.1. Representation of a Pile Supported Foundation.



Note: Batter and Direction of Load on Laterally Loaded Piles Illustrated.

- - Instrumented Pile
- ⊕ - Noninstrumented Pile
- L - Laterally Loaded Pile
- A - Axially Loaded Pile
- PO - Pullout
- B - Bearing

Fig. 3.2. Plan View of Layout of Piles and Pile Groups.

Also, single piles are frequently used in construction practice and methods for their analysis are needed. Thus, the results from the tests of the individual piles may be thought of as having a two-fold objective. These objectives may be stated as follows:

1. To develop experimental data on the behavior of the individual piles for use in the analytical method for predicting the group behavior.
2. To develop criteria for predicting pile-soil interaction curves for single piles in sand from sand properties.

In this report, the specific portion of the test program considered is the analysis of the test of the individual piles. The test conditions and scope of the tests of the individual piles will be presented in the next section. In the final section, the design of the model piles will be discussed.

Selection of Test Conditions

The complexity of a pile-soil interaction problem precludes conducting a test program to study all factors which might have a bearing on the problem. For this reason, the scope of the study must be limited to consideration of the most important parameters. A critical consideration is the size of the piles to be used in the tests, because the cost of the tests increases as the size of the piles increases. From the standpoint of cost, the small-scale test would be the most desirable. However, a number of studies using very small "pencil-piles" have been run, but the applicability of the results is debatable, because of the

unclarified scale effects. From a standpoint of correlation with real problems, the "full-scale" test would be the most desirable. However, the cost of a test employing large piles may be prohibitive.

Consideration of these factors lead to the choice of two-inch diameter pipe piles. This size was small enough so that the cost of facilities and equipment needed for the installation and testing was not prohibitive, and large enough so that most of the arguments against very small models would not apply.

Another factor considered was the soil conditions. There are differences in the load transfer of piles in sand, clay, silt, or any combination of these three, and it would be desirable to run tests for a wide range of soil conditions. However, cost and time limit the amount of testing that can be performed. For this study, a prepared sand was selected for several reasons. From the standpoint of checking the procedure for analyzing pile foundations, the ability to accurately predict the response of the individual piles is of primary importance. An artificially prepared sand can be placed and maintained in a uniform condition with relative ease, so that the response of the individual piles should be reasonably consistent. From the standpoint of developing soil criteria, a sand was desirable because of the scarcity in the literature concerning the behavior of sand around laterally and axially loaded piles.

A detailed discussion of the properties of the sand used is presented in Chapter IV.

Several other factors that were considered were the method of installation of the piles and the type of loading to be applied. The

method of installation which was used was to place the sand around the pile. During the installation process, support was provided at the top and at points approximately 3.5 feet above the tip. Sand was placed until the surface was about six inches from the bottom supports. The bottom supports were then removed and the filling continued. This method was employed, rather than driving or jacking, for several reasons. One reason was to avoid damage to the instrumentation located on the piles. Another reason was that this procedure permitted accurate alignment of the piles.

Only static loads were applied. No cyclic, dynamic, or long term effects were considered. The loading was accomplished by applying a load, axial or lateral, and allowing the deflection to stabilize before applying another load.

All of the factors considered in the selection of pile size, soil conditions, method of installation, and loading will influence the results obtained. These factors limit the scope of the study and should be considered before applying the results to other conditions.

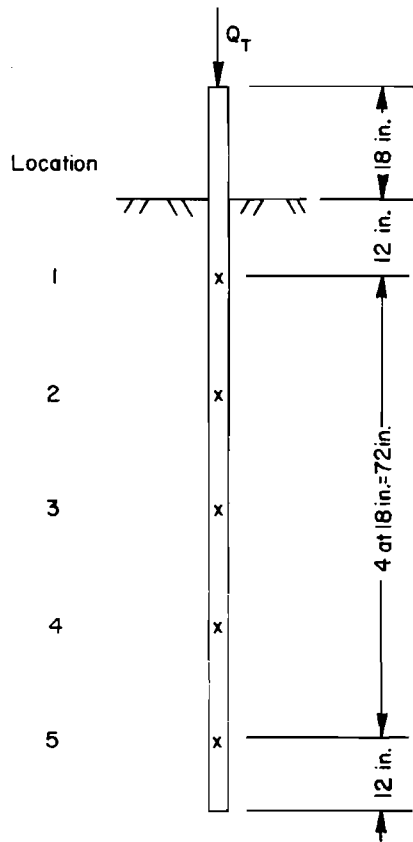
Design of the Piles

Six piles were loaded axially, and are designated 1-A through 6-A in Fig. 3.2. The embedded length of these piles was 96 inches. From these tests the average load-deformation response of the pile top was obtained for use in the prediction of the group behavior. All of the piles tested were vertical, but the measured response was also used for the batter piles in the analysis of the pile groups.

Two of the six piles which were tested, one in bearing and one in pullout, were instrumented with electrical resistance strain gages. These gages were utilized to measure the distribution of axial load in the pile. From the measured load distributions, the axial load transfer, in the form of s_x -z curves, was obtained. The location of the gages along the pile is shown in Fig. 3.3(a). At each location on the pile, two gages were located diametrically opposite each other. The two gages at a location permitted the measurement of the axial force in the pile while eliminating the effect of any bending moment. Instrumentation and calibration techniques are discussed in Appendices B and C. The analysis of the results of the axial tests are presented in Chapter V.

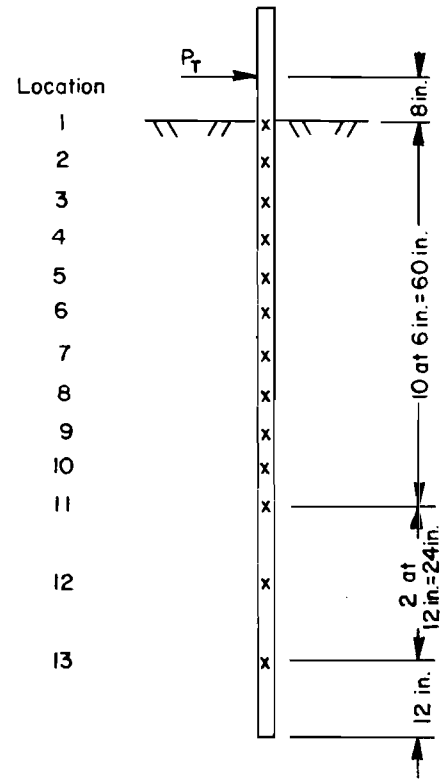
Six piles were loaded laterally, and are designated 1-L through 6-L in Fig. 3.2. The embedded length of these piles was 96 inches. In Fig. 3.2 the direction of the applied horizontal load and the batter of the piles are illustrated. Piles 3-L and 6-L are vertical. Piles 1-L and 5-L are designated as "out-battered" piles, and the direction of loading results in a force perpendicular to the pile axis, and a small compressive force parallel to the pile axis. Piles 2-L and 4-L are designated as "in-battered" piles, and the direction of loading results in a force perpendicular to the pile axis, and a small tensile force parallel to the pile axis. These various combinations of loading and batter were designed to give some indication of the effect of the pile batter on the lateral behavior.

Three of the six piles tested, one vertical, one out-battered, and one in-battered, were instrumented with electrical resistance strain gages. These gages were used to measure the distribution of bending



a. Axially loaded piles.

Notes:
 Two gages per location
 located diametrically
 opposite on the 2-inch
 diameter pipe pile.
 Axial load or bending
 moment may be measured,
 depending on the loca-
 tion of the gages in a
 Wheatstone Bridge.



b. Laterally loaded piles

Fig. 3.3. Strain Gage Placement Along the Piles.

moment in the piles. Lateral interaction curves were computed by integrating and differentiating the measured moment distributions. The layout of the gages along the pile is shown in Fig. 3.3(b). At each location on the pile, two gages were located diametrically opposite each other. The two gages at each location permitted the measurement of the bending moment in the pile while eliminating the effect of any axial load. Instrumentation and calibration techniques are discussed in Appendices B and C, and the analysis of the results from the lateral tests are presented in Chapter VI.

CHAPTER IV
PROPERTIES OF SAND

The two principal reasons for using sand in the test program were the relative ease with which sand can be placed and the maintenance of uniform conditions during and after the test. In this chapter the properties of the sand are discussed. In the first section, the basic properties of the sand are presented. The density of the compacted sand is discussed in the second section; and in the final section, the strength and stress-strain characteristics of the sand will be presented. The methods employed in placing the sand and measuring the density are presented in Appendix E.

Basic Properties of the Sand

The sand used was taken from a pit located near Austin, Texas, on the property of Capitol Aggregates, Inc. The pit was situated approximately 300 feet from the Colorado River, and the sand in its natural state was in a very loose condition ($\gamma_D \approx 90$ pcf). Because of its location and natural density, the sand was probably transported and deposited by the river.

The grain size distribution illustrated in Fig. 4.1 indicates a uniform fine sand. The band shown is the range obtained from the sieve analyses on six different samples. Microscopic examination indicated that the sand was composed mostly of subangular quartz particles, but

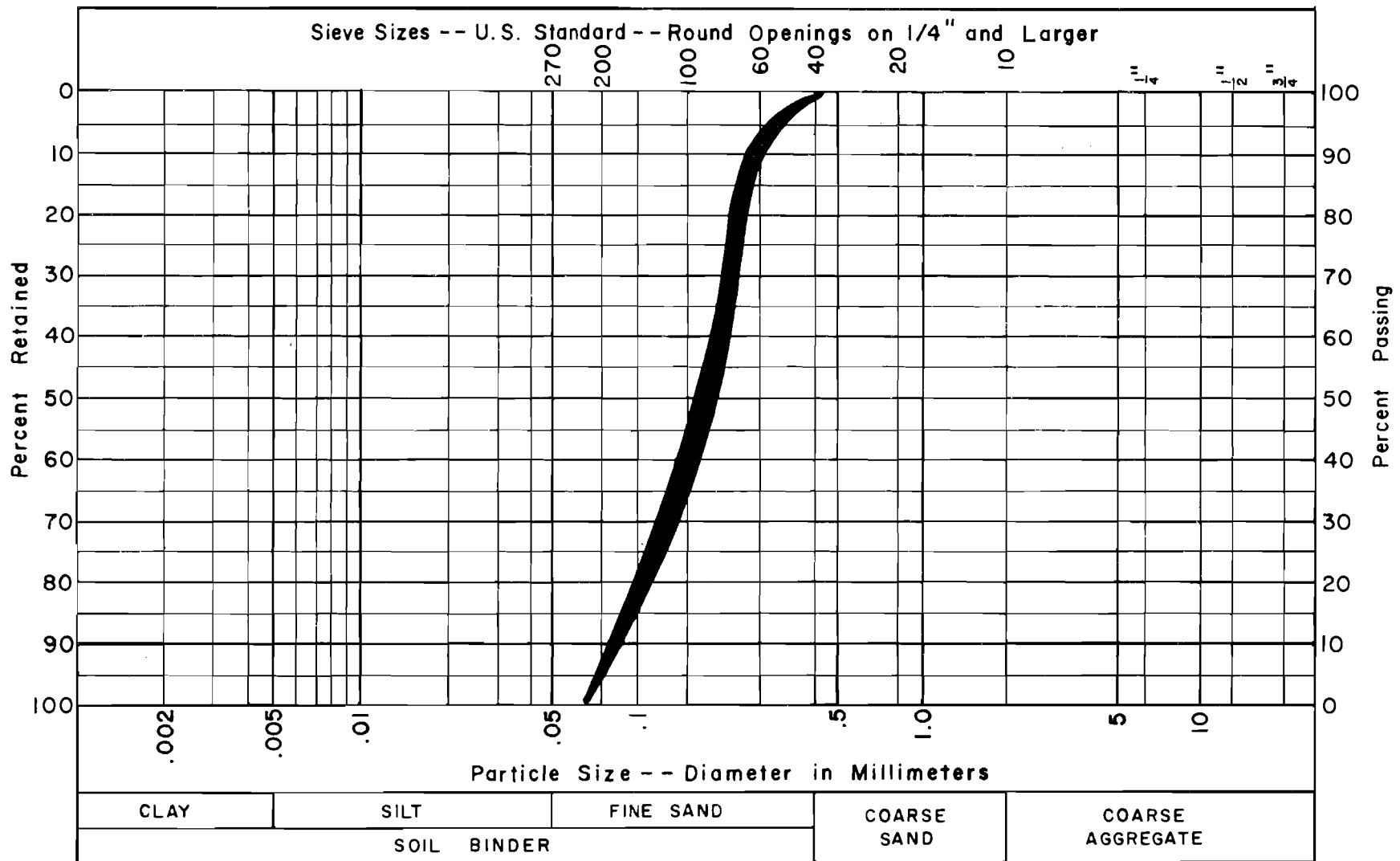


Fig. 4.1. Grain Size Distribution Curve.

with a few feldspar particles. The specific gravity of the particles was found to be approximately 2.68.

The maximum and minimum dry densities obtained in the laboratory were 102.3 pcf and 82.4 pcf. These values were the maximum and minimum values obtained from several techniques that were tried. The techniques employed were basically those suggested by Burmister and Yemington in ASTM Procedures for Testing Soils (1964). The maximum dry density was obtained by vibrating air-dried sand in a Standard Procter mold. Air-dried sand was placed in the mold in three layers. A surcharge of approximately 1.5 psi was placed on the surface, and each layer vibrated for approximately 7 minutes. The minimum dry density was obtained by pouring air-dried sand into a 1000-milliliter graduated cylinder through a 1 1/4-inch diameter tube with a perforated bottom. The values of maximum and minimum dry density were used in the computation of the relative density of the compacted sand.

Density of the Compacted Sand

Results from the density measurements taken during the placing and removal of the sand are summarized in Table 4.1. In the tabulation, the methods used for making the measurements are noted. The histogram in Fig. 4.2 illustrates the distribution of the measured values of dry density. The arithmetic mean for the distribution is 100.2 pcf, the median is 100.0 pcf, and the standard deviation is 2.2 pcf. The distribution indicates that the deposit was fairly uniform, and that an assumed value of dry density of 100 pcf would be sufficiently accurate for analysis of

TABLE 4.1. MEASURED DRY DENSITY OF SAND

Depth (Inches)	Dry Density, in pcf, Measured During Placement of Sand		Dry Density, in pcf, Measured During Removal of Sand	
	Push Tube	Push Tube	In Place Boxes	Volumeter
0	101.2**	100.1***	-	-
8	97.9***	-	-	-
16	99.7****	99.8*	101.5*	-
24	99.5****	97.8***	-	-
32	101.2***	-	-	-
40	-	-	103.2*	-
48	98.9***	101.1***	98.5*	98.7***
56	-	-	98.2*	-
64	-	-	100.4**	-
72	-	100.5***	101.2*	100.7***
80	97.8**	-	99.0*	-
88	100.5***	-	-	-
96	100.8***	101.8***	101.1*	101.9***
104	99.3***	-	-	-
112	100.5*	-	-	-
120	-	-	102.3***	-

*One measurement

**Average of two measurements

***Average of three measurements

****Average of four measurements

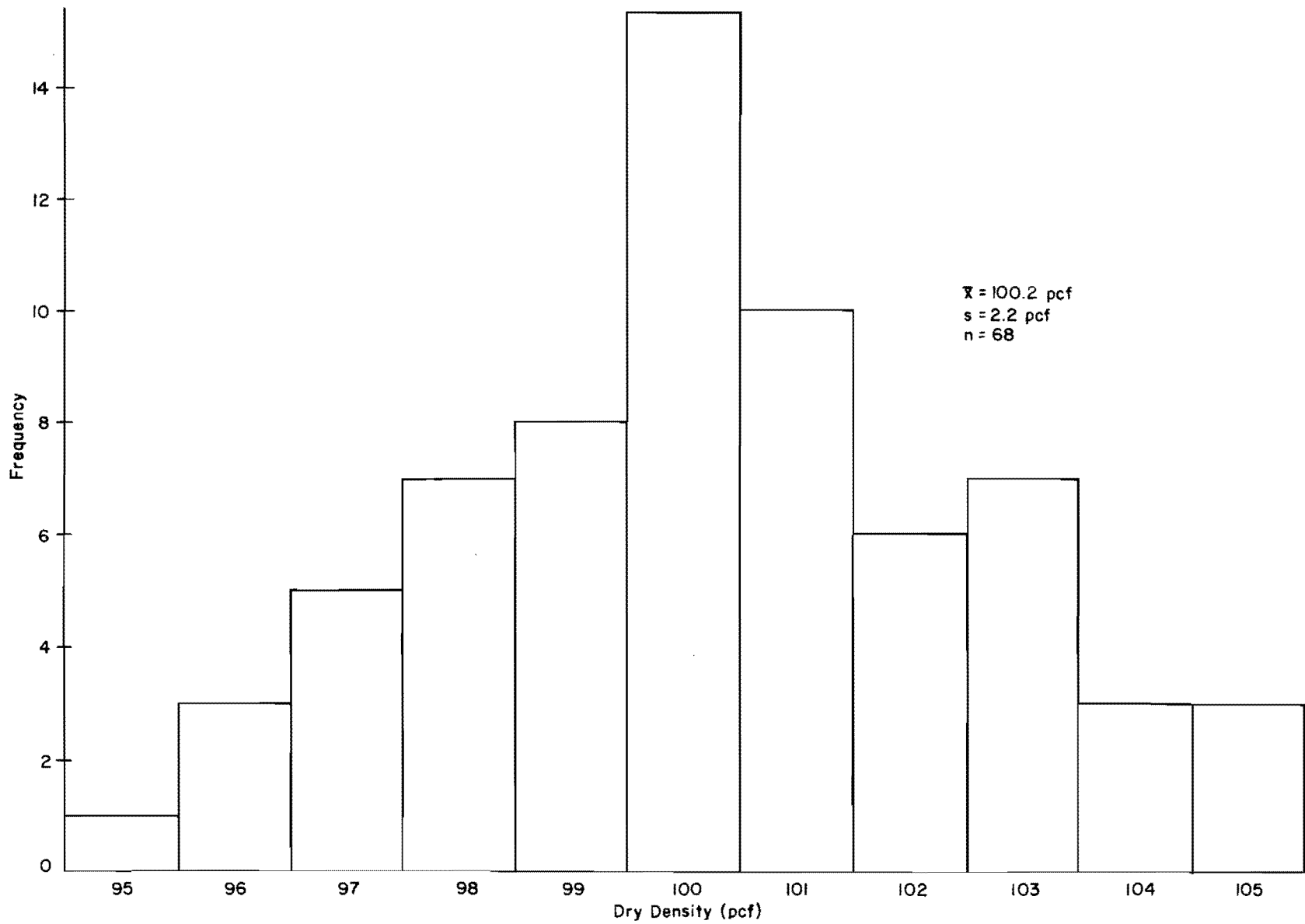


Fig. 4.2. Histogram of Measured Dry Densities.

test results. Based on the maximum and minimum measured values of dry density, a density of 100 pcf corresponds to a relative density of about 95 per cent. An assumed value of 100 pcf seems to be justified even if all of the deviation were attributed to an actual variation in density, with no consideration given to the inaccuracies in the measuring techniques. However, the distribution about the median is probably due to a combination of actual variation and errors in the measuring techniques.

The combined analysis of the density checks made during placement and removal give no indication of any change which might have occurred after placement or any variation of density with depth. An indication of a small change in density after placement was noted in comparing the means for the distributions obtained during placement and during removal. During the placing, thirty-one push-tube samples were taken and a mean value of 100.0 pcf obtained. A total of thirty-seven samples, with the methods described previously, were taken during the sand removal and a mean value of 100.4 pcf obtained. The median in both cases was 100.0 pcf but the larger mean value obtained during removal indicates that there may have been some increase in density after placement. As to any variation with depth, the dry densities obtained during removal are shown plotted with depth in Fig. 4.3. There is considerable scatter in the data, but no appreciable increase in density with depth is noted.

Measurement of Strength and Stress-Strain Characteristics of Sand

The angle of internal friction and stress-strain characteristics were the properties of the compacted sand used in the correlation with

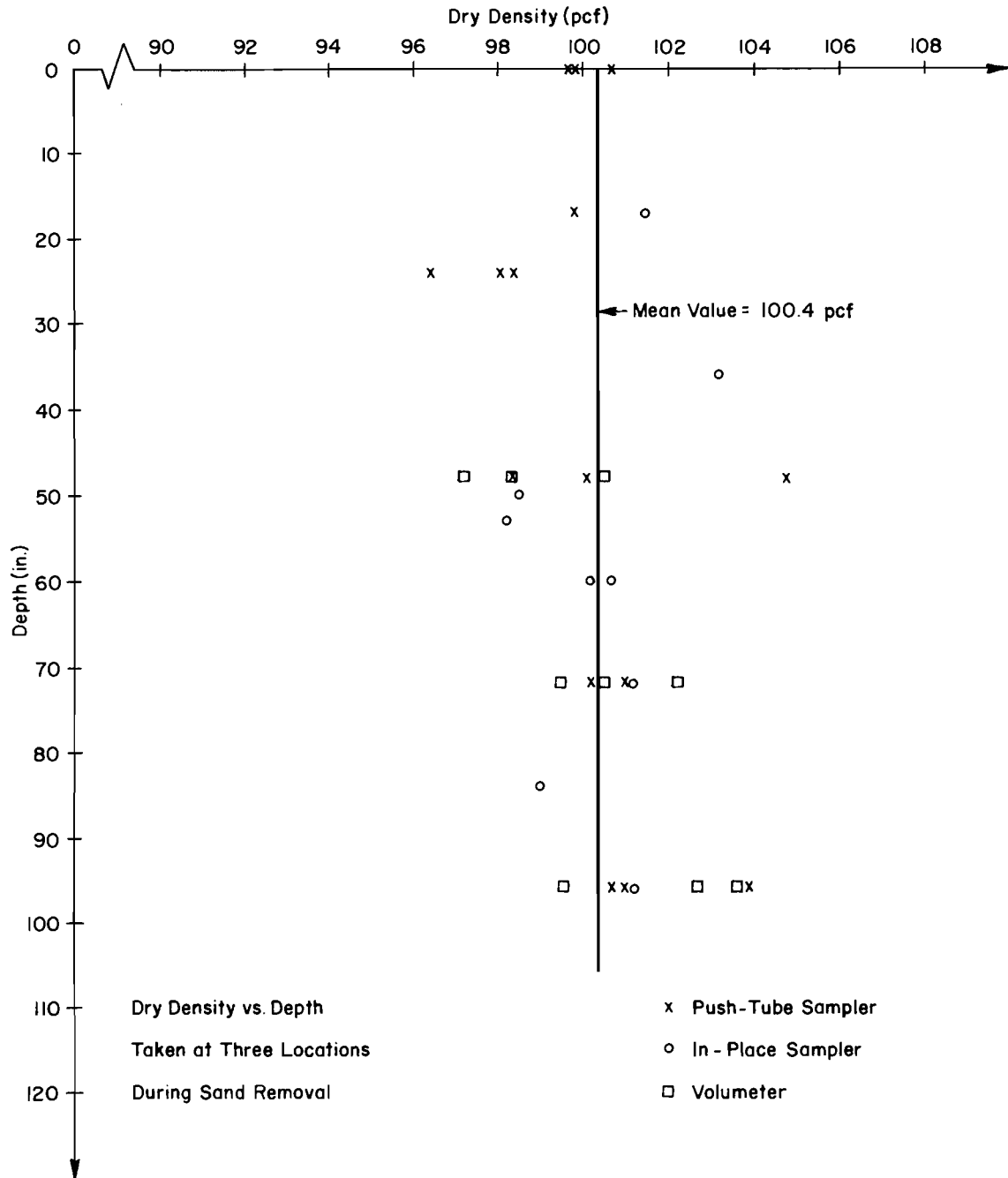


Fig. 4.3. Distribution of Dry Density with Depth Measured During Sand Removal.

results from the pile tests. To insure that the values used were representative of the in situ properties, a number of direct shear and triaxial tests were run on specimens prepared in the laboratory and on undisturbed specimens.

Determination of Angle of Internal Friction

Direct shear tests were run on specimens prepared from air-dried sand. Seven tests were run on specimens that were prepared and sheared in the dry state, and four tests were performed on specimens prepared from air-dried sand but saturated prior to shearing. For test conditions the sand was submerged, but Lambe (1967) states that the angle of internal friction for saturated and air-dried conditions are nearly identical. The tests confirm that there is no measurable difference between values of the angle of internal friction from the air-dried and saturated specimens. Results from the tests are summarized in Table 4.2.

Values of angle of internal friction obtained are plotted versus dry density in Fig. 4.4. From this plot, no apparent difference between values from air-dried or submerged specimens is indicated. The dashed lines bound the values obtained, and indicate an approximately linear relationship between friction angle and dry density. If the dashed lines accurately bound the true relationship between friction angle and dry density, then a value of friction angle of 40 degrees would be reasonable for a density of 100 pcf, based on results from direct shear tests.

Triaxial tests were run on specimens prepared from air-dried sand and on undisturbed specimens. The prepared specimens were compacted with a vibrator and sheared in the air-dried state. No special equipment

TABLE 4.2. DATA FOR DIRECT SHEAR TESTS

Test No.	Dry Density (pcf)	Normal Pressure (psi)	Friction Angle (degrees)	Sample Preparation and Test Conditions
1	102	9.0	41	Vibrated, Air-Dried
2	102	13.5	43	Vibrated, Air-Dried
3	103	18.0	41	Vibrated, Air-Dried
4	100	9.0	41	Vibrated, Submerged
5	96	13.5	36	Vibrated, Submerged
6	102	13.5	41	Vibrated, Submerged
7	102	18.0	42	Vibrated, Submerged
8	86	13.5	30	Poured, Air-Dried
9	86	18.0	27	Poured, Air-Dried
10	85	9.0	31	Poured, Air-Dried
11	91	9.0	35	Poured, Air-Dried

Rate of Shear \approx 0.025 in./min.

Sample Size: Width = 6 centimeters
 Length = 6 centimeters
 Depth = 3.75 centimeters

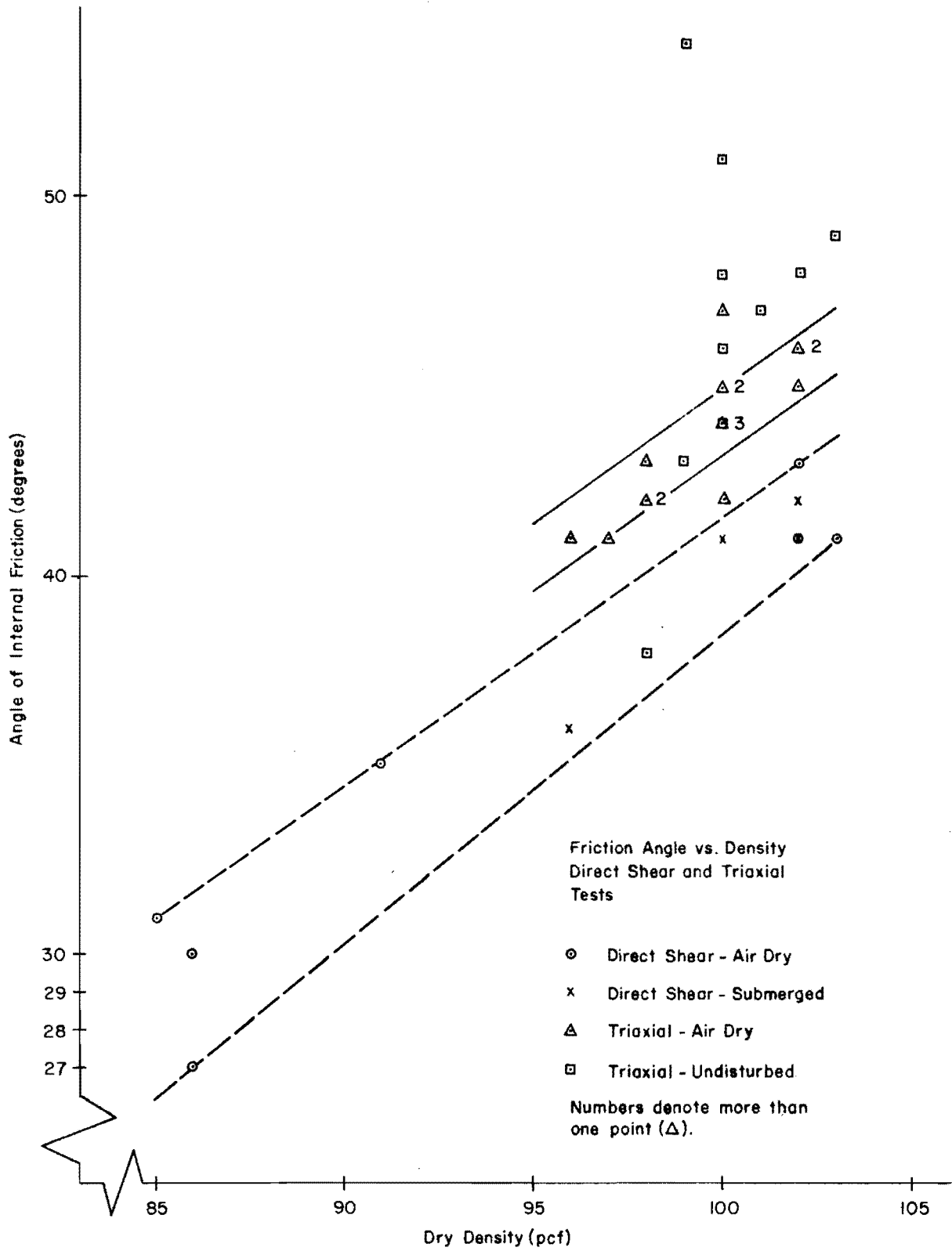


Fig. 4.4. Variation of Friction Angle with Dry Density.

or procedures were necessary for these tests. Results from tests of air-dried specimens are summarized in Table 4.3.

The procedure for testing the undisturbed samples was more involved than for the prepared specimens. Since the soil used was a sand, the testing of undisturbed samples required special handling techniques. It was possible to obtain and test undisturbed samples, because of the apparent cohesion which exists when the sand is partially saturated. Because of the small size of the sand particles, the magnitude of the apparent cohesion was sufficient to hold a sample together for sampling.

Chunk samples were taken during the removal of the sand. The sand was removed in layers, and before a layer was removed the water level was lowered. This created a partially saturated condition in the layer, approximately 85 per cent degree of saturation, so that a chunk sample could be trimmed and removed.

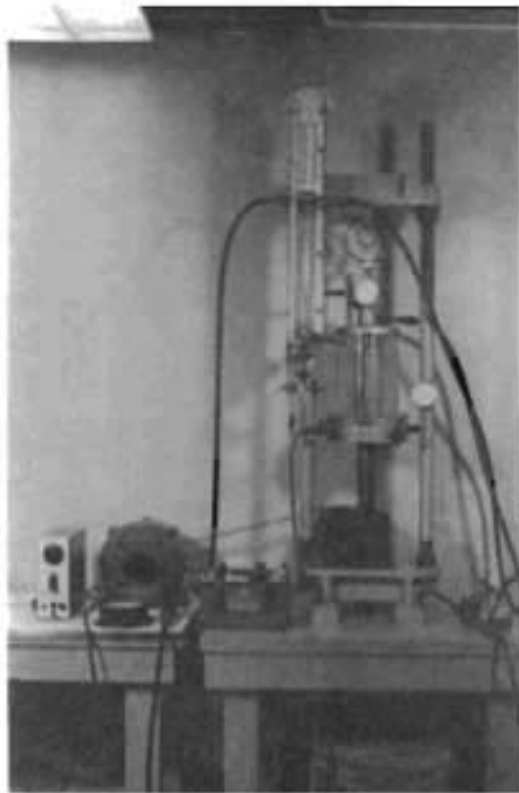
The sampling technique used was to trim around a chunk of sand that would fit into a plastic container 6 inches in diameter and 10 inches deep. The container was placed over the sample, and the sample cut free and trimmed. The top of the sample was covered with paraffin and the voids between the sides of the container filled with paraffin. The samples were then brought to the laboratory and stored in a moisture chamber until tested.

Specimens for triaxial tests were trimmed from the chunk samples, and an attempt was made to saturate them before testing. The apparatus for saturating and shearing the specimens is pictured in Fig. 4.5. This apparatus allows saturation by percolation or by applying back pressure, and also can maintain a specified back pressure during drained shear.

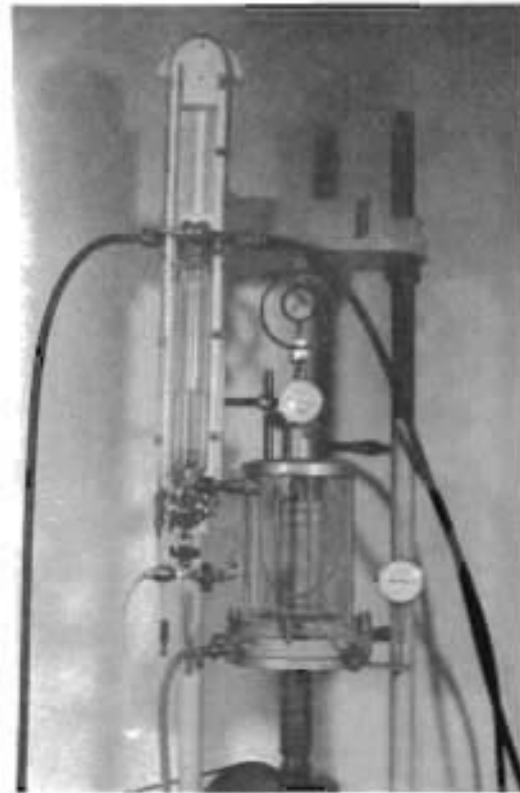
TABLE 4.3. DATA FOR TRIAXIAL TESTS ON AIR-DRIED SPECIMENS

Test No.	Dry Density (pcf)	Confining Pressure (psi)	Friction Angle (degrees)	Shear Rate (% strain/min.)
1	98	10	42	0.75
2	98	12	43	0.50
3	98	8	42	0.50
4	102	10	46	0.50
5	102	12	46	0.50
6	102	20	45	0.50
7	100	10	44	0.50
8	100	12	44	0.50
9	100	20	44	0.50
10	97	10	41	0.50
11	96	10	41	0.50
12	100	2	45	0.25
13	100	2	45	0.25
14	100	4	47	0.25
15	100	6	42	0.25

Sample Size: Diameter = 2.8 inches
 Height = 5.75 inches



a. Overall test set up



b. Closeup of triaxial cell and pressure measuring device

Fig. 4.5. Triaxial Apparatus for Testing Undisturbed Specimens.

Several procedures involving various combinations of percolation and back pressure application were tried in an attempt to saturate completely the specimens. No combination was found which would insure 100 per cent saturation, as indicated by the measurement of the pore pressure parameter B defined by Skempton (1954). The largest value of B which was obtained was 0.45, but because the sand had a relative density of 95 per cent this may correspond to a fairly high degree of saturation. Because of the difficulty in obtaining 100 per cent saturation, and because the degree of saturation of the sand for pile test conditions was probably not 100 per cent, the procedure described below was selected. This procedure produces values of B near 0.45.

The procedure used was to apply a vacuum of 10 inches of mercury to the top of the specimen, admit water at atmospheric pressure at the bottom, and allow drainage for 30 minutes. The vacuum was then removed and confining pressures of varying magnitudes and a back pressure of 2 psi was applied and the specimen was allowed to drain for 30 minutes. The magnitude of the initial confining pressure was such that the effective confining pressure was of the desired magnitude. The confining pressure and back pressure were increased in increments of 2 psi and the specimen was allowed to drain for 30 minutes after the application of each increment. This procedure was repeated until the back pressure equaled 10 psi. With the final values of confining and back pressures applied, drainage was permitted for 60 minutes. The drainage line was then closed and all pressure maintained for 60 minutes prior to shearing.

The specimens were then sheared while maintaining the final confining and back pressures. Data for these tests are summarized in Table 4.4.

Values of angle of internal friction obtained from both types of specimens are plotted versus dry density in Fig. 4.4. From this plot, it is apparent that the triaxial test gives higher values of angle of internal friction than do the direct shear tests. For the air-dried specimen there also appears to be less scatter in the points, and the solid lines that bound the values obtained from the air-dried specimens indicate an approximately linear relationship between dry density and angle of internal friction. Points from tests of undisturbed specimens show considerable scatter, and the majority of the values are higher than for the prepared specimens. The scatter and larger values may possibly be explained by the incomplete saturation of the specimens, or sample disturbance during preparation and saturation. Another possible explanation may be that some cementation between the particles had occurred with time, as suggested by Denisov, Dudlers, Durante, and Khazanov (1963) and Kerisel (1964). Because of the uncertainty as to the reason for the larger values and greater scatter in the tests of the undisturbed specimens, a value of friction angle of 44 degrees was selected as reasonable for a density of 100 pcf. This value is based on the values obtained from the triaxial tests of the prepared specimens and was used throughout the analysis of the test results.

Determination of Stress-Strain Curves

The stress-strain relationship of interest for this study were the stress-strain curves obtained from the triaxial tests. Stress-strain

TABLE 4.4. DATA FOR TRIAXIAL TESTS ON SATURATED UNDISTURBED SPECIMENS

Test No.	Dry Density (pcf)	Confining Pressure (psi)	Pore Pressure (psi)	Friction Angle (degrees)	Comments
101	100	30.5	26.5	46	
102	101	10.0	0.0	47	Poor Saturation
103	99	4.0	2.0	54	Sheared too fast
104	102	14.0	10.0	48	
105	100	16.0	10.0	48	Poor Saturation
106	100	16.0	10.0	44	
107	98	11.0	10.0	38	
108	99	12.0	10.0	43	
109	100	12.75	10.0	51	
110	103	13.5	10.0	49	

Rate of Shear \approx 0.25% strain/min.

Sample Size: Diameter = 2.8 inches
 Height = 5.25 inches

curves for some of the tests on the prepared specimens are shown by the solid lines in Fig. 4.6. The effective confining pressure and test number for each curve is noted. Stress-strain curves for some of the tests on undisturbed specimens are shown by the solid lines in Fig. 4.7. Effective confining pressures and test numbers for each curve are indicated. In both of these figures, the characteristic increase in stiffness with increase in confining pressure is noted. The irregular patterns of the measured family of stress-strain curves are illustrated in Fig. 4.6 and 4.7. Theoretically the family of curves for various confining pressures should be uniform, but the irregularities are caused by experimental errors. The curves for the undisturbed specimens are more erratic than those for the prepared specimens. The greater scatter for the undisturbed specimens may possibly have been caused by several factors mentioned previously; such as poor saturation, sample disturbance, or cementation.

Also shown in Figs. 4.6 and 4.7 are a series of hyperbolas which have been fitted to experimental curves for the stress-strain behavior of the sand. The hyperbolas are shown as the dashed lines, and the corresponding confining pressure is noted. The procedure used to generate these curves utilizes properties of the measured curves, and was suggested by Kondner and Zelasko (1963). One reason for developing analytical curves was to smooth the measured curves and to try to minimize the effect of experimental errors. Another reason was that, in the analysis of the test results, curves are needed for a number of confining pressures. With an equation a curve may be generated for any confining pressure. The analytical fitting procedure is especially useful for low confining

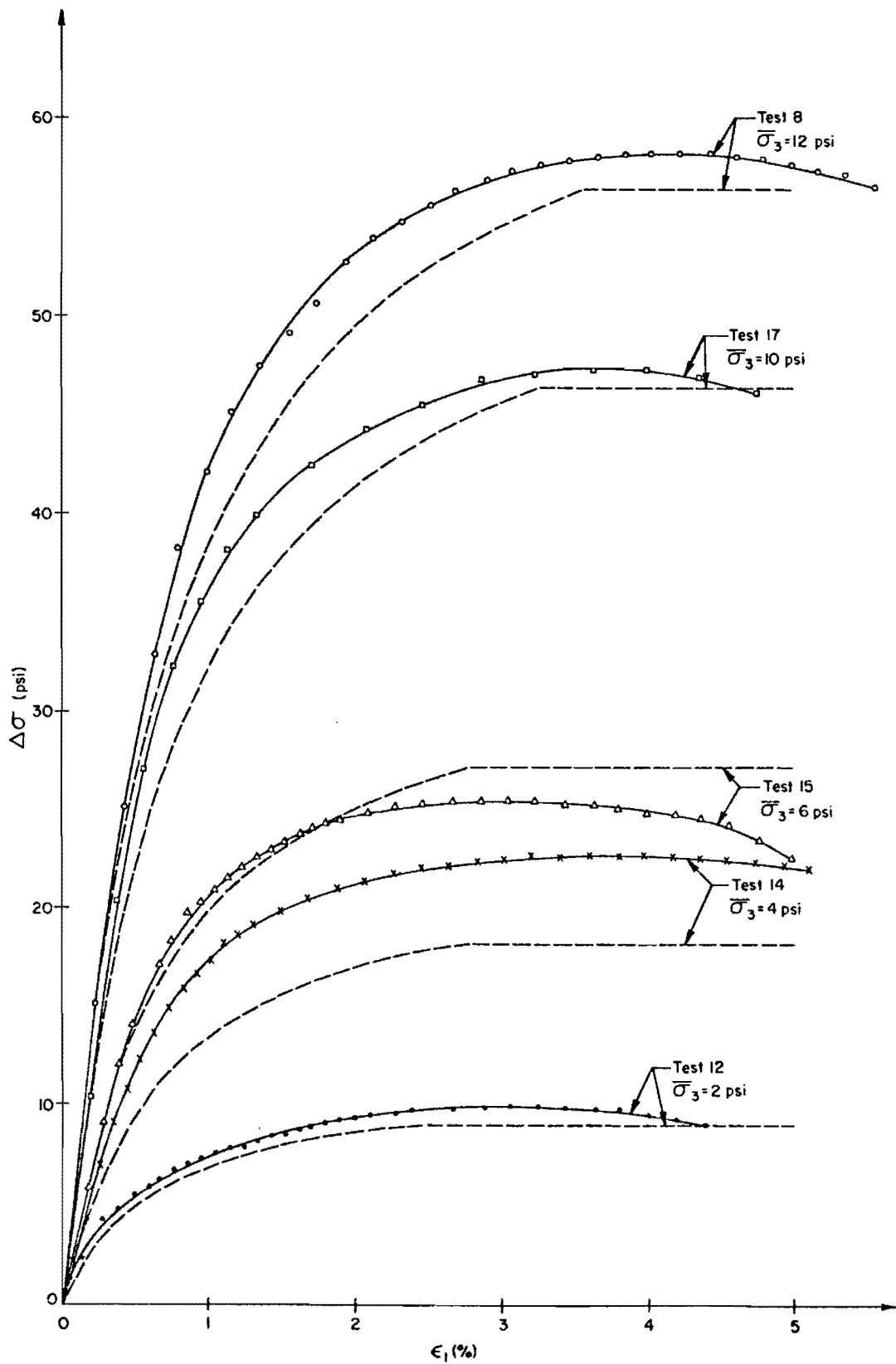


Fig. 4.6. Measured and Predicted Stress-Strain Curves for Prepared Samples.

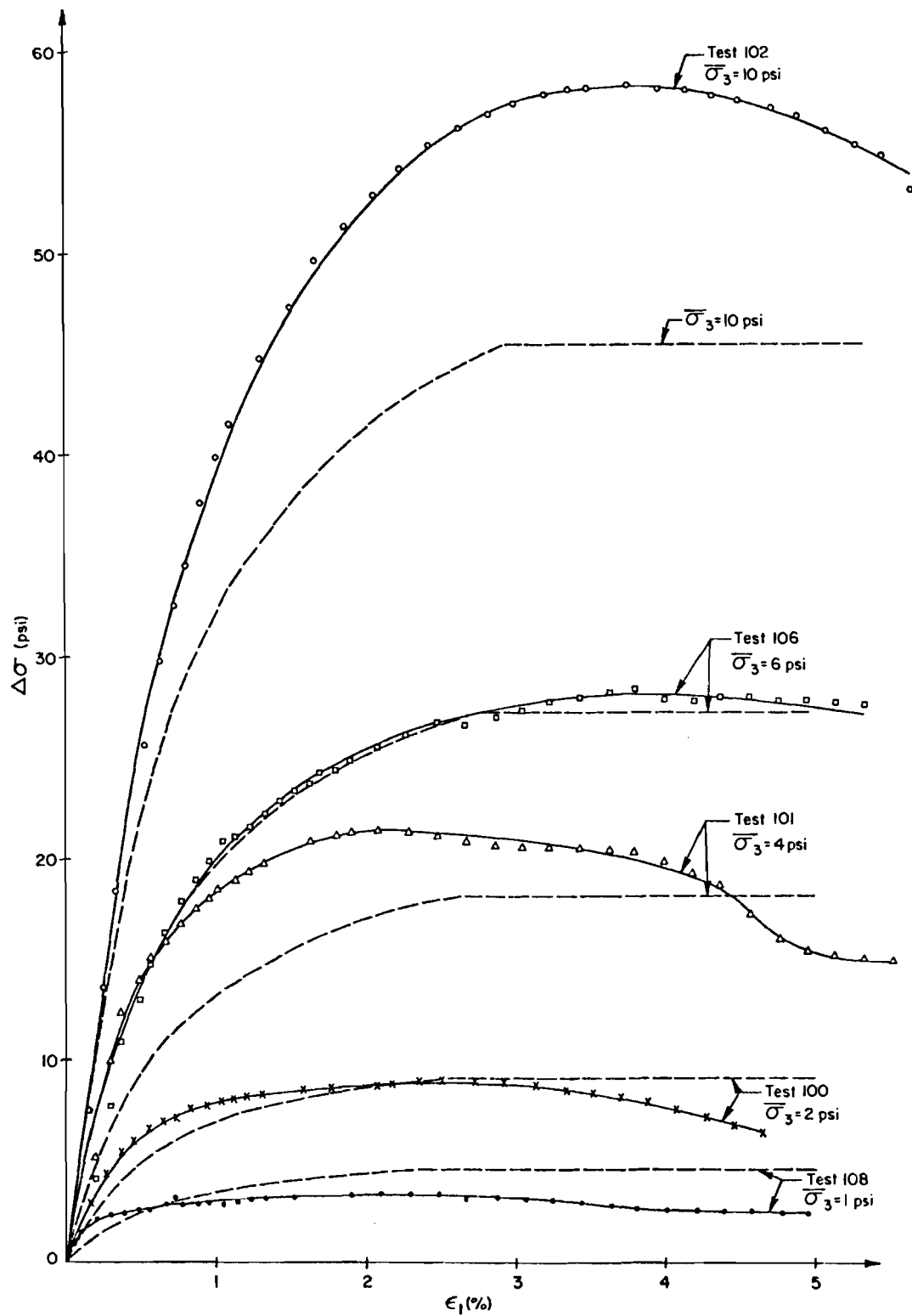


Fig. 4.7. Measured and Predicted Stress-Strain Curves for Undisturbed Samples.

pressures, for which it is impossible to run a valid triaxial test. However, it was assumed that the behavior of the sand at the low pressures could be extrapolated from the behavior at the higher pressures for which the tests were run.

The procedure suggested by Kondner and Zelasko (1963) involves the generation of a set of curves with the equation of the hyperbola

$$(\bar{\sigma}_1 - \bar{\sigma}_3) = \frac{\epsilon_1}{a + b\epsilon_1} \dots \dots \dots (4.1)$$

where

$\bar{\sigma}_1$ = effective axial stress in a triaxial specimen

$\bar{\sigma}_3$ = effective confining stress on a triaxial specimen

ϵ_1 = axial strain in a triaxial specimen

a and b = coefficients derived from triaxial test data.

In Eq. 4.1 the terms a and b are derived from the triaxial test and are written in terms of the confining stress $\bar{\sigma}_3$. For the derivation of these terms, the tests on the prepared samples were used. The first step in the procedure was to plot, for each test, the axial strain (ϵ_1) versus strain divided by the deviator stress ($\epsilon_1/\Delta\sigma$). This plot is shown in Fig. 4.8. The straight lines are drawn by hand through the points, and are the straight lines which will best fit the points. The variation of the points for small strains was expected. The intercept of the lines with the vertical axis is defined as the a coefficient for that particular confining stress. Physically the coefficient defines the inverse of the initial tangent modulus. The coefficient may be defined

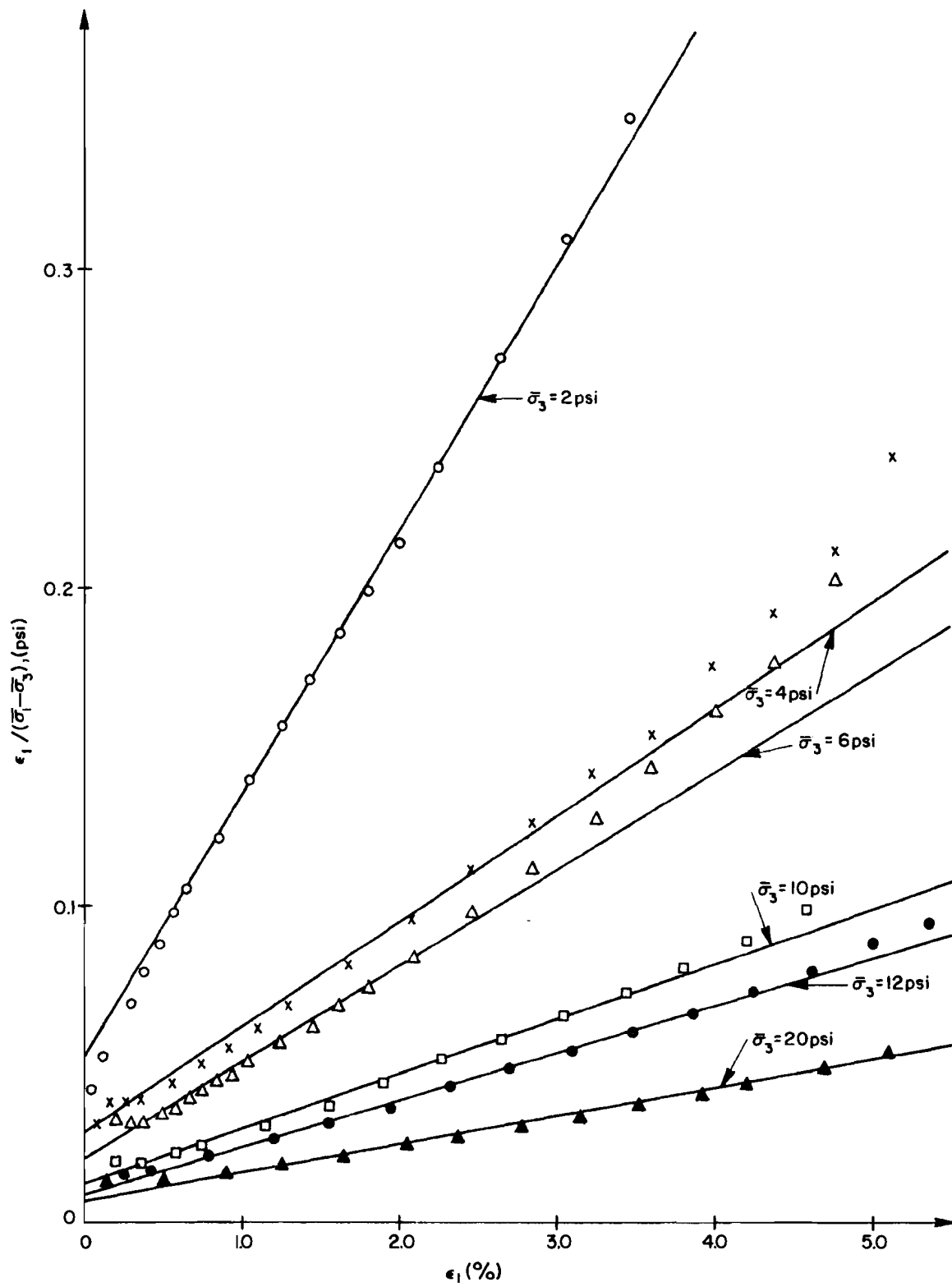


Fig. 4.8. Definition of a and b Terms for Equation 4.1.

mathematically as

$$a_i = 1/S_i \dots \dots \dots (4.2)$$

where

$$S_i = \text{slope of the } i\text{th curve at zero strain.}$$

To obtain a general expression for the coefficient a_i , in terms of the confining stress, the plot illustrated in Fig. 4.9 was made. Values of S_i and the corresponding values of confining stress are tabulated in Table 4.5. In Fig. 4.9 values of S_i/p_a and $\bar{\sigma}_3/p_a$ are plotted on log-log paper. The use of the atmospheric pressure p_a normalized the expressions. A straight line is drawn through the points and defined by the equation

$$S_i = k p_a \left(\frac{\bar{\sigma}_3}{\bar{\sigma}_{30}} \right)^n = 16.75 \left(\frac{\bar{\sigma}_3}{1.5} \right)^{0.915} \dots \dots \dots (4.3)$$

where

- k = intercept on the vertical axis in Fig. 4.9 = 1.14
- p_a = atmospheric pressure = 14.7 psi
- n = slope of the straight line in Fig. 4.9 = 0.915
- $\bar{\sigma}_{30}$ = smallest value of confining pressure ≈ 1.5 psi.

The coefficient a_i may now be defined in terms of the confining stress as

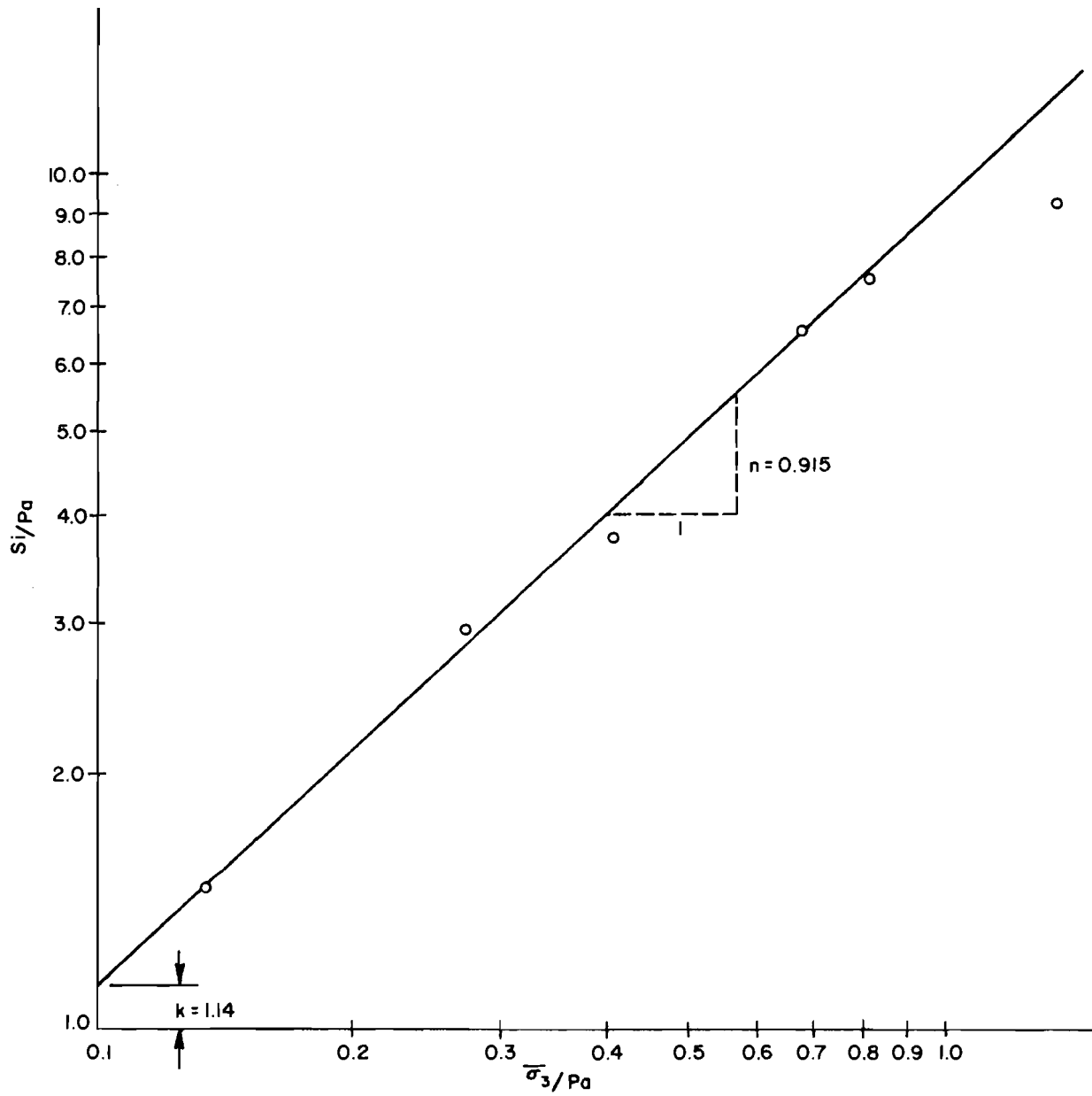


Fig. 4.9. Definition of k and n for Equation 4.3.

TABLE 4.5. CONSTANTS USED IN THE DERIVATION OF THE HYPERBOLAS

Test No.	Confining Pressure (psi)	a (in ² /lb)	S (psi)	b (in ² /lb)	$(\bar{\sigma}_1 - \bar{\sigma}_3)_{fh}$ (psi)	$(\bar{\sigma}_1 - \bar{\sigma}_3)_f$ (psi)	R_f
12	2	0.046	21.75	0.084	11.90	9.08	0.763
14	4	0.023	43.50	0.036	27.80	18.15	0.653
15	6	0.018	55.50	0.031	32.20	27.20	0.845
7	10	0.009	110.10	0.019	52.60	45.45	0.864
8	12	0.008	125.00	0.015	66.70	54.50	0.817
9	20	0.007	134.00	0.009	116.00	90.80	0.783

$$(R_f)_{avg} = 0.788$$

$$p_a = 14.7 \text{ psi}$$

$$k = 1.14$$

$$n = 0.915$$

$$a = 1/k p_a \left(\frac{\bar{\sigma}_3}{\bar{\sigma}_{30}} \right)^n = 1/16.75 \left(\frac{\bar{\sigma}_3}{1.5} \right)^{0.915} \dots \dots \dots (4.4)$$

To define the coefficient b , Fig. 4.8 is again used. In this figure, b is defined as the slope of the straight lines. Values of b are tabulated in Table 4.5. Physically the coefficient b represents the inverse of the ultimate value of deviator stress and may be written as

$$b = 1/(\bar{\sigma}_1 - \bar{\sigma}_3)_{fh} \dots \dots \dots (4.5)$$

where

$$(\bar{\sigma}_1 - \bar{\sigma}_3)_{fh} = \text{ultimate deviator stress for the hyperbolic representation.}$$

This value of deviator stress will be different from the measured ultimate value. If the measured ultimate value is written as

$$(\bar{\sigma}_1 - \bar{\sigma}_3)_f = \left[\tan^2 (45 + \phi/2) - 1 \right] \bar{\sigma}_3 = 4.545 \bar{\sigma}_3 \dots \dots (4.6)$$

where

$$\phi = \text{angle of internal friction of the sand in degrees,}$$

then the ratio between the values may be defined as

$$R_f = \frac{(\bar{\sigma}_1 - \bar{\sigma}_3)_f}{(\bar{\sigma}_1 - \bar{\sigma}_3)_{fh}} \dots \dots \dots (4.7)$$

Values of R_f are tabulated in Table 4.5. The average value of R_f is calculated and used to define the coefficient b as

$$b = \frac{(R_f)_{\text{avg}}}{\left[\tan^2 (45 + \phi/2) - 1 \right] \bar{\sigma}_3} = \frac{0.788}{4.545 \bar{\sigma}_3} \dots \dots \dots (4.8)$$

With coefficients a and b defined in terms of the confining pressure, the equation of the hyperbola for the stress-strain curves may be written as

$$\begin{aligned} (\bar{\sigma}_1 - \bar{\sigma}_3) &= \frac{\epsilon_1}{\frac{1}{k p_a \left(\frac{\bar{\sigma}_3}{\bar{\sigma}_{30}} \right)^n} + \frac{\epsilon_1 R_f}{\left[\tan^2 (45 + \phi/2) - 1 \right] \bar{\sigma}_3}} \\ &= \frac{\epsilon_1}{\frac{1}{16.75 (\bar{\sigma}_3/1.5)^{0.915}} + \frac{\epsilon_1}{5.77 \bar{\sigma}_3}} \dots \dots \dots (4.9) \end{aligned}$$

This equation produces curves which are tangent, at $\epsilon_1 = 0$, to lines with slopes defined by Eq. 4.3 and which are asymptotic to horizontal lines defined by the equation

$$(\bar{\sigma}_1 - \bar{\sigma}_3)_{\text{fh}} = \frac{(\bar{\sigma}_1 - \bar{\sigma}_3)_f}{(R_f)_{\text{avg}}} = \frac{4.545 \bar{\sigma}_3}{0.788} \dots \dots \dots (4.10)$$

However, the procedure used in this study was to define the initial portion of the curve by Eq. 4.9, but to limit the deviator stress to maximum values defined by Eq. 4.6. This procedure was used rather than

defining the entire curve by Eq. 4.9, and results in the flat-topped curves, illustrated by the dashed lines in Figs. 4.6 and 4.7.

Equations 4.6 and 4.9 will be used to define axial shear transfer curves. Coefficients are developed, from the results of the axial load tests of the small piles, which correlate the stress-strain curves with the axial shear transfer curves. Equation 4.3 will be used to approximate the stress-strain behavior of the sand for small strain. Values from the equation will be used in a linear elasticity solution to define the lateral load-deflection response of the pile for small deflections.

This page replaces an intentionally blank page in the original.

-- CTR Library Digitization Team

CHAPTER V

AXIAL LOAD TRANSFER

The mechanics of an axially loaded pile were developed in Chapter II. Equations were derived to represent mathematically the behavior of the pile under load, and a scheme was presented for solving the equations to obtain a load-deformation curve for the top of the pile. The equations contained terms for the transfer of load to the soil through shear stresses along the shaft and through pressure on the tip. In this chapter, the mechanics of load transfer for piles in sand will be considered, and also, criteria developed for predicting the load transfer from soil properties.

The first section will deal with the theoretical concepts of axial load transfer, and available analytical techniques for describing this transfer. In the second section, the results from the load test on the model piles are presented. Load transfer curves, in the form of s_x - z curves, are developed and correlated with stress-strain curves for the sand. A load-deformation curve for the tip of the pile is also developed. In the next section, the predicted s_x - z curves will be used to predict analytically load-deformation curves for the top of the piles tested. The predicted curves will then be compared with the measured curves. The criteria for describing the s_x - z curves will be modified to account for the variations in shear transfer caused by differences in sand density and method of installation. The modified criteria will be used to predict analytically the load-deformation curves for the tops

of three 4-inch diameter piles, a 12.75-inch diameter pile, and a 16-inch diameter pile. The predicted curves will then be compared with measured curves. In the final section, the results of the study of the axial pile behavior will be discussed.

Concepts of Axial Pile-Soil Interaction

The majority of the research on axially loaded piles has been carried out for the purpose of determining the ultimate capacity of the piles. A number of theoretical and empirical expressions have been developed for maximum shear transfer and ultimate bearing capacity of the tip of a pile. Such expressions can be used in an equation similar to Eq. 2.1 to compute the ultimate capacity of a pile. The approach described provides no insight into the deformation pattern of the pile which is necessary to develop the ultimate load. However, the concepts of the interaction which have been developed are valuable for explaining the action of an axially loaded pile, and the expressions obtained for ultimate load transfer serve as guidelines for developing techniques to describe the load transfer as a function of pile movement.

In the following two sections load transfer to the sand through skin friction is considered, and in the final two sections the load-transfer through the pile tip is considered.

Ultimate Shear Transfer Along the Pile Shaft

The usual form of the ultimate expression for the maximum shear transfer from an axially loaded pile to the surrounding sand is

$$s_{xm} = \mu_x \sigma_{nx} \dots \dots \dots (5.1)$$

where

$$\begin{aligned}
 s_{xm} &= \text{maximum shear stress transferred to the soil at depth } x \\
 \mu_x &= \text{coefficient of friction along shear surface at depth } x \\
 \sigma_{nx} &= \text{effective normal stress on shear surface at depth } x .
 \end{aligned}$$

The normal stress is usually written as

$$\sigma_{nx} = K_x \bar{\gamma}_x \dots \dots \dots (5.2)$$

where

$$\begin{aligned}
 K_x &= \text{coefficient of lateral earth pressure at depth } x \\
 \bar{\gamma} &= \text{effective unit weight of the soil above depth } x
 \end{aligned}$$

and x is the depth as defined in Chapter II. Equation 5.1 may now be written as

$$s_{xm} = K_x \bar{\gamma}_x \mu_x \dots \dots \dots (5.3)$$

Equation 5.3 represents a rational approach for the determination of the skin friction along a pile, but as a practical matter, the accurate determination of appropriate value of K_x and μ_x is a difficult task. The value of K_x probably lies somewhere between the value for the active and passive earth-pressure coefficients. The exact value will be a function of depth, and will depend on a number of factors such as method of pile installation and existing stresses in the soil. Mazurkiewicz (1968) tabulates 27 theoretical expressions that have been proposed for K_x , for different methods of placing the piles and types

of loading (compression and pullout). The proposed coefficients for the lateral earth pressure are not functions of depth, and are usually assumed to be constant.

The determination of the appropriate value of μ_x is also dependent on a number of variables. In the tabulation of Mazurkiewicz (1968), corresponding expressions for the coefficient of friction are noted. These expressions are independent of depth, and a majority of investigators suggest that the shear surface is probably at the pile-soil interface so that an expression for μ_x may be written as

$$\mu_x = \tan(\delta) \dots \dots \dots (5.4)$$

where

δ = apparent angle of friction between the pile and soil.

Potyondi (1961) has determined values of the coefficient of friction for a variety of soils and pile materials. Potyondi suggests the following expression for apparent angle of friction

$$\delta = f_r(\phi) \dots \dots \dots (5.5)$$

where

ϕ = angle of internal friction of sand

f_r = reduction factor.

The value for f_r is a function of four major factors: (1) moisture content, (2) surface roughness, (3) soil density, and (4) normal stress.

These factors are probably not very accurately known but will depend on the particular conditions. The equation for skin friction may now be written as

$$s_{xm} = K_x \bar{\gamma}_x \tan(f_r \phi) \dots \dots \dots (5.6)$$

Since there is a great deal of uncertainty involved in the determination of K_x and $\tan(f_r \phi)$, an approach often used is to combine the two into one factor so that Eq. 5.6 may be written as

$$s_{xm} = N \bar{\gamma}_x \dots \dots \dots (5.7)$$

where

N = skin friction coefficient.

The value of N will depend on the type of loading and Eq. 5.7 is often written as

$$s_{xm}^t = N_t \bar{\gamma}_x \dots \dots \dots (5.8)$$

or

$$s_{xm}^c = N_c \bar{\gamma}_x \dots \dots \dots (5.9)$$

where the superscripts denote tension or compression loading. Values of N_c and N_t are calculated by the expressions tabulated in Mazurkiewicz (1968) for a pile diameter of 0.4 meter, a pile length of 10.0 meters, a sand density of 1.68 gm/cm^3 , an angle of internal friction of 35 degrees, and an apparent angle of friction between the pile and soil of 30 degrees.

The values of N_c calculated range from 0.190 to 5.854 and values of N_t range from 0.190 to 0.457. Equations similar to Eqs. 5.8 and 5.9 are also usually used in empirical methods for determination of skin friction. From test data, values of the skin friction coefficient are computed. A number of such methods are listed in Mazurkiewicz (1968).

Before discussing the relative movement between the pile and soil necessary to develop shear transfer, several aspects of the above equations will be considered. If the skin friction coefficients are assumed to be constant, then Eqs. 5.8 and 5.9 indicate that the skin friction will increase with depth; assuming that the effective unit weight remains constant or increases with depth. Experimental observations by Kerisel (1964), Vesić (1965), and Coyle and Sulaiman (1967) have failed to verify that there is a continuous increase in skin friction with depth, but have shown that an increase with depth occurs only to relatively shallow depths. At greater depths the rate of increase in skin resistance may decrease, and may asymptotically approach a constant value. The limiting depth to which the increase will continue depends on a number of factors including the density of the sand, method of placement, and pile size. Vesić (1965) suggests that the skin friction may become constant below depths of 15- to 20-pile diameters. Coyle and Sulaiman (1967) present results from tests on three full-scale field tests which show that the maximum value of skin friction decreases with depth. They also present results from small-scale tests run in a tri-axial chamber which show that the skin friction increases with increasing confining stress. Results reported by Kerisel (1964) indicate that no maximum value of skin friction is reached, but that the rate of increase

with depth decreases. Results from the small-scale tests run for this study, which will be presented later, indicate a trend similar to that observed by Kerisel (1964). The piles tested had a depth to diameter ratio of forty-eight, and it appeared that as the depth increased, values of skin friction were approaching a constant value. The depth at which the rate of increase in skin friction with depth begins to decrease, or reaches a constant value is dependent on a number of factors, including pile size and sand density. Another complication is that there will always be some interference near the pile tip, regardless of the length pile.

In the development of Eqs. 5.8 and 5.9, the effect on the skin friction coefficient of the type sand and its condition, method of placing the pile, and pile material have been noted. One aspect which has not been mentioned is the effect of the pile size. No conclusive evidence exists to clarify this effect, but from the limited data presented by Vesic (1965) the size of the pile appears to have no influence on the ultimate value of skin friction.

To this point nothing has been said about the relative movement between the pile and soil necessary to develop the ultimate shear transfer, or the movement for values of shear transfer less than the ultimate. However, the concepts developed will be applicable for values less than the ultimate, and relationships developed for the ultimate shear transfer will be used in the following section as a starting point for relating shear transfer and pile movement.

Pile Movement - Shear Transfer Relationships

The application of the techniques, described in Chapter II, for determining the top load-deformation curve for the top of a pile requires not only a knowledge of the ultimate shear transfer, but also a knowledge of the pile movement necessary to develop the shear transfer. If the uncertainties involved in predicting an ultimate value of shear transfer are considered, it is not surprising to find that the majority of research has been aimed at a more accurate determination of an ultimate value, rather than a determination of the movements that are necessary to develop the shear transfer. However, several procedures have been developed which consider the shear transfer and the corresponding movement.

Analytical methods based on theory of elasticity have been proposed by Thurman and D'Appolonia (1964), Thurman and D'Appolonia (1965), Poulos and Davis (1968), and Mattes and Poulos (1969). All of these methods employ the equation proposed by Mindlin (1936) for a point load applied in the interior of a semi-infinite elastic medium, and a maximum value of shear stress set by an expression such as Eq. 5.7 to relate the shear transfer to the pile movement. This procedure results in an idealized elastic-plastic representation of the pile-soil interaction. The shear stress will be linearly proportional to the pile movement until the maximum value of shear stress is attained; after which the shear stress remains constant for any pile movement.

Empirical methods relating the shear transfer to the shear strength of the soil have been proposed by Coyle and Reese (1966) for steel piles in clay, and by Coyle and Sulaiman (1967) for steel piles in sand. The

procedures were developed using full-scale field tests and laboratory tests on small piles.

The procedure used for analyzing the test results from the small piles in this study is similar to that used by Coyle and Sulaiman (1967), in that the shear transfer is related to the shear strength of the soil. However, for this study, an attempt was made to carry the correlation a step further and relate the movements of the pile to strain values from triaxial tests on the sand rather than using pile movements obtained from the field test. The procedure employed is essentially empirical but it has some rational physical basis. In the remainder of this section, the correlation procedure employed will be developed.

To correlate the shear transfer with the stress-strain characteristics of the sand, Eqs. 4.6 and 5.7 are utilized. These equations are the expressions for the maximum deviator stress for a triaxial test and the maximum shear transfer between a pile and the surrounding soil, and are rewritten below as

$$\Delta\sigma_f = \left[\tan^2 (45 + \phi/2) - 1 \right] \bar{\sigma}_3 \dots \dots \dots (4.6)$$

and

$$s_{xm} = N \bar{\gamma} x \dots \dots \dots (5.7)$$

For Eq. 5.7, it is noted that if N is assumed constant then the maximum shear transfer will increase linearly with depth, and for Eq. 4.6, it is noted that if ϕ is constant then the shear strength will increase linearly with confining pressure. The variations of maximum shear

transfer and shear strength are graphically illustrated in Fig. 5.1. The curves in Fig. 5.1 illustrate the increase in maximum deviator stress that occurs with increasing confining pressure, and the increase in maximum shear transfer that occurs with increasing depth. Since the two families of curves are similar it should be possible to establish a correlation between the two.

To accomplish the correlation a coefficient U is introduced so that the maximum shear transfer is defined, in terms of the shear strength of the sand, by the equation

$$s_{xm} = U \Delta\sigma_f \dots \dots \dots (5.10)$$

where

U = coefficient for correlating shear transfer to soil shear strength.

Equation 5.10 involves only a redefinition of the skin friction coefficients and the coefficient U may be defined mathematically from Eqs. 4.6 and 5.7 as

$$U = N / \left[\tan^2 (45 + \phi/2) - 1 \right] \dots \dots \dots (5.11)$$

If a triaxial test is run for a confining pressure of $\bar{\sigma}_3 = \bar{\gamma}x$, then equations for maximum shear transfer for tension or compression loading may be written as

$$s_{xm}^c = U_c \Delta\sigma_f \dots \dots \dots (5.12)$$

and

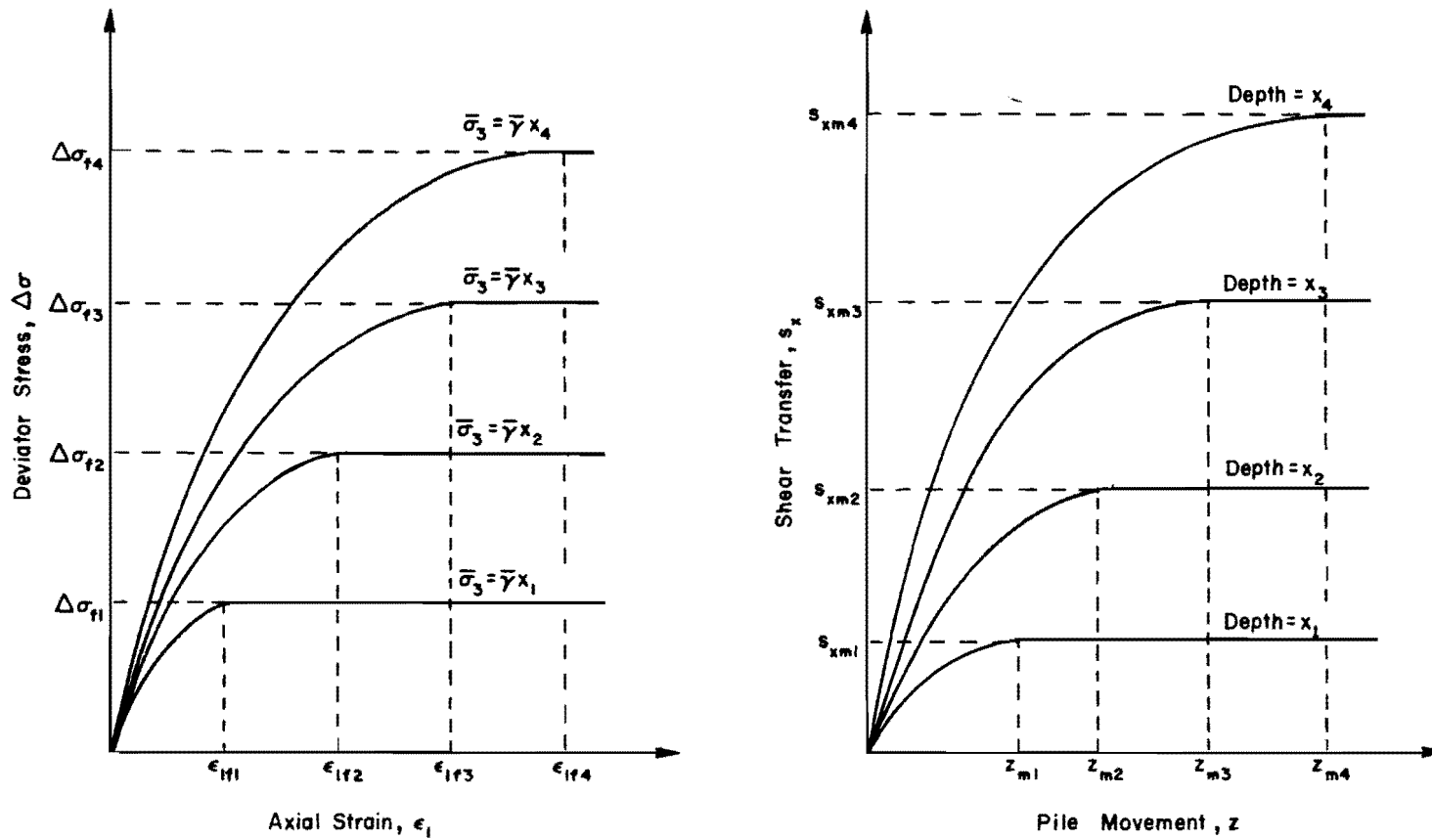


Fig. 5.1. Idealized Families of Stress-Strain Curves and Shear Transfer-Pile Movement Curves.

$$s_{xm}^t = U_t \Delta \sigma_f \dots \dots \dots (5.13)$$

The coefficients U_c and U_t will be empirically determined from the results of the pile tests. In the preceding section, the assumption of a constant N value was discussed and the currently available information on the subject presented. The values of the U coefficients will have to reflect the same trends as the N coefficients, and they will be functions of the same parameters, such as method of installation and type of pile material.

Equations 5.12 and 5.13 are expressions for ultimate shear transfer, and give no indication of the pile movement necessary to develop the shear transfer. To extend the correlation to intermediate values of deviator stress and shear transfer, it was assumed that the shape of the stress-strain and shear transfer curves would be similar, and Eqs. 5.12 and 5.13 written for all values of shear transfer and deviator stress, as

$$s_x^c = U_c \Delta \sigma \dots \dots \dots (5.14)$$

and

$$s_x^t = U_t \Delta \sigma \dots \dots \dots (5.15)$$

Equations 5.14 and 5.15 are combined with equations, which will be developed in the following paragraphs, that relate the axial strain to the pile movement to define a complete family of s_x - z curves from a family of triaxial stress-strain curves.

The procedure used to relate the pile movement to the strain from a triaxial test is similar to the approach used to relate the shear transfer to the deviator stress. The correlation relationships are first established for maximum values and then extended to intermediate values. The properties of the stress-strain curves and the shear transfer-pile movement curves illustrated in Fig. 5.1 are utilized to establish the correlation relationships.

In Fig. 5.1, it is noted that the strain at which the maximum deviator stress is developed increases as the confining pressure increases, and that the value of pile movement at which the maximum shear transfer is developed increases as the depth increases. The correlation is accomplished by introducing a coefficient R so that the pile movement for maximum shear transfer is related to the axial strain for the maximum deviator stress by the equation

$$z_m = \epsilon_{1f} R f(D) \dots \dots \dots (5.16)$$

where

z_m = pile movement at which the maximum shear transfer is developed

ϵ_{1f} = axial strain at which the maximum deviator stress is attained

R = correlation coefficient for relating pile movement to axial strain

$f(D)$ = function which expresses the influence of the pile diameter on the pile movement.

The inclusion of the effect of the pile diameter in Eq. 5.16 warrants some consideration, before developing the procedure further. The inclusion of the diameter indicates that the movement of the pile necessary to develop the shear transfer is a function of the diameter of the pile. Some investigators indicate that the pile movement is independent of the diameter, but there is considerable disagreement on this point and very little data to substantiate an argument either way. Vesic' (1963 and 1965) presents data which, according to the author, shows that the displacements needed to develop ultimate skin friction are independent of the pile size. However, an approach based on theory of elasticity and a limiting value of shear stress, such as those mentioned previously in this section, will result in an interaction relationship which is influenced by the size of the pile. The procedure utilized by Thurman and D'Appolonia was to represent the pile-soil interaction with a series of point loads in the interior of a semi-infinite elastic solid. The pile was divided into segments and the loads assumed to act at the center of the segments. The force for a segment is found by the equation

$$F = T C h \dots \dots \dots (5.17)$$

where

F = force transferred to the soil

C = pile circumference

h = increment length.

Equation 5.17 suggests that the force for a segment will be directly proportional to the diameter of the pile. This force is then used in Mindlin's

equation to obtain a corresponding displacement. Therefore, the displacement obtained is directly proportional to the force and, therefore, directly proportional to the diameter of the pile.

In a similar manner, the reasoning may be further substantiated by considering the zone of soil which will be influenced by the pile. For a normally loaded plate or footing, the deflection is proportional to the size of the footing. This is explained by considering the bulb of pressure developed beneath the loaded area. The size of the bulb of pressure or zone of influence is proportional to the size of the loaded area and, therefore, the deflection is also proportional to the size of the loaded area. It would seem logical to apply the same reasoning to the case of a pile where the load is applied parallel to the soil surface through shear. Because of the difference in the zone of soil influenced, the development of the maximum shear transfer may result in the same shear strain in the sand for any size pile, but because of the difference in the zone of soil effected, the movement at the interface will be a function of the pile size.

For this study, it was assumed that the pile movement is directly proportional to the pile size and that

$$f(D) = D \dots \dots \dots (5.18)$$

Equation 5.16 may now be written as

$$z_m = \epsilon_{1f} R D \dots \dots \dots (5.19)$$

To extend the correlation to intermediate values of pile movement and axial strain, it was assumed that the shape of the curves was similar, and Eq. 5.19, for compression and tension loading, written as

$$z^c = \epsilon_1 R_c D \dots \dots \dots (5.20)$$

and

$$z^t = \epsilon_1 R_t D \dots \dots \dots (5.21)$$

The coefficients R_c and R_t will be empirically determined from the results of the pile tests. The R coefficients will be functions of the same parameters as the U coefficients; such as, method of installation and type of pile material.

The correlation between the triaxial stress-strain curves and the shear transfer pile-movement curves, expressed by Eqs. 5.14, 5.15, 5.20, and 5.21, is empirical in the sense that the determination of the correlation coefficients will have to be from actual load test data. These coefficients will reflect the effects of such factors as method of installation and pile material. However, there is also some rational, physical basis for the correlation; since, the shear of sand in a triaxial test should result in stress-strain curves that exhibit characteristics similar to the shear transfer curves that result when a pile in the sand is loaded. Triaxial test stress-strain curves are relatively easy to obtain and with appropriate correlation coefficients should provide reasonable approximations for shear transfer curves.

Ultimate Pile Tip Resistance

The usual form of the expression for the ultimate tip resistance for a pile in sand is

$$q_o = \bar{\gamma} \times N_q^* \dots \dots \dots (5.22)$$

where

- q_o = tip bearing capacity
- N_q^* = bearing capacity factor for deep foundation with a circular or a square shape.

A number of theoretical and empirical expressions for determining the bearing capacity factor have been proposed. In all of these procedures, the bearing capacity factor is a function of the angle of internal friction of the sand. The range of the proposed values is illustrated in Fig. 5.2, from Vesic' (1965). In this figure, it is noted that there is a wide range in the proposed values, just as there was a wide range in the proposed values of skin friction coefficient. This wide range of proposed values is indicative of the state of present theory.

The accurate prediction of the ultimate tip capacity from Eq. 5.22 is further complicated by the fact that N_q^* is not a constant depending only on the angle of internal friction, but depends also on the ratio of depth to diameter and on the relative density of the sand. Experimental results presented by Kerisel (1965) and Vesic' (1964, 1965, and 1968) indicate that the bearing capacity increases linearly with depth only for relatively shallow depths. At a particular depth, which depends on the size of the pile and density of the sand, the rate of increase of

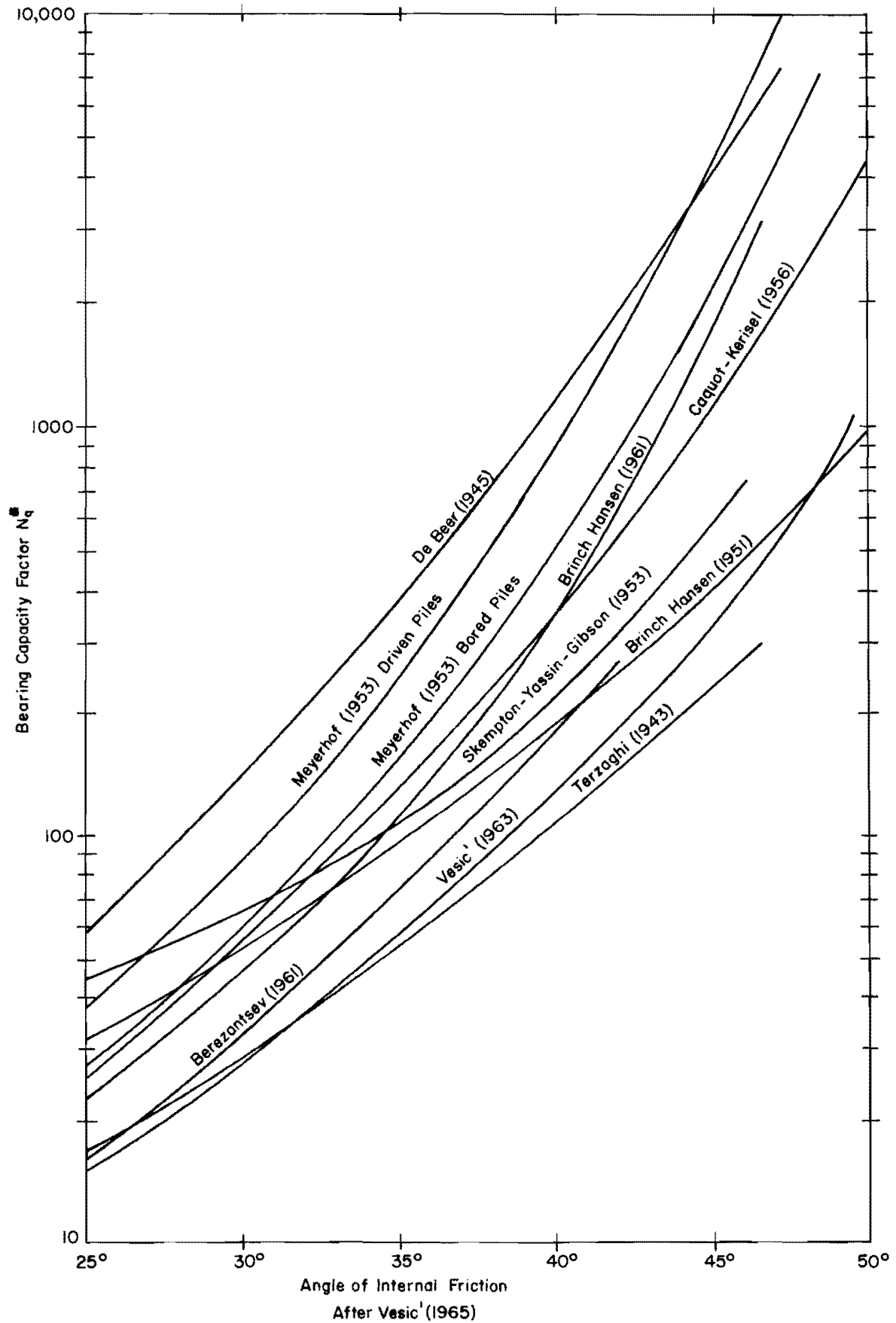


Fig. 5.2. Bearing Capacity Factors for Circular Deep Foundations.

point resistance with depth will decrease and a constant value of bearing capacity will be approached. At shallower depths, the size of the base will influence the unit point resistance, but at greater depths the size appears to have little influence on the value obtained. At depths exceeding 10 to 20 pile diameters, the unit point resistance appears to be a function of only the relative density of the sand. The situation is further complicated by the nonuniformity of the initial stress conditions in the soil around the tip, caused by the various methods of installation. The differences between the bearing capacity of the tip of a buried pile, a bored pile, and a driven pile will be considerable.

As mentioned previously, the wide range of proposed N_q^* values indicate that present knowledge of ultimate pile-tip capacity is limited. This is also true of the movement of the pile tip necessary to develop the ultimate load. A summary of the information on the relationship between the tip movement and the soil resistance at the tip will be presented in the following section.

Tip Movement - Tip Resistance Relationships

Equations for the ultimate tip resistance developed in the preceding section, give no indication of the tip movements prior to failure. The usual procedures used to predict these movements are theoretical solutions based on theory of elasticity, or empirical methods, based on field observations.

The usual form of the equation for a theory of elasticity solution is

$$z_B = \frac{q_B D (1 - \nu^2)}{E_m} I_B \dots \dots \dots (5.23)$$

where

z_B = tip movement

q_B = unit pressure on the tip

ν = Poisson's ratio of soil below tip

E_m = modulus of elasticity of soil below the tip

I_B = influence coefficient.

The influence coefficient depends on the base shape, base size, base rigidity, depth to base, as well as the type of elasticity solution used. Thurman and D'Appolonia (1964) recommend that the solution proposed by Mindlin (1936) be used to define the influence coefficient for friction piles and that the Boussinesq solution be used for end bearing piles. The elastic deformation from these equations may be used with a value of ultimate bearing capacity to form a complete curve for tip load versus tip deformation, consisting of two straight lines.

Studies by Bullen (1958) indicate that tip movement is nearly linear until approximately one-half of the ultimate tip resistance is reached; then the relationship between resistance and movement becomes increasingly nonlinear until the ultimate is reached. Bullen also indicates that the movement preceding the failure is about 10 per cent of the width of friction piles. D'Appolonia and Romualdi (1963) report that, for end bearing piles, the movement preceding failure is about 5 per cent of the pile width. These values are based on test results of driven piles in a variety of soils. Studies by Vesic' (1965) indicate that, at ultimate, the tip movement is less for driven piles than for bored or buried piles. Vesic' defines a function λ such that Eq. 5.23 for tip movement may be

written as

$$z_B = \frac{q_B D}{\lambda q_o} I_B \dots \dots \dots (5.24)$$

where

λ = empirically derived function.

For buried piles λ was found to vary from 6 to 9 and for driven or jacked piles from 25 to 50, with the smaller figures corresponding to looser deposits.

The prediction of the tip deformation, from either of the above-mentioned methods, must be considered as very approximate. For the methods based on the theory of elasticity, the accurate prediction of the modulus of elasticity and Poisson's ratio of the soil below the tip is very difficult. It is also an established fact that soil under load does not deform linearly. From empirical methods, a wide range of factors have been proposed; and the use of these factors, for conditions other than the test conditions from which they were developed, may not be valid. When using the movements obtained from either of these methods, the approximations and assumptions involved should be considered. However, it should be noted that presently these two procedures are all that is available for predicting a tip load-deformation curve. If a load-deformation curve for the pile top is to be obtained from the procedure discussed in Chapter II, some estimation of the tip behavior is necessary. In the following section, a tip load-deformation curve is developed from the load distribution curve for one of the instrumented piles.

Test Results

The results of the tests for the six axially loaded piles will be presented in this section. The top load-deformation curves for the six piles are presented first. In the next section the load distribution in the two instrumented piles will be presented, and in the final section, s_x -z and tip load-movement curves developed from the measured load-distribution curves will be presented.

Measured Axial Load-Deformation Curves for the Top of the Piles

The curves showing top movement versus top load obtained from the tests of the six axially loaded piles are shown in Fig. 5.3. The loading procedure used to obtain these curves was described in Chapter III, and the equipment for monitoring load and deflection are described in Appendix D. The top load was measured with a load cell, and the deflection was the average of measurements from three dial gages located around the pile.

Several characteristics of the curve shown in Fig. 5.3 are listed below.

1. The curves for the piles loaded in tension (1-A and 5-A) are very similar, and have the same maximum load of 4,200 pounds.
2. The curves for the piles loaded in compression (2-A, 3-A, 4-A, and 6-A) are similar for smaller loads, but begin to diverge for loads exceeding approximately 3,000 pounds.
3. One plausible explanation for the low maximum load of 3,600 pounds carried by pile 6-A is that there was large eccentricity in the applied load. This eccentricity caused a large lateral deformation which reduced the axial capacity.

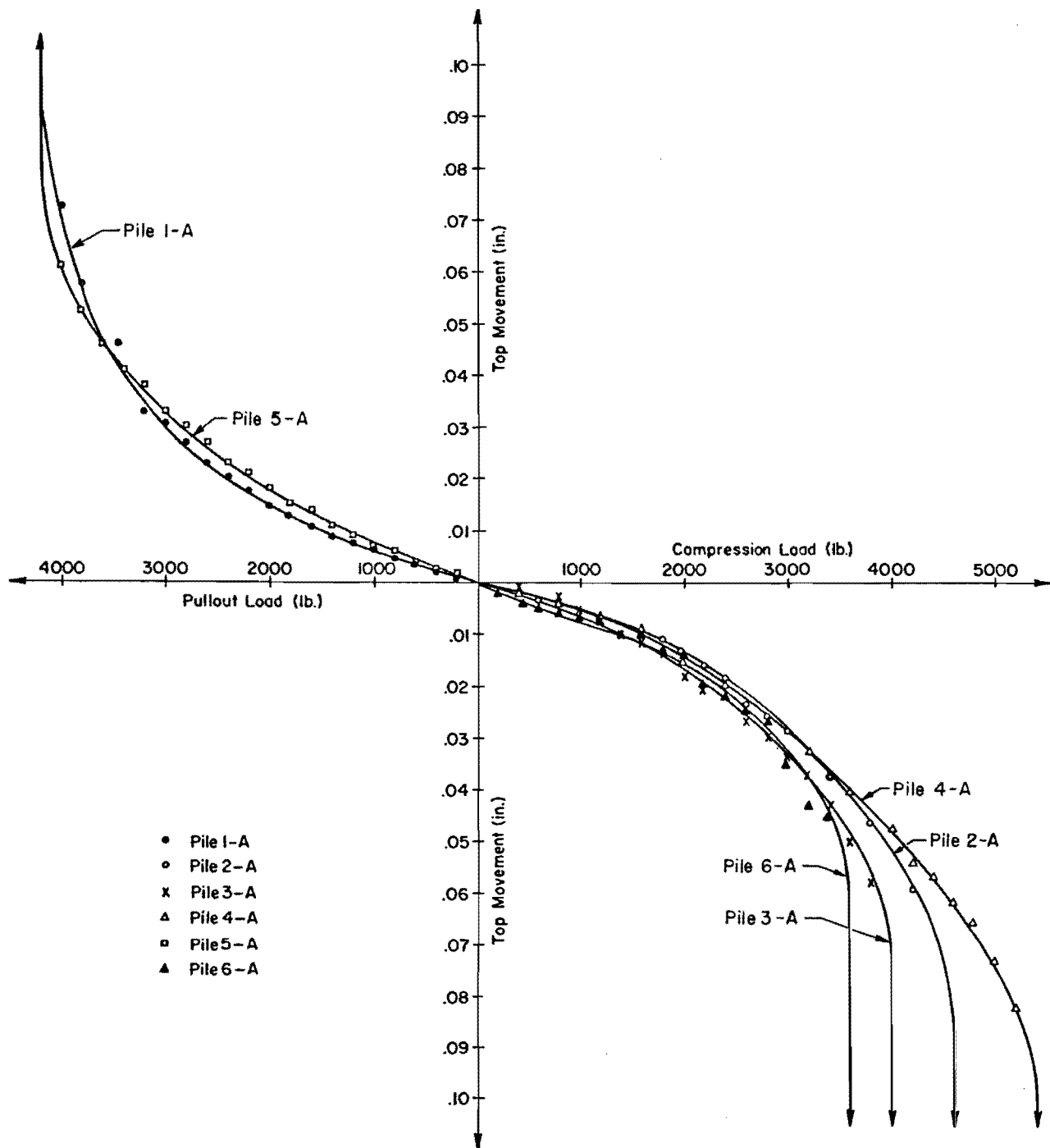


Fig. 5.3. Measured Axial Load-Deformation Curves for the Tops of the Test Piles.

4. The only explanation that can be proposed for the large load of 5,400 pounds resisted by pile 4-A is that, since pile 4-A was tested about two months after the other piles, the sand could possibly have increased in strength with aging. Kerisel (1965) points out that this increase may be significant, but no evidence is available to indicate that there actually was an increase in soil strength.
5. The initial portions of the pullout and compression curves are essentially linear, and have approximately the same slope up to a load of about 2,000 pounds.
6. The maximum loads for pullout and compression are reached when the movement is about 0.07 inch.
7. The average value of maximum load from piles 2-A, 3-A, and 4-A is 4,667 pounds.

An average curve for the two pullout tests and an average curve for the three compression tests which gave higher loads were used in the analysis of the loaded caps. In the final section of this chapter, these average curves will be compared with curves predicted using the computation procedure described in Chapter II.

Experimental Curves Showing Distribution of Axial Load Along the Piles

The load-distribution curves for piles 1-A and 2-A are illustrated in Figs. 5.4 and 5.5. The forces at the ground line were measured with a load cell, and the forces at locations one through five were measured by strain gages.

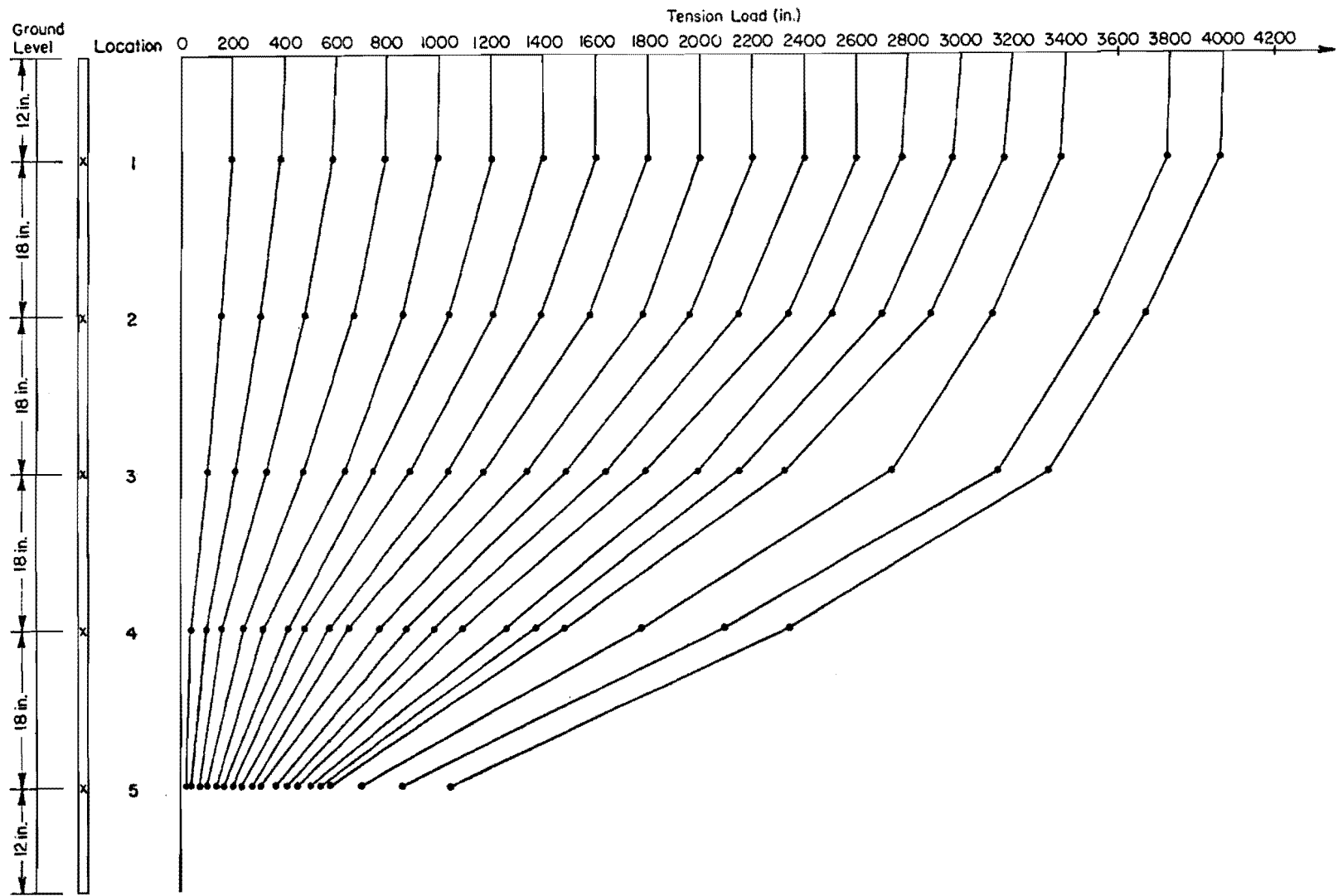


Fig. 5.4. Axial Load-Distribution Curves for Pullout Loading of Pile 1-A.

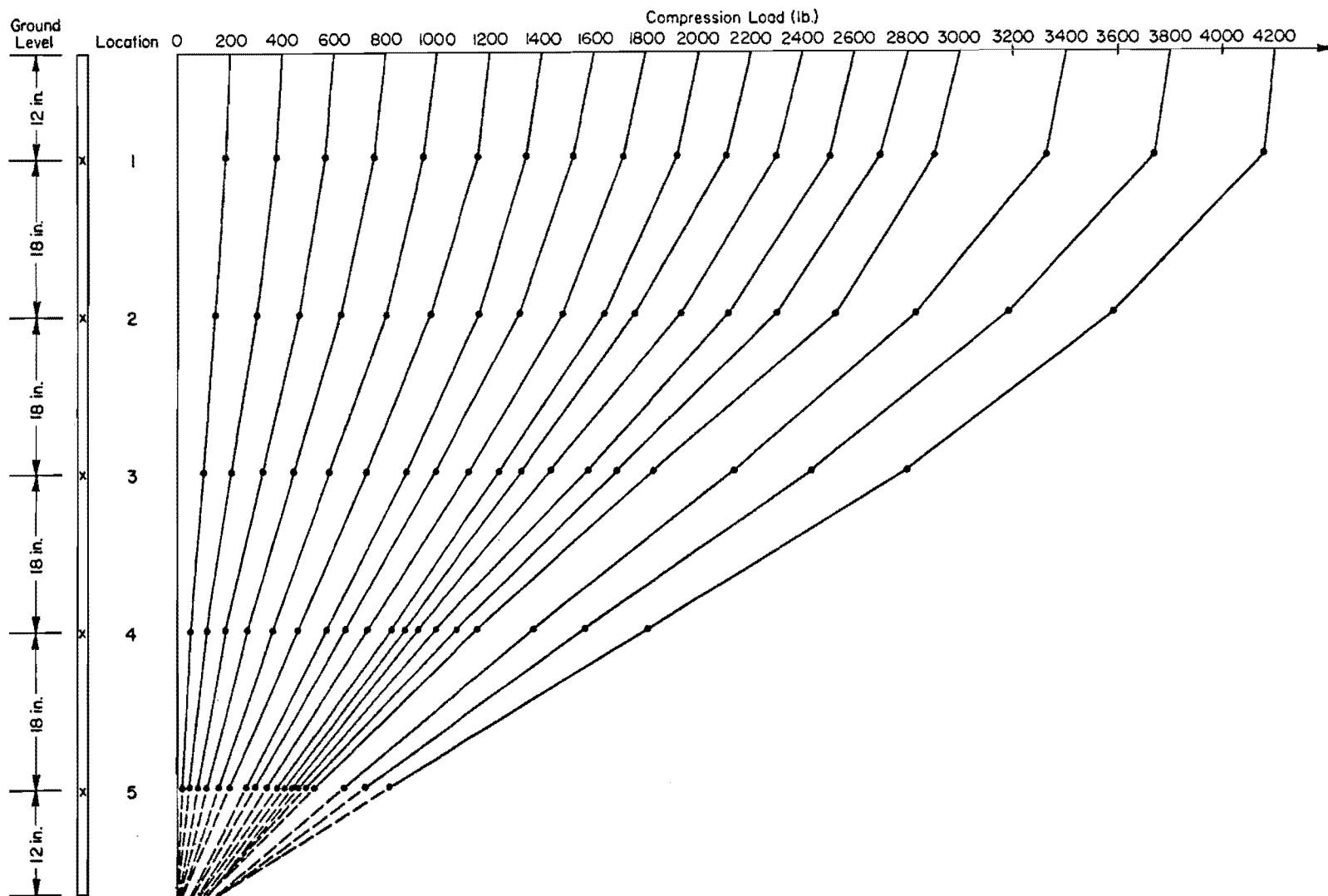


Fig. 5.5. Axial Load-Distribution Curves for Compression Loading of Pile 2-A.

Curves such as those in Figs. 5.4 and 5.5 and the top load-deformation curves are used to develop s_x -z curves. For pile 2-A, the load distribution is used to obtain a load-deformation curve for the tip of the pile. For the development of the load-transfer curves, the load-distribution curves as shown in Fig. 5.4 and 5.5 were used without any smoothing.

Development of Shear Transfer Curves from Measured Loads and Deflections

The procedure used for developing s_x -z curves from the top deflection and load distribution is illustrated in Fig. 5.6. The location of the points at which the load was measured is shown in Fig. 5.6(a). The load distribution in the pile is illustrated in Fig. 5.6(b), and the movement along the pile is illustrated in Fig. 5.6(c).

The computation procedure is as follows:

1. Compute the load transferred to the soil between points where force is known by taking the difference between the forces.

The procedure is illustrated in Fig. 5.6(b).

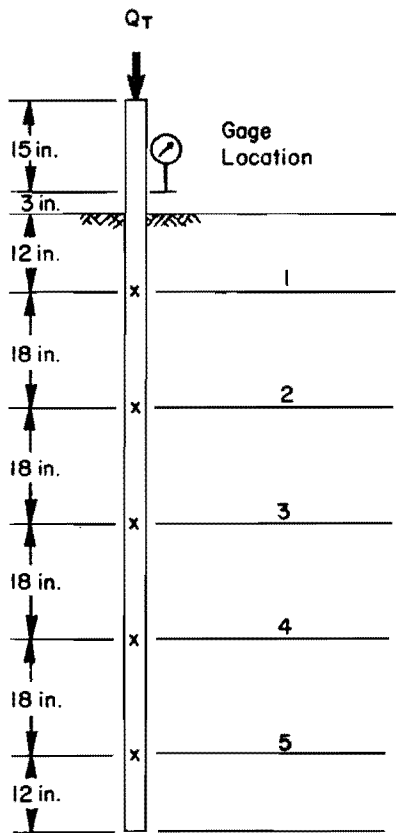
2. Compute the average load per unit area transferred to the soil between the points where the force is known. The formula used is

$$s_x = \frac{\Delta Q}{\pi D H} \dots \dots \dots (5.25)$$

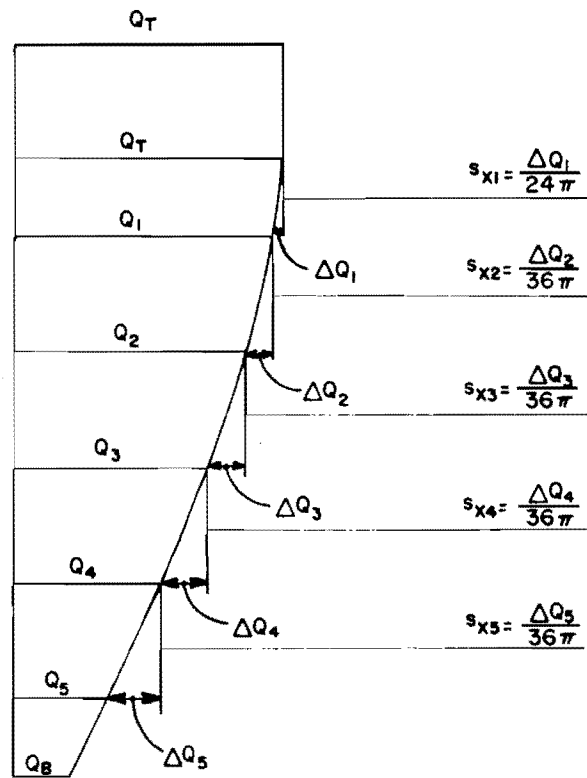
where

ΔQ = difference between forces in pile

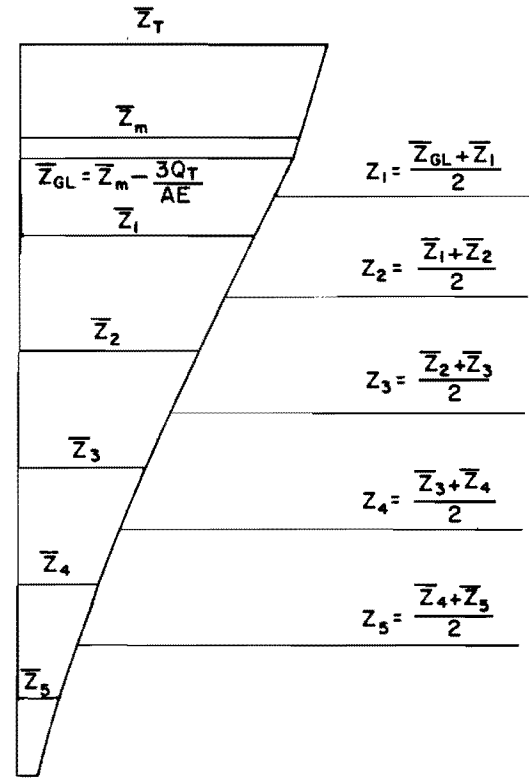
H = distance between points where force is known.



a. Layout of gages along the pile



b. Axial load distribution along the pile



c. Axial movement along the pile

Fig. 5.6. Graphical Illustration of the Development of s_x-z Curves.

This average shear transfer is assumed to be the value at the midpoint between points of known force.

3. Compute the movement at the ground line from the measured movement and applied load. The equation used is illustrated in Fig. 5.6(c).
4. Starting at the ground line and proceeding down the pile, compute the movements of the points on the pile where the forces are known. The equation used is

$$\bar{z}_l = \bar{z}_u - \frac{H(Q_l - Q_u)}{2 AE} \dots \dots \dots (5.26)$$

where the subscripts u and l denote the upper and lower points, and the bars denote movement at points where the force is known.

5. Starting at the ground line and proceeding down the pile, compute the movement at the midpoint between points of known movement. The equation used is

$$z = \frac{\bar{z}_u - \bar{z}_l}{2} \dots \dots \dots (5.27)$$

and the computation procedure used is illustrated in Fig. 5.6(c).

6. The average shear transfer and the average movement for each location is combined to form a s_x - z curve for the corresponding depth.

For the model piles, this procedure resulted in five s_x - z curves at depths of 6 inches, 21 inches, 39 inches, 57 inches, and 75 inches. The

curves developed from the pullout test of pile 1-A are shown in Fig. 5.7, and those from the compression test of pile 2-A are shown in Fig. 5.8.

Several characteristics of the two sets of curves are listed below.

1. Both sets of curves showed an increase in maximum value of load transfer with depth. Because of the controlled stress loading, maximum values were not obtained for the curves at depths of 57 and 75 inches for the compression loading, but the trend seems to indicate that the largest value of load transfer would be obtained for the 75-inch depth.
2. The rate of increase in load transfer with depth appears to be decreasing with depth.
3. The pile movement at which the maximum load transfer was developed increased with depth.

The above characteristics will be considered in the correlation with the stress-strain properties. The increase in load transfer with depth is the basis for the correlation with the stress-strain curves from triaxial tests of the sand. The increase in shear transfer with depth is assumed to be analogous to the increase in shear strength of the sand with increasing confining pressure. Correlation coefficients which relate s_x - z curves to stress-strain curves will be developed in the following section.

Correlation of Shear Transfer Curves with Stress-Strain Curves for the Sand

The correlation of the s_x - z curves with the stress-strain curves for the sand involves the determination of coefficients U_c , U_t , R_c , and R_t ,

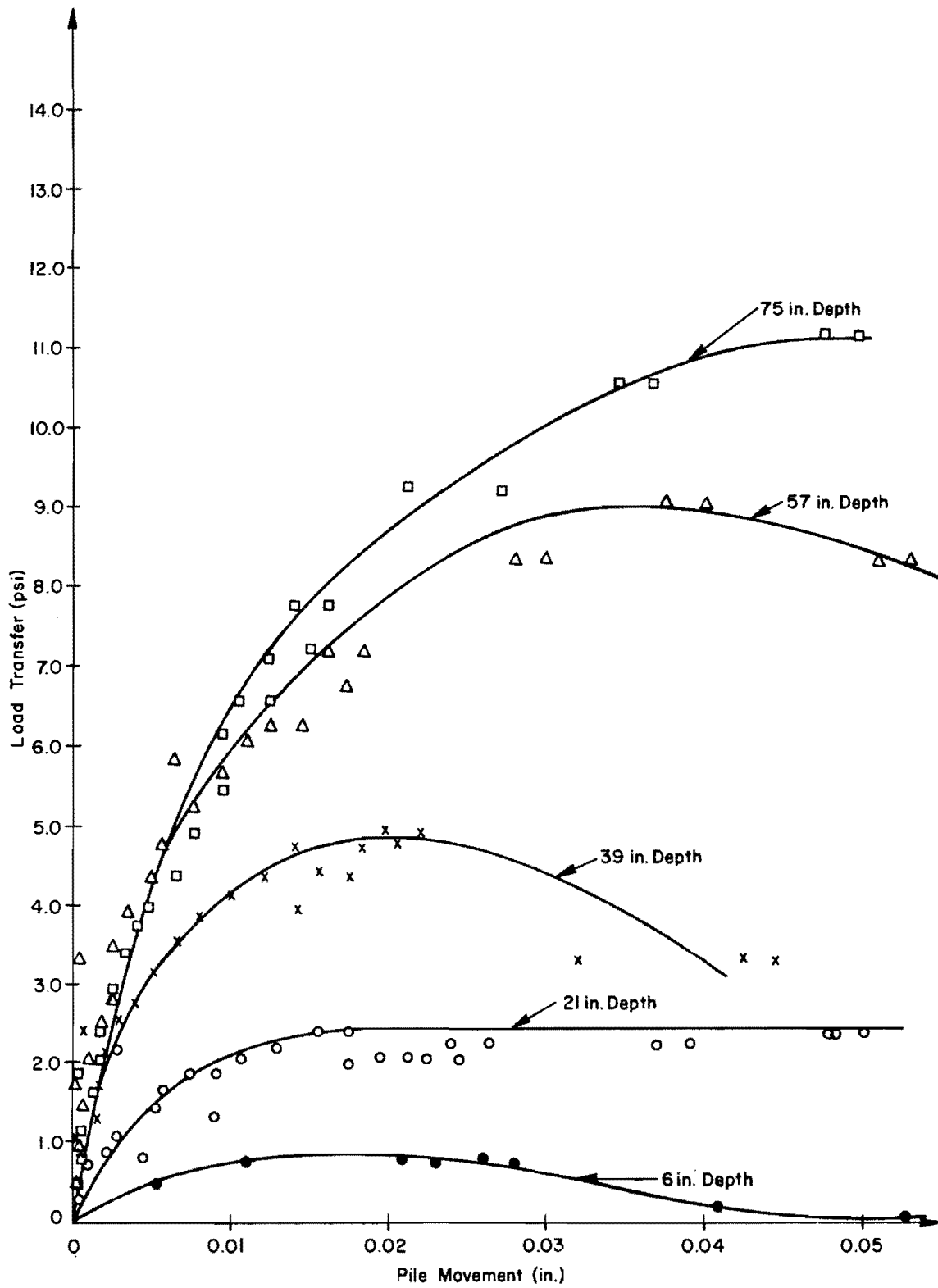


Fig. 5.7. Axial Load Transfer Curves for Pullout Test of Pile 1-A.

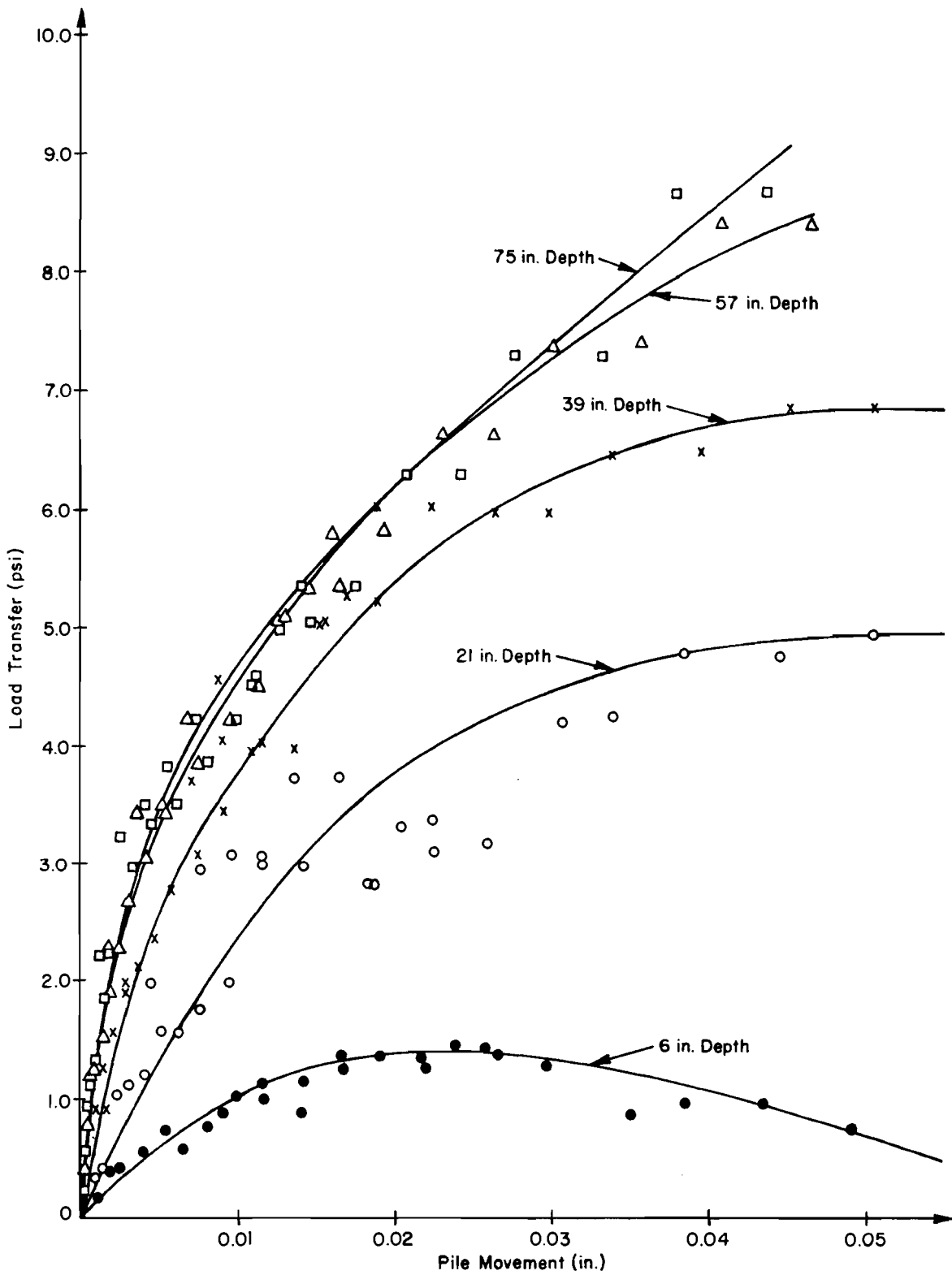


Fig. 5.8. Axial Load Transfer Curves for Compression Test of Pile 2-A.

as defined in Eqs. 5.14, 5.15, 5.20, and 5.21. These coefficients relate the s_x -z curves, illustrated in Figs. 5.7 and 5.8, to the stress-strain curves shown in Fig. 5.9. The procedure followed is outlined below.

1. For each s_x -z curve, compute the ratio of the maximum load transfer to the overburden pressure. This ratio is the definition of the skin-friction coefficient N as defined by Eqs. 5.8 and 5.9. Values are tabulated in Table 5.1.
2. Plot the values of N_c and N_t against depth as shown in Fig. 5.10. The dashed vertical line fits all the points for the pullout test and will be used to define the correlation factor U_t . For values of N_c , two equations were used to describe the variation with depth. The solid line is the best fit for the points. This line indicates a decrease in N_c with depth. However, a more practical approach may be to use a constant value, as defined by the dotted vertical line, for the top portion of the pile and to assume that the shear transfer is constant below a certain depth. The value of 5.3 is the average of the five values.
3. The value of angle of internal friction for the sand is equal to 44 degrees, and the values of U_t and U_c are computed as follows:

$$U_t = \frac{N_t}{\tan^2 (45 + \phi/2) - 1} = \frac{4.0}{4.545} = 0.88 \dots \dots (5.28)$$

$$U_{c1} = \frac{N_c}{\tan^2 (45 + \phi/2) - 1} = \frac{7.0 - 0.04x}{4.545} = 1.5 - 0.01x \dots (5.29)$$

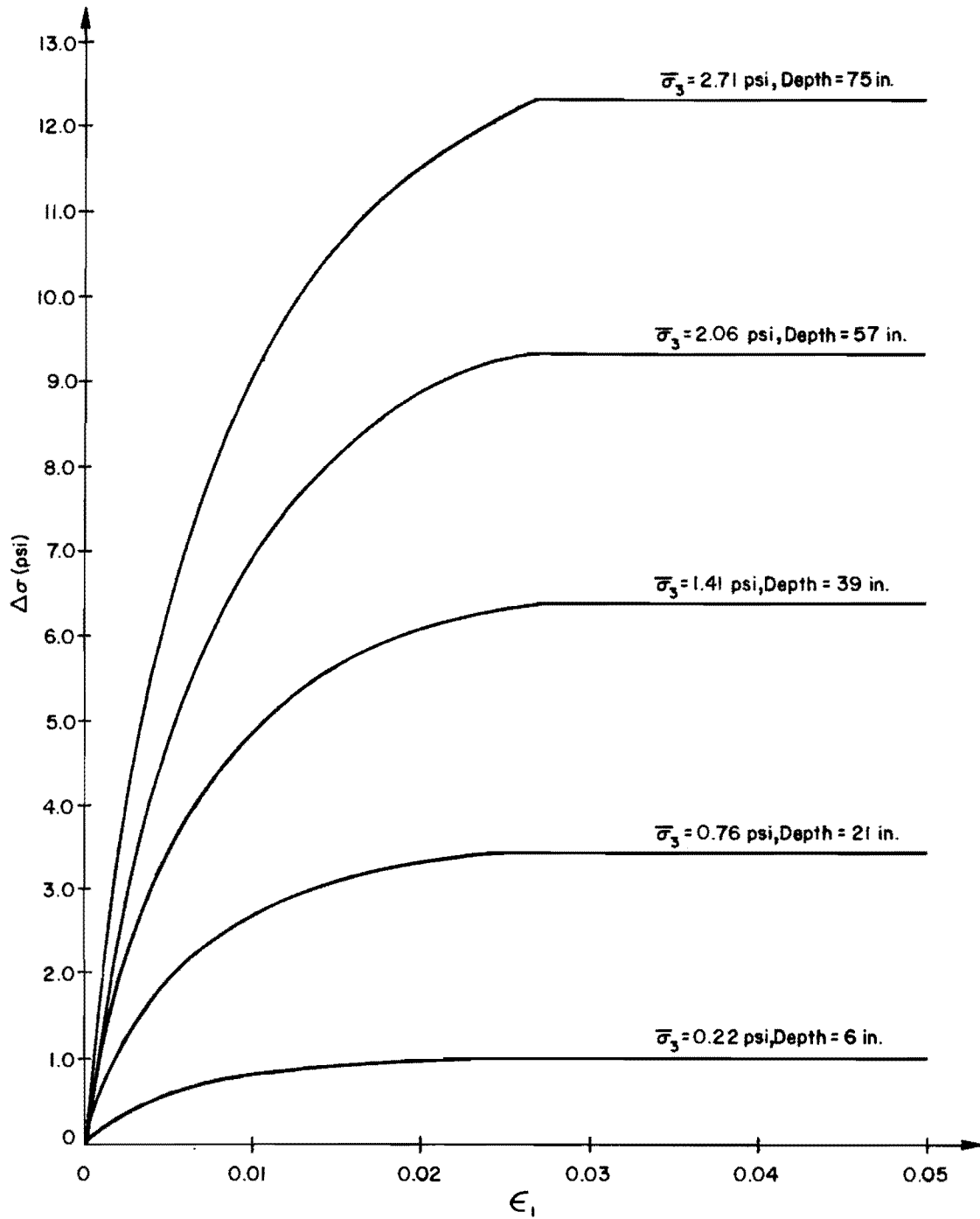


Fig. 5.9. Hyperbolic Stress-Strain Curves for Confining Stresses Corresponding to Overburden Pressure at Depths of s_x -z Curves.

TABLE 5.1. SKIN FRICTION COEFFICIENTS FROM TEST RESULTS

Depth (Inches)	Overburden Pressure (psi)	Maximum s_{xm}^c (psi)	N_c	Maximum s_{xm}^t (psi)	N_t
6	0.22	1.45	6.7	0.90	4.1
21	0.76	4.95	6.5	2.50	3.3
39	1.41	6.85	4.9	5.05	3.6
57	2.06	*9.40	4.6	9.05	4.4
75	2.71	*10.00	3.7	11.15	4.1

*Values obtained by visual extrapolation of the curves to maximum values.

TABLE 5.2. PILE MOVEMENT CORRELATION COEFFICIENTS FROM TEST RESULTS

Depth (Inches)	Movement z_c (Inches)	R_c	Movement z_t (Inches)	R_t
6	0.025	0.50	0.011	0.22
21	0.037	0.74	0.017	0.34
39	0.052	1.04	0.028	0.56
57	*0.060	1.20	0.042	0.84
75	-	-	0.050	1.00

*Values obtained by visual extrapolation of the curves to maximum values.

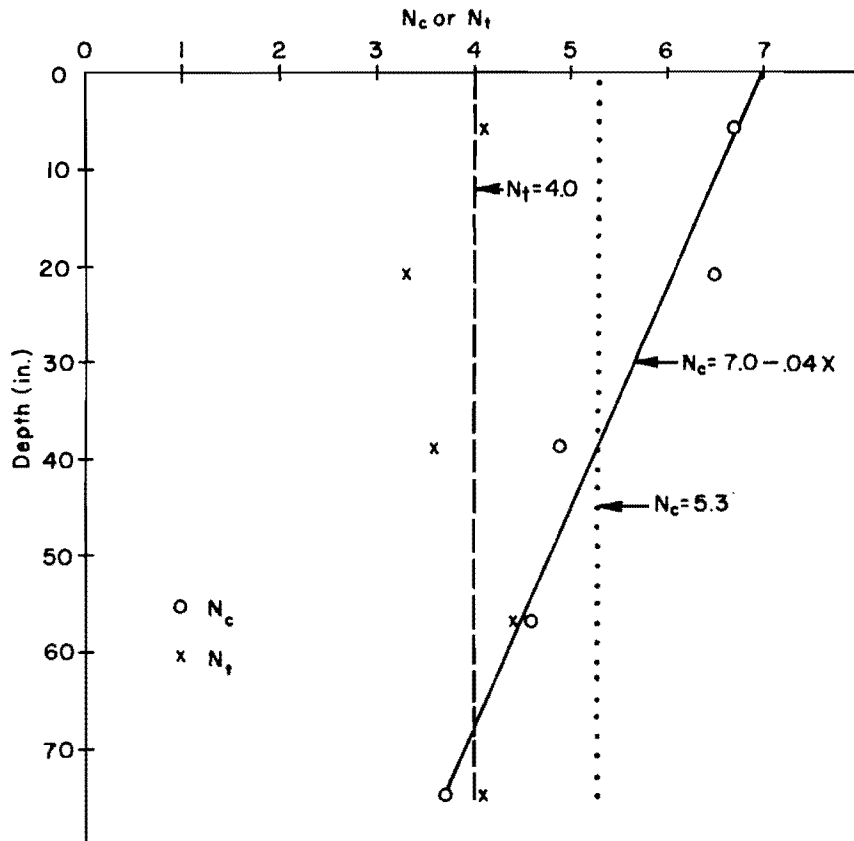


Fig. 5.10. Variation of Skin Friction Coefficients with Depth.

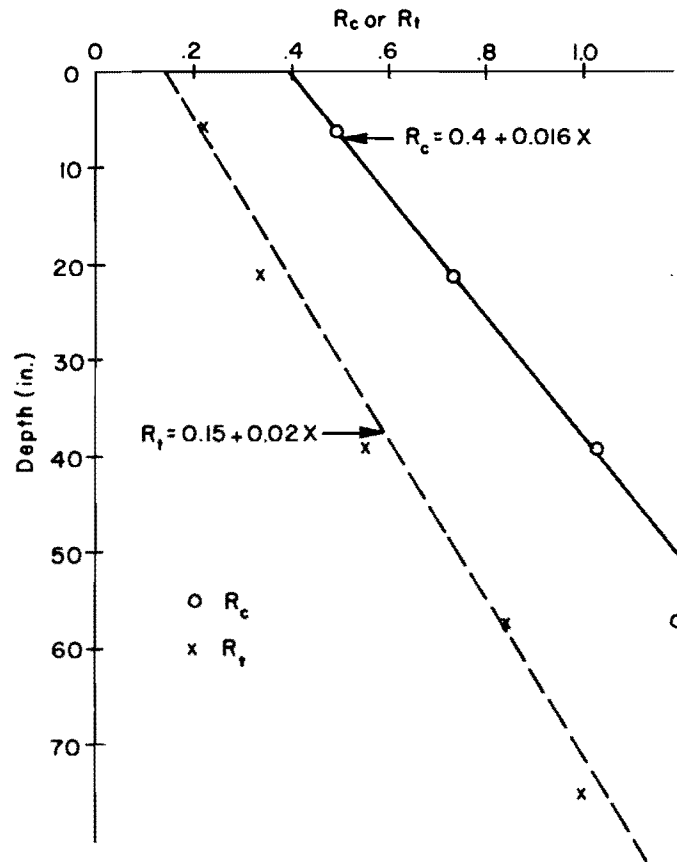


Fig. 5.11. Variation of Correlation Coefficients with Depth.

or

$$U_{c2} = \frac{5.3}{4.545} = 1.16 \dots \dots \dots (5.30)$$

4. From Fig. 5.9, it is observed that the maximum value of deviator stress is reached for an axial strain of about 0.025, for all confining pressures. From Figs. 5.7 and 5.8, it is observed that the maximum value of load transfer is developed for a pile movement which increases with depth. For each s_x -z curve, compute the ratio of pile movement at ultimate load transfer to the product of the axial strain (0.025) and the pile diameter (2.0 inches). This ratio is the definition of the correlation coefficient R as given by Eqs. 5.20 and 5.21. Values for the test results are tabulated in Table 5.2.

5. Plot the values of R_c and R_t against depth as shown in Fig. 5.11. The solid line fits the points from the compression test, and the dashed line fits the points from the pullout test. The equations for the straight lines define the correlation coefficients, and are written as

$$R_t = 0.15 + 0.012x \dots \dots \dots (5.31)$$

and

$$R_c = 0.4 + 0.016x \dots \dots \dots (5.32)$$

The coefficients U_t and R_t are multiplied by the values of $\Delta\sigma$ and ϵ_1 from the stress-strain curves, shown in Fig. 5.9, to generate

the predicted s_x -z curves illustrated by the dashed lines in Fig. 5.12. The measured curves from the test on pile 1-A are shown in Fig. 5.12 as solid lines. The coefficients U_{c1} , U_{c2} , and R_c are multiplied by values of $\Delta\sigma$ and ϵ_1 to generate the two sets of predicted s_x -z curves illustrated by the dashed lines in Fig. 5.13 and 5.14. The measured curves from the test on pile 2-A are shown in Figs. 5.13 and 5.14 as solid lines.

The comparison of the measured and predicted curves for pullout loading, as illustrated in Fig. 5.12, indicates that the correlation obtained was good for all curves. For compression loading the comparison, illustrated in Figs. 5.13 and 5.14, indicates that the correlation for the three upper curves is good. Complete curves are not available for the two lowest levels, but the trend of the curves seems to indicate that curves predicted using U_{c1} result in better approximations to the measured curves. Another justification for this contention is that the last increment of load applied, before the pile failed, would not have resulted in values for the two lower curves as large as those predicted using U_{c2} . In the final section the predicted s_x -z curves will be used to develop analytically a load-deformation curve for the top of the pile which will be compared with the measured curves. The criteria for describing the s_x -z curves will be modified to account for the differences due to density and method of installation, and the modified criteria applied to several field tests.

Development of Load-Deformation Curve for the Tip of the Pile

No provisions were made in the instrumentation of the piles to measure the load at the tip or the movement of the tip. Because of this, it

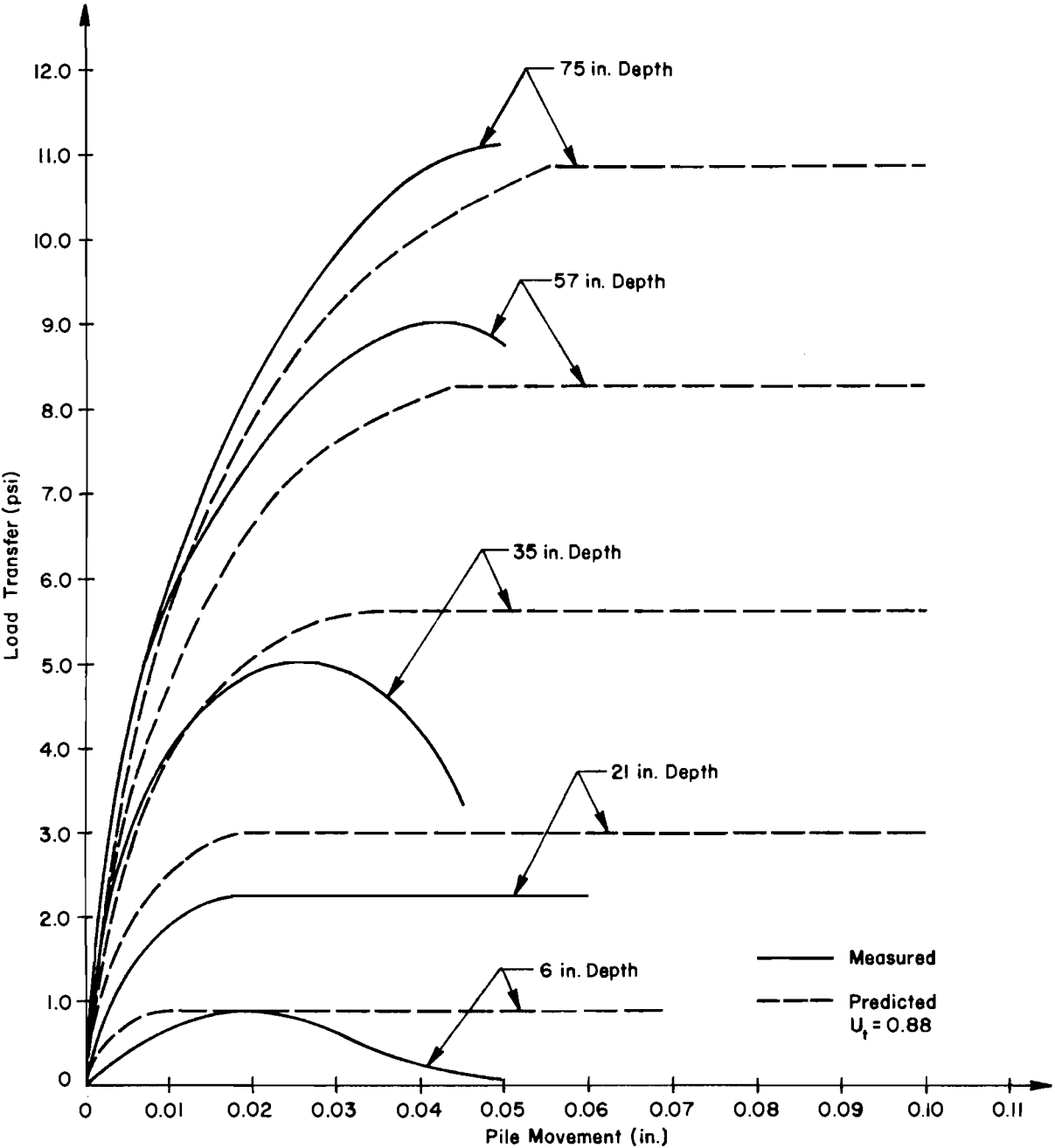


Fig. 5.12. Comparison of Measured and Predicted s_x -z Curves for Pullout Loading.

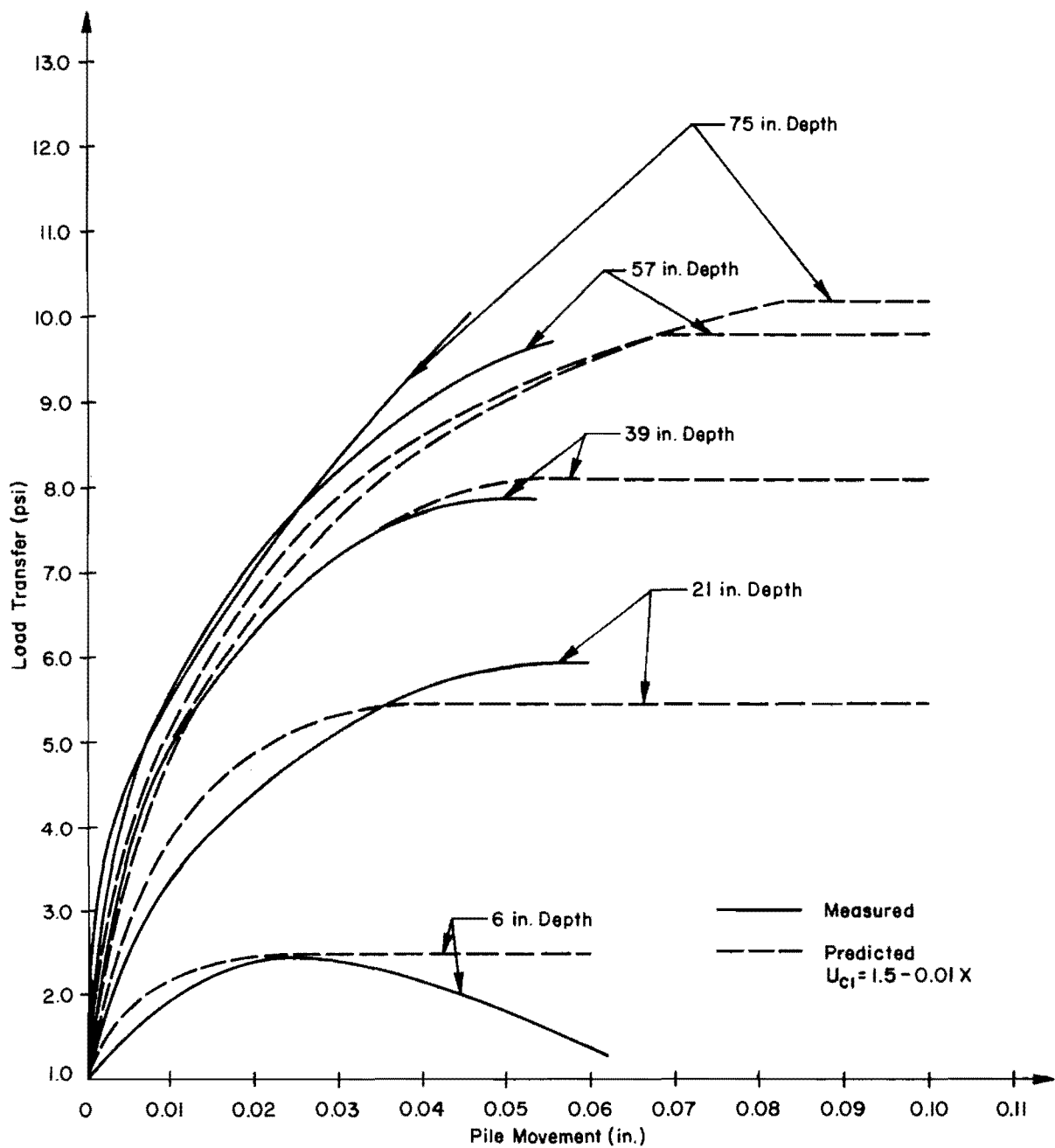


Fig. 5.13. Comparison of Measured and Predicted s_x -z Curves for Compression Loading.

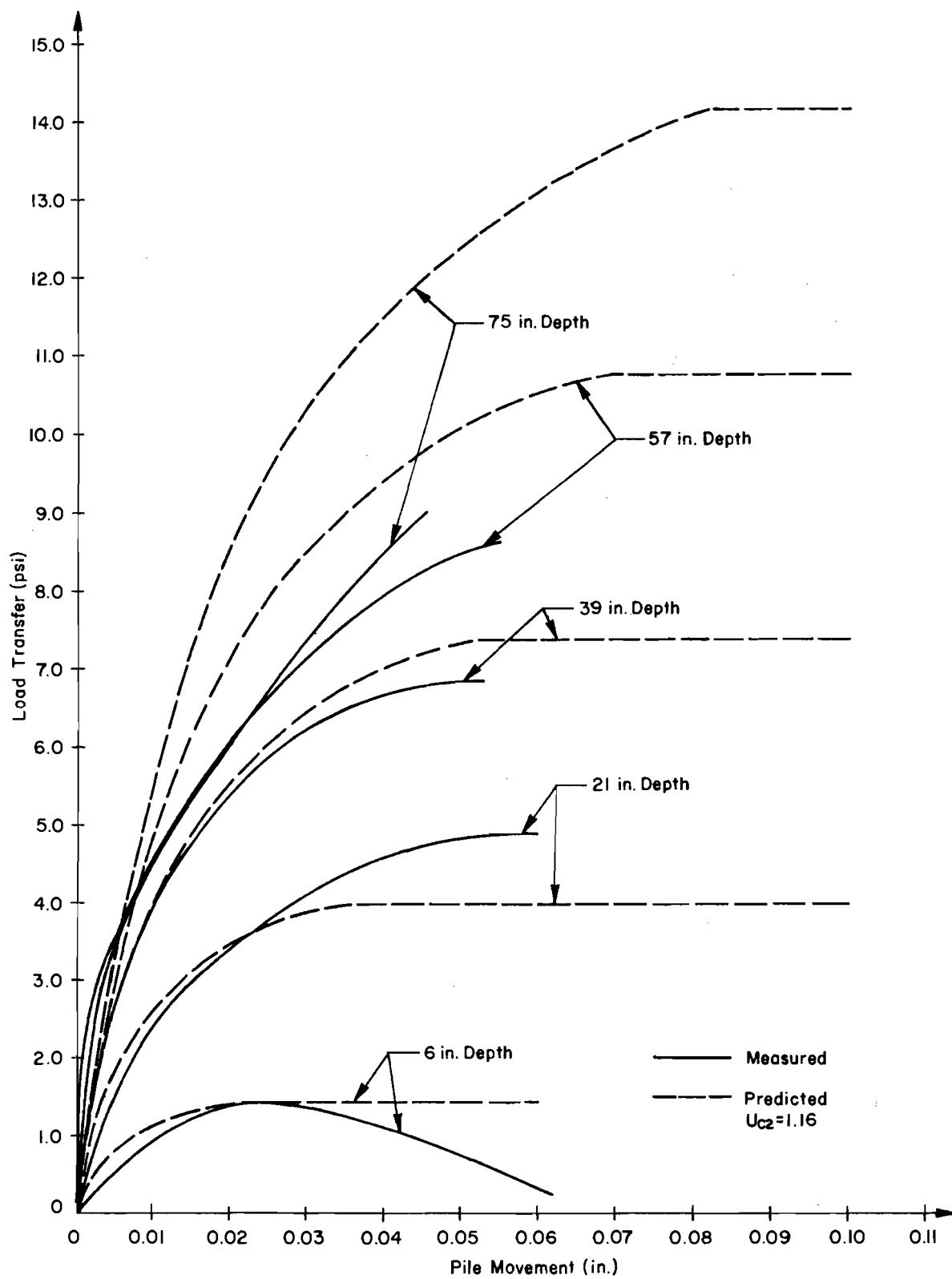


Fig. 5.14. Comparison of Measured and Predicted $s_x - z$ Curves for Compression Loading.

was necessary to utilize the measured load distribution for pile 2-A to approximate a tip load. The procedure followed was to extrapolate the load-distribution curve to the tip to approximate the tip load. This procedure is illustrated in Fig. 5.5 by the dashed lines. With the value of the tip load, from the extrapolation, the tip movement was calculated using the equation

$$z_B = z_5 - \frac{6(Q_5 + Q_B)}{AE} \dots \dots \dots (5.33)$$

This procedure was followed to generate the load-deformation curve for the tip illustrated in Fig. 5.15.

All available information indicates that a maximum tip load larger than the 160 pounds estimated should have been obtained, and that a movement larger than the approximately 0.025 inch should have been obtained for the development of the maximum tip load. The small value of ultimate tip load estimated and the sharp break in the load deformation curve at a load of 160 pounds are probably caused by the extrapolation procedure used rather than the occurrence of a bearing failure at the soil beneath the pile tip.

The load distribution curves were extrapolated to the tip with the same slope as the curve between locations four and five. This procedure may not have been valid because the arching of the sand near the pile tip may have caused an increase in the slope of the load-distribution curve near the tip and, thus, a decrease in the load transferred to the soil over the bottom 12 inches of the pile. For smaller loads the effect of the arching was probably small, so that the errors in the predicted tip

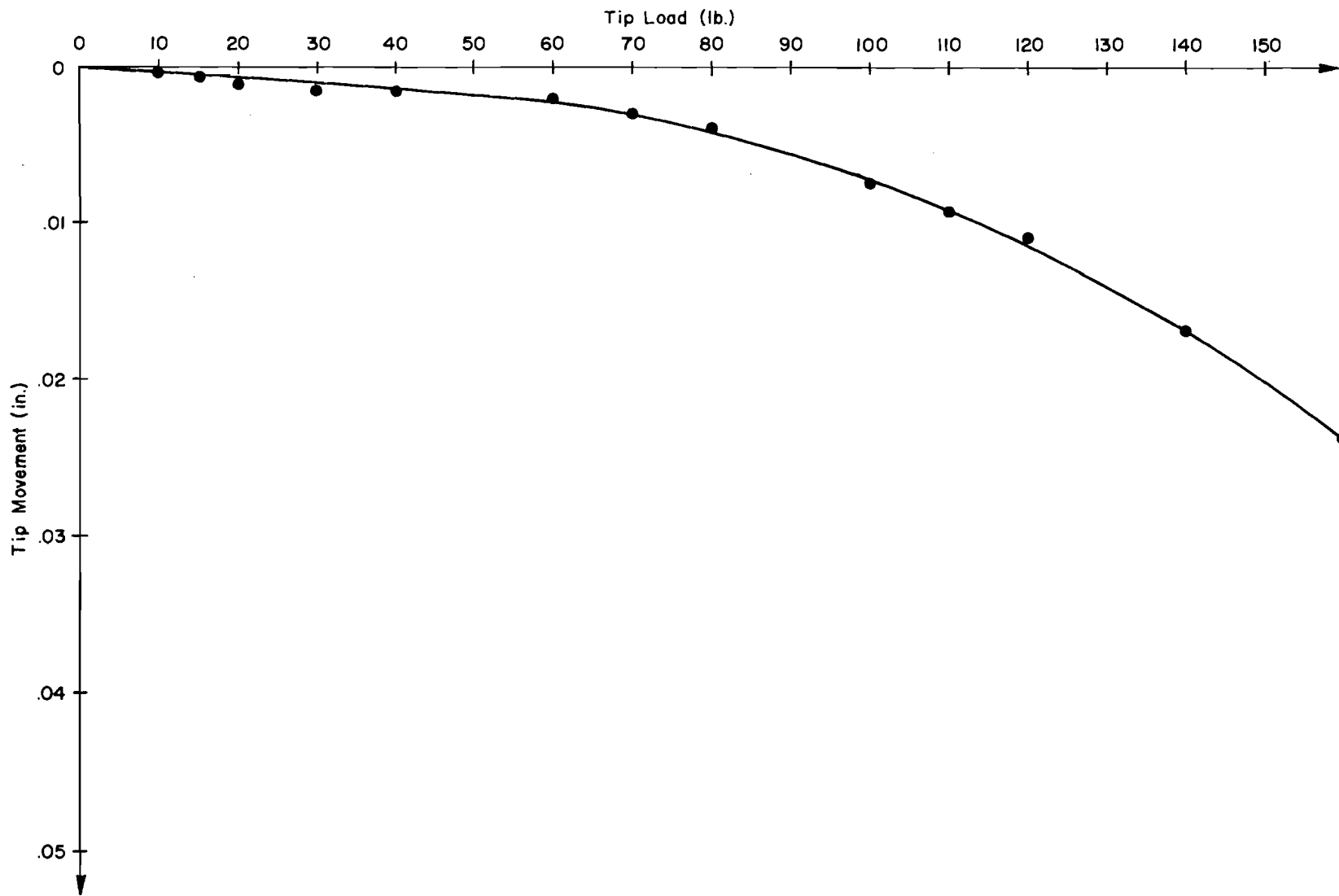


Fig. 5.15. Approximate Tip Load-Deformation Curve for Pile 2-A.

loads were small; but as the loads increased, the effect of the arching also increased, so that the errors in the predicted tip loads also increased. The arching of the sand near the pile tip combined with the inherent inaccuracies involved in visually extrapolating the curves, probably explain the small value of ultimate tip load estimated.

Because of the very approximate nature of the load-deformation behavior of the pile tip, and because the available data are limited to the results from one test, no attempt will be made to correlate the observed behavior with the properties of the sand. The load-deformation curve will be used, without modification, in the following section to predict analytically a load-deformation curve for the top of the piles, which will then be compared with the measured curve.

Comparisons of Computed and Measured Load-Deformation Curves

In this section load-deformation curves for compression and pullout loading of the test piles will be predicted analytically, using the proposed criteria for describing shear transfer-pile movement curves, and compared with measured curves. In addition, the criteria for describing the s_x - z curves will be used to predict load-deformation curves for three 4-inch diameter piles reported by Vesić (1964 and 1968). These piles had various lengths and were placed by driving or jacking into sand prepared with various densities. Based on the comparisons between the measured and predicted response of the piles, additional test data will be analyzed and an attempt made to develop a procedure for adjusting the proposed criteria to account for the observed

differences in shear transfer caused by the different methods of installation and different relative densities of the sand. The modified criteria will then be used to predict the behavior of a 12.75-inch diameter and a 16-inch diameter driven pile which will be compared with the measured behavior.

For the computation of the load-deformation curves for the tops of the piles, described in the preceding paragraph, the measured load-deformation curves for the pile tips were used. The computations were performed on a computer, and the procedure was essentially the same as described in Chapter II for solving the differential equations for an axially loaded pile. A computer program for performing the necessary computations is presented by Awoshika and Reese (1971).

Comparison for Two-inch Diameter Test Piles

Measured and predicted curves for compression loading of the test piles are shown in Fig. 5.16. The measured curve is an average curve that was computed from the curves for piles 2-A, 3-A, and 4-A. The curve for pile 6-A was omitted in computing the average curve for reasons mentioned previously.

In Fig. 5.16, it can be seen that the curve predicted using the s_x - z curves obtained with a correlation factor that varied with depth is a better approximation to the measured curve than the curve predicted using the s_x - z curves obtained with a constant correlation factor. The observed difference in the two predicted curves was expected, because there were differences in the s_x - z curves predicted using the two different correlation factors. The comparisons substantiate the contention

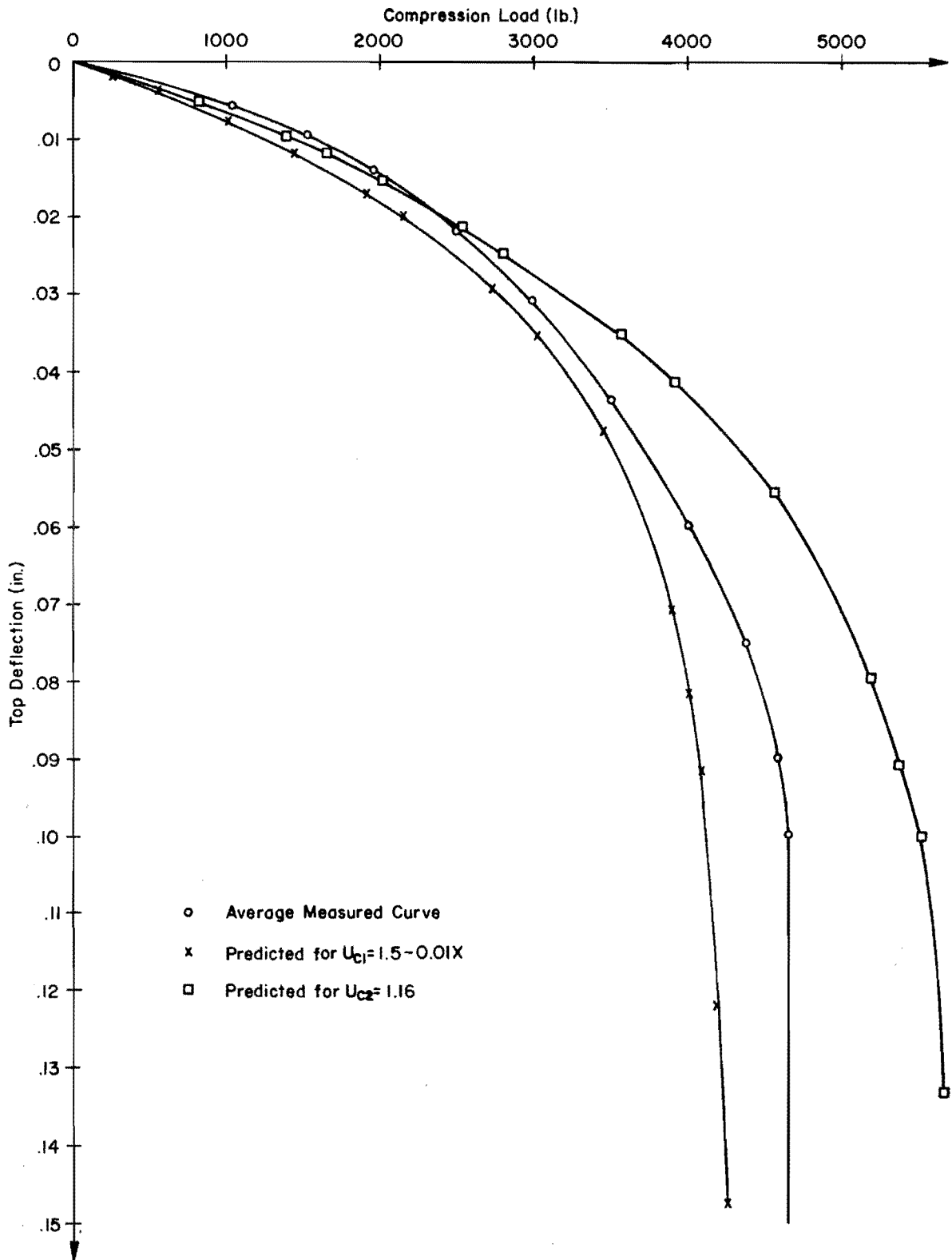


Fig. 5.16. Measured and Predicted Load-Deformation Curves for Compression Loading of the Test Piles.

that the shear transfer is not a linear function with depth, but that the rate of increase in shear transfer decreases with depth.

Measured and predicted curves for pullout loading are shown in Fig. 5.17. The measured curve is an average curve that was computed from the curves for piles 1-A and 5-A. The good agreement between the curves was expected since the agreement between the measured and predicted s_x - z curves was good, and it was not necessary to make any approximations for the tip load-deformation behavior.

The comparisons of the measured and predicted behavior of the two tests indicate that the computation procedure gives reasonable results; however, the applicability of the proposed criteria to other conditions is as yet unproved. In order to check the applicability of the proposed criteria for s_x - z curves for other conditions, studies of other experiments reported in the literature will be presented in the following section.

Comparisons for Four-inch Diameter Piles

Vesic' (1964 and 1968) conducted experiments on a number of four-inch diameter piles that were driven and jacked into sand prepared at various relative densities. The driven piles were steel and the jacked piles were aluminum. Instrumentation was provided for measuring the shear transfer, tip load, and the movement of the tip. The sand was a Chattahoochee River sand and has been described in detail by Vesic' (1963).

Load-deformation curves for three piles reported by Vesic' will be compared with computed curves. Values of ultimate shear transfer from additional tests reported by Vesic' will be used to develop a tentative procedure for adjusting the criteria for generating s_x - z curves.

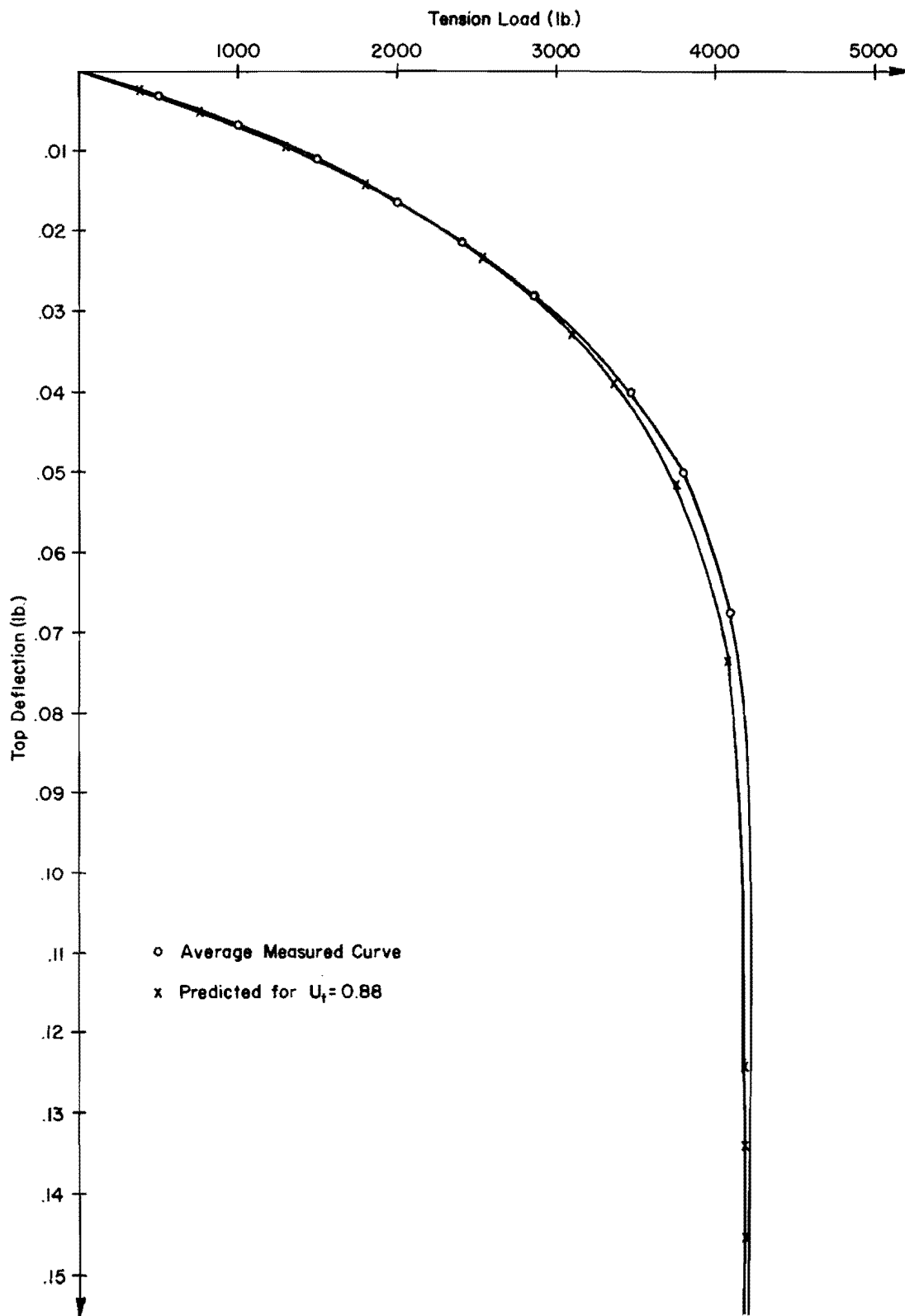


Fig. 5.17. Measured and Predicted Load-Deformation Curves for Tension Loading of the Test Piles.

No stress-strain curves were given for the Chattahoochee River sand, so that it was necessary to use the equations for the hyperbolas developed in Chapter IV for the Colorado River sand in order to approximate stress-strain curves. Values of angle of internal friction were given by Vesic' for various relative densities, and these values were used in Eqs. 4.6 and 4.9 to approximate stress-strain curves. All of the piles were loaded in compression and Eqs. 5.29 and 5.32 were used to define correlation coefficients for relating s_x -z curves to stress-strain curves. Shear stress-pile movement curves were generated and used with measured load-deformation curves for the tip of the piles to predict load-deformation curves for the tops of the piles.

Measured tip load-deformation curves are used rather than computed curves. This was done because available computational procedure will give only approximate tip load-deformation curves. Since a comparison of the measured and computed shear transfer is of primary importance, measured curves were used so that any errors in computing the tip behavior could be eliminated.

The first analysis was made for a pile 120 inches long, driven into a sand prepared with a relative density of 85 per cent. In order to differentiate between the several tests, this test will be referred to as test G-36, which was the designation given by Vesic'. The sand was placed and the pile driven and tested with the sand in an air-dried condition. The dry density of the sand was 98.2 pcf and the angle of internal friction given as 45 degrees. The measured and the predicted load-deformation curves are shown in Fig. 5.18. The predicted curve is the curve designated without adjustment, and it is noted that there

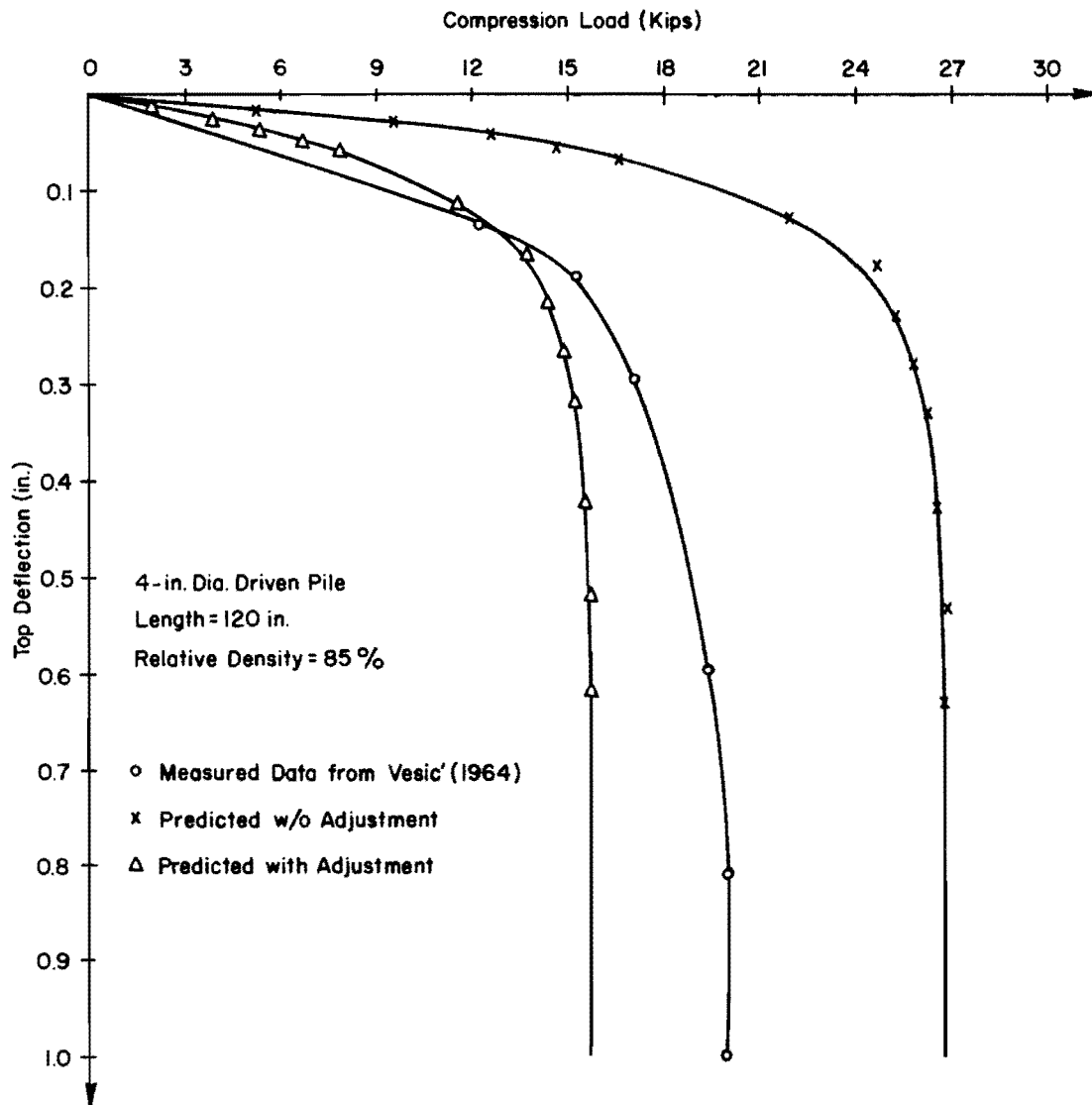


Fig. 5.18. Measured and Predicted Load-Deflection Curves for Test G-36.

is considerable difference between the measured and predicted curves. It is also noted that the predicted curve is unconservative.

The second test analyzed was for a pile 60 inches long jacked into a sand prepared with a relative density of 74 per cent. The test will be referred to as test P-13. The sand was placed and the pile jacked in place and tested with the sand in an air-dried condition. The dry density of the sand was 95.0 pcf and the angle of internal friction given was 43 degrees. The measured and predicted load-deformation curves for the top of the pile are plotted in Fig. 5.19. The predicted curve is the curve designated without adjustment, and it can be seen that there is considerable difference between the two curves. It is also noted that the predicted curve is unconservative.

The third test analyzed was for a pile 60 inches long jacked into a sand prepared with a relative density of 56 per cent. The test will be referred to as test S-11. The sand was placed in an air-dried condition, but prior to placing and loading the pile, the sand was submerged. The dry density of the sand was 90.8 pcf and the angle of internal friction given as 38 degrees. The measured and predicted load-deformation curves for the top of the pile are shown in Fig. 5.20. The predicted curve is the curve designated without adjustment, and it can be seen that the curves are considerably different. It is also noted that the predicted curve is unconservative.

In all three tests considered above, the ultimate predicted capacity of the pile was larger than the measured ultimate capacity. Measured loads on the tips of the piles were used for the computations, so that the differences in the ultimate load can be attributed to the prediction of maximum skin loads which were larger than the actual skin loads. The

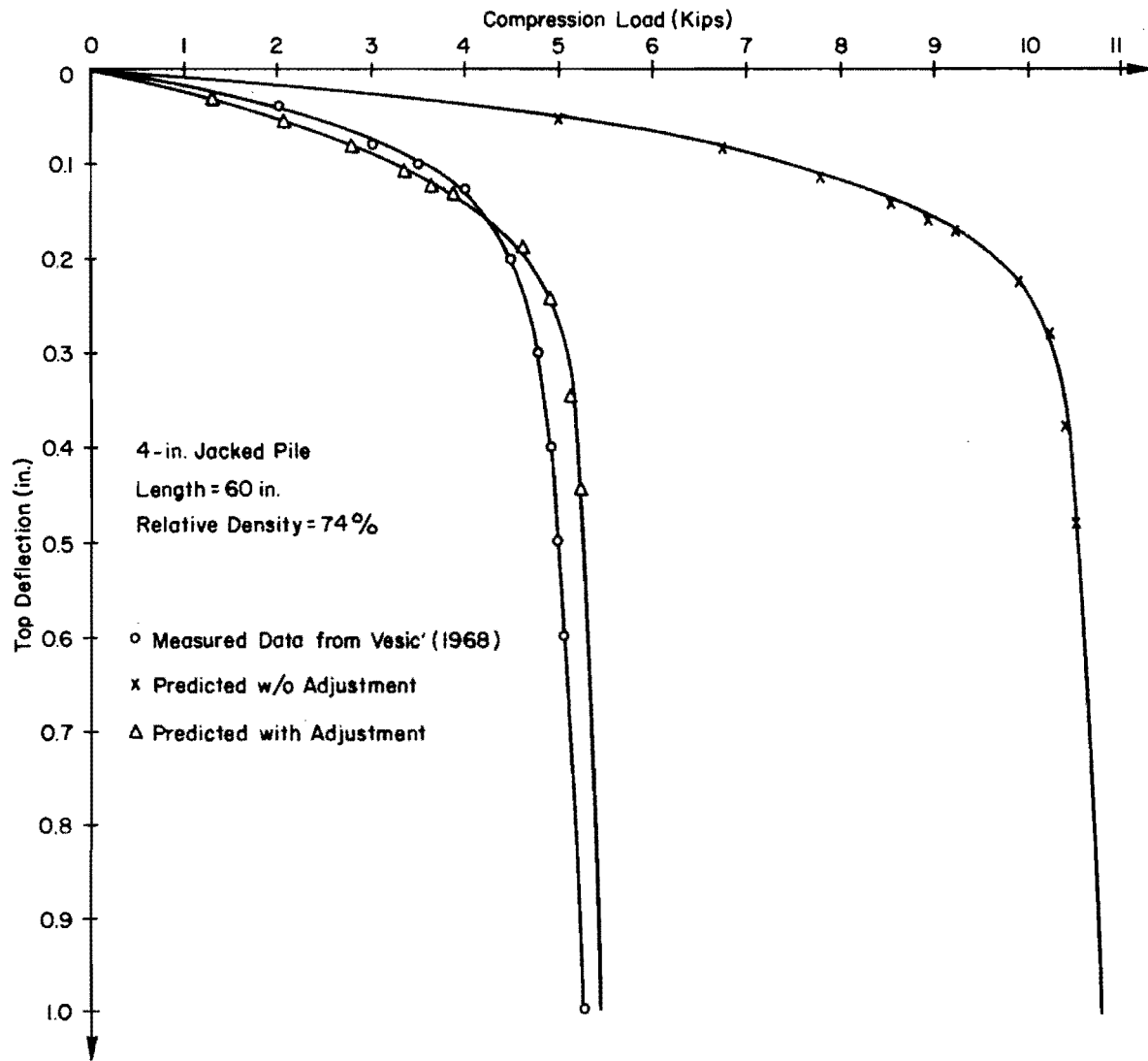


Fig. 5.19. Measured and Predicted Load-Deflection Curves for Test P-13.

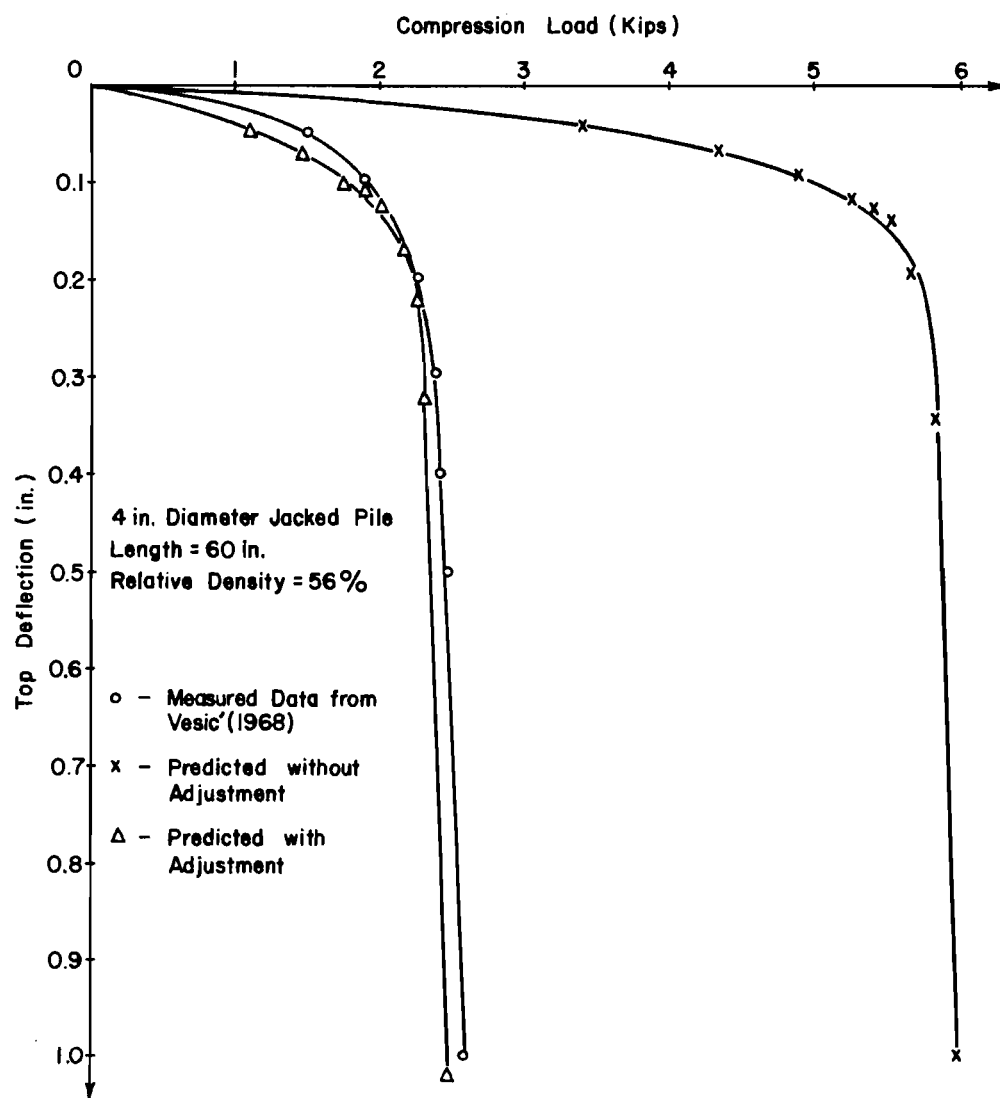


Fig. 5.20. Measured and Predicted Load-Deflection Curves for Test S-11.

criteria for describing the shear transfer was based on the results of the tests on the two-inch diameter piles, and it is felt that the method used to install the piles caused the observed differences in the measured and predicted ultimate skin loads.

The method used in installing the two-inch diameter test piles was to position the piles in the test pit and then fill the sand around the piles. The sand was placed in eight-inch layers and each layer was heavily compacted. The walls of the pit were rigid and, because of the large compactive effort, high lateral stresses resulted. Thus, the coefficient of lateral earth pressure was very high. This phenomena has been observed by Mackey and Kirk (1968). They measured coefficients of lateral earth pressure as high as 3.4 for sand compacted in layers with an electric hammer. Lambe and Whitman (1968) state that the coefficient of lateral earth pressure may approach the passive coefficient if the compactive effort is large. It is felt that the high lateral stresses which existed in the sand for the tests of the two-inch diameter piles was the principal reason for the overestimation of the skin loads for the driven and jacked piles.

For practical problems, piles will be driven, vibrated, bored, or cast-in-place so that the lateral pressure on a pile will be different from the lateral pressure on the test piles. As an example, driving a pile into a sand may densify the sand around the pile, but the vibrations may also cause a downward and outward movement of the sand grains. The movement of the sand grains may cause arching of the sand around the pile. Thus, there is a possibility that lateral pressures against the pile will be quite small. The magnitude of the arching will depend on the initial relative density of the sand; thus, the shear transfer will also be a

function of the relative density of the sand. Because arching could produce a random variation in lateral earth pressure against a pile, shear transfer would not likely be a linear function of depth if arching is present.

To investigate the possible influence of the method of installing piles in sand with various relative densities, additional test data presented by Vesic' (1964 and 1968) were utilized. The data will be used to formulate a procedure for adjusting the criteria developed for defining shear transfer curves so that the modified criteria will be applicable for piles that are driven or pushed into sands with various relative densities. The procedure employed will be strictly empirical, and will be based on a limited number of tests. Therefore, the resulting procedure should be regarded as an attempt to check the validity of the proposed method for defining s_x -z curves rather than as a general procedure that could be strongly recommended for use for a wide variety of problems.

The procedure employed was to modify the correlation coefficients used to relate the deviator stress for a triaxial test to the shear transfer. No modification was applied to the correlation coefficients that are used to relate the axial strain for a triaxial test to the pile movement, because the predicted deflections for the three tests considered were reasonable approximations to the measured deflections.

The data presented by Vesic' (1964 and 1968) consisted of the measured maximum point resistance and skin load for a number of 4-inch diameter piles that were driven and jacked into sand beds prepared with various relative densities. The length of the piles varied from 20

inches to 120 inches. To develop adjustment factors, the first step was to compute the ultimate skin load for the piles, presented by Vesić, using an equation for the ultimate shear transfer. The equation for ultimate shear transfer was obtained by combining Eqs. 4.6 and 5.29. The resulting equation is written as

$$s_{xm}^c = (7.0 - 0.04x) \bar{\gamma}_x \dots \dots \dots (5.34)$$

The ultimate skin load is found by integrating Eq. 5.34 over the outer area of the pile. The integral is written as

$$F_s = \pi D \int_0^L (7.0\bar{\gamma}_x - 0.04\bar{\gamma}_x^2) dx \dots \dots \dots (5.35)$$

where

F_s = ultimate skin load

L = pile length.

The second step involved the calculation of the ratios of the computed skin loads to the measured skin loads. The ratios calculated for the various tests are tabulated in Table 5.3. The ratios computed are plotted against relative density in Fig. 6.21. There is considerable scatter in the points but the trend appears to be for higher ratios for lower relative densities. The straight line was drawn as an upper bound for all but one point from the tests of the driven piles. Values of the ratio obtained from the line will be used to modify the correlation coefficients developed from the tests of the buried 2-inch diameter piles.

TABLE 5.3. RATIO OF COMPUTED TO MEASURED
ULTIMATE SKIN LOAD

Test Number	Installation Procedure	Relative Density of sand (%)	Ratio
G-11	Driven	36	3.6
G-12	Driven	30	7.6
G-13	Driven	37	14.1
G-14	Driven	30	11.0
G-15	Driven	39	10.7
G-16	Driven	33	11.6
G-21	Driven	48	4.0
G-22	Driven	60	5.0
G-23	Driven	64	7.4
G-24	Driven	67	6.9
G-25	Driven	62	6.9
G-26	Driven	52	8.2
G-31	Driven	78	6.7
G-32	Driven	81	2.0
G-33	Driven	81	2.1
G-34	Driven	82	2.0
G-35	Driven	86	2.1
G-36	Driven	85	1.7
P-12	Jacked	64	9.0
P-13	Jacked	74	6.9
P-14	Jacked	77	7.9
S-11	Jacked	56	8.0

Measured data from Vesic' (1964 and 1968)

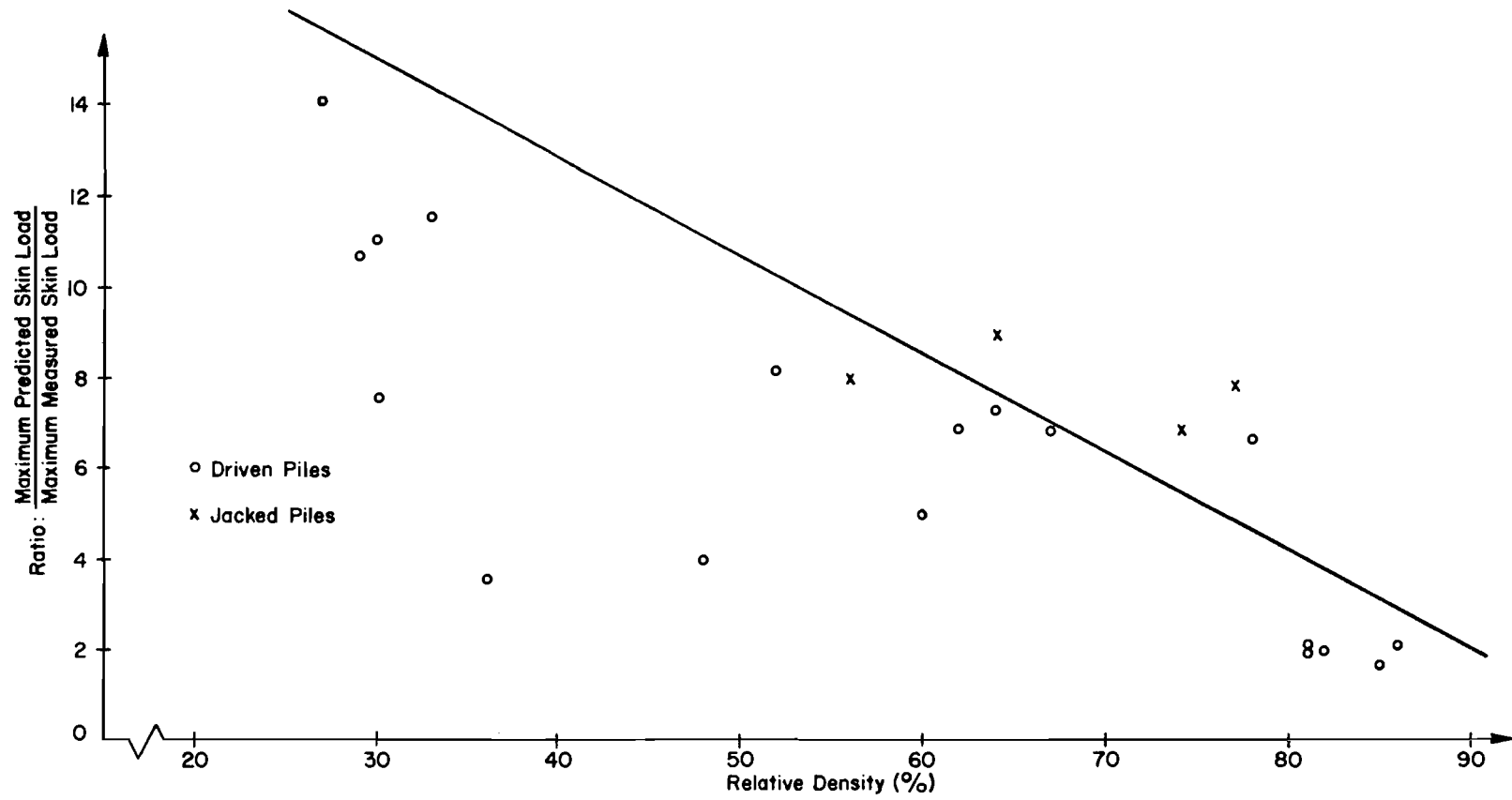


Fig. 5.21. Correction Factor Versus Relative Density.

Since the line is an upper bound for the points from the tests of the driven piles, the resulting correlation coefficient should be conservative.

As an example of the use of Fig. 5.21 to adjust the correlation coefficients, consider test G.36. The correlation coefficient used earlier to relate the shear transfer to deviator stress was obtained from Eq. 5.29 and may be written as

$$U_c = \frac{7.0 - 0.4x}{\tan^2(45 + \phi/2) - 1} = \frac{7.0 - 0.04x}{4.82} = 1.45 - 0.008x \dots \dots \dots (5.36)$$

The relative density of the sand was 85 per cent and the ratio obtained from the straight line in Fig. 5.21 is 3.2. Therefore, dividing Eq. 5.36 by 3.2 adjusts the correlation coefficient to account for the effects of driving the pile into the particular sand. The modified coefficient is written as

$$U_{cm} = \frac{1.45 - 0.008x}{3.2} = 0.45 - 0.0025x \dots \dots \dots (5.37)$$

The modified correlation coefficient was used to generate s_x -z curves, which were then used to compute a load-deformation curve for the top of the pile. The computed curve is plotted in Fig. 5.18 and is designated as the curve that has been adjusted. It can be seen that the curve computed using the modified coefficients is a better approximation to the measured curve than is the curve computed using the original coefficient. It is also noted that the estimate is conservative. The modification procedure was applied to tests P-13 and S-11 and the computed

load-deformation curves plotted in Figs. 5.19 and 5.20. For both of the tests the agreement between the measured and computed curves is very good.

When the proposed criteria for describing the s_x -z curves is modified to account for the influence of driving the pile, the resulting load-deformation curves are reasonable approximations of the measured curves. Good agreement was expected because the results compared were used to develop the adjustment factors. In the following section the procedure will be applied to four field tests of piles with diameters of 12.75 and 16 inches.

Comparisons for Field Tests

Field test data were obtained from a report by Fruco and Associates (1964). This report contains data from pile loading tests conducted for the design of a lock and dam on the Arkansas River. The test site consisted of a medium-to-fine silty sand below the water table. The average submerged unit weight of the sand was given as 63 pcf and the average angle of internal friction given as 32 degrees. Penetration tests were run and the average number of blows per foot was 27. Based on the standard penetration tests and curves presented by Gibbs and Holtz (1957), it was estimated that the relative density of the sand was between 70 and 80 per cent.

The piles considered were 12.75 and 16 inches in diameter, and had a length of 53 feet. Instrumentation was provided for measuring the loads and movements of the tips of the piles. Both size piles were loaded in compression and tension.

Stress-strain curves were not available for the sand, so that it was necessary to use Eqs. 4.6 and 4.9, developed for the Colorado River

sand, to approximate stress-strain curves. For the piles loaded in compression, Eq. 5.30 was used to define a correlation coefficient for relating deviator stress to shear transfer. For the piles loaded in tension, Eq. 5.28 was used to define the correlation coefficient. Equations 5.31 and 5.32 were used to define correlation coefficients for relating axial strain to pile movement. The use of Eqs. 5.28 and 5.30, which give the correlation coefficient as a constant, indicates that the ultimate shear stress transferred to the soil increases linearly with depth. However, as has been discussed previously, experimental data indicate that the rate of increase in shear transfer usually decreases with depth. Equation 5.30 reflects the nonlinear change in shear transfer with depth, but the expression was developed for the small piles and it is not applicable to the larger piles being considered. Therefore, it was necessary to use the simpler expressions for the correlation coefficients, and to approximate the variation of shear transfer with depth. Most experimental data indicate that the variation of shear transfer with depth is a function of the pile diameter. Vesic' (1970) states that the increase in shear transfer with depth is linear for depth not exceeding ten pile diameters, and that below a depth of approximately twenty pile diameters the shear transfer becomes nearly constant. These conclusions were based on the results of tests on an 18-inch diameter pile driven into a dense sand. For the 12.75- and 16-inch diameter pile studied, it was assumed that all the shear transfer-pile movement curves were identical below a depth of fifteen pile diameters.

The procedure employed was to generate s_x - z curves from the ground surface to a depth of fifteen pile diameters, from stress-strain curves given by Eqs. 4.6 and 4.9. Correlation coefficients for relating shear stress to deviator stress were defined by dividing values obtained from Eqs. 5.28 and 5.30 by factors obtained from Fig. 5.21. A value of relative density of 75 per cent was used, which resulted in a correction factor of 5.3. Correlation coefficients for relating pile movement to axial strain were given by Eqs. 5.31 and 5.32, and these factors were used without modification. The s_x - z curve for a depth of 15 pile diameters was used for all points below this depth. Predicted shear transfer curves and measured load-deflection curves for the tips of the piles were used to compute load-deformation curves for the top of the piles.

The first test analyzed was the compression loading of a 12.75-inch diameter pile. Computed and measured load-deflection curves for the top of the pile are shown in Fig. 5.22. It can be seen that the predicted curve is conservative, and that the shapes of the two curves are similar. The ultimate tip load measured was 90 kips so that the ratio of the ultimate measured skin load to the ultimate computed skin load is approximately 1.8.

The second test analyzed was the compression loading of a 16-inch diameter pile. The computed and measured load-deflection curves for the top of the pile are shown in Fig. 5.23. It can be seen that the predicted curve is conservative, and that the shapes of the two curves are similar. The ultimate tip load was 150 kips so that the ratio of the ultimate measured skin load and the ultimate computed skin load is approximately 1.5.

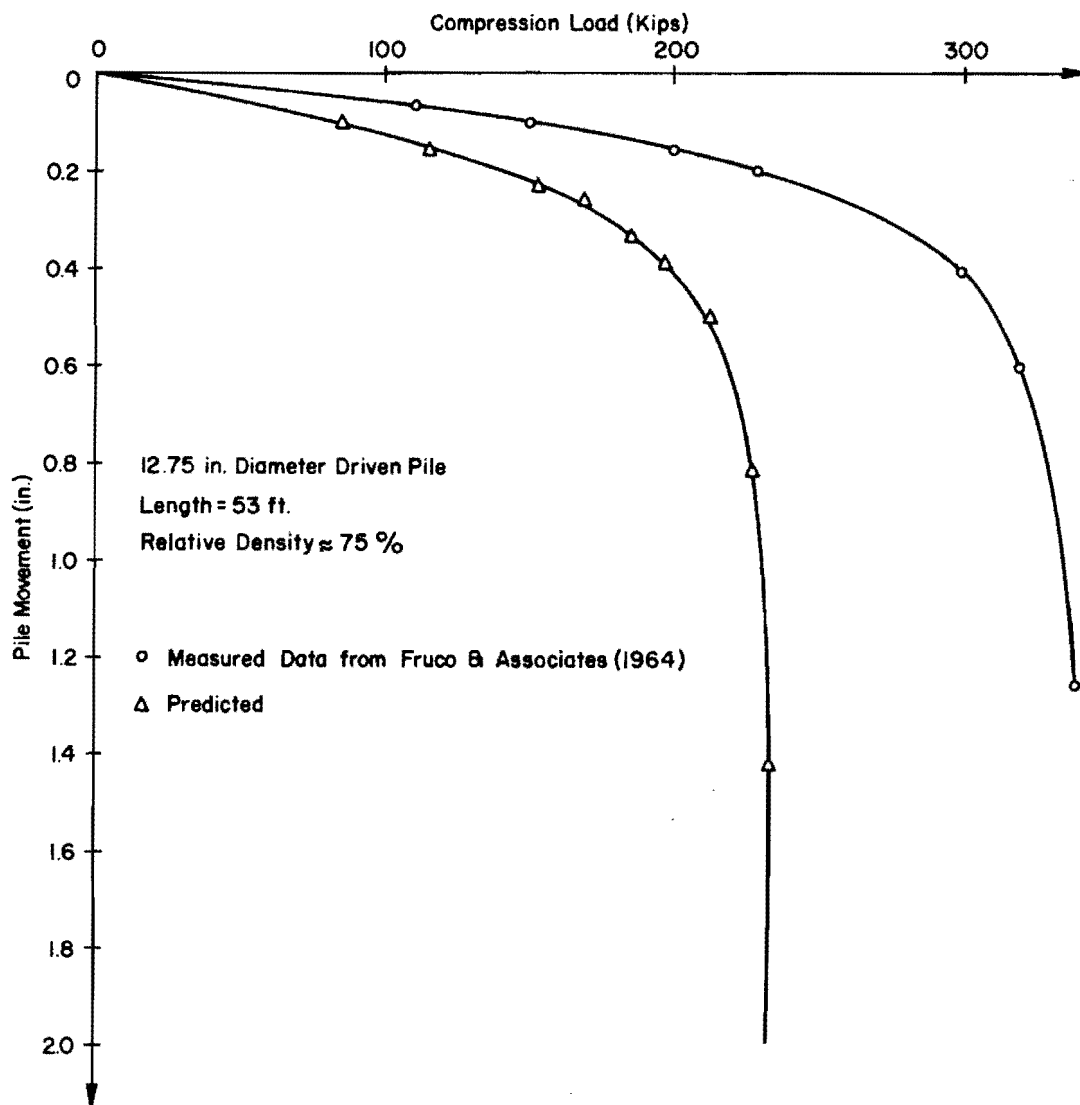


Fig. 5.22. Measured and Predicted Load-Deflection Curves for Compression Loading of a 12.75-inch Diameter Pile.

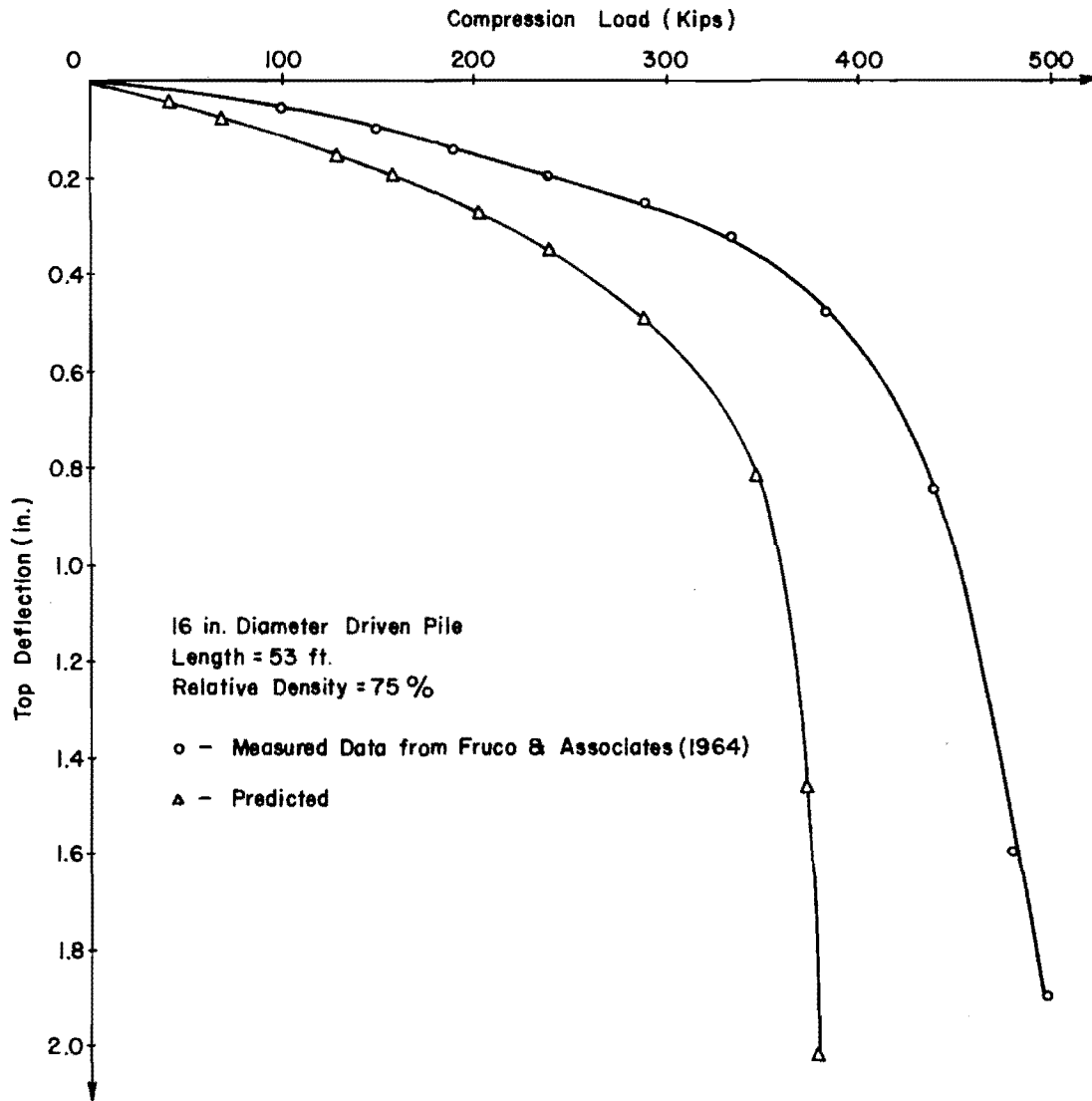


Fig. 5.23. Measured and Predicted Load-Deflection Curves for Compression Loading of a 16-inch Diameter Pile.

The third test analyzed was the tension loading of a 12.75-inch diameter pile. The computed and measured load-deflection curves for the top of the pile are shown in Fig. 5.24. It can be seen that the predicted curve is conservative, and that the shape of the predicted curve is a reasonable approximation of the shape of the measured curve. The ratio of the calculated and predicted ultimate load is about 1.6.

The fourth test analyzed was the tension loading of a 16-inch diameter pile. The computed and measured load-deflection curves for the top of the pile are shown in Fig. 5.25. It can be seen that the predicted curve is conservative, and that the shape of the predicted curve is a reasonable approximation of the shape of the measured curve. The ratio of the computed and predicted ultimate load is about 1.3.

Summary of Criteria for Describing Axial Load Transfer

For compression and tension loading of the 12.75- and 16-inch diameter piles, the computed load-deflection curves for the tops of the piles were conservative estimates of the measured curves. The reasonable agreement between the measured and computed curves for the field test suggests that the proposed procedure for describing s_x -z curves may be used with some degree of confidence for a practical field problem. When the differences between the measured load distribution curves for the test pile illustrated in Fig. 5.3 are considered, the degree of accuracy obtained for the computed curves appears to be reasonably good. However, the method is only tentative because only a limited number of checks have been made.

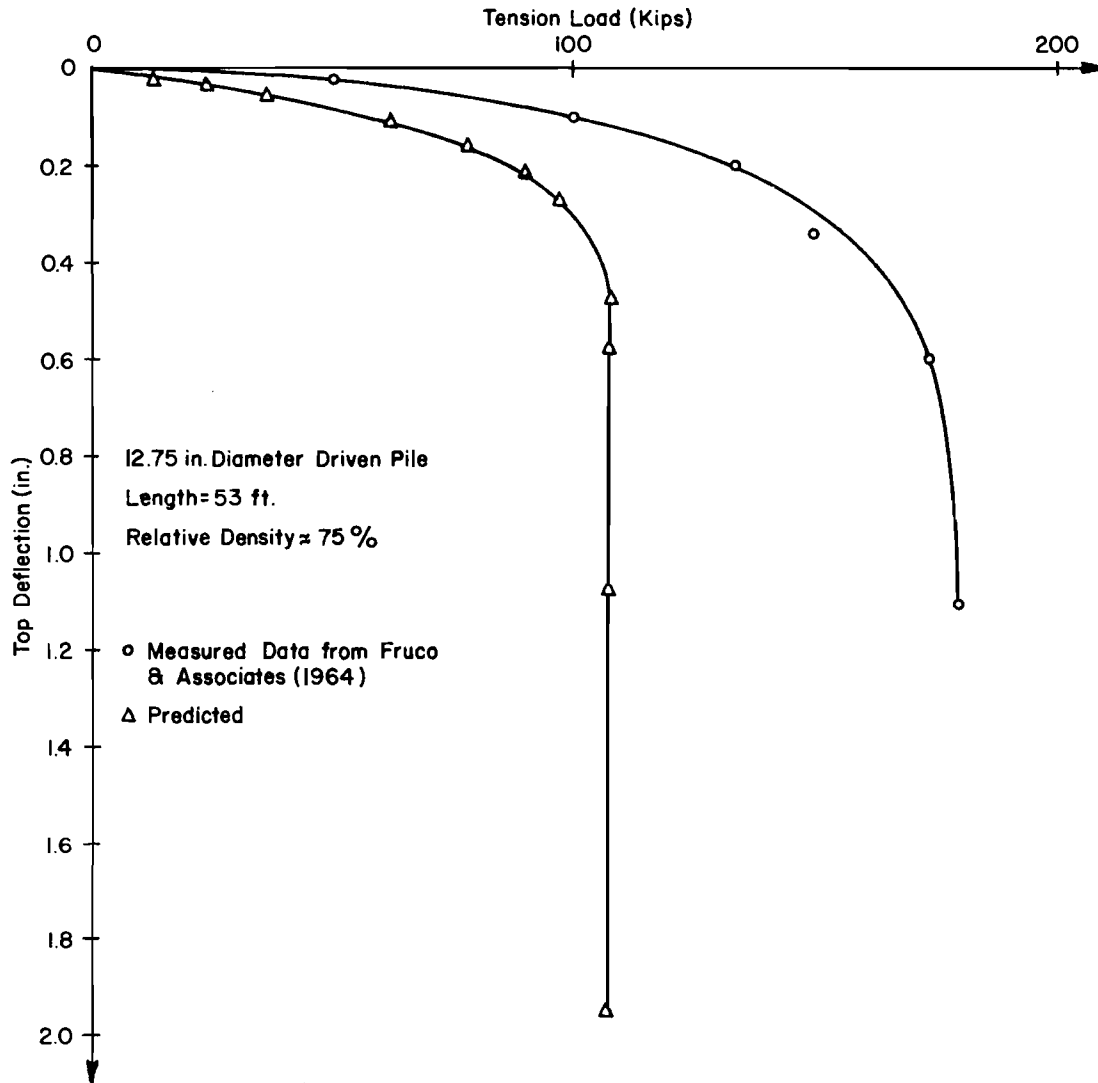


Fig. 5.24. Measured and Predicted Load-Deflection Curves for Tension Loading of a 12.75-inch Diameter Pile.

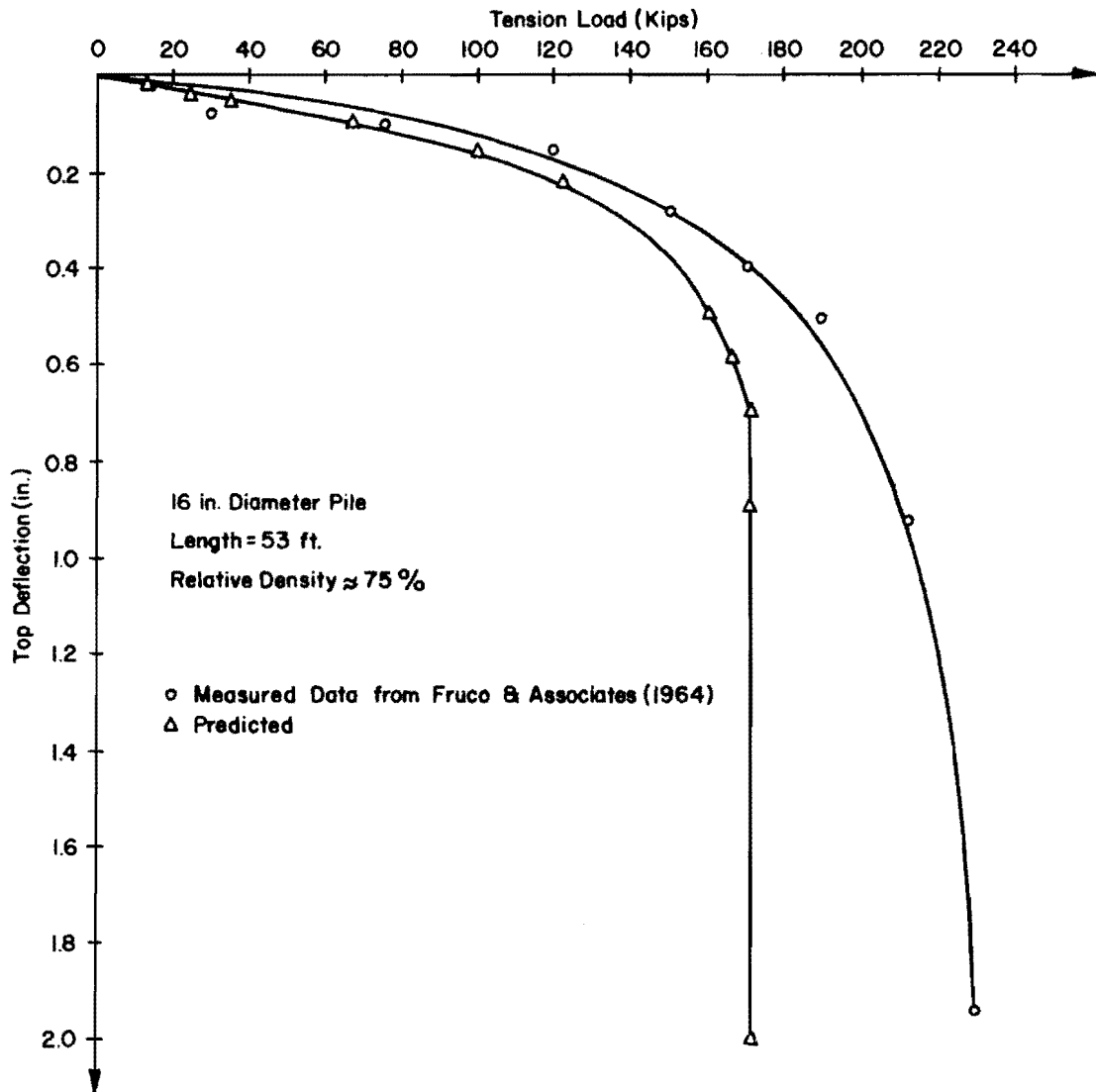


Fig. 5.25. Measured and Predicted Load-Deflection Curves for Tension Loading of a 16-inch Diameter Pile.

The step-by-step procedure to be followed when applying the proposed method to the problem of computing the load-deformation behavior of a pile is as follows:

1. Obtain properties of the sand; preferably complete triaxial stress-strain curves as well as the density. If stress-strain curves are not available, rough approximations may be obtained by using a value of angle of internal friction in the equations for the hyperbolas that were developed in Chapter IV.
2. Obtain an adjustment factor from Fig. 5.21.
3. Obtain modified correlation coefficients by dividing the appropriate expression by the adjustment factor. For tension loading use Eq. 5.28, for compression loading use Eq. 5.30.
4. Obtain s_x -z curves from stress-strain curves by multiplying deviator stress by the appropriate modified coefficient and axial strain by values obtained from Eqs. 5.31 or 5.32. Curves are needed only for depths up to fifteen times the pile diameter. The curve for this depth is used for the remainder of the pile.
5. Obtain an approximation for the tip load-deformation curve by combining an ultimate load obtained from a recommended expression for bearing capacity with an initial straight-line portion obtained from a theory of elasticity solution or from an empirical procedure.
6. Obtain the load-deformation curve behavior of a pile by using the predicted interaction curves with the procedure described in Chapter II for solving the differential equations for an

axially loaded pile. A computer program for performing the necessary computations is presented by Awoshika and Reese (1971).

Comments and Discussion of Results

The satisfactory agreement between the predicted and measured pile response, obtained for the tests analyzed in the preceding section, seems to justify the overall computation procedure and method of representing the axial pile-soil interaction. A great deal of attention was given the problem of predicting s_x - z curves from soil properties, and it appears that the suggested method that uses stress-strain curves from triaxial tests is valid. However, the procedure formulated for adjusting the correlation coefficients was based on a limited amount of data and should be used with caution. The principal reasons for formulating the procedure were to illustrate the variation in shear transfer that is caused by various methods of installing piles in sand with different relative densities, and to check the applicability of the procedure for generating shear transfer s_x curves from stress-strain curves for various conditions. It is felt that the only way that valid correlation coefficients for a wide range of sand conditions and methods of installation can be obtained is through additional testing.

So far, only limited consideration has been given the problem of determining the tip behavior. In all of the tests analyzed in the preceding section, the effect of the tip behavior on the computed behavior of the pile top was eliminated by using the measured load-deflection curve in the computation procedure. The tip behavior has been

given only limited consideration not because it is unimportant, but because only a limited amount of information concerning the tip load-deformation behavior is available in the literature, and because only a limited amount of information was obtained from the test. Therefore, the only recommendation which can be made is that an ultimate value be calculated using a suggested bearing capacity equation, and combined with a movement, calculated from either a solution based on the theory of elasticity or an empirical recommendation, to form a curve composed of two straight lines.

Another factor that should be considered is the possible influence of lateral deformation on the transfer of axial load from the pile to the soil. In Chapter II it was stated that, from the standpoint of soil behavior, the axial and lateral behavior of the pile could be uncoupled. However, for practical problems, a realistic representation of the axial load transfer will require that the curves for the upper portion of the pile be modified to account for the reduction in shear transfer caused by any lateral deformation which might occur. The procedure for adjusting the shear transfer curves is rather arbitrary, and further consideration will be delayed until the lateral behavior is analyzed in Chapter VI.

Consideration of the influence of the tip behavior and the effect of lateral deflections on the axial load transfer add to the already complex problem, and any solution obtained using the simplified procedures suggested for describing the pile-soil interaction should be regarded as only a very rough approximation of the behavior which might occur.

CHAPTER VI
LATERAL LOAD TRANSFER

The mechanics of a laterally loaded pile were developed in Chapter II, and equations were presented to represent mathematically the behavior of the pile under load. Numerical techniques were introduced for solving the equations, which yield the deformation pattern of the pile when loaded. The equations contained terms for the transfer of load to the soil through the lateral pressure along the shaft. In this chapter, the mechanics of the load transfer and, also, criteria for describing the family of interaction curves will be presented for piles in sand.

The first section will deal with the theoretical concepts of the load transfer, and the available criteria for describing the interaction curves. In the second section, the results from the load test on the 2-inch diameter piles will be presented. Load transfer relationships, in the form of p-y curves, will be developed and compared with curves developed using available techniques. Based on this comparison, a modification of an existing criteria is proposed, and equations developed to define p-y curves. In the next section, the proposed p-y curves will be used to predict analytically the behavior of the 2-inch diameter test piles, and the predicted response will be compared with the measured response. Also in this section, the proposed criteria for defining p-y curves will be used to predict analytically the lateral behavior of three tests reported in the literature, and the predicted response compared with the measured response. In the final section, the proposed criteria and its applicability to practical cases will be discussed.

Concepts of Lateral Pile-Soil Interaction

In Chapter V, it was noted that the problem of axial load transfer has been, to a large extent, handled by consideration of ultimate strength characteristics. In contrast with long laterally loaded piles, the ultimate soil resistance is seldom achieved except very near the soil surface. Because of this, the prediction of the lateral pile-soil interaction involves not only some estimate of the ultimate resistance, but also, the load-deformation characteristics prior to the development of the ultimate resistance.

A number of investigators have treated the pile as a beam on a series of linear elastic springs. One procedure followed has been to assume that the coefficient of soil reaction varies linearly with depth. This may be expressed mathematically as

$$k_s = Kx \dots \dots \dots (6.1)$$

where

$$K = \text{a constant.}$$

Palmer and Thompson (1948), Mason and Bishop (1954), and Prakash (1961) have compared test results and predicted results using Eq. 6.1 to describe the pile-soil interaction. Reese and Matlock (1956) proposed nondimensional solutions for a laterally loaded pile where the soil resistance is described by Eq. 6.1. Terzaghi (1955) proposed values of K for a variety of soils. Gleser (1953) used the expression

$$k_s = Kx^m \dots \dots \dots (6.2)$$

where

$$m = \text{a constant}$$

to compare measured and predicted results, and Matlock and Reese (1960) proposed nondimensional solutions for this variation of modulus of soil reaction. One important aspect noted in all of the above-mentioned references, is that for a realistic problem, the parameters, K and m may not be constant, but may be functions of a number of parameters, one of which is the deflection. The variation in K and m , which may occur with deflection, is illustrated in Fig. 6.1, from Reese and Matlock (1956). Since the variation in soil modulus with depth may be approximated by a straight line for a particular deflected shape, the use of Eq. 6.1 as a computational technique is valid. However, as a method for rigorously describing the pile-soil interaction, the method is limited to linear behavior.

Broms (1964a and 1964b) has considered the problem of a laterally loaded pile in two parts. Broms calculated the lateral deflections under working loads by considering that the modulus of soil reaction is defined by Eq. 6.1. For a short stiff pile, an ultimate load which the pile can sustain, is assumed to be governed by the lateral resistance of the surrounding soil. For long piles, an ultimate load is controlled by the formation of a plastic hinge. This method offers no additional information for the soil behavior since the criteria for the soil modulus is that recommended by Terzaghi (1955), and the ultimate soil resistance is based on the development of passive pressure calculated using the Rankine earth pressure theory.

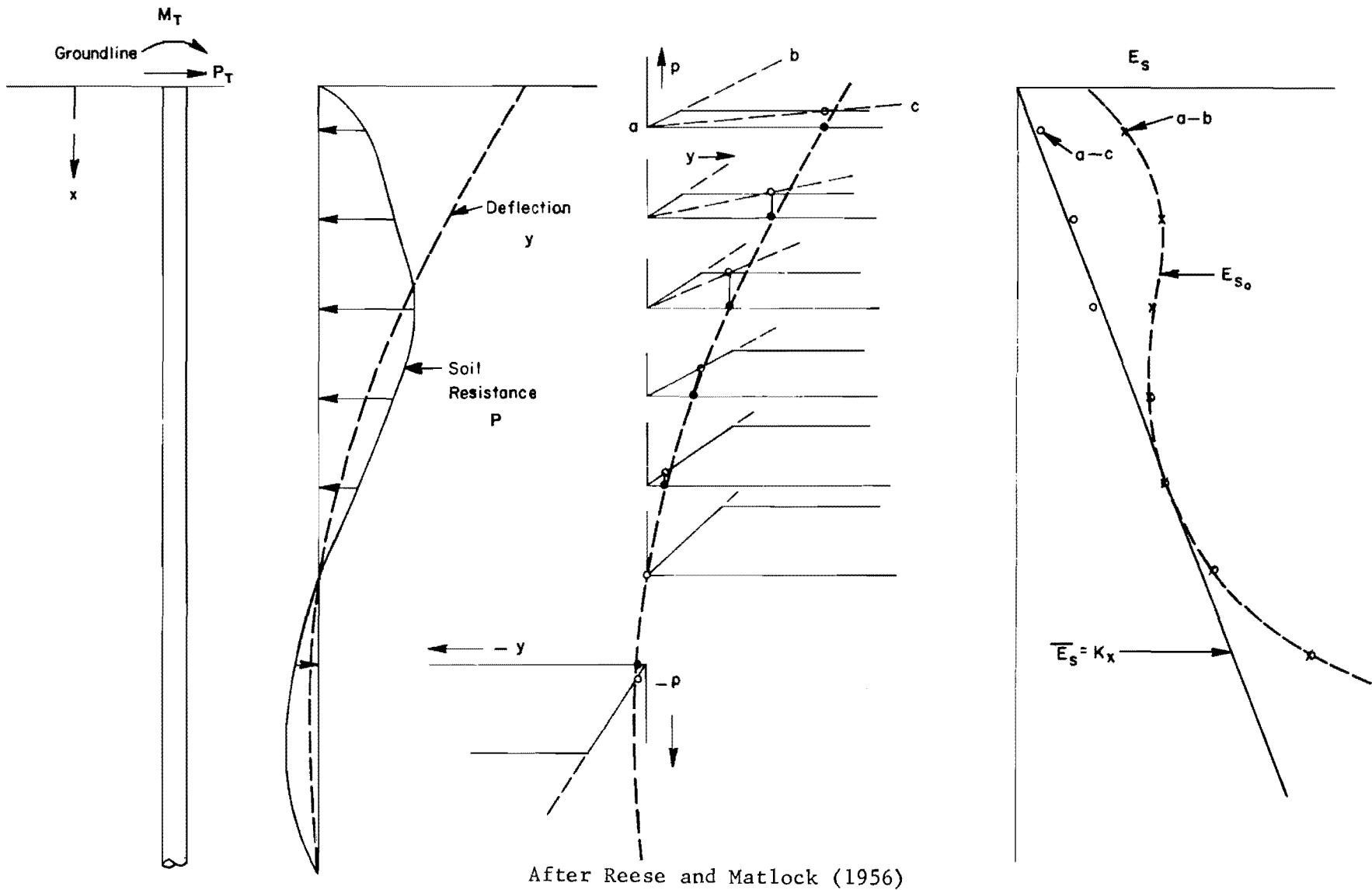


Fig. 6.1. Hypothetical Laterally Loaded Pile Illustrating Possible Variation of Soil Resistance Modulus with Deflection.

Improved computational capabilities, brought about by larger and faster computers, allow any arbitrary variation of soil modulus to be handled with relative ease. Computers have enabled more emphasis to be placed on determining a more exact soil response, rather than trying to find an approximation which could be handled by available computational procedures and still give reasonable results. The use of computers has resulted in the consideration of the soil response in the form of non-linear p-y curves. McClelland and Focht (1956) proposed criteria for predicting p-y curves for clay from measured stress-strain curves. Since this paper was presented, a great deal of work has been done on developing criteria for determining p-y curves from soil properties. A paper by Matlock (1970) gives criteria for soft clay.

For sands there are no published criteria for generating complete p-y curves. There are, however, several references which offer some suggestions concerning several aspects of lateral pile-sand interaction. The criteria for sand, presented in the following two sections, are a combination of several suggested techniques. The p-y curve is considered in two parts. In the first section, the ultimate lateral resistance which can be developed is considered; and in the second section, the behavior prior to the development of the ultimate resistance is considered.

Ultimate Lateral Soil Resistance

It is assumed that two modes of failure may occur when a pile moves laterally through the soil. Near the surface the ultimate resistance is assumed to be limited by the formation of failure surfaces which allow the movement of a wedge of soil, as the pile is deflected laterally.

For greater depths, the ultimate resistance is assumed to be limited by the flow of sand around the pile as the pile is deflected laterally. Equations describing both types of failure in sand will be developed in the remainder of this section.

An expression for the ultimate soil resistance of a cohesionless soil is developed from an expression, suggested by Reese (1962), for the ultimate passive force resisting the lateral movement of a rigid cylinder. The expression for the passive force was formulated by considering the forces developed along the failure surfaces of the assumed passive wedge, illustrated in Fig. 6.2. In the actual case of a rigid cylinder moving through the soil, the rupture surfaces are actually curves; but experimental studies by Bowman (1958) have shown that the straight-line approximations give reasonable results which are, for the most part, conservative. The forces, acting on the pile and the assumed passive wedge, are illustrated in Fig. 6.3.

The equation developed by Reese for the ultimate passive force on the cylinder may be written as

$$F_p = \bar{\gamma} H^2 \left[\frac{1}{2} D(K_p - K_a) + \frac{1}{3} K_p H \tan \alpha \tan \beta + \frac{1}{3} K_x H \tan \beta (\tan \phi - \tan \alpha) \right] \dots \dots \dots (6.3)$$

where

- F_p = ultimate passive force on cylinder
- H = depth of cylinder as illustrated in Fig. 6.2
- K_p = coefficient of passive earth pressure = $\tan^2(45 + \phi/2)$

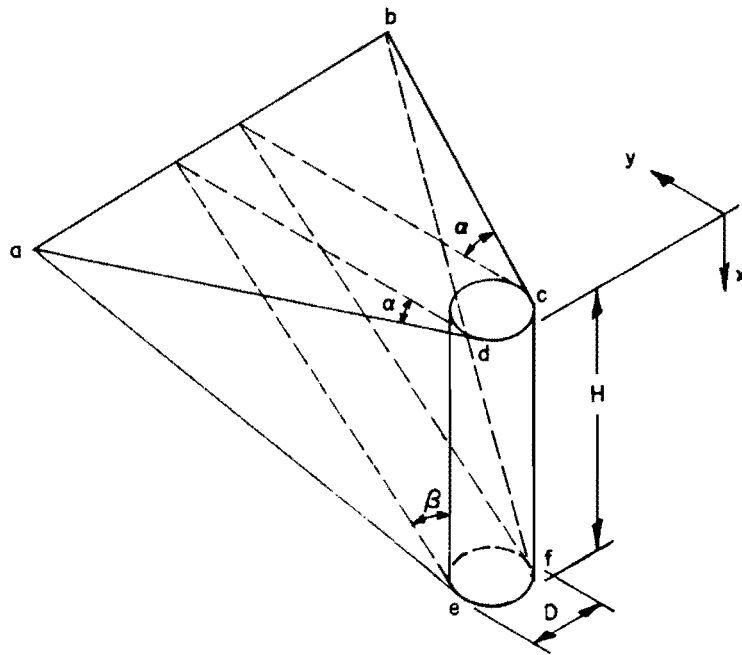


Fig. 6.2. Assumed Passive Wedge Formed Near the Surface.

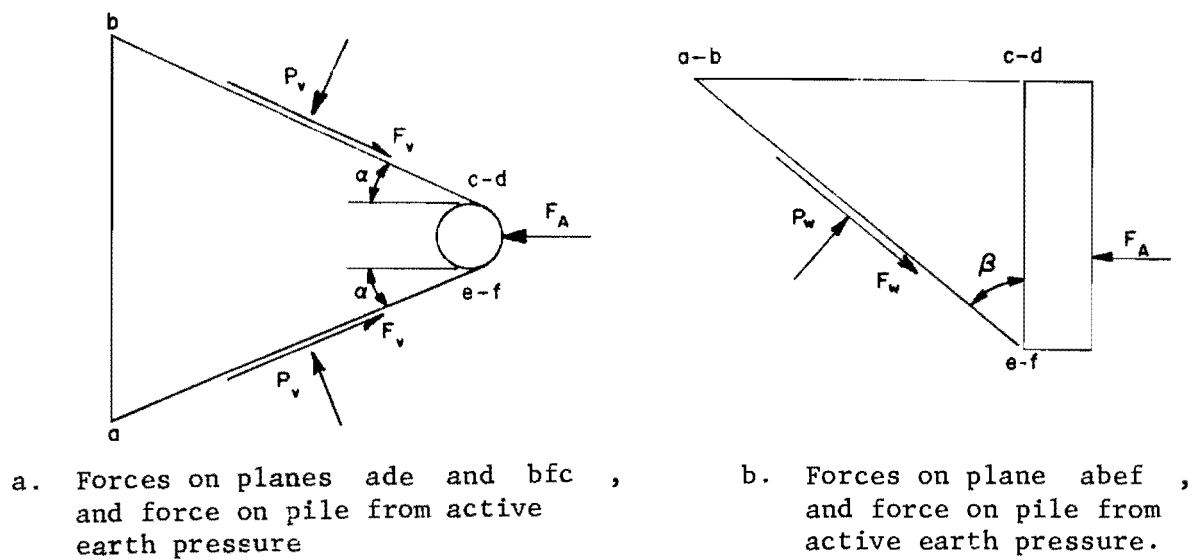


Fig. 6.3. Forces on the Pile and Assumed Passive Wedge.

K_a = coefficient of active earth pressure = $\tan^2(45 - \phi/2)$

K_x = coefficient of lateral earth pressure

α = angle illustrated in Fig. 6.2

β = angle illustrated in Fig. 6.2 and defined from the Mohr-Coulomb strength theory as, $\beta = 45 + \phi/2$.

The assumptions and approximations made in the derivation are summarized in the following list:

1. The pile moves rigidly through the soil; thus, the effects of bending are omitted.
2. No vertical shear stresses are developed between the pile and the soil.
3. The failure surfaces are straight lines.
4. The force F_v is assumed to act parallel to the soil surface.

The force per unit length of pile may be developed from Eq. 6.3 by writing the expression in terms of an arbitrary depth x and differentiating with respect to x . The resulting expression for the ultimate soil resistance, at any depth x , is written as

$$\frac{dF}{dx} = p_{uw} = \bar{\gamma}x \left\{ D(K_p - K_a) + x \tan \beta \left[K_p \tan \alpha + K_x (\tan \phi - \tan \alpha) \right] \right\} \dots \dots \dots (6.4)$$

For a particular pile and sand, all of the terms in Eq. 6.4, except K_x and α , are defined. Values of K_x and α are not very well defined, but will depend on a number of variables, such as relative density, the method of placing the sand, and the method used for installing the piles.

In the section on test results, a range of possible values are considered, and the resulting values of ultimate soil resistance compared with measured values.

At some depth below the ground surface, it will be easier for the sand to flow around the pile than to form a wedge as described above. An expression for the ultimate resistance for this mode of failure is developed by extending the procedure suggested by Reese (1956) for a clay, to a sand. The expression for the ultimate resistance is developed by considering a slice of unit thickness through the pile and soil, as illustrated in Fig. 6.4. The simplified failure mechanism is shown in Fig. 6.5. In this model the pile is represented by a block one unit thick and with the other two dimensions equal to the projected width of the pile, as shown in Fig. 6.5. The blocks A, B, C, D, and E have the same dimensions. Another simplifying assumption made in developing the failure mechanism is that no shear forces are developed on the top or bottom of blocks A, B, C, D, and E. Other assumptions and approximations will be noted during the derivation.

The derivation is started by considering the stress σ_1 acting on the back of the pile and on block E. A minimum value of σ_1 will be conservative, and assuming that a Rankine condition develops the minimum value of σ_1 , is written as

$$\sigma_1 = K_a \bar{\gamma} x \dots \dots \dots (6.5)$$

With this assumed value of σ_1 , the value of σ_2 may be computed.

Block E is assumed to fail in shear, so that σ_2 may be computed from

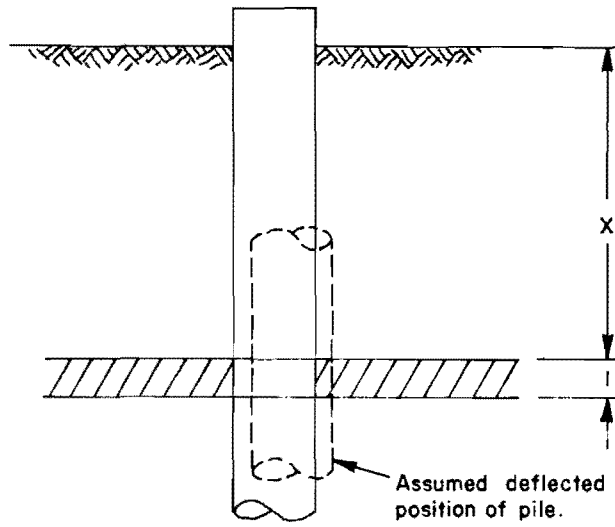


Fig. 6.4. Slice of Soil Analyzed.

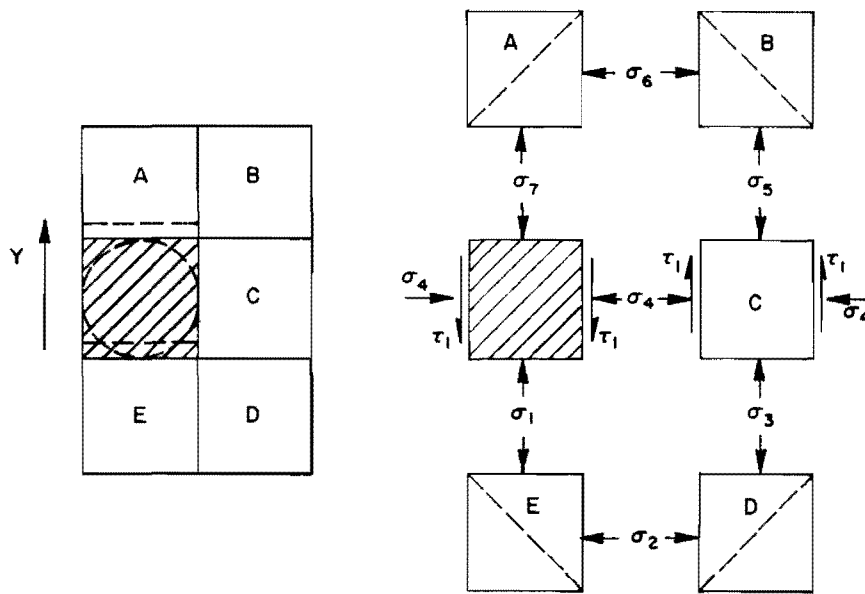


Fig. 6.5. Failure Mechanism for Computation of Ultimate Flow-Around Resistance.

the Mohr-Coulomb diagram shown in Fig. 6.6. The expression for σ_2 is, therefore,

$$\sigma_2 = K_p \sigma_1 = K_p K_a \bar{\gamma}_x = \bar{\gamma}_x \dots \dots \dots (6.6)$$

A discrepancy exists between the assumed failure plane, shown by the dashed lines in Fig. 6.5, and the actual failure plane which would exist, based on the Mohr-Coulomb theory. The assumed failure plane in block E is 45 degrees from the directions of σ_1 and σ_2 , whereas, the actual failure plane would be at $45 \pm \phi/2$ degrees. In Fig. 6.6, the actual failure plane is illustrated as the dashed line through block A, but the same configuration would also be applicable to blocks E, D, and B. The derivation is continued by considering the shear of block D so that from Fig. 6.6

$$\sigma_3 = K_p \sigma_2 = K_p \bar{\gamma}_x \dots \dots \dots (6.7)$$

No shear occurs in block C, but shear stresses are developed on the sides. Expressions for the normal stress and the shear stress on block C are written as

$$\sigma_4 = K_x \bar{\gamma}_x \dots \dots \dots (6.8)$$

and

$$\tau_1 = \sigma_4 \tan \phi = K_x \bar{\gamma}_x \tan \phi \dots \dots \dots (6.9)$$

and finally

$$\sigma_5 = \sigma_3 + 2 \tau_1 = K_p \bar{\gamma}_x + 2 K_x \bar{\gamma}_x \tan \phi \dots \dots \dots (6.10)$$

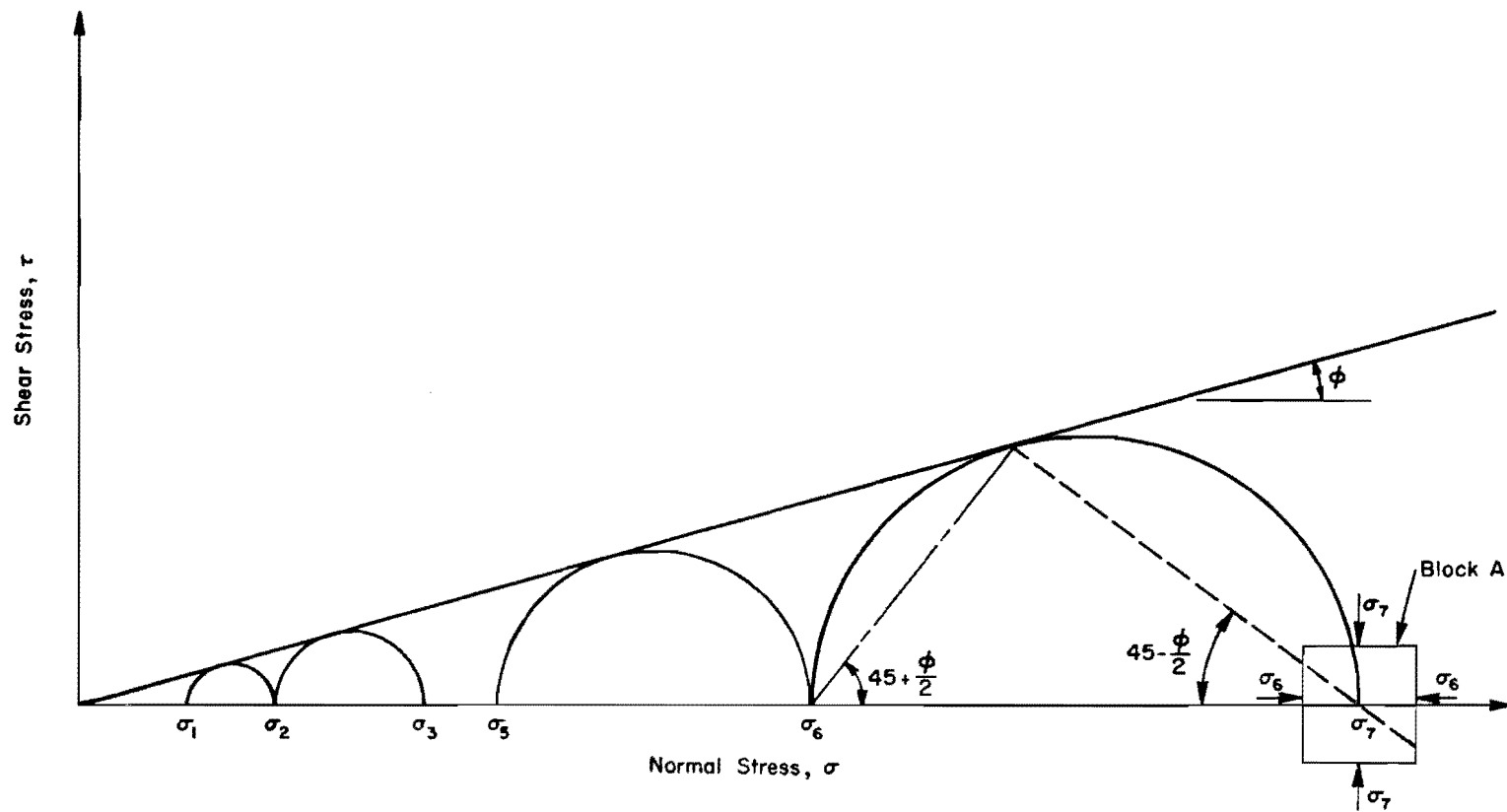


Fig. 6.6. Mohr-Coulomb Diagram for Flow-Around Failure.

In Fig. 6.6, the shift between σ_3 and σ_5 which is equal to the shear stresses on the sides of block C is illustrated. However, starting at σ_5 the procedure is straightforward, and since blocks B and A fail in shear, the expressions for σ_6 and σ_7 are written as

$$\sigma_6 = K_p \sigma_5 = K_p^2 \bar{\gamma}_x + 2 K_x K_p \bar{\gamma}_x \tan \phi \dots \dots \dots (6.11)$$

and

$$\sigma_7 = K_p \sigma_6 = K_p^3 \bar{\gamma}_x + 2 K_x K_p^2 \bar{\gamma}_x \tan \phi \dots \dots \dots (6.12)$$

The expression for the ultimate soil resistance to horizontal movement may be obtained by considering equilibrium of the segment of pile. The equilibrium expression may be written as

$$F_{uf} = D (\sigma_7 + 2 \tau_1 - \sigma_1) \dots \dots \dots (6.13)$$

where

$$F_{uf} = \text{resultant lateral force on the pile segment.}$$

The expression for the ultimate resistance per unit length of pile is obtained by substituting Eqs. 6.5, 6.9, and 6.12 into Eq. 6.13, so that

$$p_{uf} = \bar{\gamma} D x (K_p^3 + 2 K_x K_p^2 \tan \phi + 2 K_x \tan \phi - K_a) \dots \dots (6.14)$$

For a pile of a given size and sand with known properties, all the terms in Eq. 6.14, except K_x are defined. As noted previously, values of K_x will depend on several variables, such as relative density of sand, method of placement of sand, and method of installation of the pile. In

the section on test results, a range of possible values for K_x are considered, and values of ultimate resistance calculated for the test piles.

Values of p_{uw} and p_{uf} can be combined with initial load-deformation relationships, which will be developed in the following section, to form a complete family of p-y curves. For a particular depth x , the smaller of the two values obtained from Eqs. 6.4 or 6.14 will be used. Near the surface, the value of p_{uw} will be smaller, but after some depth is reached, p_{uf} will become smaller.

Initial Lateral Load-Deformation Relationships

When a state of plastic equilibrium is reached in the soil there will be no increase in resistance as deflection increases. For small deflections there will be a linear relationship between soil resistance and pile deflection. As the deflection of the pile is increased, a state of plastic equilibrium is reached and there will be a relatively constant soil resistance with additional deflection. Presently there are no available techniques for predicting the nonlinear response, and a linear approximation is employed. With the assumption of linear behavior, theory of elasticity can be used to develop an expression for the lateral soil resistance as a function of pile deflection.

The following development is taken from Terzaghi (1955), and is based on the equation

$$y = \frac{\rho D}{E_m} I_y \dots \dots \dots (6.15)$$

where

- ρ = unit pressure
 I_y = influence coefficient
 E_m = modulus of elasticity of sand.

This equation is taken from Terzaghi (1943), and the value of the influence coefficient suggested, $I_y = 1.35$, is derived from a theory-of-elasticity solution for a line of pressure ρ acting on an elastic layer with thickness of $3D$. Substituting for the influence coefficient and rearranging, Eq. 6.15 may be rewritten as

$$\rho = \frac{yE_m}{1.35D} \dots \dots \dots (6.16)$$

An expression for the soil resistance per unit length of pile may be obtained by multiplying Eq. 6.16 by the projected diameter, which yields

$$p = \frac{yE_m}{1.35} \dots \dots \dots (6.17)$$

Terzaghi (1955) noted that the variation of the modulus of elasticity of a sand with confining pressure may be approximated reasonably well with a linear variation. Therefore, the variation of the modulus with depth should be approximately linear, if the unit weight is constant, and the modulus of elasticity of sand was expressed mathematically by Terzaghi as

$$E_m = J \bar{\gamma} x \dots \dots \dots (6.18)$$

where

J = nondimensional coefficient depending on the relative density of the sand.

For sand classified as loose, a range of values of J from 100 to 300 was suggested; for medium sand, from 300 to 1,000; and for dense sand, from 1,000 to 2,000. The equation for the initial slope of the p - y curve, previously defined as the coefficient of soil reaction, may now be written as

$$k_s = p/y = \frac{E_m}{1.35} \dots \dots \dots (6.19)$$

Substituting the empirical expression for modulus of elasticity into Eq. 6.19 yields

$$k_s = \frac{J\bar{Y}_x}{1.35} \dots \dots \dots (6.20)$$

Equation 6.19 may be used to establish the slope of the initial portion of the p - y curve, if values of soil modulus of elasticity are known. If the soil modulus values are not known, Eq. 6.20 and the suggested values for J may be used to establish the slope.

The straight lines, with the slopes defined by Eq. 6.19 or Eq. 6.20, may be combined with a value of maximum soil resistance from Eq. 6.4 or Eq. 6.14 to form a complete p - y curve. In the following section, the family of curves established by this procedure are compared with a measured family of curves. Based on the comparison, a minor modification to the criteria is suggested.

Test Results

The results from tests of the six laterally loaded piles are presented in the following sections. In the first section, curves are presented for all six piles showing load at the top versus deflection at the top and load at the top versus the slope at the top. The measured moment-distribution curves, from two of the instrumented piles, are presented in the second section. The measured bending moments, from the third instrumented pile, are not presented and were not used in the analysis, because the precision of the measurements was very poor. In the third section, p-y curves will be developed from measured top deflections and slopes, and measured moment distributions; and in the next section the measured p-y curves will be compared with theoretical curves. Based on this comparison, a refinement of the available criteria is suggested. Equations for describing the p-y curves will be presented in the final section.

Measured Load Versus Deflection and Load Versus Slope Curves for the Tops of the Piles

Measured curves, for all six, showing load at the top of the pile versus the deflection and the slope at the top are given in Figs. 6.7 through 6.10. Curves for the deflection at the ground line are shown for the three instrumented piles (1-L, 2-L, and 3-L) in Fig. 6.7, and for the three noninstrumented piles (4-L, 5-L, and 6-L) in Fig. 6.8.

The effect of pile batter on the load-deflection behavior is illustrated in Figs. 6.7 and 6.8. The batter of the piles and the direction of the loading was illustrated in Fig. 3.2. Piles 3-L and 6-L were vertical. Piles 1-L and 2-L had a batter of 1:12, and the loading was such that, pile 1-L was designated as an out-battered pile, and pile

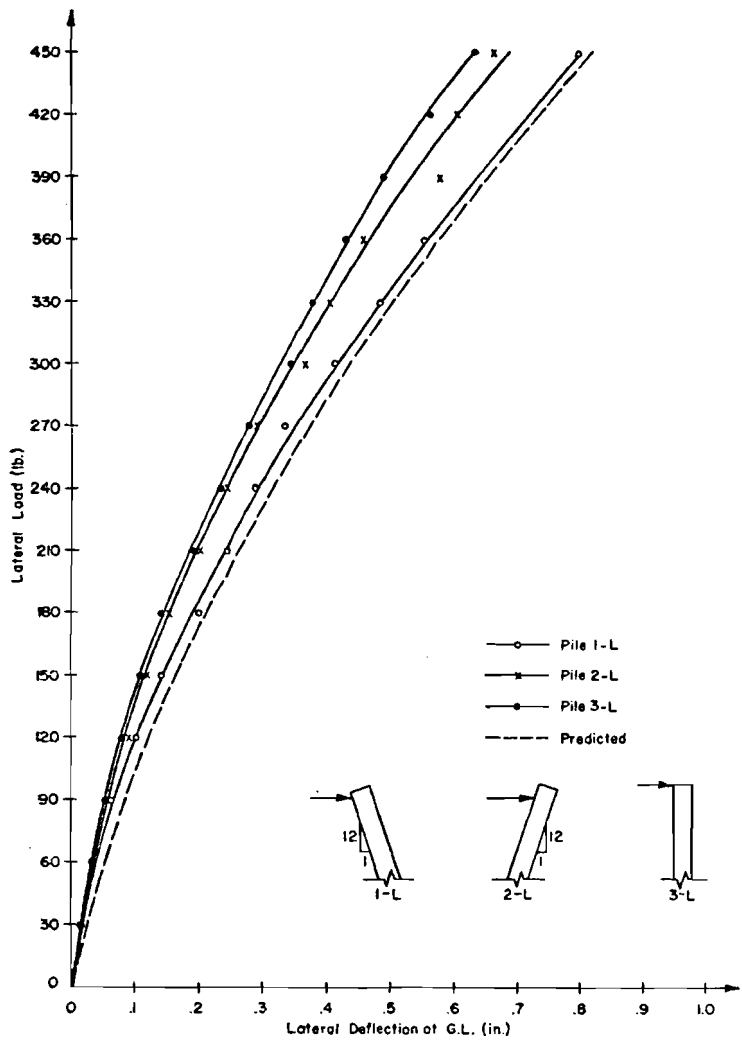


Fig. 6.7. Lateral Load-Deflection Curves for the Instrumented Piles.

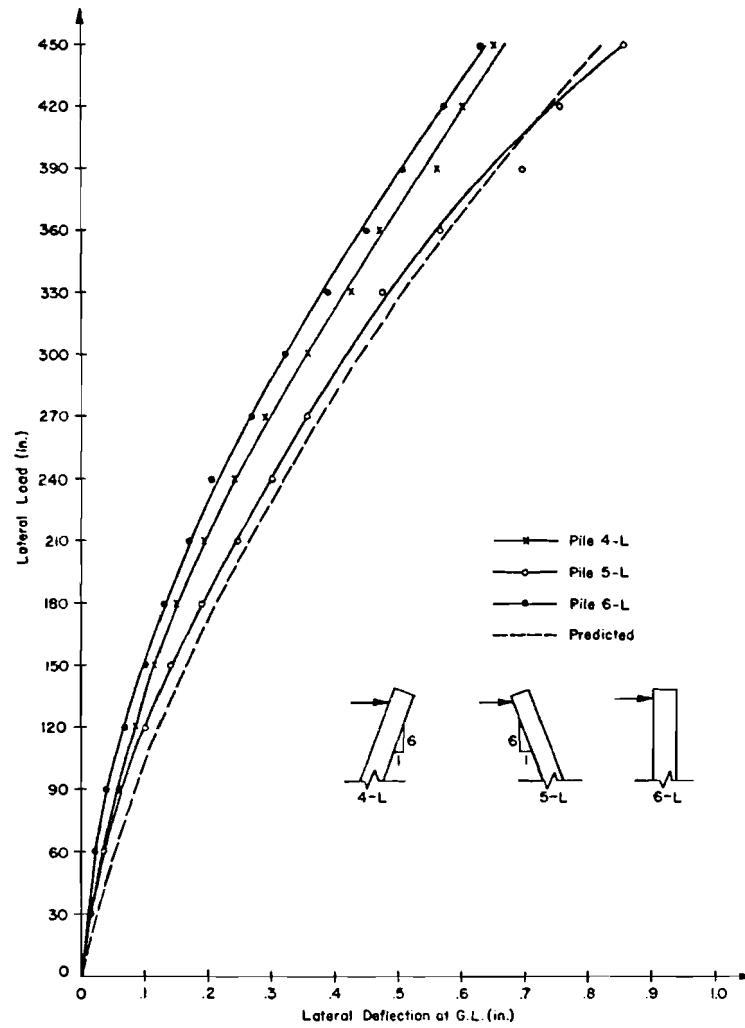


Fig. 6.8. Lateral Load-Deflection Curves for the Noninstrumented Piles.

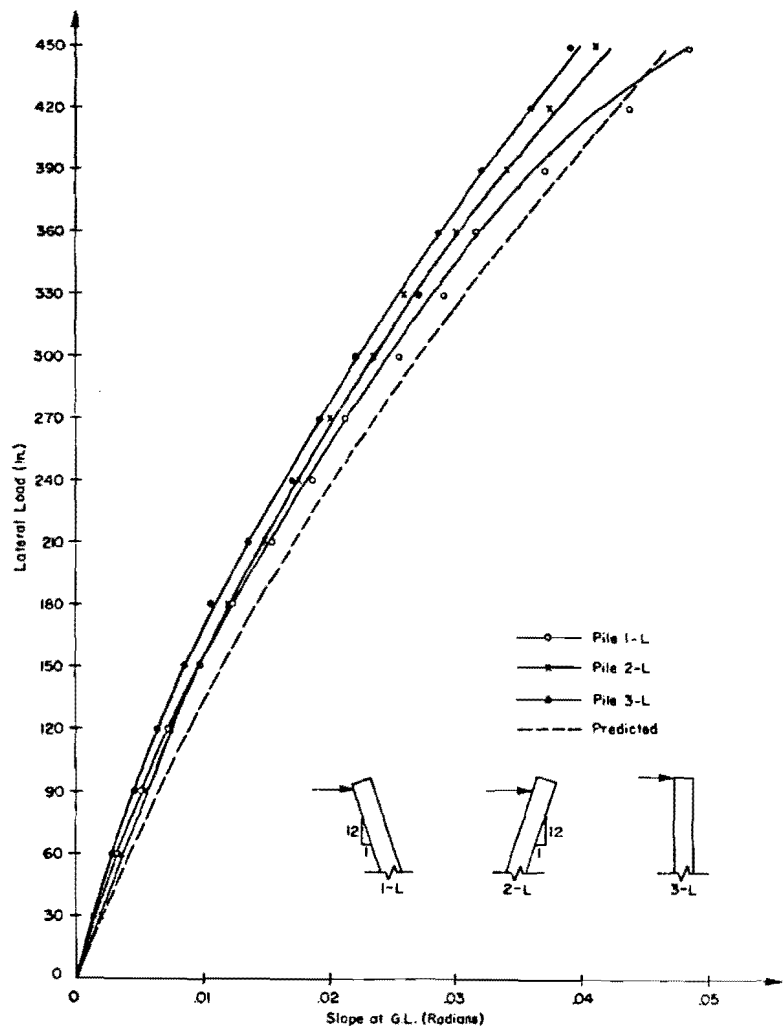


Fig. 6.9. Lateral Load-Slope Curves for the Instrumented Piles.

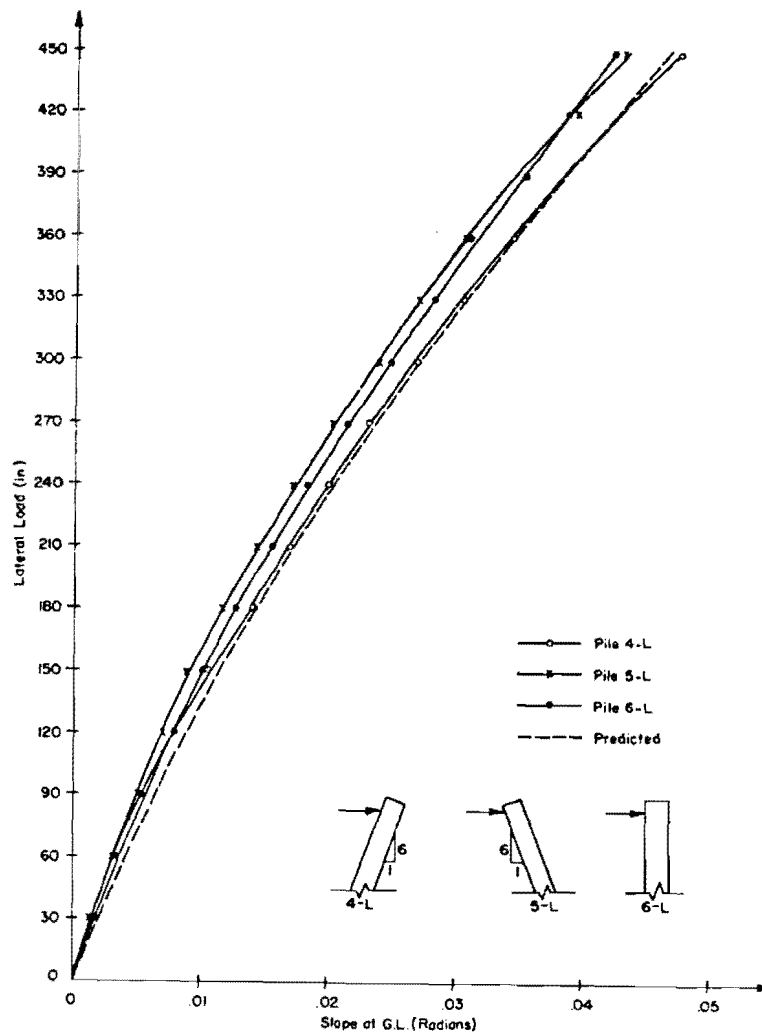


Fig. 6.10. Lateral Load-Slope Curves for the Noninstrumented Piles.

2-L as an in-battered pile. Piles 4-L and 5-L had a batter of 1:6, and were designated, respectively, as in-battered and out-battered piles. With the above designation of the batter and direction of loading, the observed effects may be discussed. Several significant effects were observed, and are enumerated as follows:

1. For out-battered piles, the deflections are larger than for vertical or in-battered piles.
2. For in-battered piles the deflections are approximately equal to those for vertical piles.
3. No measurable difference was observed in the behavior of piles with batters of 1:12 or 1:6.

Essentially, the same effect is indicated in Figs. 6.9 and 6.10, which show curves for the slope at the ground line versus load. However, the difference in the curves for the various types of loading are not as pronounced as they were for the deflection curves.

The smaller observed lateral resistance for out-battered piles was expected, since the wedge-type failure mechanism described in the previous section would result in a smaller soil resistance if the pile was battered. Matsuo (1938 and 1939) also observed that out-battered piles were more flexible than vertical piles. If out-battered piles showed an increase in deflection, then in-battered piles should have shown a decrease in deflection. However, an increase in stiffness was not observed and the in-battered piles were actually more flexible than the vertical piles. The magnitude of the difference between vertical and in-battered piles was small, and if the accuracy of the dial gages used is considered, the differences are probably insignificant. No logical explanation can be

given as to why the in-battered piles did not show a decrease in flexibility, but for batters of 1:6 and 1:12 the in-battered piles apparently behave much like vertical piles. Matsuo (1938 and 1939) also observed that in-battered piles behaved similar to vertical piles. Another apparent discrepancy in the observed behavior, is that there is no apparent difference in the deflections for pile with batters of 1:6 or 1:12. It is possible that there was some variance, but that it was too small to be detected by the measurements made. However, for larger batters the dissimilarity will probably be more pronounced.

From the limited results of the six tests, no specific conclusions can be drawn; however, several important trends were indicated. The first is that out-battered piles tend to be more flexible than vertical piles or in-battered piles. The second is that in-battered piles tend to behave similar to vertical piles. A discussion of the significance of these observed phenomena and a comparison of the measured results with predicted results will be presented later.

Measured Moment Distribution Curves

The measured moment distributions for piles 1-L and 3-L are shown in Figs. 6.11 and 6.12. For clarity, curves are only shown for each 90-pound increment of load; however, loads were applied and curves obtained for 30-pound increments. One characteristic of the curves that was observed was that the point of maximum moment moves downward as the load increases. Another phenomenon that was observed was that, near the point of maximum moment, the curvature of the curves increased as the load increased.

For pile 1-L complete curves were not obtained because bridge numbers 10 and 11 did not function properly. Moments were obtained for pile 2-L,

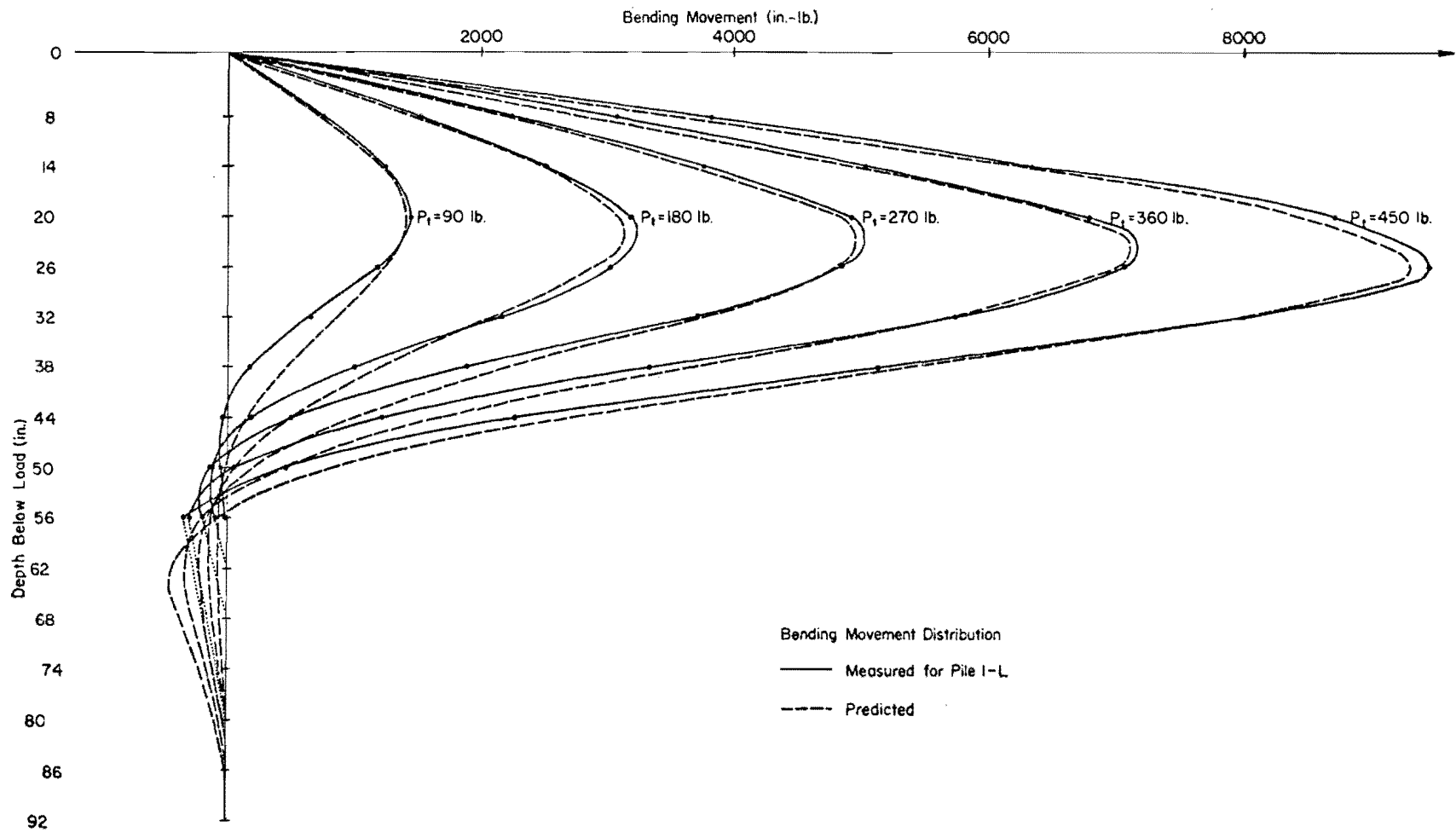


Fig. 6.11. Moment Distributions for Pile 1-L.

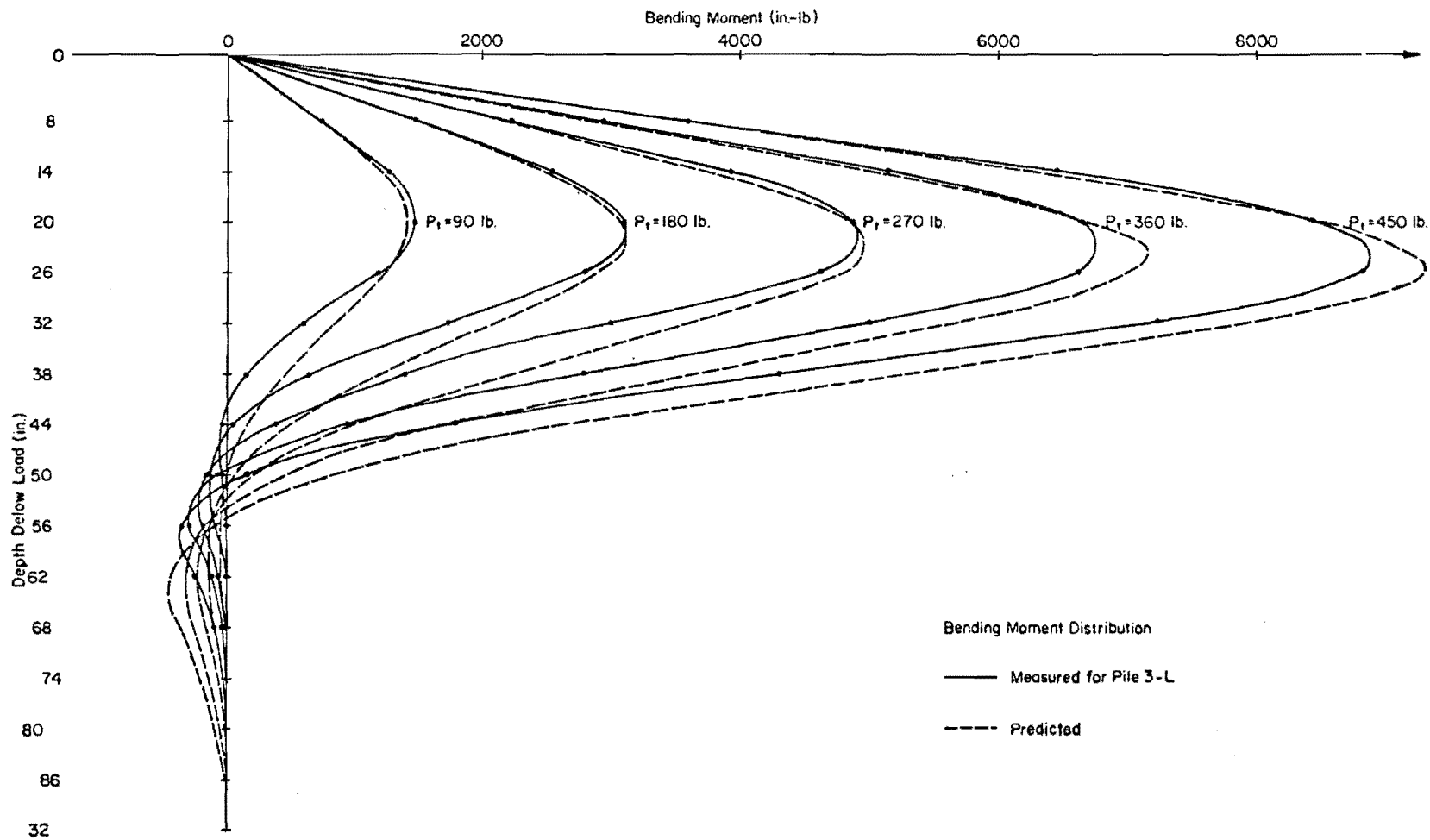


Fig. 6.12. Moment Distributions for Pile 3-L.

but the accuracy was very poor; and the values of soil resistance and movement obtained from the differentiation and integration of the measured distribution were very erratic. The poor quality of the measured moments was caused by equipment failures as described in Appendix D. Since the load-deformation curves for the tops of the in-battered piles were similar to those for vertical piles, it would be expected that the results from pile 3-L would also be applicable to pile 2-L.

In the following section, the deflections and slopes at the ground line and the moment distributions will be used to develop p-y curves. These curves will be compared with theoretical curves, and based on this comparison, expressions for describing the curves will be formulated. The proposed criteria will then be used to predict analytically the moment distribution which will be compared with the measured distribution.

Development of p-y Curves

Two procedures for developing p-y curves were tried. One procedure was to differentiate numerically the moment distribution to find values of soil resistance, and to integrate the moment distribution to obtain values of lateral deflection. The other procedure was a curve fitting technique, based on the nondimensional coefficients suggested by Matlock and Reese (1960) and applied by Reese and Cox (1969) to two large piles. The top deflection and the magnitude and location of the maximum moment were the fitting points.

The procedures for the numerical differentiation and integration may be derived by considering Fig. 6.13. Values of deflection were found by using Simpson's Rule to integrate numerically the equation

$$\frac{d^2y}{dx^2} = \frac{M}{EI} \dots \dots \dots (6.21)$$

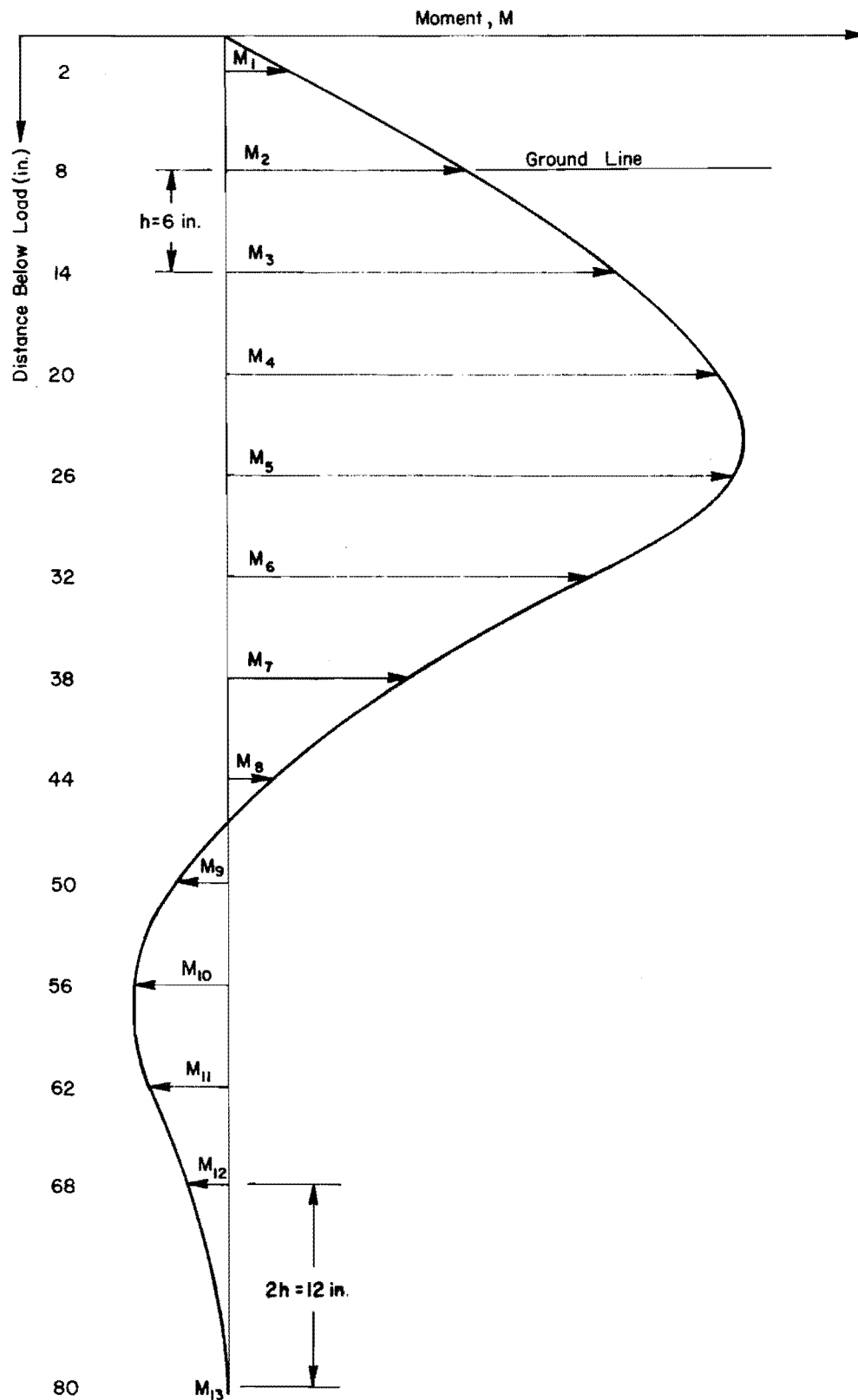


Fig. 6.13. Numbering System for Numerical Integration and Differentiation.

In order to solve Eq. 6.21, two boundary conditions were applied. These were the slope and deflection at the ground line, which was at location 2, for the numbering system shown in Fig. 6.13. Starting with the known value of slope at location 2 and proceeding down the pile, the slope at each location was found from the equation

$$\left(\frac{dy}{dx}\right)_i = \left(\frac{dy}{dx}\right)_{i-1} - \frac{h}{3EI} (M_{i-1} + 4M_i + M_{i+1}) \dots \dots \dots (6.22)$$

for $i = 3, 11$. The deflections were then calculated using the equation

$$y_i = y_{i-1} - \frac{h}{3} \left[\left(\frac{dy}{dx}\right)_{i-1} + 4 \left(\frac{dy}{dx}\right)_i + \left(\frac{dy}{dx}\right)_{i+1} \right] \dots \dots \dots (6.23)$$

for $i = 3, 11$. With the upper limit on i set at 11, deflections below location 11 are not defined, but at these depths the deflections were very small. The values of deflection were combined with values of soil resistance to obtain complete p-y curves.

Values of soil resistance were found by numerically differentiating the equation

$$\frac{d^2M}{dx^2} = p \dots \dots \dots (6.24)$$

The effect of the small axial force in the batter piles was neglected. Referring to Fig. 6.13 the soil resistance was computed by numerically differentiating the moment distribution. One method used, referred to as Method 1, was to solve the central difference equation

$$P_i = \frac{1}{h^2} (M_{i-1} - 2M_i + M_{i+1}) \dots \dots \dots (6.25)$$

for $i = 3, 11$ where $h = 6$ inches. Another method, referred to as Method 2, was to solve the central difference equation

$$P_i = \frac{1}{h^2} (M_{i-2} - 2M_i + M_{i+2}) \dots \dots \dots (6.26)$$

for $i = 3, 10$ where $h = 12$ inches. Method 3, suggested by Matlock and Ripperger (1956), consisted of fitting a cubic polynomial, by the least squares method, to five equally spaced points and then differentiating the polynomial. This procedure resulted in the equation

$$P_i = \frac{1}{7h^2} (2M_{i-2} - M_{i-1} - 2M_i - M_{i+1} + 2M_{i+2}) \dots \dots \dots (6.27)$$

for $i = 3, 10$ where $h = 6$ inches.

Method 4 was the curve fitting procedure for top deflection and maximum moment. This procedure utilized the following two expressions, suggested by Matlock and Reese (1960):

$$y = \left(\frac{P_T \Gamma^3}{EI} \right) A_y + \left(\frac{M_T \Gamma^2}{EI} \right) B_y \dots \dots \dots (6.28)$$

$$M = (P_T \Gamma) A_m + (M_T) B_m \dots \dots \dots (6.29)$$

where

- $A_y, B_y, A_m,$ and B_m = nondimensional deflection and moment coefficients
- Γ = relative stiffness of the pile.

The nondimensional coefficients and the relative stiffness of the pile depend on the form of the soil modulus variation. The form selected is expressed by Eq. 6.2 and is written as

$$k_s = Kx^m \dots \dots \dots (6.2)$$

where x is measured downward from the soil surface. With the form of the soil modulus variation defined, the relative stiffness of the pile may be expressed as

$$\Gamma^{m+4} = \frac{EI}{K} \dots \dots \dots (6.30)$$

The nondimensional depth coefficient is defined as

$$Z = \frac{x}{\Gamma} \dots \dots \dots (6.31)$$

and the nondimensional soil modulus function may be expressed as

$$\phi(Z) = (Z)^m \dots \dots \dots (6.32)$$

where

Z = depth coefficient

$\phi(Z)$ = nondimensional soil modulus function.

With the soil modulus function defined by Eq. 6.32, values of the nondimensional deflection and moment coefficients may be obtained for a particular value of m , by solving nondimensional differential equations similar to Eq. 6.33. Equation 6.33 is an example of the form of the

expressions obtained and is the equation for the deflection coefficient for lateral force.

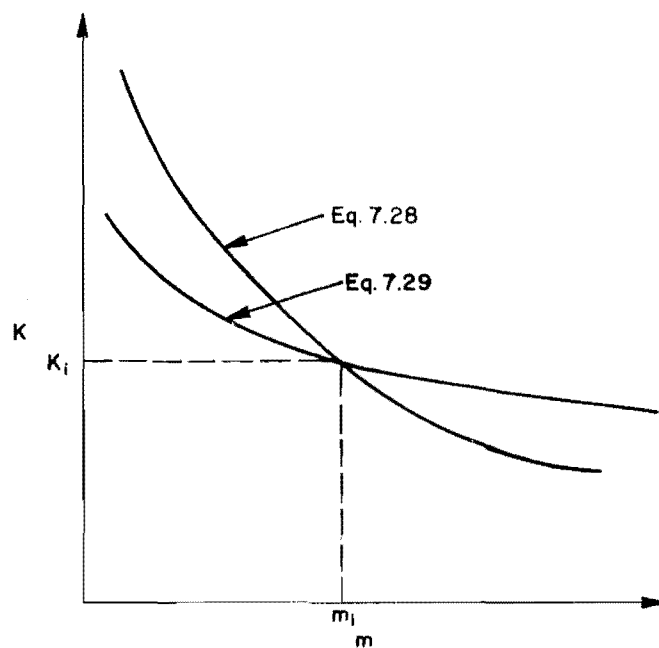
$$\frac{d^4 A_y}{dz^4} + \phi(z) A_y = 0 \dots \dots \dots (6.33)$$

Because the deflection at the soil surface is one of the known values, values of A_y and B_y are generated for a range of m values, but only for the case where $Z = 0$, since $x = 0$ at the soil surface. Values of A_m and B_m are generated for a range of m values, and also a range of Z values, because the maximum moment is one of the known values and it will occur at various values of x .

The sets of nondimensional coefficients are used in conjunction with Eqs. 6.28, 6.29, and 6.30, in a trial and error procedure to find an appropriate value of K and m . The procedure is outlined in the following steps:

1. Assume a value of m .
2. Obtain values of A_y , B_y , A_m , and B_m . Selection of values of A_m and B_m will also involve a trial and error type solution for selecting the appropriate value of Z .
3. Solve Eqs. 6.28 and 6.29 for values of Γ .
4. Solve Eq. 6.30 for values of K .
5. Plot values of K and m as shown in Fig. 6.14 and find the point of intersection of the curves from Eqs. 6.28 and 6.29.

With the correct values of K and m , the deflected shape of the pile and the distribution of soil reaction were obtained and cross plotted to obtain p - y curves.



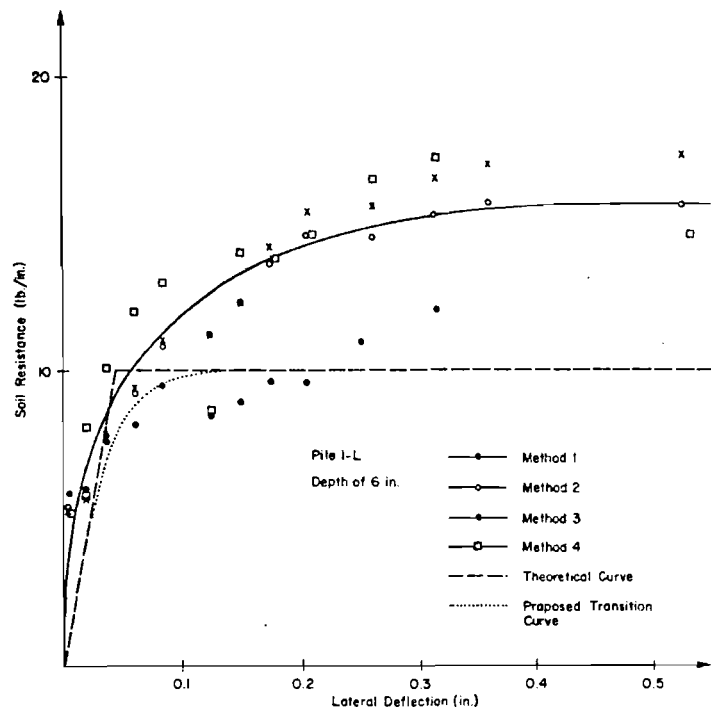
After Reese and Cox (1969)

Fig. 6.14. Plot of Values of m and K From Eqs. 6.28 and 6.29.

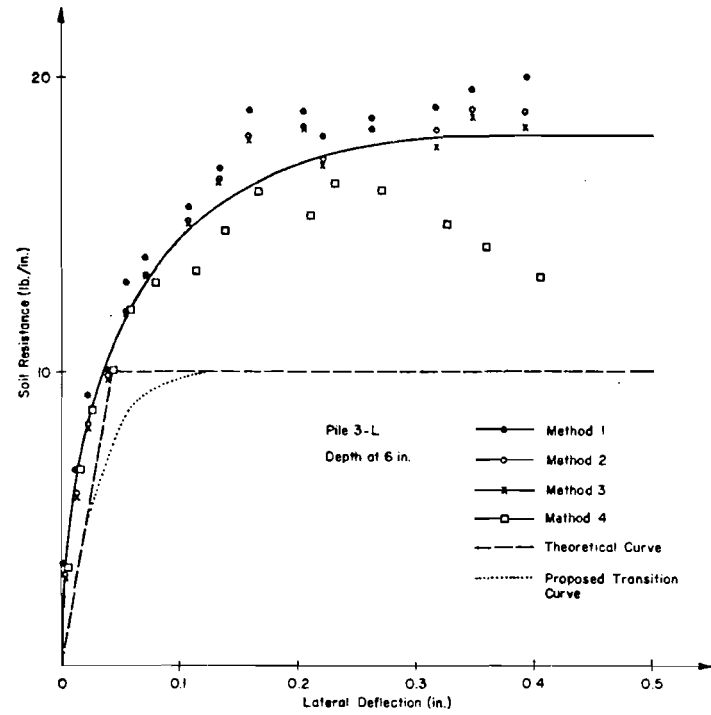
Values of soil resistance and deflection obtained from the four methods described above are shown plotted in Figs. 6.15 through 6.18. In these four figures, points for depths of 6, 12, 18, and 24 inches are plotted for piles 1-L and 3-L. There is considerable scatter in the points for each method and, also, differences between the methods. The solid lines through the experimental points were drawn in by hand to best represent the trends indicated by the points. Several of the expected trends are illustrated by these curves. There was the expected increase in resistance and increase in initial slope with depth. The curves for pile 3-L, which was vertical, also indicated a larger resistance than did the curves for pile 1-L, which was an out-battered pile.

Curves are only shown for the top 24 inches, since for larger depths the deflections were too small for accurate determination. Another limiting factor is that, of the four depths considered, the ultimate resistance was developed only at the 6- and 12-inch depths, because the application of larger loads would have stressed the steel beyond the linear stress-strain range.

There were several reasons for selecting the pile cross section which resulted in the limited load that could be applied. For one thing, the pile size was based on an expected density of sand less than that which was obtained. Another factor which influenced the selection of a size of the pile, was the desirability of keeping the section modulus of the pile as small as possible, because the calibration constant is directly proportional to the stiffness of the pile cross section. If the stiffness of the section was increased, the calibration constant would also be increased, and therefore, the precision of the measured moment would be decreased.

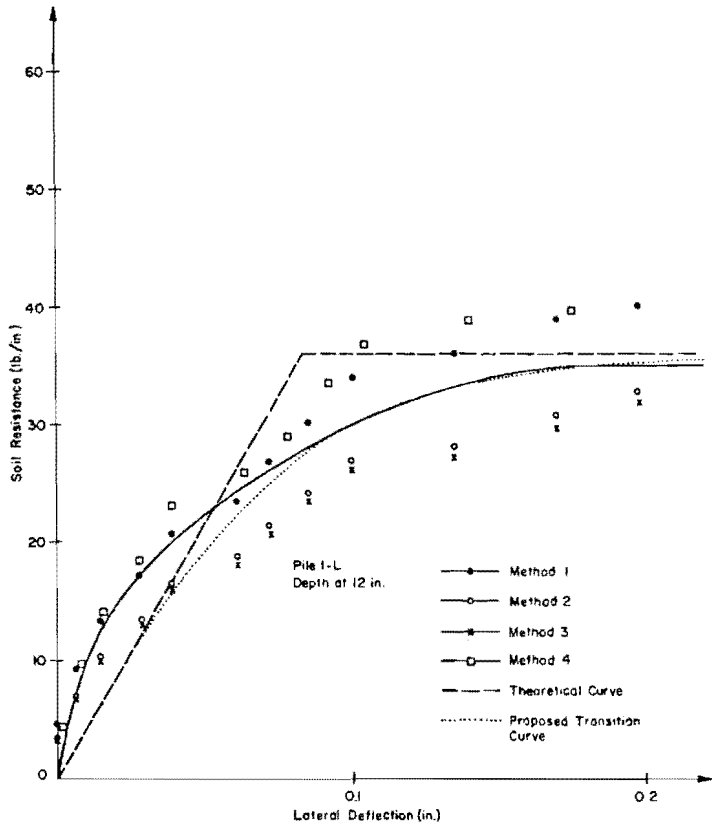


a. Curve for Pile 1-L

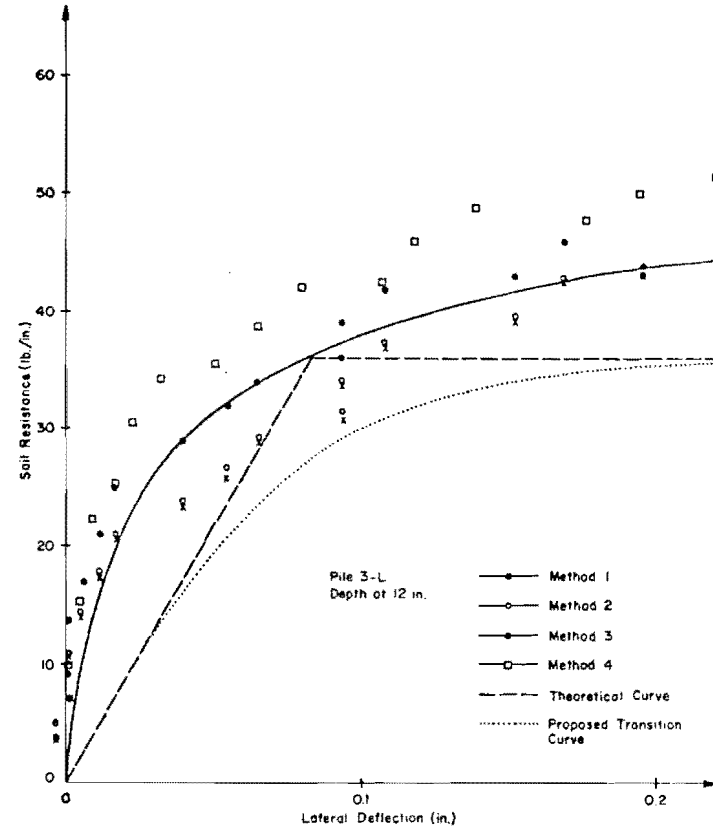


b. Curve for pile 3-L

Fig. 6.15. Lateral Soil Resistance Curves for a 6-inch Depth.

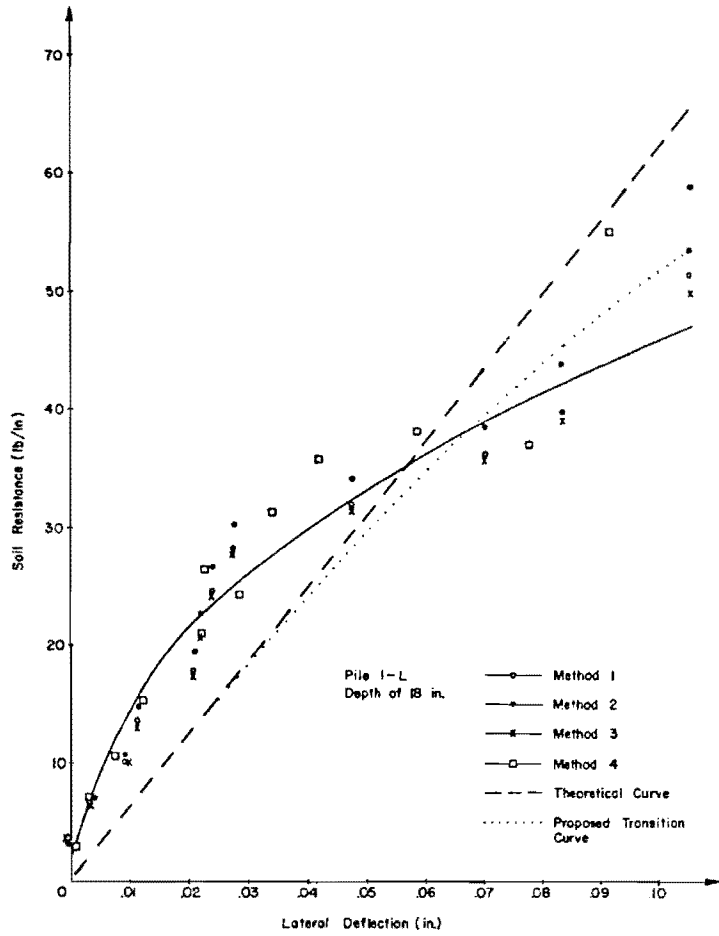


a. Curve for pile 1-L

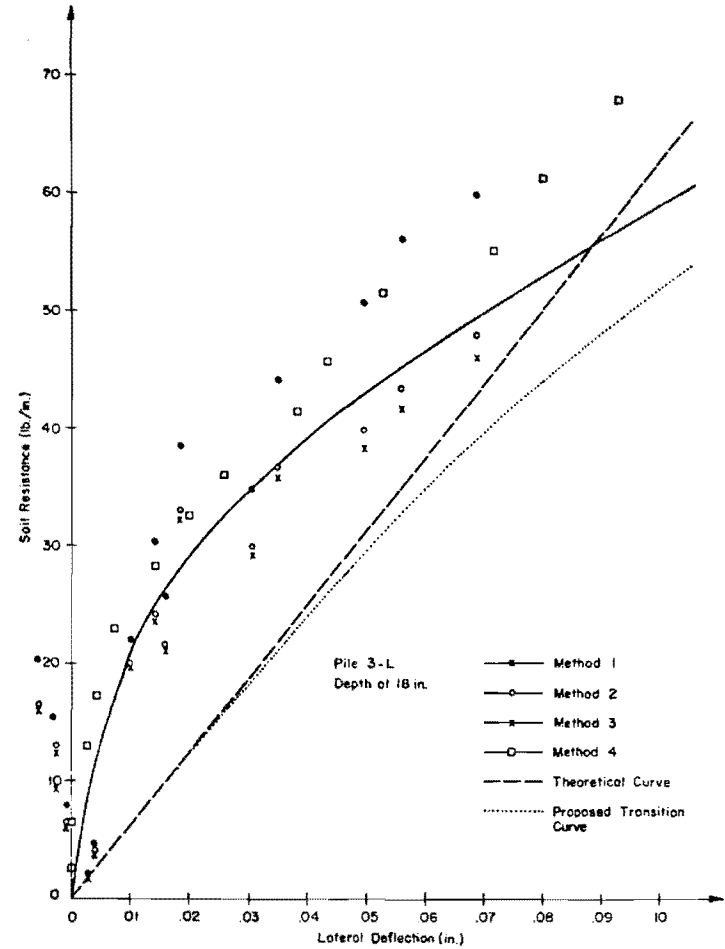


b. Curve for pile 3-L

Fig. 6.16. Lateral Soil Resistance Curves for a 12-inch Depth.

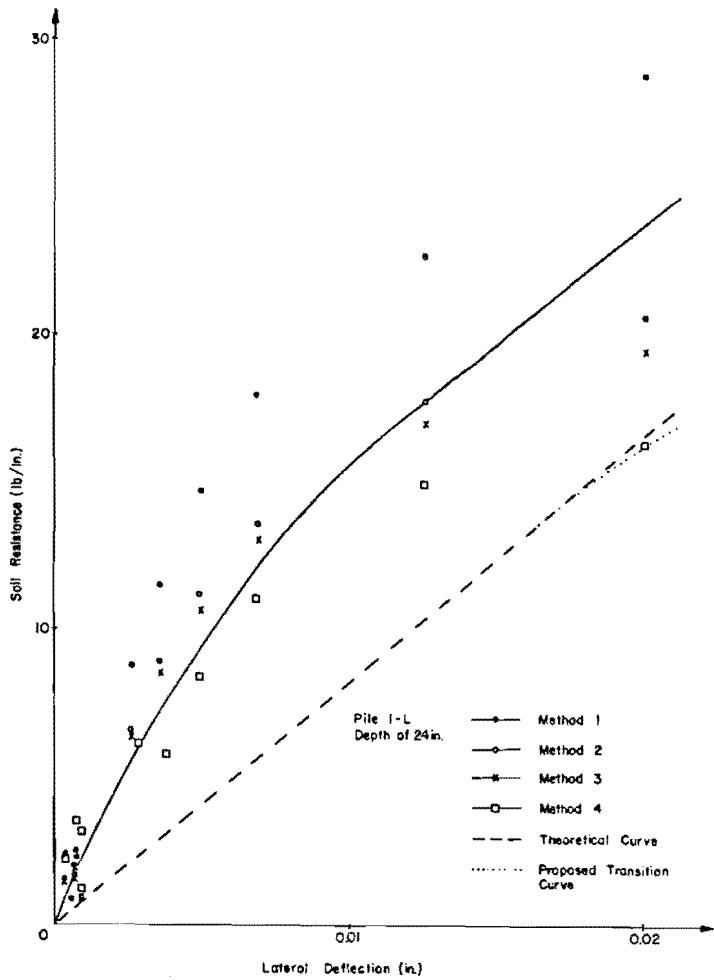


a. Curve for Pile 1-L

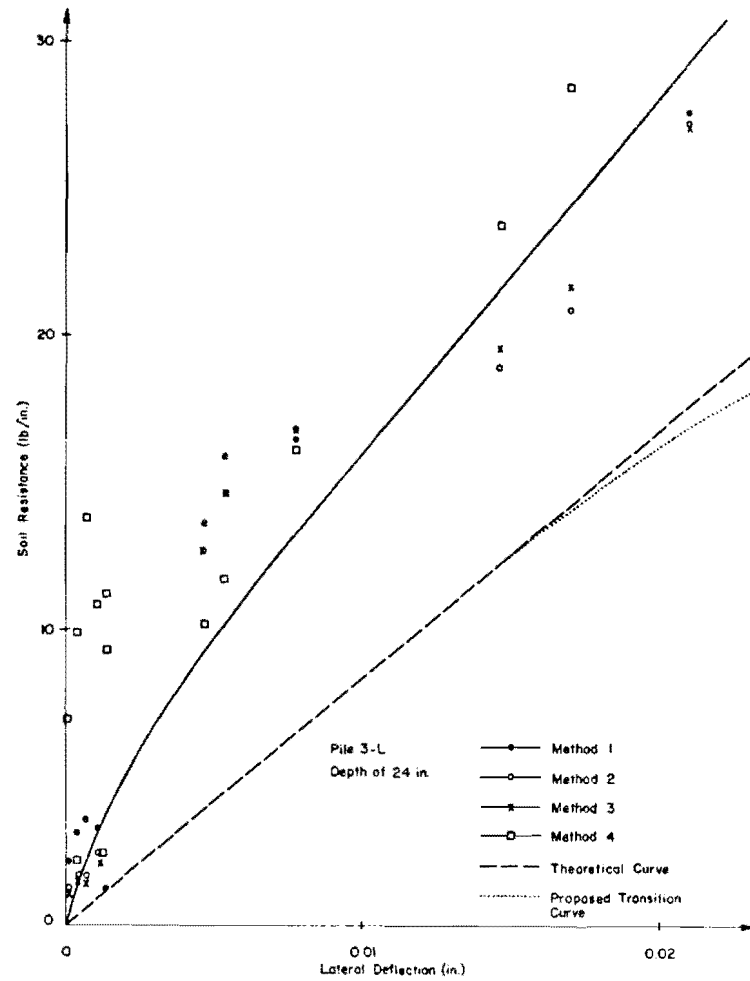


b. Curve for pile 3-L

Fig. 6.17. Lateral Soil Resistance Curves for an 18-inch Depth.



a. Curve for pile 1-L



b. Curve for pile 3-L

Fig. 6.18. Lateral Soil Resistance Curves for a 24-inch Depth.

In the following section the p-y curves computed from the measured moment distributions will be compared with curves obtained from theoretical criteria. Complete curves were obtained for depths of 6 and 12 inches, and the criteria for ultimate resistance and the initial portion of the curve are compared with the computer curves. For depths of 18 and 24 inches complete curves were not obtained, and it was only possible to compare the initial portions of the theoretical and measured curves at these depths.

Comparison of Measured and Theoretical p-y Curves

Curves obtained from the available criteria consist of two straight lines defined by Eqs. 6.4 or 6.14 and Eq. 6.19. For the test conditions, Eqs. 6.4 and 6.14 giving the ultimate resistance may be written as

$$P_{uw} = 0.389x + x^2 \left[\tan \alpha (0.474 - 0.085 K_x) + K_x (0.683) \right] \dots \dots \dots (6.34)$$

and

$$P_{uf} = 0.072x (170.798 + 61.429 K_x) \dots \dots \dots (6.35)$$

The values obtained from Eqs. 6.34 and 6.35 depend on the values selected for α and K_x . Bowman (1958) states that α may be a function of the void ratio of the sand, and suggests that α may range from $\phi/3$ for a loose sand to ϕ for a dense sand. The relative density of the sand used was about 95 per cent, so that it would appear that a

value of $\alpha = \phi$ would be applicable. However, from the limited test results, it appears that an average value of $\alpha = \phi/2$ best fits the measured curves.

Terzaghi and Peck (1967) suggest a range of values for K_x from 0.4 to 0.8. The value of $K_x = 0.8$ is suggested for sand placed in layers and tamped, which was the installation procedure used. In Chapter V, it was concluded that large lateral stresses probably existed in the sand in the test pit because of the method used to place the sand. It was noted that the coefficient of lateral earth pressure may have approached the coefficient of passive earth pressure. However, any movement in the sand, such as that caused by shear along the rupture surfaces and the upward movement of the wedge of soil, probably reduced the lateral pressure considerably along the rupture surfaces. This contention seems to be justified by the values of ultimate soil resistance measured for depths of 6 and 12 inches. In the following paragraph the possible range in ultimate resistance is considered.

The probable range in ultimate resistance values is illustrated in Table 6.1. These values were obtained from Eqs. 6.34 and 6.35, by using a range of values of α and K_x . For the maximum values, $\alpha = \phi$ and $K_x = 0.8$ were used. For the minimum values, $\alpha = 0$ and $K_x = 0.4$ were used, and for the average values, $\alpha = \phi/2$ and $K_x = 0.6$ were used.

If the modulus of elasticity of the sand is known, the slope of the initial portion of the curve is defined by Eq. 6.19. If the modulus of elasticity of the sand is not known, the slope can be approximated by Eq. 6.20. Since the sand had a relative density of about 95 per cent, the suggested values for a dense sand should be applicable. The possible

TABLE 6.1. RANGE OF VALUES FOR ULTIMATE SOIL RESISTANCE AND INITIAL SLOPE OF p-y CURVE

Depth (in.)	Max. P_{uw} (lb./in.)	Min. P_{uw} (lb./in.)	Avg. P_{uw} (lb./in.)	Max. P_{uf} (lb./in.)	Min. P_{uf} (lb./in.)	Avg. P_{uf} (lb./in.)	Max. k_s (lb./in. ²)	Min. k_s (lb./in. ²)	Avg. k_s (lb./in. ²)	Mea. k_s (lb./in. ²)
6	19	4	10	96	85	90	322	161	242	230
12	71	9	36	191	170	181	644	322	483	434
18	155	18	78	287	255	271	966	483	724	627
24	272	28	136	382	340	361	1290	644	967	817
30	423	41	210	478	425	451	1610	805	1208	1000
36	607	57	299	574	510	542	1930	965	1450	1170
67	2076	175	1014	1050	950	1008	3535	1800	2700	2100
96	4253	341	2066	1530	1359	1444	5140	2570	3865	2920

range of suggested slopes is illustrated in Table 6.1. These values were obtained from Eq. 6.20, using the suggested range of J values for a dense sand. For the maximum values $J = 2000$, for minimum values $J = 1000$, and for average values $J = 1500$, was used. The initial slopes of the stress-strain curve for the sand were established for use in fitting the hyperbolic curves. The expression obtained for the slope, may be written as

$$ES = 1675 (0.026x)^{0.915} \dots \dots \dots (6.36)$$

Values from this expression were used in Eq. 6.19 to obtain the slopes, designated as measured (Mea.) in Table 6.1. In Table 6.1, it is noted that the agreement between the slopes using the measured soil modulus and the average suggested values of J are quite good. It is also observed that the ranges between the maximum and minimum values for the ultimate wedge resistance and for the slopes are quite large.

However, the range of the values for the flow around failure are small, which indicates that the flow around criteria is insensitive to the value of K_x selected.

The slopes calculated using the measured soil modulus of elasticity and the ultimate values calculated using the wedge-failure theory with average values of α and K_x are shown as the dashed lines in Figs. 6.15 to 6.18. For the curves at a depth of 6 inches, the initial slopes of the measured and predicted curves compare well, but the predicted ultimate values are smaller than the measured values. For the curves at a depth of 12 inches, the comparison between the initial slopes and the ultimate values are quite good. For the 18- and 24-inch depth no

comparison can be made between the ultimate values, but for the limited range of deflections shown, both curves show the same trends.

The comparisons indicate that very near the soil surface, the proposed wedge-failure theory and method for predicting the initial slope give reasonable results. However, the comparisons provide no insight into the validity of either of the failure theories or the method of predicting the initial slope for depths greater than about 24 inches.

In the next section, a relationship is proposed to provide a smooth transition between the two straight lines. The transition relationship does not drastically change the curves, but it results in a more realistic shape. Comparisons made later between the measured and calculated deflected shapes and moment distributions will provide some indication as to the validity of the over-all procedure.

Transition Between Initial Slope and Ultimate Resistance

The comparison between the measured curves and the theoretically defined curves indicated that the two straight lines are fairly good approximations. In this section, a relationship will be developed which provides a smooth transition between the two straight-line portions. This relationship will not greatly alter the values for the curve, but it will provide a more realistic shape for the curve. Another reason for developing the relationship is that it will allow the curve to be described analytically as a continuous function.

Since a hyperbola was used for representing the sand stress-strain curves and axial load transfer, it was tried for the p-y curves. The equation tried had the same form as the one used for the stress-strain curves and was written as

$$p = \frac{y}{a' + b'y} \dots \dots \dots (6.37)$$

where

$$a' = 1/k_s$$

$$b' = 1/p_u$$

This curve provided the desired transition between the two straight lines, but the resulting curves were much flatter than the measured curves. The transition-type equation finally selected was the hyperbolic equation of the form

$$p = p_u \tanh\left(\frac{k_s y}{p_u}\right) \dots \dots \dots (6.38)$$

This equation describes a function which is tangent at $y = 0$ to the line with a slope of k_s , and which is asymptotic to the line described by the ultimate resistance p_u . The ultimate soil resistance p_u is defined by the smaller of the two values obtained from Eqs. 6.4 or 6.14, and the initial slope k_s may be defined by Eqs. 6.19 or 6.20.

Curves defined by Eq. 6.38 are shown plotted in Figs. 6.15 to 6.18 as the dotted lines. These curves are based on the average values for the initial slope and the ultimate resistance. In Figs. 6.15 and 6.16, it is noted that the transition curves provide good approximations to the shape of the measured curves. Figure 6.19 provides another comparison between the measured curves and the predicted curves. Based on the limited available measured curves, the comparison in Fig. 6.19 illustrates that the shape and trends indicated by the predicted curves are

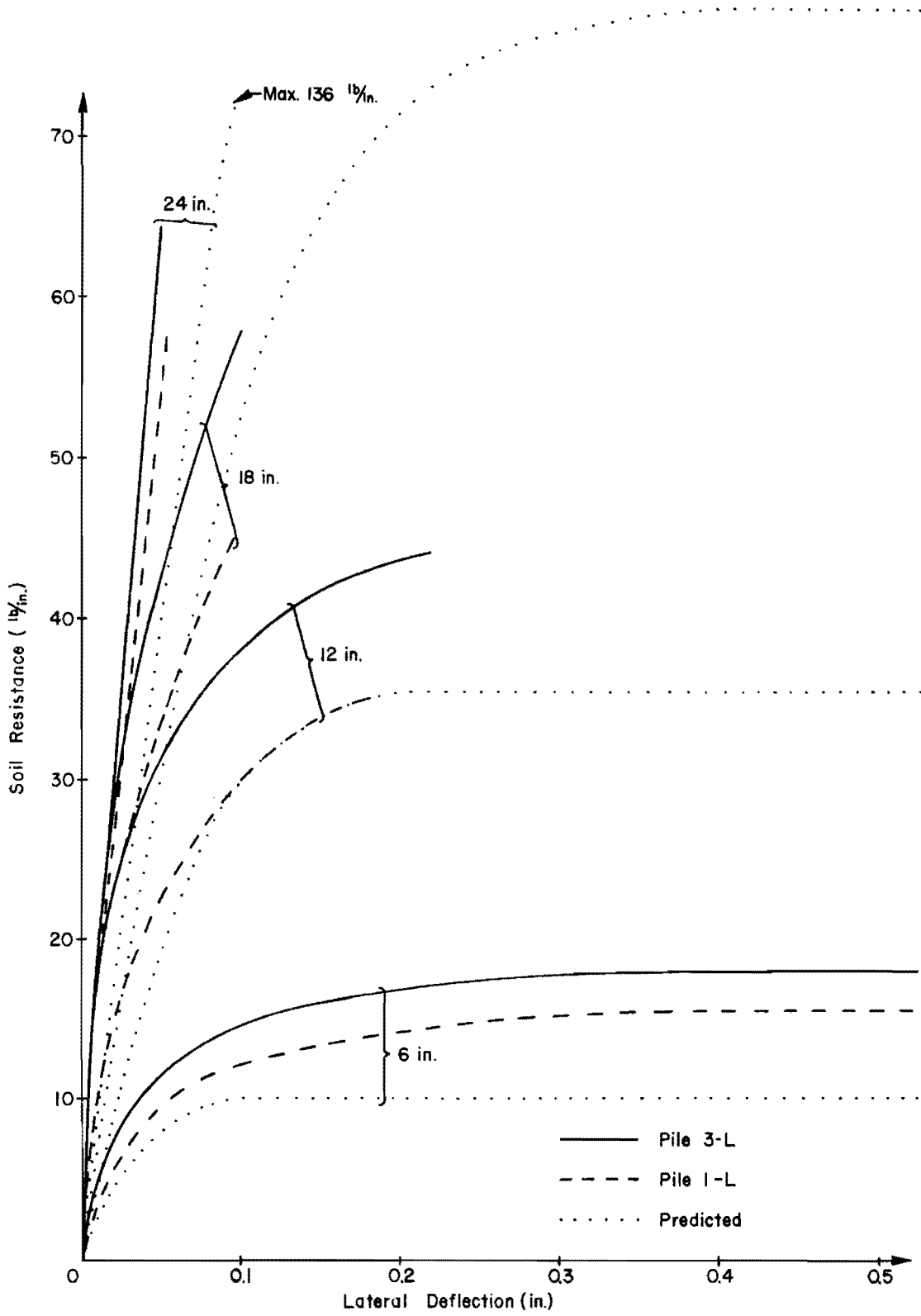


Fig. 6.19. Measured and Predicted p-y Curves.

reasonable approximations to the measured behavior. In the following section, the predicted p-y curves will be used to predict analytically the response of the test piles which will be compared with the measured response. The proposed criteria for generating p-y curves will also be applied to three tests reported in the literature and the predicted response compared with the measured response.

Comparisons of Measured and Predicted Lateral Pile Response

In this section, load-deformation curves, deflected shapes, and moment distributions, for the 2-inch diameter test piles, will be predicted analytically and compared with the measured values. In the computation of the pile behavior the soil response was represented by curves defined by Eq. 6.38. Values of initial slope used in Eq. 6.38 were obtained from soil modulus of elasticity obtained from laboratory stress-strain curves, and the ultimate resistance used was the smaller of the two values for the wedge or flow-around failures. In addition, the proposed criteria for describing p-y curves will be used to predict lateral response for three piles which were tested and the results reported in the literature. The tests analyzed were a 2-inch diameter pile reported by Shinohara and Kubo (1961), a 16WF36 pile reported by Mason and Bishop (1954), and a 16-inch diameter pile reported by Fruco and Associates (1964).

The computations were performed on a computer. The differential equation described in Chapter II is solved by the finite difference method, and a computer program for performing the necessary computations is presented by Awoshika and Reese (1971).

Comparisons for the 2-inch Diameter Test Piles

Comparisons between the measured and predicted load-deformation behavior of the top of the test piles may be made by referring to Fig. 6.7 through 6.10. The load-deflection curves for the top of the piles, shown in Figs. 6.7 and 6.8, indicate that the agreement is very good between the measured curve for pile 1-L and the predicted curve. These curves also indicate that the predicted deflections are approximately 25 per cent greater than the measured values for piles 2-L and 3-L. The same trends are illustrated in Figs. 6.9 and 6.10 for the load-slope curves. The closer agreement for pile 1-L was expected since the agreement between the predicted and measured p-y curves was better for the curves obtained from pile 1-L than for pile 3-L.

Measured and predicted moment distributions for piles 1-L and 3-L are illustrated in Figs. 6.11 and 6.12. As expected, the overall agreement between the curves is better for pile 1-L than for pile 3-L. For both piles, the agreement between the two curves is very good in the upper portions, but below the location of the maximum moment the curves begin to diverge. Below the location of the maximum moment the rate of decrease in the moment is smaller for the predicted curves than for the measured curves. This results in the downward movement of the points of zero moment. As illustrated in Fig. 6.12, the magnitude of the maximum negative predicted and experimental moments are approximately equal. One possible explanation for the downward movement of the points of zero moment is that with increasing depth there was a greater increase in the stiffness of the soil resistance than was reflected in the predicted curves. This trend is also illustrated by the steeper slopes of the

measured p - y curves in Fig. 6.19; but it is to be expected, since the assumptions and approximations made in developing the theoretical expressions for the ultimate resistance and initial slope were all on the conservative side. For practical problems, the most important aspect illustrated by the comparison is the close agreement obtained between the magnitude and location of the maximum moment. For design problems the location and magnitude of the maximum moment will be of primary importance.

Measured and predicted deflected shapes are shown in Figs. 6.20 and 6.21, for piles 1-L and 3-L. For pile 1-L, very good agreement is obtained for the upper portions of the pile. For pile 3-L, the agreement in the upper portion is not as good as it is for pile 1-L. As was observed for the moment distribution curves, the measured and predicted curves for the deflected shapes diverge with increasing depth. This divergence is illustrated by the deeper locations of the points of zero deflection for the predicted curves. One possible explanation for the differences in the curves is that the predicted p - y curves reflect a smaller increase in stiffness with depth than actually occurs. For the moment curves this explanation was sufficient, but for the deflected shapes a discrepancy arises, because the measured negative deflections are larger than the predicted values. The prediction of large negative deflections is contrary to what would be expected if the actual stiffness of the sand was greater than the predicted stiffness. A possible explanation for this discrepancy in negative deflections, and another possible cause for the difference in the locations of the points of zero deflection may be illustrated by considering the equations for calculating the deflections. Equations 6.22 and 6.23 are the equations used, and the slope and deflection at the ground

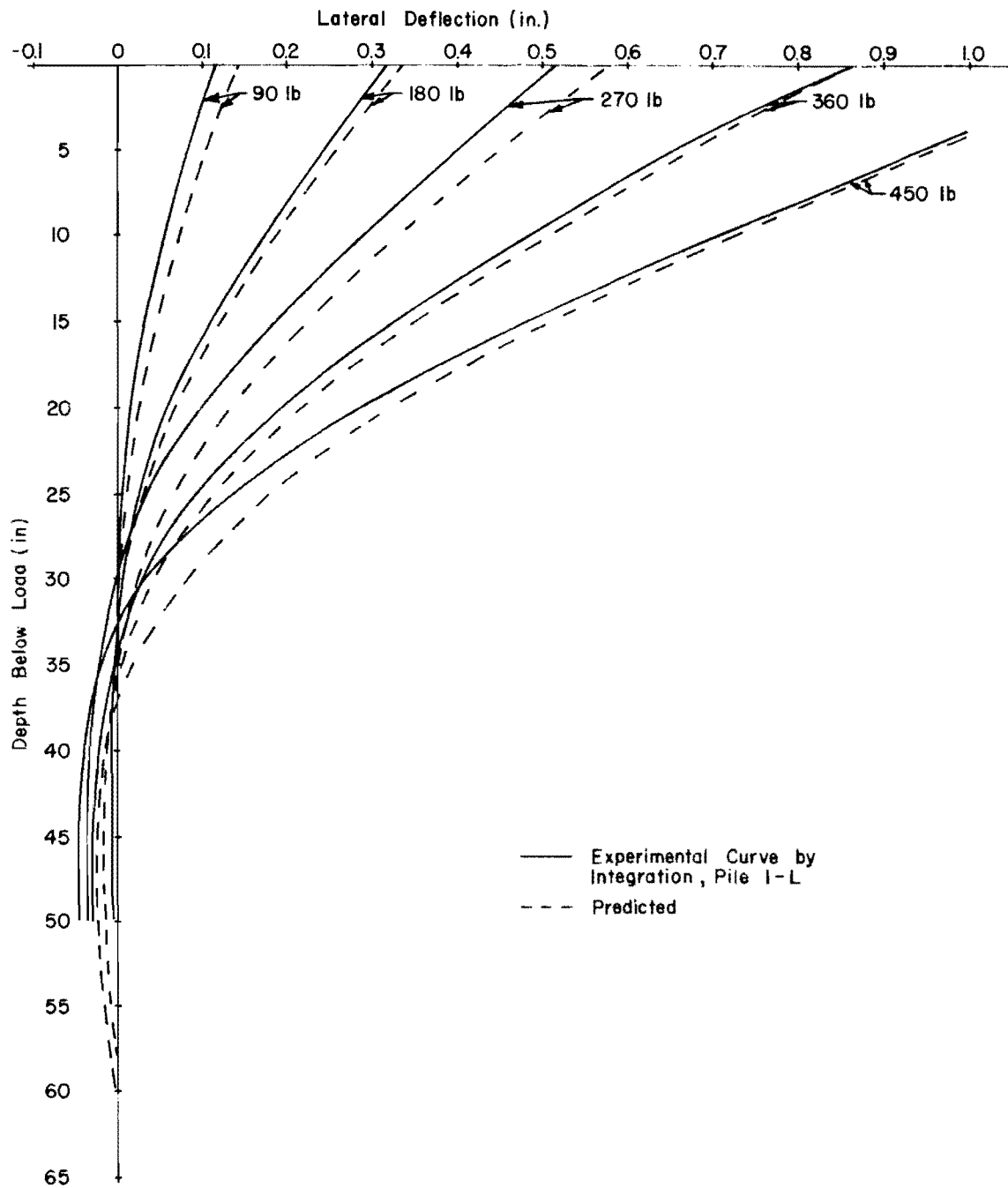


Fig. 6.20. Deflected Shapes for Pile 1-L.

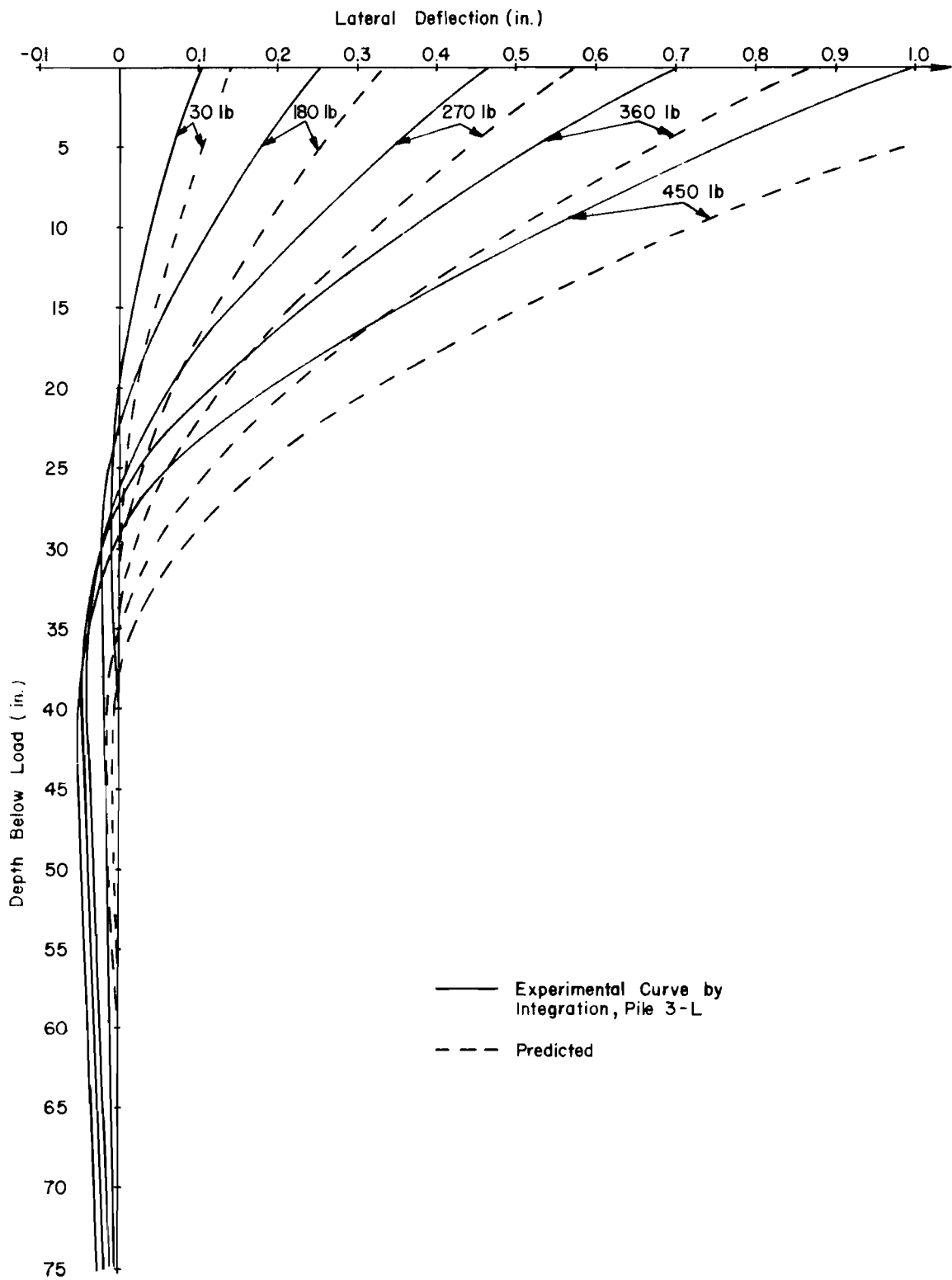


Fig. 6.21. Deflected Shapes for Pile 3-L.

line are the applied boundary conditions used in the equations to find the deflections. It is felt that the accuracy of the measured deflection at the ground line was much better than the accuracy of the slope. If the slope at the ground line, $i = 2$, is only slightly too large, the effect on the deflections in the upper portion will be small; but the effect is cumulative with depth and may become significant for larger depths. The errors in the measured deflections and slopes for the top of the pile could have caused part of the observed differences in the points of zero deflection, and could also account for the significant negative deflections which remain in the piles at larger depths.

From the standpoint of understanding the behavior of the piles, the deflections in the lower portions are important; but for practical problems the behavior of the top of the pile is of primary importance. Therefore, the most important aspect illustrated by the comparisons is the relatively good agreement obtained between the measured and predicted deformations in the upper portions of the pile.

The comparisons between the measured and predicted behavior of the test piles indicate that the computation procedure gives reasonable results, but they provide no indication of the applicability of the proposed criteria to other conditions. In the following sections the proposed criteria for describing p-y curves will be applied to three piles which have been tested, and the results reported in the literature.

Comparisons for Tests of Shinohara and Kubo

Shinohara and Kubo (1961) measured the bending moments along a 2-inch diameter free-head pile in sand. The deflection of the top of the pile was also measured. The pile was steel and had a flexural stiffness of $7.75 \times$

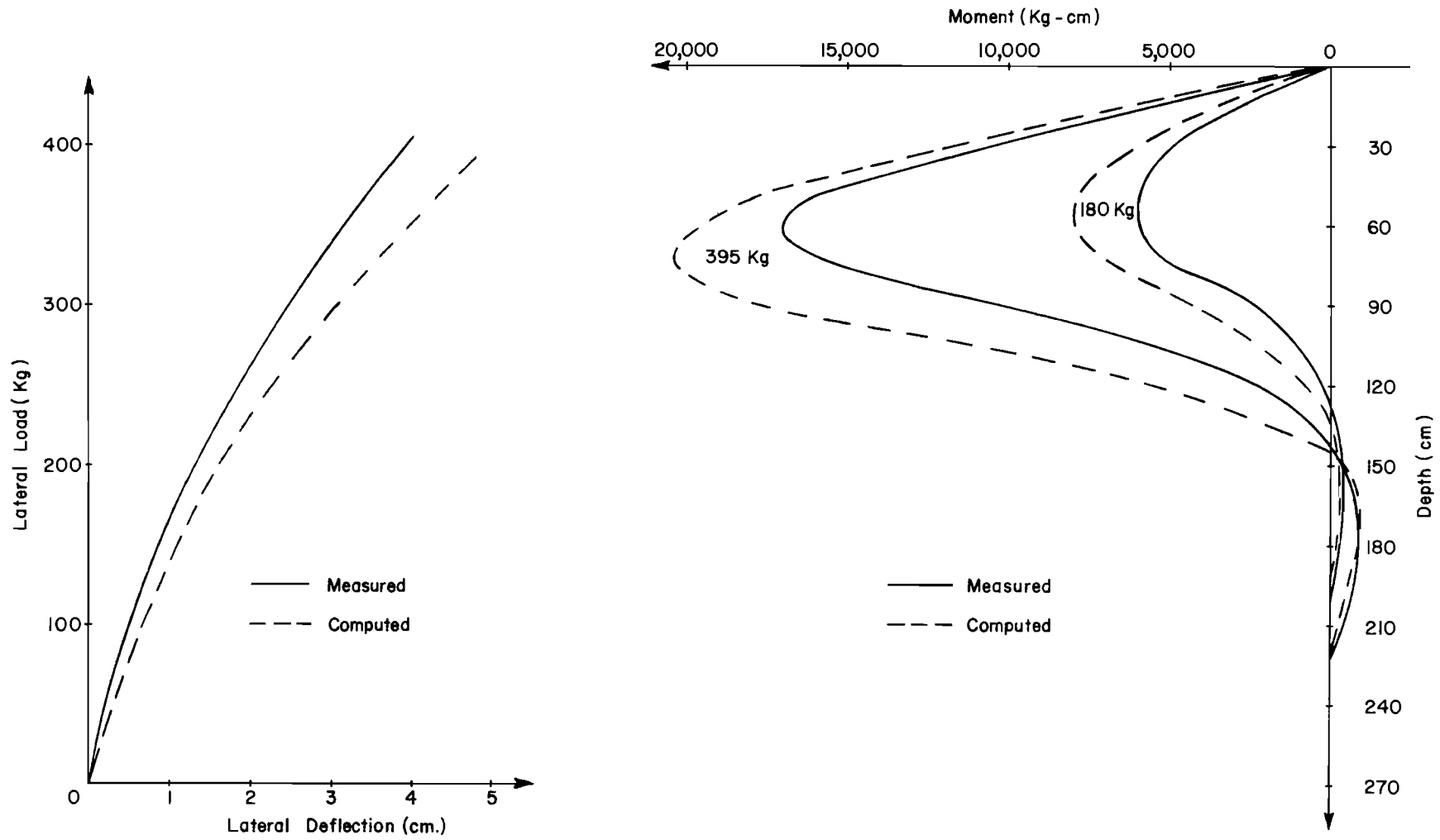
10^6 lb. - in.² The pile was positioned in a pit, and sand placed around the pile, so that 94 inches of the pile was embedded. The load was applied 6 inches above the soil surface. Compaction of the sand produced a dry density of 111.1 pcf. This density corresponded to a relative density of 86 per cent, and an effective unit weight when submerged of 60 pcf. The angle of internal friction of the sand was determined to be 44 degrees. The coefficient of lateral earth pressure K_x was assumed equal to one-half, and the angle α was assumed to equal to $\phi/2$.

The deflections at the point of application of the load and bending moments at points along the pile were measured for loads of 62, 117, 180, 237, 311, 353, 395 kilograms. The measured deflections are shown in Fig. 6.22(a) along with deflections from computer solutions using the proposed criteria for p-y curves. The measured moment distributions, for applied loads of 180 and 395 kilograms, are shown in Fig. 6.22(b) along with the moment distributions from computer solutions using the proposed criteria for p-y curves.

As shown in Fig. 6.22, the computed values of deflection and moment compare favorably with the measured ones. The computed deflections and moments are conservative. The difference between the measured and computed deflections is approximately 25 per cent. For the load of 180 kilograms, the difference between the measured and predicted maximum moment is approximately 30 per cent; and for the load of 395 kilograms, the difference is about 20 per cent.

Comparisons for Test of Mason and Bishop

Mason and Bishop (1954) measured the deflection and earth pressure along a free-head pile in sand. The steel 16WF36 section was 44.8 feet



a. Deflection at the load

b. Moment distribution

Fig. 6.22. Comparison Between Measured Results by Shinohara and Kubo and Results Computed with the Proposed Criteria.

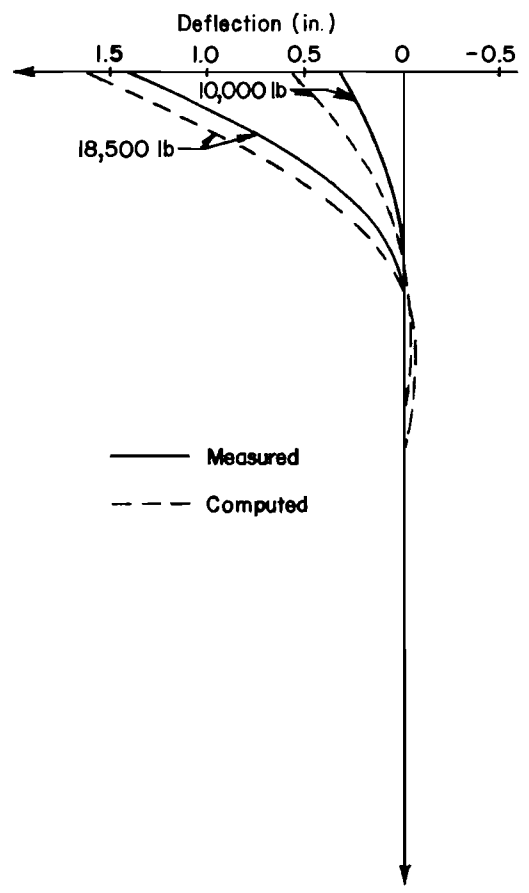
long and had 3/8 inch plates welded transversely between the flanges. The flexural stiffness of the pile was 2.3×10^9 lb. - in.² The pile was placed in an excavation, and sand placed around the pile, so that 40 feet of the pile was embedded. The load was applied at the surface of the soil.

The sand fill was constructed by compacting the sand in 6 inch layers. The density obtained was 98 pcf at a moisture content of 3 per cent. The angle of internal friction of the sand was determined to be 35 degrees. The coefficient of lateral earth pressure K_x was assumed equal to one-half, and the angle α was assumed equal to $\phi/2$.

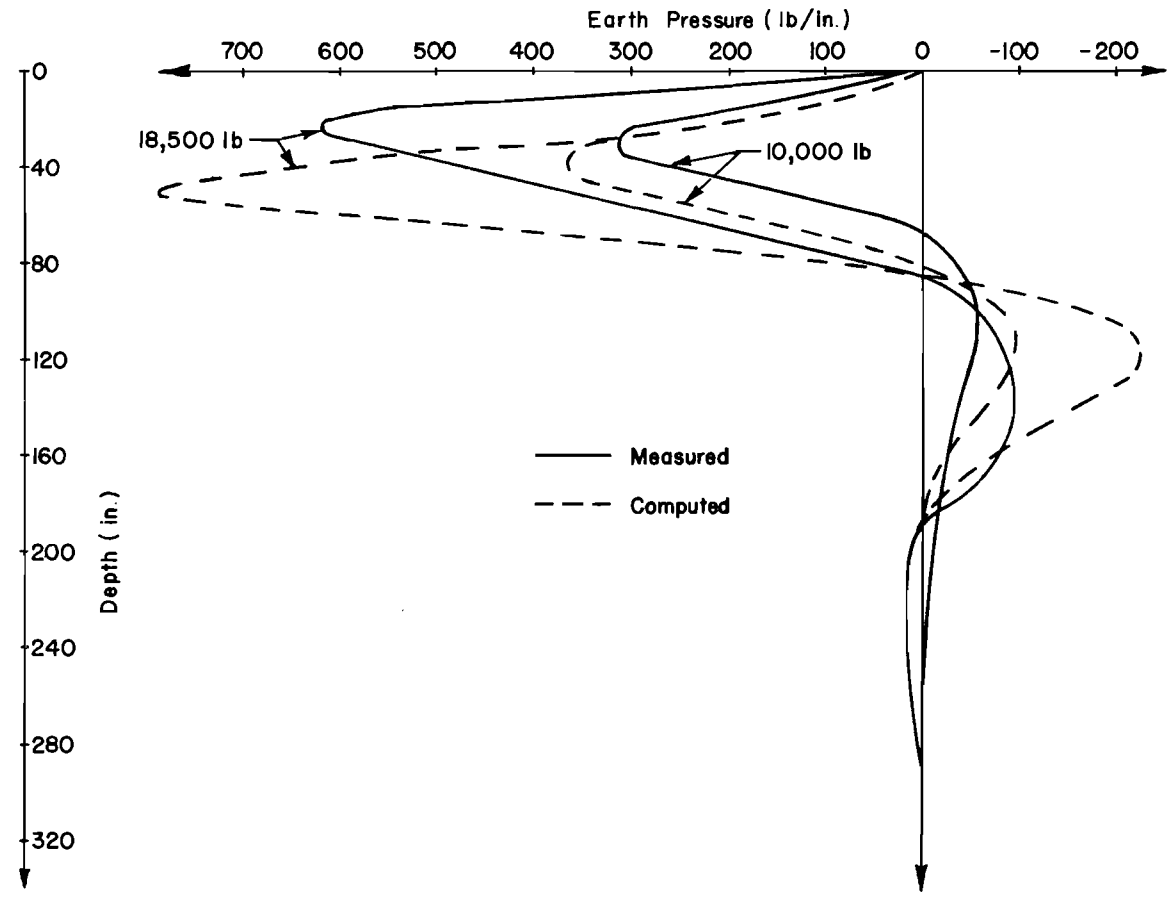
Before testing, an oscillator was strapped to the top of the pile and the pile vibrated. The vibrations produced additional compaction of the sand around the pile, but the magnitude of the densification and the influence on the angle of internal friction are not known.

Deflections and earth pressures at points along the pile were measured for applied loads of 10 and 18.5 Kips. The measured values are shown in Fig. 6.23 along with results from computer solutions using the proposed criteria.

As shown in Fig. 6.23(a), the computed deflected shapes compare favorably with the measured ones. For both loads, the computed deflections are conservative, and the differences between the measured and predicted values are about 40 per cent for the 10 Kip load and about 10 per cent for the 18.5 Kip load. The difference between the measured and computed maximum earth pressure, illustrated in Fig. 6.23(b), is about 15 per cent. The differences in the locations of the points of maximum earth pressure are probably due to the densification of the sand around the pile by the vibration of the pile.



a. Deflected shape



b. Distribution of earth pressure

Fig. 6.23. Comparison Between Measured Results by Mason and Bishop and Results Computed with the Proposed Criteria.

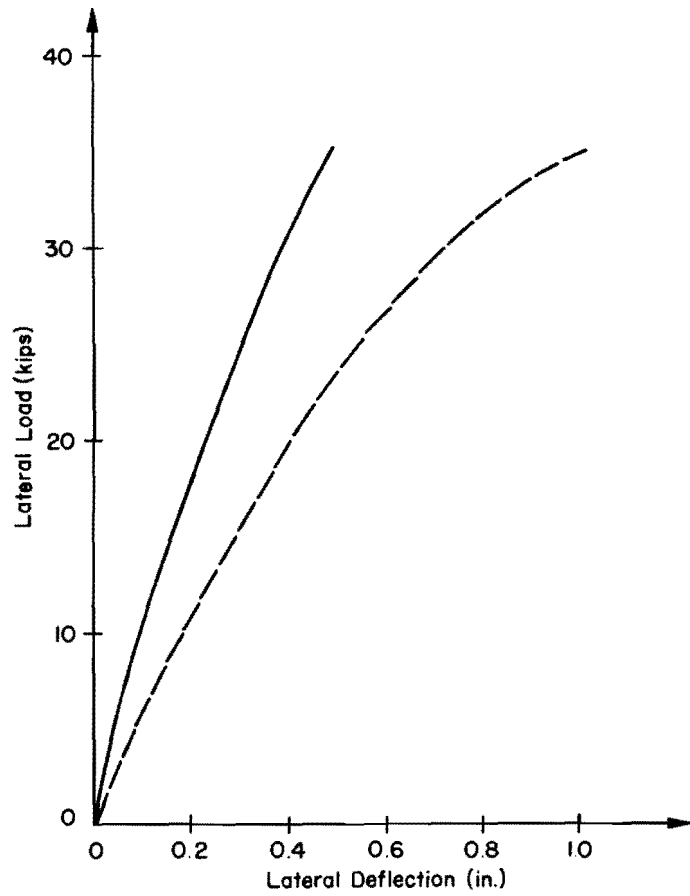
Comparisons for Arkansas River Test

The test considered here is one of a number of tests performed for the Corps of Engineers by Fruco and Associates at a location on the Arkansas River near Pine Bluff, Arkansas. The pile considered was designated as number 16, and consisted of a 16-inch diameter pipe with 3/8 inch walls. The flexural stiffness was 24×10^9 lb. - in.² The pile was driven and static loads applied at the surface of the soil. The water table was located 2 feet below the soil surface.

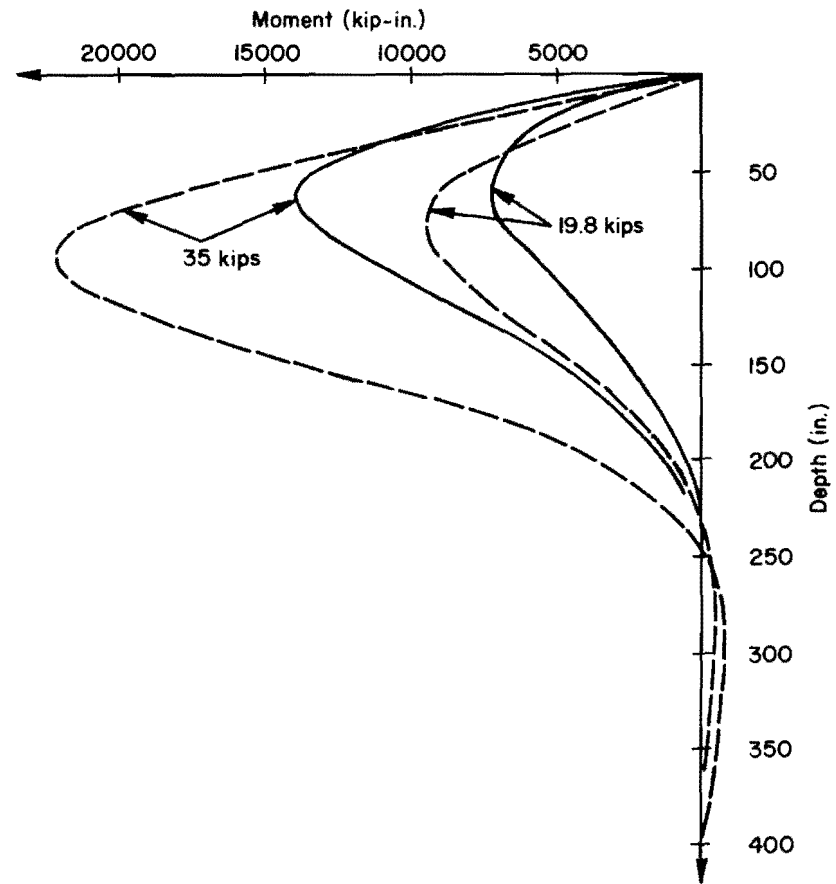
The sand had an average dry unit weight of 100 pcf and a submerged unit weight of 62.8 pcf. The relative density, estimated from standard penetration tests, was 75 per cent. The measured angle of internal friction ranged from 31 to 35 degrees with an average of 32 degrees. For the purpose of comparison in this report a value of 32 degrees will be used. The coefficient of lateral earth pressure K_x was assumed to be equal to one-half, and the angle α was assumed to be equal to $\phi/2$.

The deflections at the ground line and bending moments at points along the pile were measured for loads of 9.8, 19.8, 30.0 and 35.0 Kips. The measured deflections are shown in Fig. 6.24(a) along with deflections from computer solutions using the proposed criteria for p-y curves. The measured moment distributions, for applied loads of 19.8 and 35 Kips, are shown in Fig. 6.24(b).

As shown in Fig. 6.24(b), the computed deflections are approximately twice as large as the measured deflections. The measured and computed moment distributions in Fig. 6.24(b) are also considerably different. For the 35 Kip load, the difference between the maximum measured and computed moment is about 50 per cent. The differences between the measured and



a. Deflection at the ground line



b. Moment distribution

Fig. 6.24. Comparison Between Measured Results from Arkansas River Tests and Results Computed with the Proposed Criteria.

computed deflections indicate that the actual lateral soil resistance was quite a bit larger than the predicted resistance. This increased resistance could possibly have been caused by densification of the sand around the pile during driving.

Summary of Criteria for Describing Lateral Soil Resistance

The good agreement between the predicted p-y curves and the p-y curves obtained from the results of the tests of the 2-inch diameter test piles, and the reasonable agreement between the predicted and measured response of the three tests studied in the preceding section indicate that the proposed procedure for describing p-y curves may be used with some degree of confidence for practical field problems.

The step by step procedure to be followed when using the recommended criteria for defining p-y curves is as follows:

1. Obtain soil properties, such as angle of internal friction, unit weight, and relative density. If stress-strain curves are available, estimate values of modulus of elasticity from initial portions of the curves.
2. Obtain values of ultimate resistance from Eq. 6.4 or Eq. 6.14. For a particular depth use the smaller of the two values. For dense or medium sand, use $\alpha = \phi/2$ and $K_x = 0.5$ in Eqs. 6.4 and 6.14. For loose sand use $\alpha = \phi/3$ and $K_x = 0.4$.
3. Obtain values of initial slope of the curves in Eq. 6.19, if values of modulus of elasticity of the soil are known,

or from Eq. 6.20, if values of soil modulus of elasticity are not known. If Eq. 6.20 is to be utilized, use the following values of J :

Loose sand $J = 200$

Medium sand $J = 600$

Dense sand $J = 1500$

4. Obtain complete p-y curves from Eq. 6.28 by substituting into the expression values of ultimate resistance and initial slope.
5. Obtain the response of a pile by using the predicted interaction curves with the finite difference procedure described in Chapter II for solving the differential equations for a laterally loaded pile. A computer program for performing the necessary computations is presented by Awoshika and Reese (1971).

Comments and Discussion of Results

The limited amount of data obtained, from the lateral load tests of the 2-inch diameter piles, restricted the measured p-y curves to the upper portion of the piles. Therefore, rather than attempting to correlate the measured p-y curves with stress-strain curves for the sand, as was done for the axial shear transfer curves, the measured p-y curves were compared with analytically defined curves. This comparison was made to check the validity of the proposed criteria for defining the p-y curves. The validity of the criteria was also checked by comparing the measured response of the 2-inch diameter test piles with the response computed, using predicted

p-y curves. Additional checks were made by comparing the measured and predicted response for three tests reported in the literature.

The good agreement obtained between the measured and predicted response of the 2-inch diameter test piles indicates that the computational procedure and the method of representing the pile-soil interaction by independent springs is valid. The reasonable agreement obtained for the three tests from the literature indicate that the proposed criteria may be applied to other conditions with some degree of confidence. However, there are several factors which make it impossible to recommend the criteria without reservations, for a wide variety of problems. For one thing, only three cases were considered. The possible inaccuracies in the test results and the given soil properties are two other factors which must be considered when analyzing the comparisons between the measured and computed response. However, for all three tests the computed response was conservative which enhances the proposed criteria.

There are several parameters which have not been considered, but which could possibly affect the lateral pile-soil interaction. The lateral soil resistance is represented by a series of independent springs and, thus, satisfies the Winkler assumption made in the derivation of the equations for describing the behavior of a laterally loaded pile. This assumption implies that the lateral soil resistance is independent of the deflected shape of the pile. Intuitively it would appear that the influence of the deflected shape would be small because of the relatively small curvature that would exist in a pile. Matlock (1970) tested both free-head and restrained-head piles in clay, and concluded that the soil resistance-lateral deflection relationships were independent of the pile

head restraint and deflected shape. It is felt that the same conclusions could be drawn for piles in sand.

In Chapter II, it was noted that the lateral and axial soil resistance are assumed to be independent. This assumption was mentioned again in discussing the axial shear transfer curves. The validity of the assumption may be studied by considering an example problem. Figure 6.25 shows the deflected shape and lateral soil resistance distribution for one of the 2-inch diameter test piles with a lateral load of 450 pounds. Also shown in the figure is the distribution of the axial load that is distributed to the surrounding soil for an axial load of 4200 pounds.

Referring to Fig. 6.25, it can be seen that the lateral deflection of the pile is quite small below a depth of 30 inches. Also shown in the figure is the fact that only about 15 per cent of the axial load is transferred to the soil above this depth. Thus, the soil near the ground surface is of major importance in transferring lateral load and the soil at some distance from the ground surface is of major importance in transferring axial load. While the figure does not prove conclusively that lateral and axial behavior can be uncoupled, it seems reasonable to say that effects of interaction between axial and lateral behavior would be small.

The batter of a pile is another parameter which warrants some consideration. The loading of the 2-inch diameter test piles indicated that an out-battered pile is more flexible than an in-battered or vertical pile. No quantitative data are available regarding this effect, but for practical design problems it should be given some attention. There is also the problem of determining the properties of the sand around the pile after

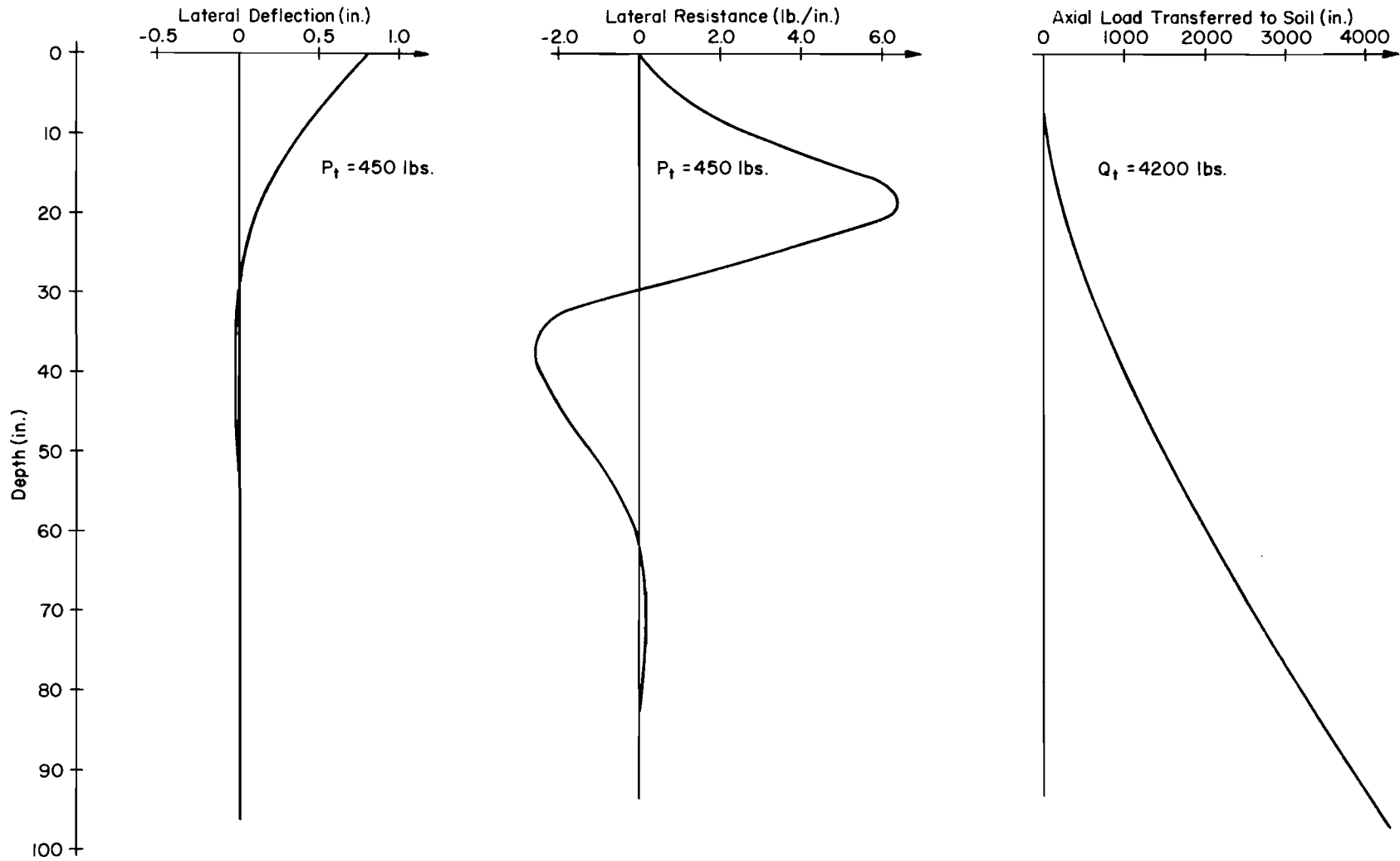


Fig. 6.25. Example Illustrating the Distribution of Lateral and Axial Load to the Sand for a Two-inch Diameter Test Pile.

the pile has been installed. For a driven pile, the sand will probably be densified, and p-y curves predicted with the in situ properties of the sand will probably be conservative. However, for a pile that was cast in place or bored pile, the installation procedure may have loosened the soil around the pile. For practical problems the batter of the pile and the method of installation should be considered.

There is also the problem of defining the parameters K_x , α , and J to be used in Eqs. 6.4, 6.14 and 6.20. For the 2-inch diameter test piles, it was assumed that $K_x = 0.6$ and that $\alpha = \phi/2$. Measured values of the soil modulus of elasticity were used. The measured values of the modulus of elasticity agreed favorably with values obtained using $J = 1500$ which was the average recommended value for a dense sand. For the three additional tests studied, values of $K_x = 0.5$, $\alpha = \phi/2$, and $J = 1500$ were used to define the ultimate soil resistance and initial slope of the p-y curves. For all three tests these assumptions resulted in conservative estimates of the soil resistance curves. However, until the parameters are better defined it may be advisable to use the most conservative of the values which are recommended.

The complexity of the interaction of a pile with the soil makes a rigorous analysis impossible. Therefore, a simplified approach was taken in order to get some approximation of the lateral interaction. However, based on the comparison of the measured and predicted p-y curves from the 2-inch diameter test piles and the comparisons of the measured and computed response for the three additional tests investigated, it appears that the proposed criteria produces results that are conservative and that are reasonable approximations of the actual behavior of a laterally loaded pile.

CHAPTER VII

CONCLUSIONS AND RECOMMENDATIONS

Axial and lateral pile-soil interaction, for piles in sand, was investigated in this study. Emphasis was placed on formulating criteria for describing the pile-soil interaction in the form of nonlinear curves, which can be used to predict the behavior of a pile when loaded. It was assumed that the axial interaction was independent of the lateral interaction, and that the two could be studied separately. Two-inch diameter piles, placed in sand prepared with controlled properties, were loaded to study the transfer of loads from the pile to the soil.

Experimental Procedures

The following conclusions can be drawn about the experimental procedures employed:

1. The method of placing sand resulted in a uniform deposit. The compacted sand had a high relative density and high horizontal residual stresses existed in the deposit.
2. The procedures for measuring density resulted in a reasonably accurate determination of the density.
3. The hyperbolas generated for representing the stress-strain curves for the sand provided reasonable approximations for the measured curves.

4. The instrumentation on the piles functioned adequately and permitted reasonably accurate measurement of axial force and bending moment in the test piles.
5. The results from the tests provide a basis for the formulation of criteria to describe axial and lateral pile-soil interaction, and accurate pile response that was used to check the validity of the criteria that were developed.

Behavior Under Axial Load

Based on the results of the study of the axial behavior, the following conclusions may be drawn regarding the criteria that were developed for representing the behavior of the sand around a pile:

1. The proposed criteria for obtaining s_x -z curves accurately represented the transfer of load from the piles to the soil for the 2-inch diameter test piles.
2. The results from the test piles indicate that shear transfer is different for pullout and compression loading, and that for compression loading the shear transfer is not a linear function of depth.
3. The proposed criteria for obtaining s_x -z curves represented reasonably well the transfer of load from the piles to the soil for the full-scale tests analyzed.
4. The proposed criteria for obtaining s_x -z curves may be applied to design problems; but with caution, since only limited checks have been made.

5. Little data are available in the literature and little information was generated in the tests run for this study on the transfer of load to the soil through the tip of a pile. The best information available will result in an approximate curve composed of an initial straight line and an ultimate value of load.
6. The finite difference technique for solving the differential equation for an axially loaded pile will produce reliable results, if representative interaction curves are used.

The need for realistic correlation coefficients for a wide range of soil conditions, methods of installation, and pile material; and the need for additional tip load-deformation data illustrates the need for additional testing. There have been a great number of load tests performed but, unfortunately, the majority of the tests fail to provide data necessary to adequately describe the interaction between the pile and soil. In order to provide the necessary information, the following five factors should be considered in further testing:

1. Pile Size. It is recommended that full-scale piles be tested. There are several reasons for this stipulation. One is to clarify the effect of size on the shear transfer and tip load-deformation curves. Another reason would be to test piles with realistic length to diameter ratios, in order to either verify or disprove the assumption that there is some limiting depth to diameter ratio at which the maximum tip load and shear transfer are no longer linear functions of depth.

2. Instrumentation. Instrumentation should be provided for measuring the load distribution in the pile. Special care should be taken near the tip in order to accurately describe the tip behavior.
3. Sand Conditions. It would be desirable to test for a wide range of sand conditions. However, a realistic approach would be to run tests in sands with loose, medium, and dense classifications of relative density. Extensive sampling and testing should be performed in order to accurately determine the sand properties.
4. Method of Installation. There are basically four methods of installing piles in sand, and theoretically, each should result in different interaction curves. Therefore, tests should be run to clarify the effect of the method of installation.
5. Pile Material. The apparent friction angle between the sand and pile material will be different for different materials; thus, the shear transfer along the shaft will be different. Therefore, tests should be run to clarify the effect of the pile material.

A testing program considering all the factors mentioned above would be very expensive and time consuming. However, the complexity of the problem and the number of variables which must be considered will require a detailed study. It is also possible that a detailed study will result in simplified criteria which would produce adequate results.

Behavior Under Lateral Load

Based on the results of the study of the lateral behavior, the following conclusions may be drawn regarding the criteria that were developed for representing the behavior of the sand around the pile:

1. The proposed criteria for obtaining p-y curves accurately represented the lateral resistance of the sand for the 2-inch diameter test piles.
2. The results from the test piles indicate that there was no difference between the response of vertical and in-battered piles, but that both were stiffer than out-battered piles.
3. The proposed criteria for obtaining p-y curves represented reasonably well the lateral resistance of the sand for the tests from the literature that were analyzed.
4. The prediction of the ultimate soil resistance near the surface depends on the values of α and K_x used, and the ultimate resistance at larger depths depends on the value of K_x . Recommended values have been given for various relative densities.
5. The prediction of the initial slope of a p-y curve depends on the value of soil modulus of elasticity used. Recommended values have been given for various relative densities.
6. The proposed criteria for obtaining p-y curves may be applied to design problems; but with caution, since only limited checks have been made.
7. The finite difference technique for solving the differential equations for a laterally loaded pile will produce reliable results if representative interaction curves are used.

In order to verify adequately the proposed criteria, the effect of several parameters such as method of installation, sand conditions, pile size, and loading will have to be clarified. The effect of the various parameters can only be clarified with additional testing, and in order to provide the necessary information the following factors should be considered.

1. Pile Size. Full-scale piles should be used in order to eliminate any scale effects, and the piles should be designed so that both assumed modes of failure can be investigated.
2. Instrumentation. Instrumentation should be provided for measuring the moment distribution in the pile.
3. Sand Conditions. Tests should be run for sands with various relative densities in order to define more precisely values of soil modulus of elasticity, K_x , and α to use.
4. Loading Conditions. Up to this point in this study, only static short term loading has been considered. However, most lateral forces on piles will be due to live loads on the structure so that the loads may be cyclic and dynamic. Cyclic loading is probably the most critical and should be considered in any additional testing.

REFERENCES

- ASTM Procedures for Testing Soils 1964 (1964), American Society for Testing Materials, 1964, p 175.
- Awoshika, K. and L. C. Reese (1971), "Analysis of Foundations with Widely Spaced Piles," Research Report No. 117-3, Center for Highway Research, The University of Texas at Austin, 1971.
- Bowman, Elliott R. (1958), "Investigation of the Lateral Resistance to Movement of a Plate in Cohesionless Soil," Thesis submitted to The University of Texas at Austin, January 1958.
- Broms, B. B. (1964a), "Lateral Resistance of Piles in Cohesive Soils," Journal of the Soil Mechanics and Foundations Division, American Society of Civil Engineers, March, 1964, p 27.
- Broms, B. B. (1964b), "Lateral Resistance of Piles in Cohesionless Soils," Journal of the Soil Mechanics and Foundations Division, American Society of Civil Engineers, May, 1964, p 123.
- Bullen, F. R. (1958), "Phenomena Connected with the Settlement of Driven Piles," Geotechnique, Vol 8, No 3, September 1958, p 121.
- Coyle, H. M., and Lymon C. Reese (1966), "Load Transfer for Axially Loaded Piles in Clay," Journal of the Soil Mechanics and Foundations Division, American Society of Civil Engineers, March 1966, p 2.
- Coyle, Harry M. and Ibrahim H. Sulaiman (1967), "Skin Friction for Steel Piles in Sand," Journal of the Soil Mechanics and Foundations Division, American Society of Civil Engineers, Vol 93, November 1967, p 261.
- D'Appolonia, E. and J. P. Romualdi (1963), "Load Transfer in End-Bearing Steel H-Piles," Proceedings, American Society of Civil Engineers, Vol 89, 1963, p 1.
- Denisov, N. Y., I. V. Dudlers, V. A. Durante, and M. I. Khazanov (1963), "Studies of Changes of Strength and Compressibility of Hydraulically Filled Sands in Time," Proceedings, European Conference on Soil Mechanics and Foundation Engineering, Wiesbaden, Vol 1, 1963, p 221.
- Focht, John A., Jr. and Bramlette McClelland (1955), "Analysis of Laterally Loaded Piles by Difference Equation Solution," The Texas Engineer, Texas Section of American Society of Civil Engineers, September, October, and November 1955.

- Fruco and Associates (1964), "Pile Driving and Loading Tests, Lock and Dam No. 4, Arkansas River and Tributaries, Arkansas and Oklahoma," Report for U. S. Army Engineer District, Little Rock, Little Rock, Arkansas, September, 1964.
- Gibbs, H. J. and W. G. Holtz (1957), "Research on Determining the Density of Sands by Spoon Penetration Testing," Proceedings, Fourth International Conference on Soil Mechanics, London, Vol 1, 1957, p 35.
- Gleser, Sol M. (1953), "Lateral Load Tests on Vertical Fixed-head and Free-head Piles," Special Technical Publication 154, American Society for Testing Materials, 1953, p 75.
- Hetenyi, M. (1946), Beams on Elastic Foundation, University of Michigan Press, Ann Arbor, Michigan, 1946.
- Kerisel, Jean (1964), "Deep Foundations Basic Experimental Facts," Proceedings, Conference on Deep Foundations, Mexican Society of Soil Mechanics, Mexico City, Vol 1, 1964, p 5.
- Kondner, R. L. and J. S. Zelasko (1963), "A Hyperbolic Stress-Strain Formulation for Sands," Proceedings, Second Pan American Conference on Soil Mechanics and Foundation Engineering, Brazil, Vol 1, 1963, p 289.
- Lambe, T. William (1967), Soil Testing for Engineers, John Wiley and Sons, Inc., New York, 1967.
- Lambe, T. William and Robert V. Whitman (1969), Soil Mechanics, John Wiley and Sons, Inc., New York, 1969.
- Mackey, R. D. and Donald Pearson Kirk (1968), "At Rest, Active and Passive Earth Pressures," Proceedings, Southeast Asian Regional Conference on Soil Engineering, Bangkok, 1968, p 187.
- Mason, H. G. and J. A. Bishop (1954), "Measurement of Earth Pressure and Deflection Along the Embedded Portion of a 40-ft Steel Pile," ASTM Special Technical Publication No. 154, American Society for Testing Materials, 1954, p 1.
- Matlock, Hudson (1970), "Correlations for Design of Laterally Loaded Piles in Soft Clay," Presented at the Second Annual Offshore Technology Conference, Houston, Texas, 1970.
- Matlock, Hudson, Rachid Abdel-Raof and John J. Panak (Research in progress), "A Computer Program for Nonlinear Bending and Support Analysis for Beam Columns," Center for Highway Research, The University of Texas at Austin.

- Matlock, Hudson and Lymon C. Reese (1961), "Foundation Analysis of Offshore Pile-Supported Structures," Proceedings, Fifth International Conference, International Society of Soil Mechanics and Foundation Engineering, Paris, Vol 2, 1961, p 91.
- Matlock, Hudson and Lymon C. Reese (1960), "Generalized Solutions for Laterally Loaded Piles," Journal of the Soil Mechanics and Foundations Division, American Society of Civil Engineers, October, 1960, p 63.
- Matlock, Hudson and E. A. Ripperger (1956), "Procedures and Instrumentation for Tests on a Laterally Loaded Pile," Proceedings, Eighth Texas Conference on Soil Mechanics and Foundation Engineering, Austin, Texas, 1956.
- Matsuo, H. (1953), "Tests on Lateral Resistance of Piles," Report No. 42 and Report No. 46, Japanese Research Institute of Civil Engineering, Ministry of Home Affairs, 1938 and 1939. (as quoted by G. P. Tschebotarioff, in ASTM, Special Technical Publication No. 154, 1953, p 48).
- Mattes, Neil S. and Harry G. Poulos (1969), "Settlement of Single Compressible Pile," Journal of the Soil Mechanics and Foundation Division, American Society of Civil Engineers, Vol 95, January 1969, p 189.
- Mazurkiewicz, B. K. (1968), "Skin Friction on Model Piles in Sand," Bulletin No. 25, The Danish Geotechnical Institute, Copenhagen, 1968, p 13.
- McClelland, Bramlette and John A. Focht, Jr. (1958), "Soil Modulus for Laterally Loaded Piles," Transactions, American Society of Civil Engineers, Vol 123, 1958, p 1049.
- Miller, F. E. and H. A. Doeringsfeld (1965), Mechanics of Materials, International Textbook Company, Scranton, Pennsylvania, 1965.
- Mindlin, R. D. (1936), "Force at a Point in the Interior of a Semi-Infinite Solid," Physics, Vol 7, No 5, 1936, p 195.
- Palmer, L. A. and James B. Thompson (1948), "Horizontal Pressures on Pile Foundations," Proceedings, Third International Conference on Soil Mechanics and Foundation Engineering, Rotterdam, Vol 5, 1948, p 156.
- Parker, Frazier, Jr. and William R. Cox (1969), "A Method of Analysis of Pile Supported Foundations Considering Nonlinear Soil Behavior," Research Report No. 117-1, Center for Highway Research, The University of Texas at Austin, June 1969.
- Perry, C. C. and H. R. Lissner (1962), The Strain Gage Primer, McGraw-Hill Book Co., New York, 1962.

- Potyondy, J. G. (1961), "Skin Friction Between Various Soils and Construction Materials," Geotechnique, Vol 11, No 4, December 1961, p 339.
- Poulos, H. G. and E. H. Davis (1968), "The Settlement Behavior of Single Axially Loaded Incompressible Piles and Piers," Geotechnique, Vol 18, No 3, September, 1968, p 351.
- Prakash, Shamsar (1961), "Behavior of Pile Groups Subjected to Lateral Loads," Dissertation submitted to The University of Illinois, December, 1961.
- Reese, Lymon C. (1958), Discussion of "Soil Modulus for Laterally Loaded Piles," by Bramlette McClelland and John A. Focht, Jr., Transactions American Society of Civil Engineers, Vol 123, 1958, p 1071.
- Reese, Lymon C. (1962), "Ultimate Resistance Against a Rigid Cylinder Moving Laterally in a Cohesionless Soil," Journal, Society of Petroleum Engineers, December 1962, p 355.
- Reese, Lymon C. (1964), "Load Versus Settlement for an Axially Loaded Pile," Proceedings, Symposium on Bearing Capacity of Piles, Central Building Research Institute, Roorkee, India, 1964.
- Reese, Lymon C. (1966), "Analysis of a Bridge Foundation Supported by Batter Piles," Proceedings, Fourth Annual Engineering Geology and Soils Engineering Symposium, Moscow, Idaho, 1966, p 61.
- Reese, L. C. and W. R. Cox (1969), "Soil Behavior from Analysis of Tests of Uninstrumented Piles Under Lateral Loading," Special Technical Publication 444, American Society for Testing Materials, 1969, p 160.
- Reese, Lymon C. and Hudson Matlock (1956), "Non-Dimensional Solutions for Laterally Loaded Piles with Soil Modulus Assumed Proportional to Depth," Proceedings, Eighth Texas Conference on Soil Mechanics and Foundation Engineering, Austin, Texas, 1956.
- Reese, Lymon C. and Hudson Matlock (1960), "Numerical Analysis of Laterally Loaded Piles," Proceedings, Second Structural Division Conference on Electronic Computation, American Society of Civil Engineers, Pittsburgh, 1960, p 657.
- Reese, Lymon C. and Hudson Matlock (1966), "Behavior of a Two-Dimensional Pile Group Under Inclined and Eccentric Loading," Proceedings, Off-shore Exploration Conference, Long Beach, California, 1966, p 123.
- Robertson, Robert N. (1961), "The Analysis of a Bridge Bent with Batter Piles," Thesis submitted to The University of Texas at Austin, January 1961.

- Seed, H. B. and Lymon C. Reese (1957), "The Action of Soft Clay Along Friction Piles," Transactions, American Society of Civil Engineers, Vol 122, 1957, p 731.
- Shinohara, Tomio and Koichi Kubo (1961), "Experimental Study on the Lateral Resistance of Piles (Part 1) - Lateral Resistance of Single Free Head Piles Embedded in Uniform Sand Layer," Monthly Reports of Transportation Technical Research Institute, Japanese Ministry of Transportation, Vol 11, No 6, July 1961, p 169.
- Skempton, A. W. (1954), "The Pore Pressure Coefficients A and B," Geotechnique, Vol 4, p 143.
- Terzaghi, Karl (1943), Theoretical Soil Mechanics, John Wiley and Sons Inc., New York, 1943.
- Terzaghi, Karl (1955), "Evaluation of Coefficient of Subgrade Reaction," Geotechnique, Vol 5, December 1955, p 297.
- Terzaghi, Karl and Ralph B. Peck (1967), Soil Mechanics in Engineering Practice, John Wiley and Sons, Inc., New York, 1967.
- Thurman, A. G. and E. D'Appolonia (1964), "Prediction of Pile Action by a Computer," Proceedings, Conference on Deep Foundations, Mexican Society of Soil Mechanics, Mexico City, Vol 1, 1964, p 141.
- Thurman, A. G. and E. D'Appolonia (1965), "Computed Movement of Friction and End-Bearing Piles Embedded in Uniform and Stratified Soils," Proceedings, Sixth International Conference on Soil Mechanics, Montreal, Vol 2, 1965, p 323.
- Vesić, A. (1963), "Bearing Capacity of Deep Foundations in Sand," Highway Research Record 39, National Academy of Sciences, National Research Council, 1963, p 112.
- Vesić, A. S. (1964), "Investigation of Bearing Capacity of Piles in Sand," Proceedings, Conference on Deep Foundations, Mexican Society of Soil Mechanics, Mexico City, Vol 1, 1964, p 197.
- Vesić, Aleksander S. (1965), "Ultimate Loads and Settlements of Deep Foundations in Sand," Proceedings, Symposium on Bearing Capacity and Settlement of Foundations, National Science Foundation, Durham, North Carolina, 1965, p 53.
- Vesić, A. S. (1968), "Experiments with Instrumented Pile Groups in Sand," Special Technical Publication 444, American Society for Testing and Materials, 1968, p 177.
- Vesić, Aleksander Sedmak (1970), "Tests on Instrumented Piles, Ogeechee River Site," Journal of the Soil Mechanics and Foundations Division, American Society of Civil Engineers, Vol 96, March, 1970, p 561.

Vijayvergiya, Vasant N., W. Ronald Hudson and Lymon C. Reese (1969), "Load Distribution for a Drilled Shaft in Clay Shale," Research Report No. 89-5, Center for Highway Research, The University of Texas at Austin, March 1969.

Winkler, E. (1867), Die Lehre von Elastizität und Festigkeit (On Elasticity and Fixity), Prague, 1867.

APPENDICES

This page replaces an intentionally blank page in the original.

-- CTR Library Digitization Team

APPENDIX A
TEST FACILITIES

This page replaces an intentionally blank page in the original.

-- CTR Library Digitization Team

APPENDIX A
TEST FACILITIES

The test facilities include a rectangular reinforced concrete pit in which the piles were placed, the drainage system for controlling the water level in the pit, and the system used in loading the piles. An overall view of the test area, located at Balcones Research Center in Austin, Texas, shown in Fig. A.1. The top of the test pit and parts of the loading system are visible in the figure.

Test Pit

The test pit, illustrated in Fig. A.2, is a rectangular reinforced concrete pit 10 feet wide, 12 feet deep, and 25 feet long. It provides sufficient area for locating the piles and the pile groups as shown in Fig. 3.2. The pit was filled with sand to a depth of 10.5 feet, providing 1.5 feet of sand below the tip of the piles. The walls are eight inches thick and provide reaction for the application of both horizontal and vertical loads.

Drainage System

The drainage system illustrated in Fig. A.2 was provided for the purpose of regulating the water level in the pit. The ability to raise and lower the water level was required for the procedure employed in placing the sand.

The system consisted of a six-inch layer of pea gravel, a four-inch diameter collection pipe, and a two-foot diameter sump. The pea gravel

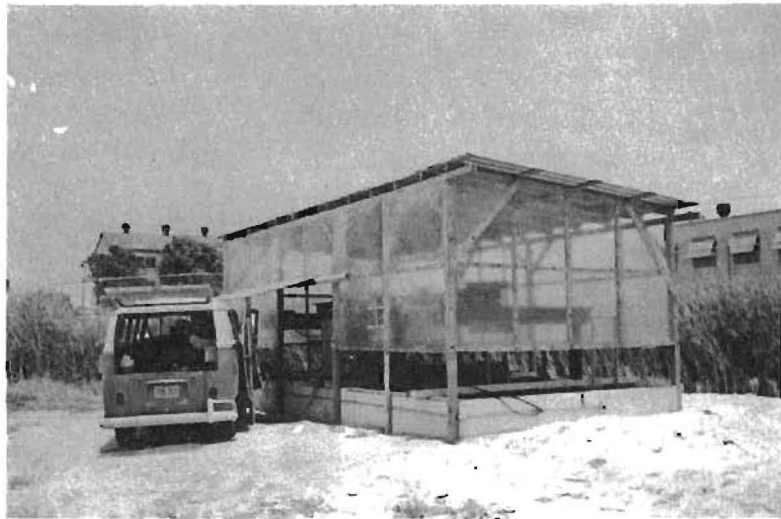


Fig. A.1. Test Site.

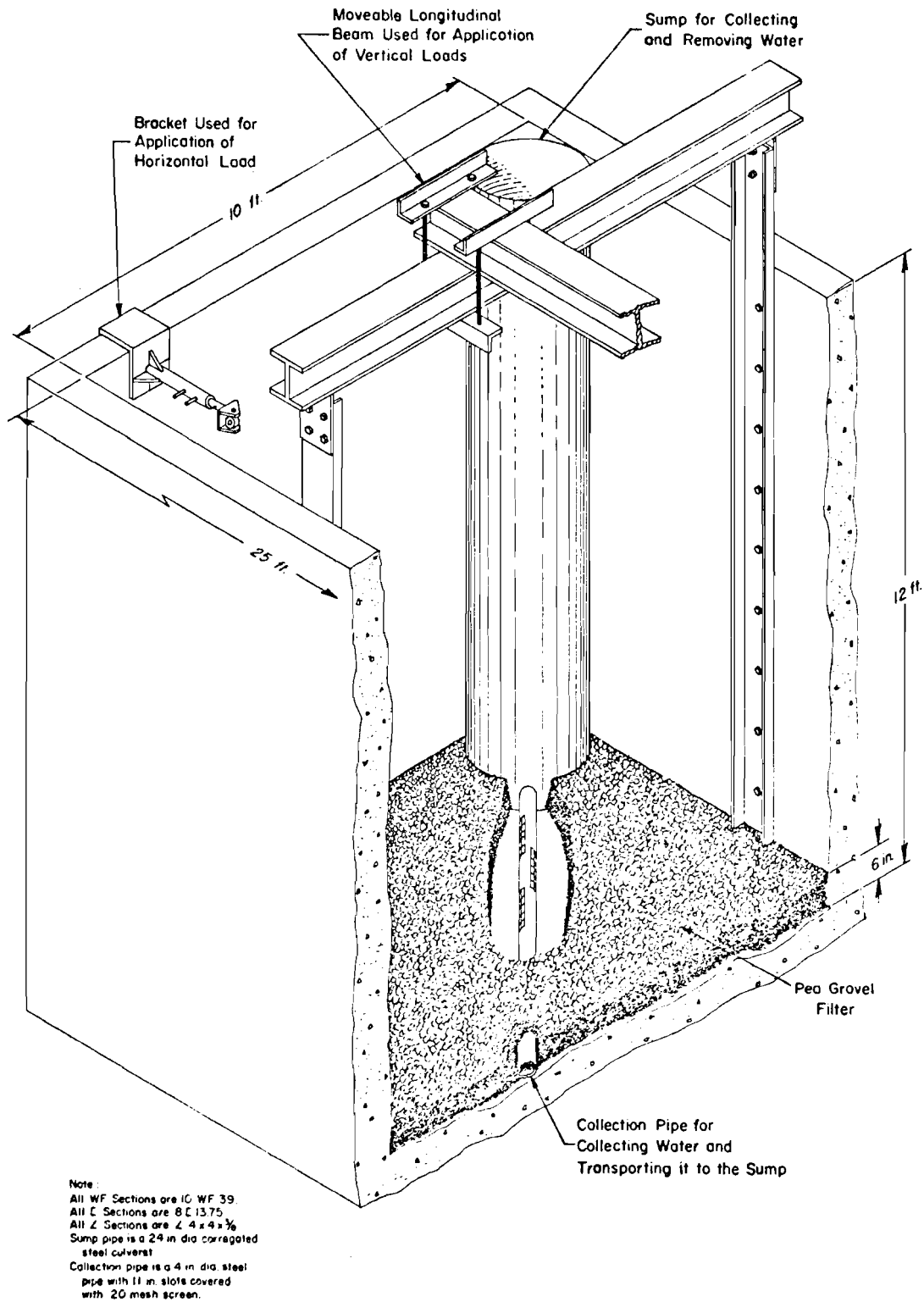


Fig. A.2. Layout of Drainage System and Loading Frame in the Test Pit.

was placed as shown in Fig. A.2, and provided a drainage layer over the entire area of the pit. This layer of pea gravel also acted as a filter to prevent the loss of sand during drainage. The four-inch collection pipe had slots cut in the side which were covered with screen wire. This pipe was placed diagonally across the pit and carried water to the sump. The sump was a two-foot diameter corrugated culvert placed in the corner of the pit, as shown in Fig. A.2, and provided access to the water which was removed from the sump by a submergible pump. This system allowed control of the water level in the sump and, therefore, the water level in the pit.

Loading Frame

Horizontal and vertical loads were applied by using a hydraulic ram. Horizontal loads were applied by a ram connected to the bracket, shown in Fig. A.2, attached to the end of the pit. This bracket transferred the applied loads to the pit wall. The bracket hung on the pit wall and could be moved to the location of the several piles to be tested.

Vertical loads were applied by a hydraulic ram attached to the longitudinal beam shown in Fig. A.2. This beam transferred the load to cross beams at both ends of the pit. These cross beams then transferred the load to vertical channels, which were attached to the walls of the pit. The longitudinal beam was attached to the cross beam with four angles and four rods, which allowed it to be moved to the location of the pile to be loaded.

APPENDIX B
INSTRUMENTATION

This page replaces an intentionally blank page in the original.

-- CTR Library Digitization Team

APPENDIX B
INSTRUMENTATION

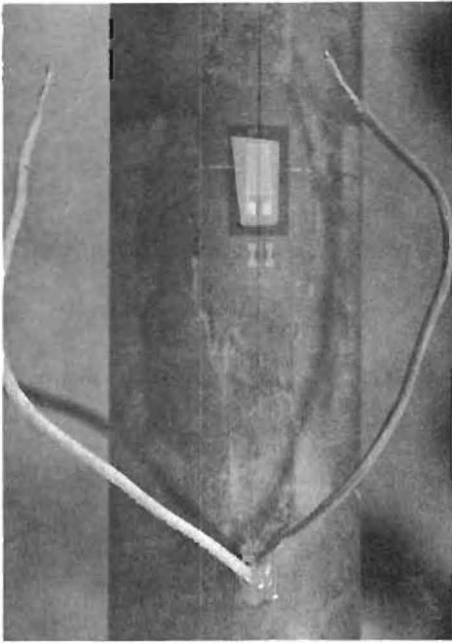
The locations of the strain gages on the axially and laterally loaded piles are shown in Fig. 3.3. There were two electrical resistance strain gages at each location, placed diametrically opposite on the pile. With this arrangement, the axial strain and bending strain could be obtained independently by changing the location of the gages in a Wheatstone Bridge. In the following sections, the techniques used in placing and waterproofing the strain gages will be discussed.

Gaging Technique

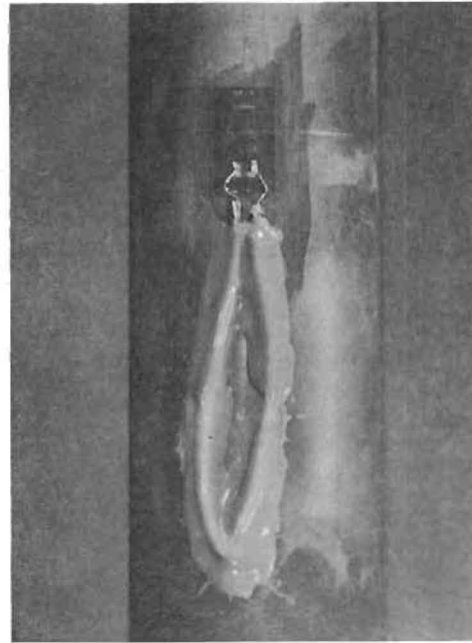
The bonding and waterproofing of the gages essentially followed the procedures suggested by Perry and Lissner (1962) and those suggested by the manufacturers of the gages and material used. Two principle sources of this information were technical bulletins by BLH Electronics, Inc., and William T. Bean, Inc.

Surface Preparation and Lead Wire Installation

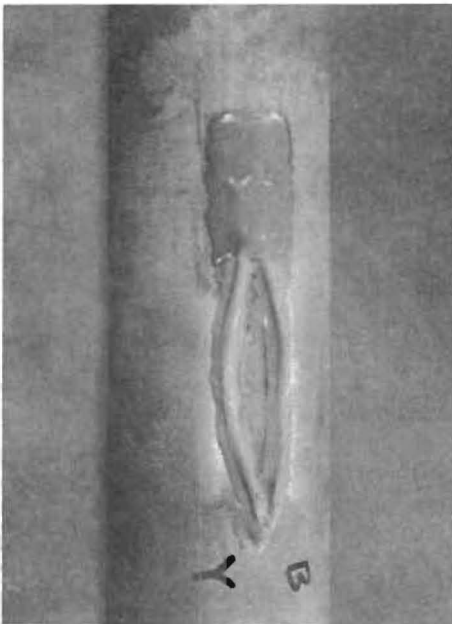
The entire outer surface of the piles was first sandblasted to remove any oil or mill scale present. The next step was to drill access holes for the lead wires. The access holes were elliptical in shape, located three inches from the center of the gage. The lead wires were next pulled through the access hole, as shown in Fig. B.1(a), and attached to the pile with Sears Filled Epoxy Cement. The two lead wires for each



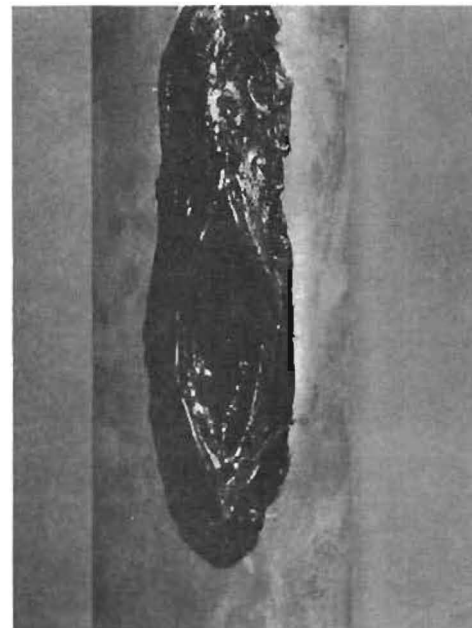
a. Gage and lead wire placement



b. Lead wire anchorage and waterproofing with Gagekote No. 2



c. Waterproofing with Gagekote No. 5



d. Waterproofing with rubber to metal cement

Fig. B.1. Strain Gage Installation.

gage were a pair of conductors from an eight-conductor, shielded, rubber-jacketed cable. The area around the position of each gage was then buffed with fine emery cloth and cleaned with Methyl Ethyl Ketone (MEK).

Gage Preparation and Bonding

The gages used were SR-4 Epoxy Back Strain Gages manufactured by BLH Electronics, Inc. The type designation was FAE-37-1256. The gage resistance was 120.0 ± 0.2 ohms and the gage factor quoted was 2.06 ± 1 per cent. The adhesive used was a room temperature curing epoxy manufactured by BLH Electronics with the designation EPY-150 Epoxy Cement.

The gages and solder tabs were placed on a piece of transparent tape. A piece of teflon was placed between the gage grid and the tape to prevent damage to the grid when the tape was removed. The backing material was then removed and the back of the gage roughed with a fiber brush and given a final cleaning with MEK. The cement was next spread on the pipe and the gages positioned. Excess cement and air bubbles were then squeezed from under the gage. A rubber pad was then placed over the gage, and a pressure of approximately 10 psi applied. The bond pressure was applied by hanging a weight from a cloth strap placed over the rubber pad. A curing time of approximately 12 hours was allowed before removing the pressure. A bonded gage is shown in Fig. B.1(a).

Lead Wire Attachment and Waterproofing

Lead wires were first connected to the solder tabs and then to the tabs on the gages. The lead wires were next securely attached to the pipe with Sears Filled Epoxy, as shown in Fig. B.1(b). The first layer

of waterproofing is also shown in Fig. B.1(b). It was a thin layer of solvent-thinned nitrile rubber, marketed by William T. Bean, Inc., and designated as Gagekote No. 2. The next layer of waterproofing is illustrated in Fig. B.1(c), and was a rubber-line epoxy resin also marketed by William T. Bean, Inc., with the designation, Gagekote No. 5. The final layer of waterproofing was a rubber-to-metal cement manufactured by G. C. Electronics. The completed gage installation is shown in Fig. B.1(d).

Checks Made During Gage Installation

Several checks were made during the installation procedure to insure that the gages functioned properly. After bonding, the first check made was a test of the continuity of the grid by measuring the gage resistance. The next check was to measure the leakage resistance between the strain gage filament and the pile. If these checks indicated permissible values, the lead wires were attached, and checks for continuity and resistance to ground repeated. A final check was made by attaching the gage to a strain indicator, balancing the bridge, and then pressing lightly on the gage and connections with an eraser or a pencil. If this check indicated adequate bond and proper connections, the waterproofing was applied. During the application of the waterproofing, care was taken to insure that each layer was bonded to the pipe around the entire perimeter of the previous layer. These steps were taken to eliminate as many of the causes of gage failure as possible, before subjecting the gages to field conditions.

APPENDIX C
CALIBRATION OF PILES

This page replaces an intentionally blank page in the original.

-- CTR Library Digitization Team

APPENDIX C
CALIBRATION OF PILES

There are several factors which require that the instrumented piles be calibrated, in order to obtain accurate values of bending moment and axial load from strain gage readings. Included in these factors are the variation from the nominal cross section and from the nominal modulus of elasticity of the pile, errors in gage orientation, and variations in the quoted gage factors. If accurate values of all of these parameters were known, then accurate values of bending moment and axial load could be obtained by analytical techniques. Consequently, the accuracy of these measured values would depend only on the precision with which the signals from the strain gages were measured. Unfortunately, the properties of the piles and gages are not known precisely, and the influence of the various factors can only be eliminated by calibrating the piles. It should be noted that the accuracy of the measured values will continue to be influenced by the precision with which the output signals from the gages are measured.

The calibration of the piles, while eliminating the unknowns mentioned in the previous paragraph, will introduce an additional approximation that must be considered. The factor that must be considered is the accuracy with which the loads and moments are measured during calibration. The care which must be taken in determining the moment and axial force will depend on the precision required in the calibration constants. For the purposes of these tests, more precision was required in the moments than in the axial loads. Therefore, more care was taken in determining

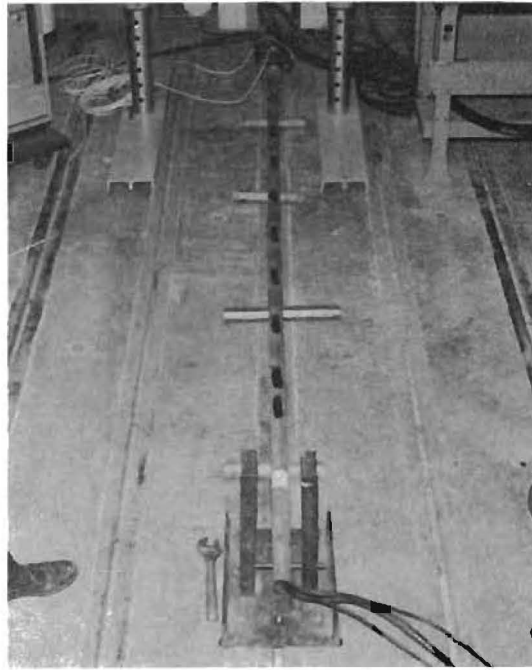
for calibration constants for bending than for the calibration constants for axial load.

The procedures followed for the axial calibration are covered in the following section, and the procedures followed for the lateral calibration are covered in the final section.

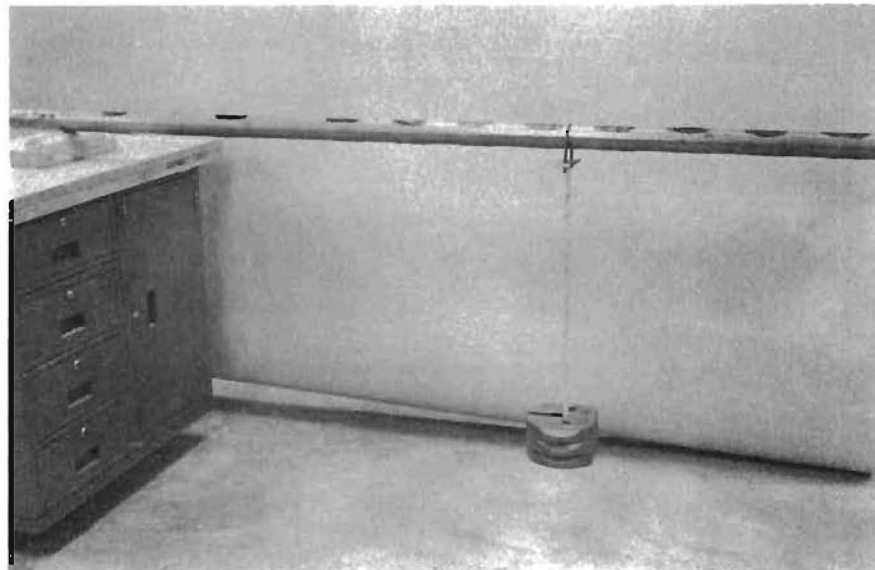
Procedure for Axial Calibration

The arrangement used in the axial calibration is shown in Fig. C.1(a). The hydraulic ram used to apply the load and the strain-gage load cell used to monitor the applied load are illustrated. The load cell is an Ormond, Model WCL-FF23-CD-10K-2102. The rated capacity is 10 kips and the rated accuracy of full-scale output is 0.25 per cent, tension or compression. The sensitivity of the load cell is 2 mV/V at rated capacity. An excitation voltage of 10 volts DC was used to power the bridge. The output from the load cell was measured with a Hewlett-Packard Model 3440 Digital Voltmeter. The rated sensitivity of the voltmeter is 0.01 per cent full-scale. The output from the Strain gage bridges was measured with the data acquisition system used throughout the entire test. The system was the Honeywell Model 620 Data Logging System, and it will be discussed later.

The piles were calibrated for axial tension and axial compression. The procedure followed involved applying a known load and measuring the output from the strain gages on the pile. A plot of load versus bridge output was made and the slope of the best straight line through the points obtained. An example of the procedure followed is illustrated



a. For axial force



b. For bending moment

Fig. C.1. Calibration Setups.

in Fig. C.2. In this figure, values for tension and compression are plotted. Because of the proximity of the points, no distinction is made between the calibration constant for tension and compression. This resulted in a calibration constant for the two gages at each location on the pile. This constant was multiplied by the output from the gages at a location to obtain the force in the pile at that location. Constants for piles 1-A and 2-A are tabulated in Table C.1.

Procedure for Lateral Calibration

The arrangement used to calibrate the piles for bending moment is shown in Fig. C.1(b). The pile was supported by a pin at the right end, and on a knife edge at the left end. With this configuration, the pile is considered as a simply supported beam. Moments were applied by placing known weights on the hanger. These weights are calibrated using a 10,000 gram Mettler Balance. The balance may be read to the nearest gram and interpolated to the nearest half gram. Distances between supports and loading points were measured with a six-foot tape, and the accuracy obtained must be considered compatible with the device used. The signals from the strain gages were measured using the Honeywell Data Logging System.

A weight was placed on the hanger, and the output from the strain gages was recorded. Since the pile was simply supported, the moment at a particular gage location could be obtained from the known load and distances. Additional weights were applied and a series of moments and bridge outputs obtained. These values were plotted, as illustrated in

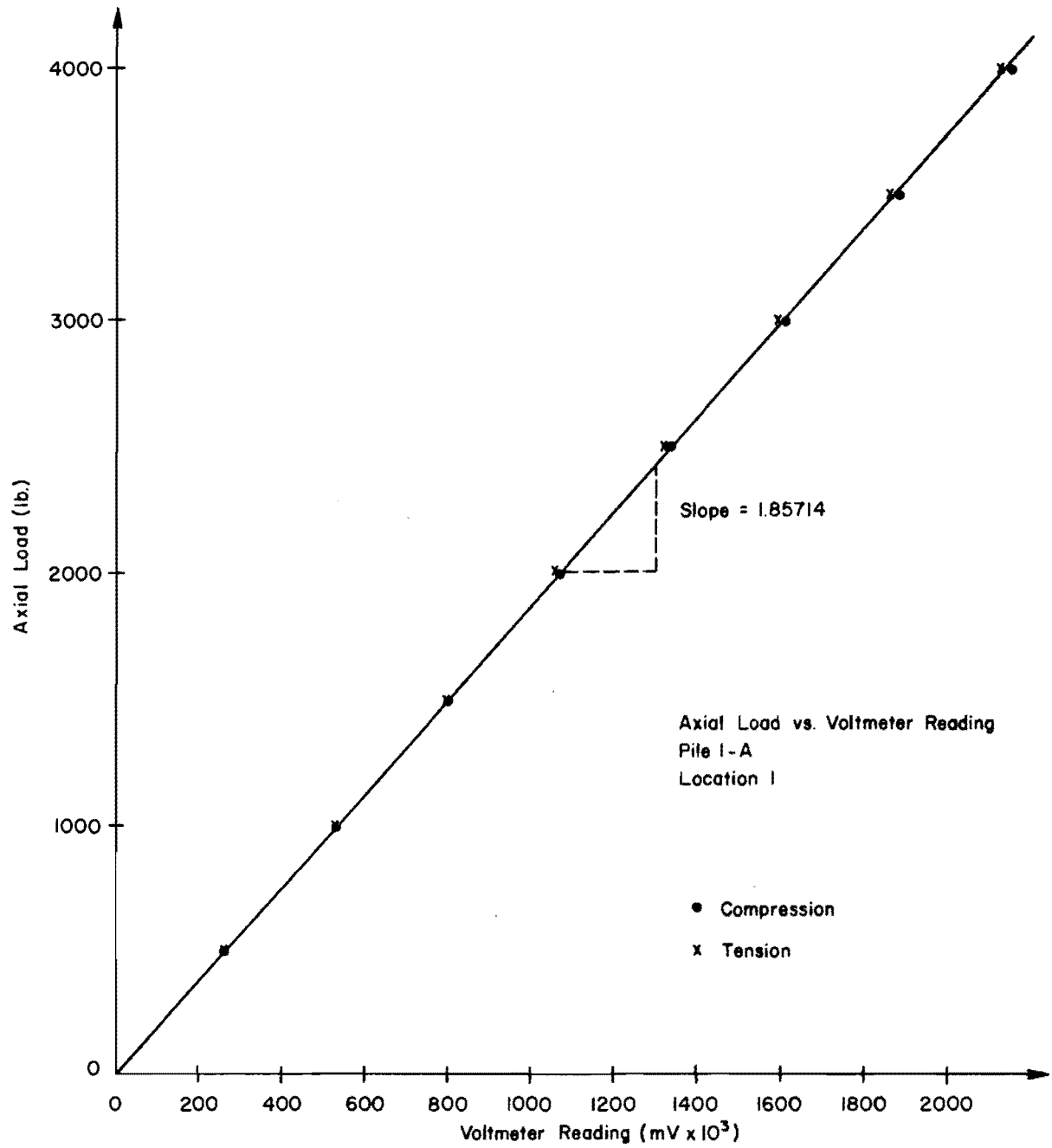


Fig. C.2. Example Axial Calibration Constant Determination.

TABLE C.1. CALIBRATION CONSTANTS FOR AXIAL FORCE

Location	Constants for Pile 1-A	Constants for Pile 2-A
1	1.85714	1.90162
2	1.84548	1.90151
3	1.89249	1.89625
4	1.87800	1.88187
5	1.82325	1.87469

Values obtained from tension and compression tests.

Fig. C.3, and the slope of the straight line through the points obtained. This slope is the desired calibration constant.

In Fig. C.1(b), the load is shown applied at the center line of the span between the supports. The load was also applied at the quarter points at each end and calibration constants obtained. The calibration constants used in the data reduction were the averages of the three values obtained.

The calibration constant for a particular location was multiplied by the output from the gages at that location to obtain the bending moment in the pile. Calibration constants for piles 1-L, 2-L, and 3-L are tabulated in Table C.2.

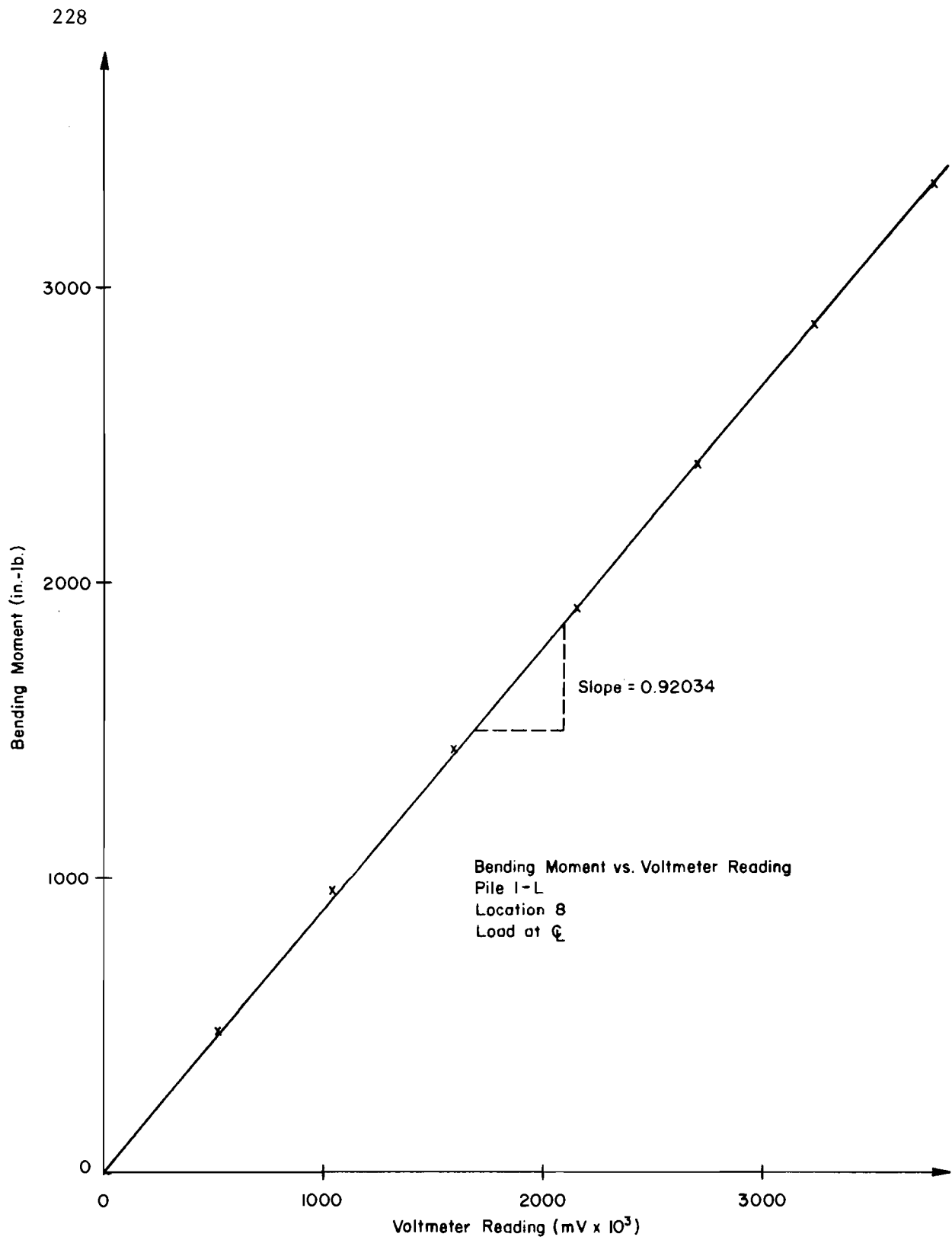


Fig. C.3. Example Moment Calibration Constant Determination.

TABLE C.2. CALIBRATION CONSTANTS FOR BENDING MOMENT

Location	Constants for Pile 1-L	Constants for Pile 2-L	Constants for Pile 3-L
1	0.90407	0.90893	0.89890
2	0.92130	0.91038	0.89420
3	0.90042	0.91094	0.89026
4	0.89758	0.91207	0.89238
5	0.89575	0.91108	0.88995
6	0.89640	0.91084	0.88862
7	0.90111	0.91075	0.88823
8	0.90093	0.91102	0.88620
9	0.90623	0.91211	0.89125
10	0.89929	0.91247	0.89672
11	0.89252	0.91254	0.89493
12	0.89052	0.91658	0.89441
13	0.90450	0.91668	0.90684

Given values are the average of three values obtained with the load applied at three different locations along the pile.

This page replaces an intentionally blank page in the original.

-- CTR Library Digitization Team

APPENDIX D
TEST EQUIPMENT

This page replaces an intentionally blank page in the original.

-- CTR Library Digitization Team

APPENDIX D

TEST EQUIPMENT

The items of test equipment described below are the loading apparatus, the read-out equipment used to measure the signals from the strain gages, and the dial gages used to measure the deflection of the tops of the pile.

Loading Equipment

The hydraulic loading equipment and the monitoring equipment is illustrated in Fig. D.1. Power for the system was provided by a hydraulic pump, driven by a 2 1/2 hp electric motor. The pump had a 3-gallon reservoir, provided a maximum pressure of 3,000 psi, and had a maximum flow rate of 1/2 gpm. The line pressure was controlled by a pressure reducing valve (V-1) and pressure relief valves (V-3 and V-4). The direction of the load was controlled by the four-way valve (V-2).

The load was transferred from the hydraulic cylinder through a load cell to the pile. The hydraulic cylinder and load cell used depend on the type of loading. For axial loading, the arrangement of the hydraulic cylinder and load cell is shown in Fig. D.2(a). The hydraulic cylinder has a four-inch bore, a six-inch stroke, and is double acting. The load cell is a BLH Type T2PIB. The rated capacity is 20 kips and the rated accuracy of full-scale output is 0.10 per cent. The sensitivity is 2 mV/V at rated capacity and an excitation of 10 volts DC was applied.

For lateral loading the arrangement of the hydraulic cylinder and load cell is shown in Fig. D.2(b). The hydraulic cylinder has a two-inch

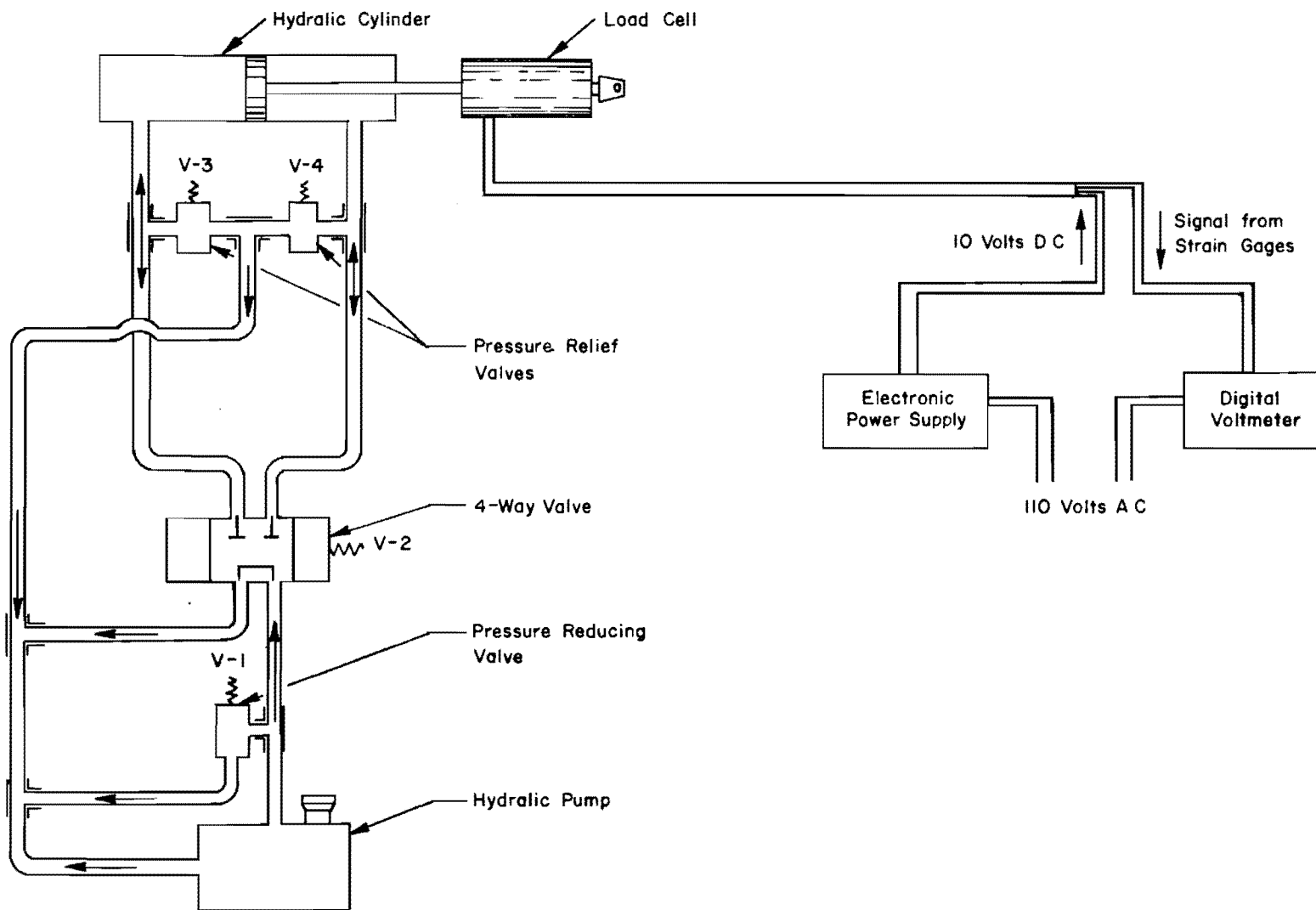
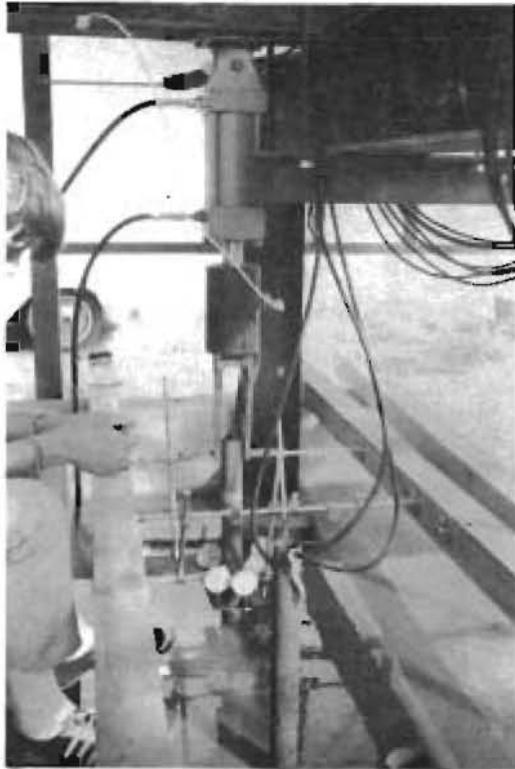


Fig. D.1. Hydraulic Loading and Electronic Load Monitoring Equipment.



a. For application of axial load



b. For application of horizontal load

Fig. D. 2. Arrangement of Hydraulic Cylinder and Load Cell.

bore, a six-inch stroke, and is double acting. The load cell was a Transducer, Inc., Model WTC-FF62-CD-2K. The rated capacity is 2 kips and the rated accuracy of full-scale output is 0.25 per cent. The sensitivity is 2 mV/V at rated capacity and an excitation of 10 volts was applied.

The excitation to the strain gage bridges was supplied by a Harrison Laboratories, Model 620A DC Power Supply, which supplied 10 volts DC regulated to 0.01 per cent. The signals from the bridges were monitored with the Hewlett-Packard Digital Voltmeter, as described in the section on axial calibration.

With the equipment described above, the signal from the load cell could be monitored to an accuracy greater than the rated accuracy of the load cell. For example, the rated accuracy of the load cell used for lateral loading was 0.25 per cent of full-scale output, which provided results that were guaranteed for ± 5 pounds. The rated accuracy of the digital voltmeter was 0.01 per cent full-scale. For 100 millivolts full-scale, the voltmeter accuracy was guaranteed for ± 0.01 millivolts, corresponding to ± 1 pound when the excitation voltage was 10 volts. For axial loading, the rated accuracy of the load cell was ± 25 pounds, but the signal was monitored to an accuracy of ± 5 pounds.

Data Acquisition Equipment

The magnitude of the applied loads was obtained by the equipment described in the previous section. The movements of the pile heads were observed from dial indicators, and will be discussed briefly in the next

section. The signals from the strain gages were recorded with the Honeywell Model 620 Data Logging System described in the last section.

Measurement of Pile-Head Movement

The axial deflection of the pile head was obtained by taking the average of three gages placed around the pile. The smallest division on the gages was 0.0001 inch, and the maximum travel was 0.5 inch. The gage arrangement is illustrated in Fig. D.2(a). Two gages used for measuring ground-surface movement are also shown in the figure.

The lateral deflection of the pile head was obtained at three positions. The smallest division on the gages was 0.001 inch, and the maximum travel was 2 inches. The arrangement is illustrated in Fig. D.2(b). Approximations of the deflection and slope of the pile at the ground line were obtained using the three measured values of deflection.

Measurement of Axial Load and Bending Moment

The signals from the strain gages were recorded with the Honeywell Model 620 Data Logging System. The unit, along with the switch and balance circuits is pictured in Fig. D.3. The axial load tests were run in late May before temperatures were high, and the equipment functioned well without any temperature control. However, the lateral load tests were run in the middle of the summer, and it was necessary to provide temperature control. To insure that the equipment functioned properly, the measuring equipment was placed inside an air-conditioned van, pictured in Fig. D.4. Another problem encountered during the lateral load tests was the operation of the switching system. The arrangement used, for



Fig. D.3. Honeywell 620 Data Logging System, Balance Circuits, and Switching System.



Fig. D.4. Measuring System Placed Inside an Air Conditioned Van for Temperature Control.

the first test on pile 2-L was a series of knife switches, but repeated switching caused a deterioration of the contacts and, thus, very erratic readings. A high quality, two-position, multipole radio switch with silver contacts was used in later tests. This switch was mounted on a chassis with a number of terminals and is pictured on the right in Fig. D.3.

The operation of the data acquisition system is shown schematically in Fig. D.5. The gages were connected to the balancing circuits, shown in the center of Fig. D.3. The balance circuits provided a potentiometer for balancing the bridges. For the axial load tests, the gages were connected directly to the balance circuits, but for the lateral load tests, the connection was made after going through the switch. The switch allows a change of the location of the gages in the bridge so that the axial load and the bending moment in the pile could be read. The dummy gages used to complete the bridges were located on a similar pile at the same level as the active gages. Voltage to the bridges was controlled by an electronic power supply that provided 6 volts DC.

Each bridge was connected to one of the 40 input channels in the data logging system. The signal from the bridges was fed into a preamplifier, which scaled the signal to the proper level to be read by the digital voltmeter. The voltmeter sampled the preamplified signal and converted the voltage to a decimal number which was sent to the printer module. The output from the gage was then printed on four-inch adding machine tape. The process was automatic, and the desired number of input channels could be scanned and printed at a rate of about one per second. For the axial load test, five bridges with the active gages in opposite arms

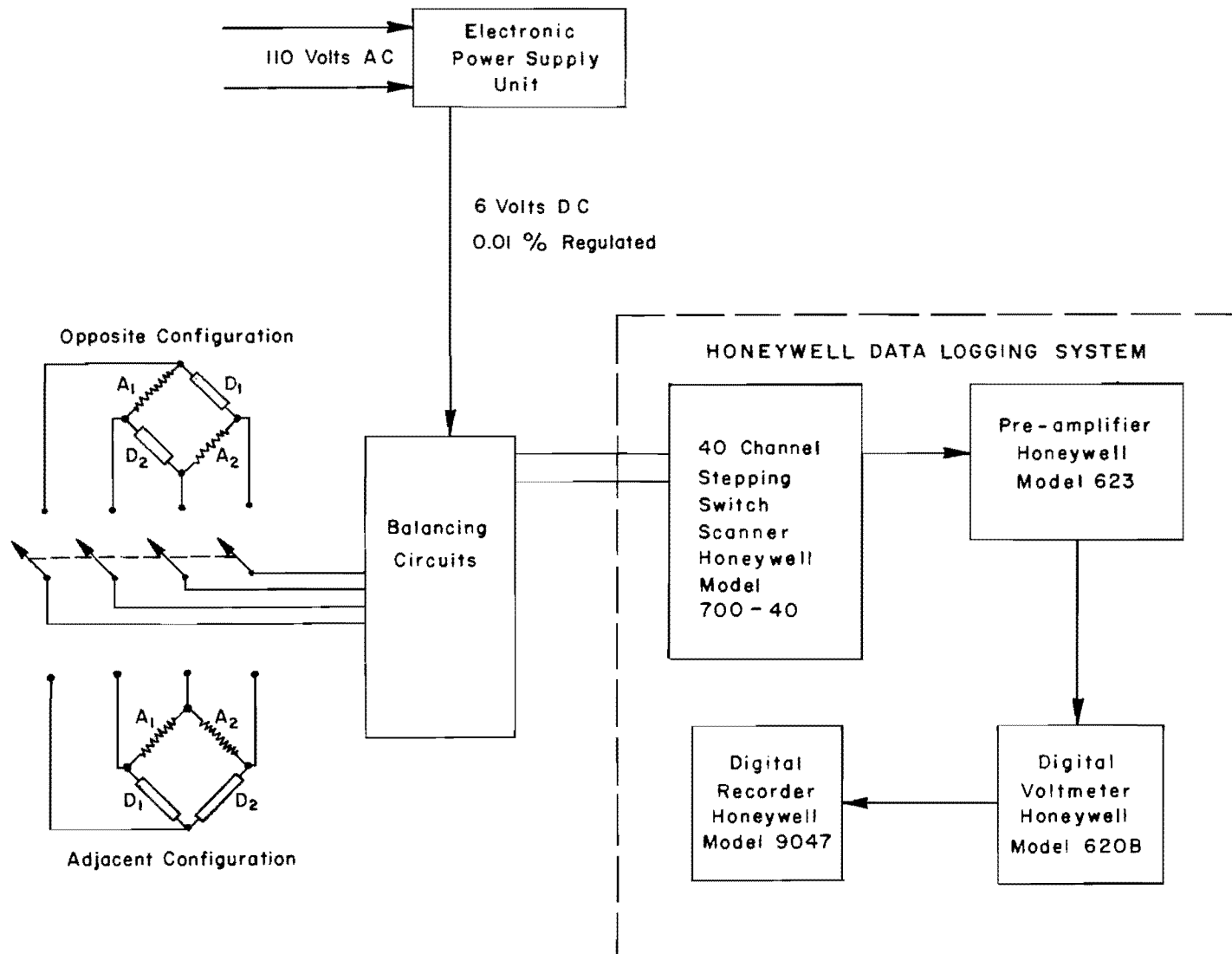


Fig. D.5. Honeywell Data Logging System.

were read. For the lateral load test, 13 bridges with the active gages in adjacent arms were read. The configuration of the bridges was then switched so that the active gages were in opposite arms and the 13 bridges scanned. For the lateral load tests, the gages were read in the configuration to measure the axial component of the horizontal force in the pile. This component was very small, which made precise measurement impossible, and the effect was ignored in the analysis of the results.

The rated accuracy of the digital voltmeter in the system was 0.01 per cent full-scale. For 10 millivolts full-scale the voltmeter accuracy was guaranteed for ± 0.001 millivolt. For axial loading, 0.001 millivolt corresponds to approximately ± 1.8 pounds and for bending moment to about ± 0.9 inch-pounds.

This page replaces an intentionally blank page in the original.

-- CTR Library Digitization Team

APPENDIX E

PROCEDURES USED IN PLACING SAND AND MEASURING DENSITY

This page replaces an intentionally blank page in the original.

-- CTR Library Digitization Team

APPENDIX E

PROCEDURES USED IN PLACING SAND AND MEASURING DENSITY

Placing of the Sand

There are several methods which have been used to place sand under controlled conditions. The most popular method is a "raining" technique with possible vibration in order to obtain the more dense states. The raining technique involves pouring air-dried sand from containers with perforated bottoms. The height of free fall and rate of deposition is controlled to produce the desired density. The vibration is usually done with some type of surface or penetration vibrator. This method has been used by a number of investigators for a wide range of pile sizes. The raining technique has been used by Mazurkiewicz (1968), and the raining technique with vibration by Prakash (1961) for tests on small pencil-piles. The raining technique and vibration has also been used by Vesić (1963, 1964, 1965, and 1968) for larger size models (2 to 7 inches in diameter). For most of the studies mentioned above, the sand was placed in an air-dried condition, and the load test run with the sand air-dried. Vesić (1968) reports tests run after the sand had been saturated.

Another technique which has been used involves ponding the sand with subsequent tamping to increase the density. This technique was reported by Sinohara and Kubo (1961) and was the method selected for this study. The tests reported by Sinohara and Kubo were for larger scale models (1.75- to 5.18-centimeter diameter piles and 10- to 30-centimeter wide plates), and the models were loaded while the sand was saturated. This

method was selected, because a relatively large quantity of sand could be placed rapidly with very little equipment (a shovel and a tamper). It also allowed the sand to be placed and maintained in a submerged condition, which eliminated any changes in moisture content. Another prerequisite that the method satisfied was that a dense condition could be obtained. This was desirable to avoid density changes during testing.

The procedure involved placing the sand in layers approximately 8 inches thick. The first step was to fill the test pit with water to a level approximately 2 inches above the top of the previous layer. Sand was then shoveled into the pit until the level of the water was about one-half inch above the sand surface. The surface of the sand was then leveled with a rake, and the water level drawn down about 8 inches. This drawdown of the water level was accomplished by the drainage system described in Appendix A. The layer of sand was then compacted with the tamper pictured in Fig. E.1. The tamper weighed approximately 25 pounds and the area of the base was one square foot. The height of drop was approximately 12 inches. At first, the entire surface area was tamped eight times but this was later reduced to four coverages. This decrease caused no apparent reduction in the magnitude or uniformity of the density obtained. The procedures utilized for checking the density will be presented in the following section.

Density Measurement

Density measurements were made during the placement and also during the removal of the sand. After each layer was placed, two or three density samples were taken with the push-tube sampler pictured in Fig. E.2.



Fig. E.1. Tamper Used for Compacting Sand.

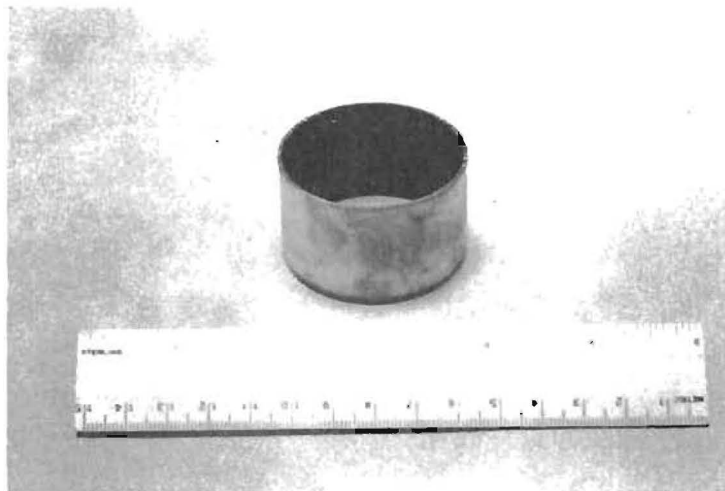


Fig. E.2. Push-Tube Sampler Used for Density Measurement.

The ring is 2 inches in diameter, 1.3 inches deep and has a wall thickness of approximately 0.03 inch. The sampler is made of brass and has a beveled face for easier penetration. The first step in the procedure was to push the ring about 2 inches into the sand. The ring was then removed and the sand trimmed flush with the top and bottom. The ring and sand were then placed in a moisture can, and weighed and dried to obtain values of density and moisture content. Thirty-one density samples were taken using this method.

During the placement of the sand, a number of in-place sample boxes, shown in Fig. E.3, were buried. Five of the smaller rings (3 inches in diameter and 2 inches in depth), five of the larger rings (5 inches in diameter and 3 inches in depth), and five of the rectangular boxes (4 inches by 6 inches by 12 inches) were placed at various depths. When the sand was removed, twelve of these samples were recovered and values of dry density calculated. The procedures followed in removing the in-place samplers were the same as for the push-tube samplers.

As the sand was removed sixteen additional push-tube samples were taken, and density checks were made using the volumeter pictured in Fig. E.4. Nine values were determined using this device. In using the volumeter, the first step in the procedure was to level the base. Then through a hole in the base a test hole was excavated, and the material from the hole weighed and dried. The volumeter was next placed on the base and the volume of the hole measured. This particular model of volumeter employed a balloon filled with an antifreeze solution to measure the volume. With the volume of the hole and the weight of the material removed, the density was calculated.

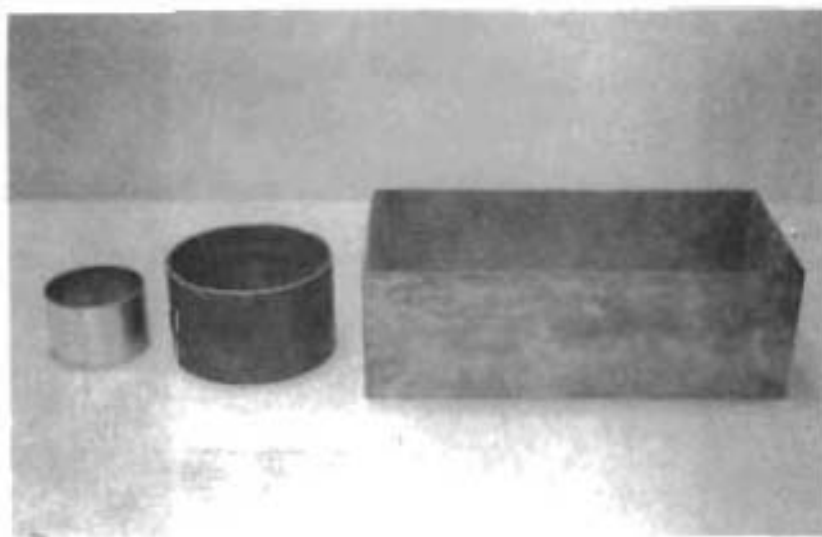


Fig. E.3. In-Place Samplers Used for Density Measurement.



Fig. E.4. Rainhart Volumeter Used for Density Measurement.

This page replaces an intentionally blank page in the original.

-- CTR Library Digitization Team

THE AUTHORS

Frazier Parker, Jr. was a graduate research assistant with the Center for Highway Research of The University of Texas at Austin. He has had experience in the areas of highway design and bridge construction and has reported on the analysis of pile foundations. He is currently involved in research in the area of flexible pavements at the Waterways Experiment Station, Vicksburg, Mississippi.



Lymon C. Reese is Professor and Chairman of the Department of Civil Engineering at The University of Texas at Austin. His specialization is in the area of soil mechanics and foundation engineering. He was the recipient of the Thomas A. Middlebrooks Award of the American Society of Civil Engineers in 1958. One of his primary interests has been in the design of offshore structures and pile foundations. In recent years he has become well known for his research in the application of the finite-element method of analysis to problems in soil and rock mechanics. He holds memberships in numerous professional and learned societies and is a Registered Professional Engineer in Texas.

